



City Research Online

City, University of London Institutional Repository

Citation: El-Kaream, A. M. G. (1983). An experimental and numerical analysis of plane layered structures subjected to impact. (Unpublished Doctoral thesis, The City University)

This is the accepted version of the paper.

This version of the publication may differ from the final published version.

Permanent repository link: <https://openaccess.city.ac.uk/id/eprint/34931/>

Link to published version:

Copyright: City Research Online aims to make research outputs of City, University of London available to a wider audience. Copyright and Moral Rights remain with the author(s) and/or copyright holders. URLs from City Research Online may be freely distributed and linked to.

Reuse: Copies of full items can be used for personal research or study, educational, or not-for-profit purposes without prior permission or charge. Provided that the authors, title and full bibliographic details are credited, a hyperlink and/or URL is given for the original metadata page and the content is not changed in any way.

AN EXPERIMENTAL AND NUMERICAL ANALYSIS OF
PLANE LAYERED STRUCTURES
SUBJECTED TO IMPACT

A THESIS SUBMITTED FOR THE DEGREE OF
DOCTOR OF PHILOSOPHY IN THE DEPARTMENT OF
CIVIL ENGINEERING AT THE CITY UNIVERSITY

BY

ALY MEHANY GAD EL-KAREAM BSc, MSc

THE CITY UNIVERSITY

1983

The first part of the paper is devoted to a description of the
method used in the present study. A new apparatus consisting of
a cylindrical chamber of aluminum, 20 cm in diameter and 10 cm
high, was used. The chamber was evacuated to a pressure of
10⁻⁴ mm Hg. The chamber was surrounded by a water jacket
which was kept at a constant temperature of 20°C. The
chamber was filled with a mixture of gases which was
maintained at a constant pressure of 100 mm Hg. The
mixture was composed of 10% oxygen and 90% nitrogen.

The second part of the paper is devoted to a description of the
method used in the present study. A new apparatus consisting of
a cylindrical chamber of aluminum, 20 cm in diameter and 10 cm
high, was used. The chamber was evacuated to a pressure of
10⁻⁴ mm Hg. The chamber was surrounded by a water jacket
which was kept at a constant temperature of 20°C. The
chamber was filled with a mixture of gases which was
maintained at a constant pressure of 100 mm Hg. The
mixture was composed of 10% oxygen and 90% nitrogen.

To My Family

The third part of the paper is devoted to a description of the
method used in the present study. A new apparatus consisting of
a cylindrical chamber of aluminum, 20 cm in diameter and 10 cm
high, was used. The chamber was evacuated to a pressure of
10⁻⁴ mm Hg. The chamber was surrounded by a water jacket
which was kept at a constant temperature of 20°C. The
chamber was filled with a mixture of gases which was
maintained at a constant pressure of 100 mm Hg. The
mixture was composed of 10% oxygen and 90% nitrogen.

The fourth part of the paper is devoted to a description of the
method used in the present study. A new apparatus consisting of
a cylindrical chamber of aluminum, 20 cm in diameter and 10 cm
high, was used. The chamber was evacuated to a pressure of
10⁻⁴ mm Hg. The chamber was surrounded by a water jacket
which was kept at a constant temperature of 20°C. The
chamber was filled with a mixture of gases which was
maintained at a constant pressure of 100 mm Hg. The
mixture was composed of 10% oxygen and 90% nitrogen.

The fifth part of the paper is devoted to a description of the
method used in the present study. A new apparatus consisting of
a cylindrical chamber of aluminum, 20 cm in diameter and 10 cm
high, was used. The chamber was evacuated to a pressure of
10⁻⁴ mm Hg. The chamber was surrounded by a water jacket
which was kept at a constant temperature of 20°C. The
chamber was filled with a mixture of gases which was
maintained at a constant pressure of 100 mm Hg. The
mixture was composed of 10% oxygen and 90% nitrogen.

ABSTRACT

This thesis considers the theoretical and experimental analysis of plane layered structures subjected to impact. A new approach combining the finite element technique with the theories of propagation wave, which is appropriate for design purposes, has been proposed. This approach is suitable for the analysis of multi-layered half-space structures subjected to impact forces. Such structures include aircraft pavements or runways. It is intended to be a realistic and a versatile method to be used for the analysis and design of structures or structural components which may be considered to act as plane or axisymmetric systems subjected to impact.

Some special features related to the propagation of elastic waves in solids are considered. In addition, problems involving the response of multi-layered structures which arise from the different types of waves created at interfaces have been discussed. A review of the analytical solutions of wave propagation in solids and multi-layered structures are summarized in this thesis.

A numerical model has been developed using the finite element technique. This technique has certain advantages for analysis of a multi-layered half-space structure subjected to an impact force. The simulation of complex applied load distribution, the representation of stress wave propagation and the reflection and refraction at interfaces are included. The different stiffness and damping characteristics in each layer are represented. The theory which has been developed has been incorporated in a complete program called DFEM to study the dynamic response and also important features such as the damping, reflection and refraction of stress waves.

The accuracy of the results obtained is demonstrated by comparison with results obtained by other published methods. In addition, an experimental investigation was carried out by using the dynamic photoelasticity technique which provides a convenient method to study stress wave propagation. A series of a multi-layered models were tested to further substantiate the theoretical results. The model dimensions and materials were chosen to minimize the effects of reflection from both boundary and free surfaces. The degree of correlation obtained shows that the theoretical developments proposed in this thesis may be applied successfully to the analysis of plane multi-layered structures subjected to impact.

The objective of the method of analysis which has been developed was the direct analysis of pavement or runway structures. Therefore, the basic methods which deal with the design of flexible airfield pavements are summarized. A dynamic factor has been assessed which depends on the time of impact force and maximum tyre deflection to be used in the analysis and design of airfield pavements.

ACKNOWLEDGEMENTS

The research described herein was undertaken in the Department of Civil Engineering of The City University. During the course of the research the author received valuable advice and helpful suggestions from many persons. In particular, the author wishes to express his gratitude to the following:

To Professor J E Gibson, Head of Department, for the helpful way in which the project was accommodated.

To Dr L F Boswell, who supervised this work, for his constant encouragement, his valuable advice and his guidance throughout the duration of the project, without which the effective fulfilment of this work would not have been possible.

To Professor L M Meyer, for his helpful suggestions which directly contributed to the scheme of the experimental investigation.

The author is extremely grateful to Mr D A Chamberlain, Dr A E Mohamed and Dr S Bolbol for their valuable advice and generous help in many ways.

The assistance and effort provided by the technical staff of the Structures Laboratories is greatly appreciated by the author.

The author is extremely grateful to the Egyptian Government for providing financial support.

A special word of thanks is given to my wife and my friends for their help, support and encouragement.

Thanks are also due to ■■■ ■■■■ ■■■■ who typed the manuscript.

NOTATION

A	Amplitude of incident wave
\bar{A}	Amplitude of reflected wave
[B]	Strain matrix
[C]	Damping matrix
[C ^e]	Element damping Matrix
C	Wave velocity
[D]	Elasticity matrix
D _S	Damping coefficient
E	Modulus of elasticity
e	Volume Expansion
f	Unit fringe value
G	Shear modulus
h	Thickness of layer
I	Intensity of light
J	Damping constant
[K]	Stiffness matrix
[K ^e]	Element stiffness matrix
L	Wavelength
[M]	Mass matrix
[M ^e]	Element mass matrix
N	Fringe order
[N]	Shape function
n	Damping exponent
P _S	Static load per leg
P _x , P _y , P _z	Time dependent forcing functions
q _n	Admittance ratio
R	Raleigh wave
{R}	Force vector
S	Distortional wave
T _o	Fundamental period of the system

T_A	Pavement thickness
t	Time
$\{U\}$	Displacement vector
$\{\dot{U}\}$	Velocity vector
$\{\ddot{U}\}$	Acceleration vector
U, V, W	Displacement in x, y, and z directions
V_p, V_s	Wave velocities
W	Weight
X, Y, Z	Global coordinates
x, y, z	Local coordinates
Z	Factor defining the character of discontinuity
α, β	Rayleigh constants
ν	Poisson's ratio
ϵ	Strain
λ, μ	Lame's constants
λ_i	Eigenvalue
ξ	Efficiency factor
σ_1, σ_2	Principal stresses
σ_a	Stress in incident wave
σ_b	Stress in reflected wave
σ_x, σ_y	Stress components in the x and y directions
τ_x	Shear stress
ρ	Density
$\{\Phi\}$	Eigenvector
ω	Circular frequency
ω_0	Natural frequency
Θ	Parameter for Wilson- Θ method
∇^2	Laplacian operator

Only the main symbols have been listed. Other symbols are defined as they first appear in the text.

CONTENTS

	PAGE	
Abstract	III	
Acknowledgements	IV	
Notation	V	
Chapter 1	General Introduction	1
1.1	Introductory Remarks	1
1.2	Objectives	3
1.3	General Outline of the Method of Analysis and Experimentation	4
1.4	Impact Problems	6
1.4.1	Brief Description of the Phenomenon of Impact	6
1.4.2	Contact Zone	7
1.4.3	Force-Time Relation of Impact	8
1.5	Methods of Solution of Impact Problems	8
1.6	Basic Considerations and Assumptions	8
Chapter 2	Theoretical Analysis of Elastic- Wave Propagation During Impact	11
2.1	Introduction	11
2.2	General Wave Theory	12
2.2.1	Waves of Dilation and Distortion in an Isotropic Elastic Medium	12
2.2.2	Surface Waves or Rayleigh Waves in a Half-Space (Single Boundary)	15
2.2.3	Plane Waves	17
2.2.4	Longitudinal Wave Propagation	19

		PAGE
2.3	Stress Wave Propagation in Soil and Granular Materials	20
2.4	Stress Wave Propagation in Multi- Layered Half-Space	23
2.5	Previous Work	25
2.5.1	Analytical Methods	25
2.5.2	Numerical Methods	27
Chapter 3	Damping Phenomena in Wave Propagation	31
3.1	Introduction	31
3.2	Types of Damping Phenomena	32
3.3	Types of Linear Damping	34
3.4	Evaluation of Material Damping	35
3.5	Interface Effects in Damping Analysis of Structures	38
3.6	Experimental Measurement of Damping	40
3.7	Numerical Formulation for Damping Analysis	41
3.8	Damping Idealization and Damping Model for Pavement Construction	46
Chapter 4	The Finite Element Analysis Numerical Model	57
4.1	Introduction	57
4.2	The Finite Element Method	58
4.3	Discretization of Infinite Media and Mesh Design	59
4.4	Mathematical Formulations	60

	PAGE	
4.4.1	Linearly Elastic, Undamped Formulation	60
4.4.2	Formulation of Damping Properties	64
4.5	Solution of Eigenvalue Problems	67
4.6	Dynamic Analysis of Layered Semi-Infinite Media	68
4.6.1	Treatment of the Effect of Wave Impinging upon Interface	69
4.6.2	The Scheme for Numerical Analysis of ReFlected, Refracted and Transmitted Waves	72
4.7	Solution of Equilibrium Equations for the Dynamic Finite Element System	74
Chapter 5	Program Description and Numerical Examples	76
5.1	Introduction	76
5.2	Brief Description	77
5.3	Program Structure	78
5.4	Numerical Examples	81
5.4.1	Cantilever Beam with Uniform Load	82
5.4.2	Damping Effect	82
5.4.3	Dynamic Snap-Through of an Arch	83
5.4.4	One-Dimensional Wave Propagation Problems	84
5.4.5	Two-Dimensional Wave Propagation	87

		PAGE
5.4.6	Response of Half-Space Excited by Trapezoidal Pulse	87
5.4.7	Dynamic Analysis of a Rubber Sheet with a Hole	88
Chapter 6	Experimental Investigation	119
6.1	Introduction	119
6.2	Photoelasticity and Applications to Elastodynamics	120
6.3	Dynamic Recording Systems	121
6.3.1	Rotating Prism High-Speed Camera	122
6.3.2	Timing Light Generator	123
6.3.3	Fidelity of Dynamic Recording	124
6.4.1	The Impact Force	125
6.4.2	Material Properties	126
6.5	The Investigation of the Isoclinic	133
6.6	Model Manufacturing and its Properties	134
6.7	Experimental Procedure	134
6.8	Processing of Photoelastic Results	136
6.9	Interpretation of Photoelastic Results	136
6.10	Theory of Computer Data Analysis of Experiments and the Analysis of Experimental Results	139

	PAGE	
6.11	Theoretical Solutions	141
6.12	Discussion of Experimental Results	141
6.13	Comparison of the Theoretical and Experimental Results	142
Chapter 7	The Influence of Impact Loading upon the Design of Airfield Pavements	184
7.1	Introduction	184
7.2	Design of Aircraft Pavements	185
7.3	Dynamic Phenomena in Airfield Pavements	193
7.4	Landing Gear and Dynamic Response Prediction	196
7.5	The Analysis of the Dynamic Response of an Airfield Pavement	199
Chapter 8	Conclusions and Recommendations for Further Research	221
References		225
Appendix I	Computer Program - DFEM	241
Appendix II	The Wilson- θ - Method	286
Appendix III	The Eigenproblem	292
Appendix IV	Program for Analysis of Experimental Results	296
Appendix V	Program for Least Squares Method for Unit Fringe Value	308

CHAPTER 1

GENERAL INTRODUCTION

1.1 INTRODUCTORY REMARKS

The analysis and design of structures which are subjected to impact loading are a particular part of the work of a civil engineer. Although a considerable amount of information is available on the subject, certain areas require further investigation. In particular, the effect of significant impact loading upon the analysis and design of aircraft runways, is an area requiring further attention.

Excepting the United States Air Force [1], all authorities which are responsible for the design of airfield runways, use static considerations. These considerations usually dictate that the runway ends have a greater thickness than elsewhere.

Since runway ends are critical, their design to resist impact forces will be considered in this thesis. The results of the proposed method, which takes account of dynamic effects, is compared with the results of the five basic methods that deal with the design of flexible airfield pavements [2, 3, 4].

An impact event usually consists of at least a transient state with wave propagation throughout the impacting and impacted bodies followed by more-or-less steady state in which the bodies involved vibrate in modes and frequencies that are natural to the system. The landing of aircraft on runways can be considered to be an impact problem in a multi-layered half space.

Impact problems are complicated and few cases can be solved directly by analytical methods [5]. Therefore, numerical methods such as the finite element technique may be used to solve all but the simplest problems. This method has several advantages, since it can account for the complex wave forms which occur, the interaction between loads and the structure and different material properties.

A finite element programme for the elastic analysis of plane and axisymmetric conditions has been developed to obtain the dynamic response of a half-space subjected to arbitrary impact loading. To verify the numerical results which have been obtained, an experimental investigation has been carried out using a multi-layered photo-elastic model.

The dynamic response of a multi-layered half-space subjected to impact has been obtained as a result of the work presented in this thesis. Also, the effect of impact on the design of runway ends has been considered.

It is worthwhile noting that the proposed method of analysis is also applicable to structures or structural components which may be considered to act as plane or axisymmetric systems subjected to impact.

1.2 OBJECTIVES

The objectives of the present project may be summarised as follows:

- (1) To develop a plane strain, plane stress and axisymmetric linear finite element analysis so that the dynamic response of a multi-layered half space subjected to impulsive or continuous dynamic loading may be obtained.
- (2) To include within the analysis a means by which a wide variety of boundary conditions, damping, wave reflection and wave refraction phenomena can be considered.
- (3) To carry out an experimental investigation of the response of different multi-layered systems subjected to impact and to compare this response with the analytical formulation.
- (4) To establish important parameters for the design of multi-layered structures to be used in runway construction.

1.3 GENERAL OUTLINE OF THE METHOD OF ANALYSIS AND EXPERIMENTATION

This thesis is presented in a form which is compatible with the objectives of the project. In this chapter, the impact phenomena is briefly described and existing analytical methods leading to the present study are reviewed. Basic considerations and assumptions are established for further investigation.

In Chapter 2, a brief description of some special features related to the propagation of elastic waves in solids is given. The distribution of wave energy at boundaries in cases of reflection and refraction of stress waves is considered. A discussion of the dissipation of energy by damping and its mathematical treatment concludes Chapter 3.

Following the mathematical formulation of the problems stated in Chapter 2, the finite element method for solution is summarised in Chapter 4. The method is extended to include within the analysis a means by which a wide variety of boundary conditions, damping effects and wave reflection and refraction phenomena can be considered.

The verification and application of the present study are given in Chapters 5 to 7. In Chapter 5, results from selected examples are given. Chapter 6 describes further the experimental scheme of the multi-layered photoelastic

model subjected to impact forces. The numerical and experimental results are compared and discussed in Chapter 6.

A brief description of the basic methods of the design of airfield pavements are reviewed in Chapter 7. Also the effects of aircraft characteristics and performance on the design of pavements is discussed. This discussion is included since this thesis is concerned with the study of impact forces on multi-layered half spaces and their effect on the design of runway ends. In Chapter 7, the dynamic factor, which may be related to an effective static loading has been assessed and its use in the structural design of pavement has been demonstrated.

Finally, in Chapter 8, the conclusions to which the present study leads and the proposals for further studies are given. The finite element programme is discussed in Appendix 1 together with a listing and information concerning the preparation of data.

1.4 IMPACT PROBLEMS

1.4.1 Brief Description of the Phenomenon of Impact

The progress of an impact may be described as follows. If it is assumed that one body is at rest and is approached by another body with a certain initial momentum and kinetic energy, both bodies deform locally, either elastically or plastically after collision and thereby generate a contact force. This force decelerates the contact zone of one body and accelerates the contact zone of the other. At this stage only part of the mass of either body is involved. The positions and types of support, if any, of the impacted body have no influence in its response.

The effects of the contact force may be so severe that a local failure occurs in one or other body before there has been any significant transfer of momentum or energy. If local failure does not occur, the impinging body continues to decelerate and contact may end [12]. Considering the case of high loading rates and that no local failure occurred, then wave propagation effects must be considered to determine the initial response.

Impact is characterized also by the generation of relatively large contact forces which act over a very short time. During this time-interval the contact area grows rapidly to a peak value as deformation increases and then reduces to zero during the restoration.

1.4.2 Contact Zone

The conditions in the contact zone between impacting bodies and contact problems have received considerable attention in the literature. Much of the literature in this area deals with an elastic slab, either loaded symmetrically from both surfaces or loaded from one surface and rigidly fixed on the other surface.

Sahlin and Milson [5] discuss an analytical method for calculating the depth of penetration of an object travelling at a very high velocity. This type of impact is somewhat less important for the purpose of this project than in relation to ballistic problems. A useful application of this phenomena has been used in rapid soil investigations, however, using high-speed earth penetrating projectiles [6]. The entire determination can be achieved from the air to assess soil or rock conditions.

By using elasticity theory Chen and Engel [7], have analysed the contact problem in a multi-layered to determine their results, they assumed that the surface compresses gradually and the dissipation of energy during impact was neglected. The quasi-static assumption of the Hertz impact theory was also assumed [7]. Chen and Engel determined the variation of contact force and surface displacements as a function of time during which rigid ball is dropped from a height on the layered medium.

1.4.3 Force-Time Relation of Impact

The force-time relationship of the impact depends upon the properties of the colliding bodies. Sahlin and Nilson [5] provide formulae for impact times and contact forces. Also, Chen and Angel [7], discuss the contact duration analytically and verify the results experimentally.

1.5 METHODS OF SOLUTION OF IMPACT PROBLEMS

Few analytical solutions exist for impact problems [8, 9, 10]. Only those cases in which the characteristic of wave propagation and the boundary conditions are simpler can be solved analytically [11]. Many practical problems are too complicated for solution by analytical techniques. In these cases, if a detailed description of the response is required, it is more convenient to use a numerical method assumption such as the finite element technique [12].

1.6 BASIC CONSIDERATIONS AND ASSUMPTION

The general topic of the research was the determination of the response of multi-layered media subjected to impact loading. In particular, the effect of impact upon the design of runway ends has been considered. Although the five basic methods of the design of airport paving will be discussed in Chapter 7, it is useful to discuss the basic considerations and assumptions of the problem in this section.

Airport pavements are constructed to provide adequate support for the loads imposed by aircraft. They should provide a firm, stable, and durable surface. Airport pavements are subjected to impact and static loads [13]. The load on the pavement is static and equal to the gross weight of the aircraft when it is standing with the motors dead. This is the heaviest load imposed on the pavement. Tests and observations have disclosed that the gross load transmitted to the pavement is reduced when the plane is standing and the propellers operating at high speed as well as when the plane is taxiing. This may be explained by the aerodynamical forces acting on the wings producing an airborne condition to a certain degree. Since the aircraft is at least partially airborne when taxiing and largely airborne when landing and taking off, the dynamic (moving) and impact loads are less critical than the static loads. Hence, pavements designed for static loads will be adequate for all conditions of loading [13].

The development of different types of aircraft for civil and military use has increased the various landing characteristics to which a runway is subjected and gives rise to impact phenomenon as an important design criterion. The results of a research programme [14], which has been conducted in the United States of America to determine the dynamic properties of soil associated with aircraft loading indicate that current flotation formulae do not predict the observed break up of concrete runways due to impact. Clearly, the impact of runways requires further investigation.

Runways are usually constructed from 2 to 3 layers of asphaltic concrete which rest upon a well compacted soil sub-base. Experimental evidence obtained from the determination of the dynamic properties of asphaltic mixes shows that the response is approximately linear for small strain conditions. Although the stress-strain characteristics of asphaltic concrete are complex and influenced by many factors [2], the assumption of linear behaviour at low stress levels seems reasonable.

The behaviour of the granular material and soil which form the sub-base to the asphaltic layers may also be considered to be linear for small strain of the order of 10^{-3} [15]. This assumption of linearity enables the secant moduli and the damping factors to be considered independently of the strain amplitude [16].

The variation of the contact area and contact force of the impacting object with respect to time will be considered in the analysis. The performance of aircraft during landing has great effect on the direction and magnitude of the impacting force and also must be considered in the analysis.

Plane and axisymmetric conditions have been assumed for the work considered in this thesis.

C H A P T E R 2

THEORETICAL ANALYSIS OF ELASTIC-WAVE PROPAGATION DURING IMPACT

2.1 INTRODUCTION

Theoretical aspects of elastic-wave propagation are well established and have been summarized in texts by Kolsky [17], Ewing, Jardetsky and Press [18], and Desi [19]. In spite of the broad theoretical background, however, it is very difficult to obtain quantitative information in terms of stress magnitudes for real types of impact, real geometries, and combinations of materials with different properties which may occur in practice [5].

In the more specific area of reflection and refraction of stress waves at an interface between two different materials, much of the theoretical work is concerned with the plane strain wave forms caused by a line source [19].

Thus in this chapter, a brief description of some special features related to the propagation of elastic waves in solids is given. Problems involving the response of multi-layered structures subjected to impact which arise from the different types of waves created at interfaces will be briefly discussed. Thus all the basic material which is relevant to the work in this thesis is being reviewed.

2.2 GENERAL WAVE THEORY

The theory of the propagation of elastic waves in solids was developed during the last century by Stokes, Poisson, Rayleigh, Kelvin and others as an extension of the theory of elasticity to the problem of vibrating bodies [18]. Significant recent progress has been made in developing theoretical procedures in elasto-dynamics [19].

In an infinite homogeneous media, waves from a source will propagate at two distinct speeds. Two types of waves can be distinguished namely waves of dilation and waves of distortion. Introduction of a plane surface of the body (half space) gives rise to additional waves with different velocities. The mathematical formulation of all these waves will now be considered.

2.2.1 Waves of Dilation and Distortion in an Isotropic Elastic Medium

The equation of motion for an isotropic elastic medium can be written as follows in cartesian coordinates [5, 19, 17]

$$(\lambda + G) \frac{\partial e}{\partial x} + G \nabla^2 U - \rho \frac{\partial^2 u}{\partial t^2} = 0$$

$$(\lambda + G) \frac{\partial e}{\partial y} + G \nabla^2 V - \rho \frac{\partial^2 v}{\partial t^2} = 0$$

$$(\lambda + G) \frac{\partial e}{\partial z} + G \nabla^2 W - \rho \frac{\partial^2 w}{\partial t^2} = 0 \quad \dots \quad \dots \quad \dots \quad (2.1)$$

The symbol e denotes the volume expansion, and the symbol ∇^2 represents the operator

$$\nabla^2 = \frac{\partial^2}{\partial x^2} + \frac{\partial^2}{\partial y^2} + \frac{\partial^2}{\partial z^2} \quad \dots \quad \dots \quad \dots \quad \dots \quad \dots \quad (2.2)$$

while u , v and w are the displacement in the x , y and z -directions. If the volume expansion e is equal to zero, the following equations result which represent waves of distortion (S-waves) with rotational deformation only.

$$G \nabla^2 U - \rho \frac{\partial^2 u}{\partial t^2} = 0$$

$$G \nabla^2 V - \rho \frac{\partial^2 v}{\partial t^2} = 0$$

$$G \nabla^2 W - \rho \frac{\partial^2 w}{\partial t^2} = 0 \quad \dots \quad \dots \quad \dots \quad \dots \quad \dots \quad \dots \quad (2.3)$$

If on the other hand the rotational deformations

$$\begin{aligned} \omega_x &= \frac{1}{2} \left(\frac{\partial w}{\partial y} - \frac{\partial v}{\partial z} \right) \\ \omega_y &= \frac{1}{2} \left(\frac{\partial u}{\partial z} - \frac{\partial w}{\partial x} \right) \\ \omega_z &= \frac{1}{2} \left(\frac{\partial v}{\partial x} - \frac{\partial u}{\partial y} \right) \quad \dots \quad \dots \quad \dots \quad \dots \quad \dots \quad \dots \quad (2.4) \end{aligned}$$

are suppressed, the equations take the form

$$\begin{aligned} (\lambda + 2 G) \nabla^2 U - \rho \frac{\partial^2 U}{\partial t^2} &= 0 \\ (\lambda + 2 G) \nabla^2 V - \rho \frac{\partial^2 V}{\partial t^2} &= 0 \\ (\lambda + 2 G) \nabla^2 W - \rho \frac{\partial^2 W}{\partial t^2} &= 0 \quad \dots \quad \dots \quad \dots \quad \dots \quad (2.5) \end{aligned}$$

OR

$$(\lambda + 2 \mu) \nabla^2 e - \rho \frac{\partial^2 e}{\partial t^2} = 0 \quad \dots \quad \dots \quad \dots \quad \dots \quad (2.6)$$

Representing irrotational waves or waves of dilation (P-waves).

The above mentioned waves can be superimposed to give a more general case of combined waves in an elastic medium. Both kinds of wave obey the common equation of motion of the the form

$$\frac{\partial^2 \psi}{\partial t^2} = a^2 \nabla^2 \psi \quad \dots \quad \dots \quad \dots \quad \dots \quad \dots \quad \dots \quad (2.7)$$

With the constant $a = c_2 = \sqrt{G/\rho}$ for the case of waves of distortion and $a = c_1 = \sqrt{(\lambda + 2G)/\rho}$ for the case of waves of dilation. With more common notation for the elastic constants

$$C_2 = \sqrt{\frac{E}{2(1 + \gamma)\rho}}$$

$$C_1 = \sqrt{\frac{E(1 - \gamma)}{(1 + \gamma)(1 - 2\gamma)\rho}}$$

and

$$C_2 = C_1 \sqrt{\frac{(1 - 2\gamma)}{2(1 - \gamma)}} \quad \dots \quad \dots \quad \dots \quad \dots \quad \dots \quad (2.8)$$

For $\gamma = 0.25$, $C_2 = C_1/\sqrt{3}$ showing that the rotational waves are slower than the dilation waves.

2.2.2 Surface Waves or Rayleigh Waves in a Half-Space (Single Boundary)

At a great distance from the source the surface waves can be considered to be two-dimensional. The wave generated displacements can generally (with the displacements denoted as u, v, w) be put in the form

$$U_1 = Se^{-ry} \sin(pt - Sx)$$

$$V_1 = -re^{-ry} \cos(pt - Sx)$$

$$W_1 = 0 \quad \dots \quad \dots \quad \dots \quad \dots \quad \dots \quad \dots \quad (2.9)$$

where p , r and s are constants. These equations are assumed to represent waves of dilation. The velocity of these waves is thus $C_3 = p/s$. If the expressions are substituted in Equation (2.5), the following relationship must hold

$$r^2 = s^2 - \frac{\rho p^2}{\lambda + 2G} \quad \dots \quad \dots \quad \dots \quad \dots \quad \dots \quad (2.10)$$

If again the solutions to Equation (2.3) are written as

$$U_2 = A b e^{-by} \sin(pt - Sx)$$

$$V_2 = - A S e^{-by} \cos(pt - Sx)$$

$$W_2 = 0 \quad \dots \quad \dots \quad \dots \quad \dots \quad \dots \quad \dots \quad \dots \quad (2.11)$$

where A is a constant and b a positive number, the following relationships must hold

$$b^2 = s^2 - \frac{\rho p^2}{G}$$

The general wave can then be obtained by superposition

$$U = U_1 + U_2$$

and

$$V = V_1 + V_2$$

Then constants A, h, p, r and s have to be determined. Making use of the fact that the body surface is stress free, it is found that the speed of the surface wave is

$$C_3 = \alpha C_2$$

For $\gamma = 0.25$, α would be 0.9194 and for $\gamma = 0.5$, α would take the value 0.9553. In both cases the velocity is always slightly less than the velocity of waves of distortion propagated through the body.

2.2.3 Plane Waves

By assuming a line source of relatively large length, or by considering only the effects at some distance from the source, the problem can be reduced to a two-dimensional one, where all the waves propagate in a directions parallel to a plane (x z plane), and the motion is therefore independent of the third coordinate (y in this case). By this assumption, the equation of motion are reduced to be

$$(\lambda + 2 G)\nabla^2 e = \rho \frac{\partial^2 e}{\partial t^2} \quad \dots \quad \dots \quad \dots \quad \dots \quad (2.12)$$

$$G \nabla^2 U_y = \rho \ddot{U}_y \quad \dots \quad \dots \quad \dots \quad \dots \quad \dots \quad (2.13)$$

$$G \nabla^2 \Omega = \rho \frac{\partial^2 \Omega_y}{t^2} \quad \dots \quad \dots \quad \dots \quad \dots \quad \dots \quad (2.14)$$

where

$$\nabla^2 = \frac{\partial^2}{\partial x^2} + \frac{\partial^2}{\partial z^2} \quad \dots \quad \dots \quad \dots \quad \dots \quad \dots \quad (2.15)$$

And the general solution for a steady state harmonic motion is [19]

$$U_x = A_p \ell_x f_p + A_{sy} \ell_z f_s$$

$$U_y = A_{sh} f_s$$

$$U_z = A_p \ell_z f_p - A_{sv} \ell_x f_s \quad \dots \quad \dots \quad \dots \quad \dots \quad (2.16)$$

where $\ell_x = \sin\alpha$, $\ell_y = \cos\alpha$ and α is the angle between the direction of propagation of the wave and the z axis.

$$f_p = \text{Exp}\left[\frac{i}{v_p}(v_p t - \ell_x X - \ell_z Z)\right]$$

$$f_s = \text{Exp}\left[\frac{i}{v_s}(v_s t - \ell_x X - \ell_z Z)\right]$$

This shows that in the case of plane waves, which is the case under investigation, the displacement U_y in the y direction is uncoupled from the displacements U_x and U_z in the x and z directions respectively. The first one results only from the propagation of SH waves while the other two are functions of both SV and P waves. Each problem can thus be studied independently [19].

2.2.4 Longitudinal Wave Propagation

As longitudinal waves are simpler to analyze than three-dimensional waves, more has been published on this subject. Also the problem of the measurement of the magnitude of longitudinal disturbances is less difficult, so that more experimental data have been published.

The simplest theory of longitudinal wave propagation in a horizontal column or cylindrical bar is that for a perfectly elastic material, it is assumed that plane cross sections remain plane and that only axial stresses are present. The governing equation can be written as one second-order partial-differential equation for one of the variables and the resulting equation is the well known wave Equation (2.5) mentioned before. The general solution of (2.5) is of the form

$$U = f_1(x - C_0 t) + f_2(x + C_0 t) \quad \dots \quad \dots \quad \dots \quad (2.17)$$

with the constant $C_0 = \sqrt{E/\rho}$

Equation (2.17) represents the sum of two travelling waves, one in positive and one in negative x-direction and their shapes are preserved since dispersion is neglected.

Pochhammer (1876) and Chree (1889), independently studied a bar with a solid circular cross section, infinite in length, of homogeneous linear elastic material and free

from restraint on the lateral surface. The results show that the shape of the pulse will change due to dispersions as it propagates along the rod [11].

The Pochhammer-Chree theory is applicable only to an infinitely long bar in which sinusoidal wave trains of infinite length propagate in either direction. It cannot be used to develop a solution for a finite or even semi-infinite bar. As a result approximate theories have been constructed which contain the essential features of the exact problem in a simplified form.

In Love's approximate theory (1927), the assumption of the elementary theory are used, but terms which take account of the mass acceleration associated with the lateral expansion or contraction are added. An approximate theory which considers the change of lateral dimensions, with the associated shearing strain, has been proposed by Mindlin and Herrmann (1951). Bishop (1952) has given an alternative theory for longitudinal waves [11].

2.3 STRESS WAVE PROPAGATION IN SOIL AND GRANULAR MATERIALS

The transmission of waves in soil is important and is the means by which the propagation of energy arising from impact is distributed. Whatever the source of the disturbance, waves of different types are generated and propagated through the medium and along the surface. Such waves

generally are attenuated as they travel and change in shape and in duration with distance from the source of disturbance. For most engineering purposes, particularly in the design of structures or of cavities in the ground, designers are interested in the maximum particle displacements, velocities, and accelerations in the ground. Consideration must be given to the effect of layering or stratification of the soil and the possible channelling of the transmitted energy in particular strata.

A detailed discussion of stress waves in soils has been presented by Richart, Hall and Woods' [20]. The review by Selig [21] has been thought to be useful and some results have been incorporated in the latter analysis of pavement, Chapter (7). Selig summarized the experimental results of stress wave propagation in constrained bars of sand. These wave propagation tests were designed to permit the study of the inter-relationship between the stress-strain characteristics and wave transmission phenomenon. The testing was limited to dry sand, principally a 20-30 mesh Ottawa Sand. Short duration loads were applied by a 50 pound ram striking against one end of the horizontally positioned, long cylindrical sample of sand confined under constant pressure.

Measurements were made of the impact velocity of the ram, wave propagation velocity and the stress-time relationship at the impact and reaction ends of the specimen. The wave

velocities computed from these tests ranged from 1080 to 1420 feet per second with the majority of the values falling around 1250 f.p.s. A pronounced initial stress peak was developed with the higher impact velocities. This peak was several times the strength of the sand under static loading at the impact and the specimen. This phenomena was attributed to the inertia of sand against lateral expansion and the frictional restraint of the end cap.

In general, especially with lower impact velocities applied to the shorter samples, the impact and stress-time curves dropped to a minimum after the initial peak and then began to increase once more. The second increase in the stress level was thought to be the result of reflection of the pressure waves from the fixed end of the sample. It is suggested that the stress levels which would have been induced in the samples by various impact velocities had no lateral inertia or strain, rate effect and can be represented by the stress level immediately after the peak. These values were seen to increase gradually with an increase in initial impact velocity.

2.4 STRESS WAVE PROPAGATION IN MULTI-LAYERED
HALF-SPACE

The impulsive loading of a multi-layered half-space can be considered as a stress wave propagation problem. It can be assumed that for each layer in a multi-layered half-space, the solution of the one-dimensional amplification problem is of the form [18, 19]:

$$U_{yn} = (A_n e^{-ip_n z_n} + \bar{A}'_n e^{-ip_n z_n}) f_{sn}(x, t) \dots \dots (2.18)$$

with

$$f_{sn}(x, t) = \text{Exp}(i\omega t) \text{Exp}\left(-\frac{i\omega}{v_{sn}} x \sin\alpha_n\right)$$

where A = amplitude of wave travelling up

\bar{A} = amplitude of wave travelling down

$$p = \frac{\omega}{v_s} \cos\alpha$$

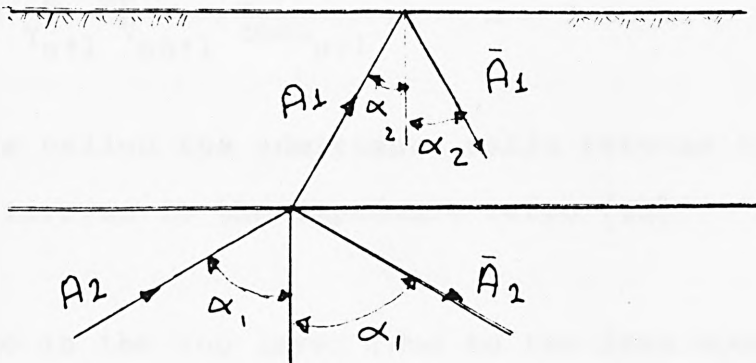


Fig. (2.1) Reflection and refraction of SH wave for layer on half-space.

The compatibility condition at the interface of two layers is

$$f_{s1}(x,t) = f_{s2}(x,t) = \dots f_{sm}(x,t) = f_{sm+1}(x,t) \dots \quad (2.19)$$

OR

$$\frac{\sin\alpha_1}{v_{s1}} = \frac{\sin\alpha_2}{v_{s2}} = \dots \frac{\sin\alpha_m}{v_{sm}} = \frac{\sin\alpha_{m+1}}{v_{sm+1}} \dots \dots \quad (2.20)$$

and

$$A_{n+1} = \frac{1}{2} [A_n(1 + q_n)e^{ip_n h_n} + A'_n(1 - q_n)e^{-ip_n h_n}] \quad (2.21)$$

$$A'_{n+1} = \frac{1}{2} [A_n(1 + q_n)e^{ip_n h_n} - A'_n(1 + q_n)e^{-ip_n h_n}] \quad (2.22)$$

where h_n is the thickness of the nth layer

$$p_n = \omega/v_{sn} \cos\alpha_n, \quad \text{and}$$

$$q_n = \frac{\gamma_n V_{sn} \cos\alpha_n}{\gamma_{n+1} V_{sn+1} \cos\alpha_{n+1}} \quad n = 1 \text{ to } m$$

q_n is called the admittance ratio between two layers and its inverse is the impedance ratio [19].

Since in the top layer (due to the free boundary condition)

$A_1 = A'_1$ and expressing A_1 in terms of A_{SH} , all other amplitudes can then be computed as a function of the

frequency ω for a steady state harmonic motion. The explicit expression for these amplification functions becomes too long even for two layers. However, the numerical computation, proceeding from layer to layer, is simple and is conveniently carried out on a digital computer.

2.5 PREVIOUS WORK

In recent years, the attention of many investigators in civil engineering has been focused on the problem concerning the response of horizontally stratified layers subjected to dynamic forces. In particular, investigators in earthquake engineering have carried out a considerable amount of research [22]. Two methods of solution to these problems are available and these are:

- (1) The analytical methods
- (2) The numerical methods.

2.5.1 Analytical Methods

Most of the analytical studies are generally based on the assumption that each soil layer exhibits "shear-beam" behaviour. It is assumed that stress waves that emanate from the focus of the source are bent by successive refraction and propagation to a near vertical position as they reach the rock surface. Further refractions within the stratified soil produce a shear wave which propagates in an almost vertical direction while the particle displacements occur in a direction perpendicular to the

direction of propagation. This approach in modelling multi-layered soil by means of shear beam has recently been discussed [22].

Idris and Seed [23] have derived a closed-form solution for evaluating the response of soil layers with linearly elastic properties varying in a prescribed manner. Bahar and Ebner [22] developed a transfer matrix method to determine the transfer function governing layered soil amplification. The method is direct and does not require the evaluation of integration constants for the solution of a differential equation governing the motion of each individual layer. Gazetas and Roesset [24] studied the vertical vibrations of a massive, infinitely-long foundation carrying constant-force or rotating-mass type oscillators on the surface of linearly-hysteretic, elastic, layered half-space. A semi-analytical procedure to determine the compliance functions of massless rigid strips has first been presented and the results have been subsequently used to evaluate the response of the massive foundation. The method was based on a direct solution of the wave equations in terms of displacements and accounts for the exact physical conditions at the rough layer interfaces and the soil surface [24]. Extending these studies by Gazetas [25], an analytical numerical formulation presented for a heterogeneous multi-layered soils.

2.5.2 Numerical Methods

In practical situations numerical solutions are the preferred to analytical because of the inherent difficulties of problem description. In the last decade there have been many applications of numerical techniques to stress wave propagation problems [19, 26].

Most numerical techniques are based on the principle of discretization; this can be defined as a procedure in which a complex problem of large extent is divided, or discretized into smaller equivalent units or components.

Alfredo and Others [27, 28] suggested a model for wave motion in axisymmetric solids. The model is composed of discrete elements of lumped masses and springs. The elements in the model are further identified collectively as mass points and stress points. The model was described in the cylindrical-polar and the spherical-polar coordinate systems. It was shown that in both reference systems, the model is mathematically consistent with a finite difference form of the corresponding classical theory of solid continua. Boundary conditions of the model are defined by displacements or derivatives of displacements at the mass points. Boundary conditions can also be defined by specifying externally applied stresses at the boundary stress points.

Costantino et al [29] developed a computer program to treat the response of general two-dimensional continuum problems subjected to dynamic loading caused by a nuclear detonation.

In satisfying the boundary conditions, the equation of motion for fixed nodes are ignored. For partially fixed nodes, equations of motion are derived in the direction in which motion is permitted.

Lysmer and Kuhlmeyer [30, 31], investigated different possibilities of expressing boundary conditions analytically. They found that the most promising way was to express it by the conditions

$$\sigma = a \rho V_p \dot{\omega} \quad \dots \quad \dots \quad \dots \quad \dots \quad (2.23)$$

$$\tau = b \rho V_s \dot{u} \quad \dots \quad \dots \quad \dots \quad \dots \quad \dots \quad \dots \quad \dots \quad (2.24)$$

In which σ and τ are the normal and shear stress respectively, $\dot{\omega}$, \dot{u} are the normal and tangential velocity of s-wave and p-wave respectively. Dimensionless parameters are represented by a and b . The proposed boundary condition corresponds to a situation in which the convex boundary was supported on infinitely small dashpots oriented normal and tangential to the boundary.

A comprehensive study of the finite element discrete parameter model of a continuum for the analysis of transient loading and wave propagation problems has been presented by Shipley, et al [32]. It was observed that the finite element model behaves like low pass filters having definite passing pounds and cut-off frequencies and that the cut-off frequencies depend upon the wave type and finite element mesh. It was noted also that waves propagating through a continuum at frequencies above the cut-off frequency cannot propagate through the finite element mesh associated with the particular cut-off frequency.

Kuhlemeyer and Lysmer [31] presented the results of a study concerning the accuracy of the displacement caused by a single harmonic, one-dimensional elastic wave propagating through a finite element mesh. They found that the basic criteria governing the accuracy was the ratio of the element length in the direction of propagation ℓ , divided by wavelength, λ , as defined $\ell_r = \frac{\ell}{\lambda}$. Results were presented for the four cases of ℓ_r , equal to one-fourth, one-sixth, one-eighth and one-twelfth. From the results it was clear that the high frequency content in transient problems cannot be modeled unless the element dimension is very small. The maximum element dimension should correspond to a value of ℓ_r equal or less than one-fourth when calculated for the highest significant

frequency; ℓ_r would also depend upon the type of mass matrix utilized.

A numerical technique for the analysis of wave motion in layered strata which accounts for the radiation into the far field was presented by Wass [15]. Harmonic waves in plane strain or antiplane shear as well as the axisymmetric waves in a layered stratum were considered. The technique was extended by Kausel [33] to nonaxisymmetric waves in an axisymmetric region of layered strata.

The solutions were obtained in regions of infinite extent on all these developments. Recently, as a further extension of the previous work, Kausel [34] developed a technique for the numerical analysis of wave motion in layered strata. Semidiscrete particular solutions satisfying inhomogeneous boundary conditions were calculated by the finite element method.

CHAPTER 3

DAMPING PHENOMENA IN WAVE PROPAGATION

3.1 INTRODUCTION

The effect of damping is usually considered in the detailed study of the dynamic behaviour of structures subjected to impact. Sometimes, however, its effect may be neglected if the impact is associated with structures having a low natural frequency. This assumption is not usually made in the case of wave propagation in which case information concerning the type and magnitude of damping is required. The effect of damping in dynamic response of pavement constructions was found to be important. Therefore, the study of the damping parameter has been considered.

The action of an impact force on a half-space creates body and Rayleigh waves which decrease in amplitude with increased distance from the point of impact. Material internal damping dissipates the wave energy and in addition further energy is dissipated at the interfaces between material layers.

Although considerable information exist on damping phenomena in general, information is still required on the magnitude of damping at different frequencies and for different materials [5]. For this reason and also for the special characteristics of the problem under

investigation, the damping problem is represented in a particular way. A review of damping phenomena is given in this chapter and in particular those methods which relate to wave propagation are discussed.

The present study deals with the response of runway pavement subjected to impact loading. The idealization of the damping parameter and its mathematical model in case of pavement construction, therefore, has been investigated. The basic assumptions for this mathematical model and the numerical formulation for damping analysis are given.

3.2 TYPES OF DAMPING PHENOMENA

The various types of damping phenomena encountered in materials and structural systems may be generally classified into the four following types [20, 35]:

1. Rate-dependent, recoverable behaviour
2. Rate-dependent, non-recoverable behaviour
3. Rate-independent, recoverable behaviour
4. Rate-independent, non-recoverable behaviour.

The term "recoverable" as used above refers to the "recoverability" of inelastic strain with time, or its reduction to zero, leaving only elastic strain. Figure (3.1.a) illustrates rate-dependent, rate-independent, recoverable and non-recoverable types of inelastic strain.

An important characteristic in the damping relation is the manner in which energy dissipation varies with stress amplitude. Although damping-stress relations are often complex for some mechanisms, nevertheless this relation can be expressed as follows:

$$D = J \sigma_a^n \quad \dots \quad \dots \quad \dots \quad \dots \quad \dots \quad \dots \quad \dots \quad (3.1)$$

where J and n are material constants

- J = damping constant, or the damping energy dissipated at a stress amplitude of unity, and
- n = damping exponent

The shape of various types of idealized curves are illustrated in Figure (3.2).

At low amplitudes of stress the operative mechanisms generally lead to two conditions:

- (a) Damping exponent $n = 2$ (quadratic damping)
- (b) The hysteretic loop is elliptical in form.

The term linear damping is used for this case since these conditions also characterize linear viscosity. Another reason for this usage is that linear differential equations and linear superposition are generally appropriate in analysis. Classification of types of damping phenomena, their characteristics and typical values are given in Figure (3.3, 3.4).

3.3 TYPES OF LINEAR DAMPING

Figure (3.3) illustrates the three types of frequency effects which can be identified in linear materials and processes. These types are given as follows.

Case (a) - Rate Independent Linear Damping

For this case η_s and D_s are all independent of frequency.

Case (b) - Linear Dashpot Damping

This is often identified as conventional linear viscosity or dashpot damping. This is only a special case of linear damping in which $P'' = C(dx/dt)$.

where C = coefficient of viscosity of the linear dashpot.

Case (c) - General Rate-dependent Linear Damping

Many inelastic and visco-elastic materials generally behave in a manner shown in Figure (3.4.c), particularly in the transition region where relaxation phenomena are active.

All three types of behaviours are identified as linear in this project. This is consistent with the definition for linear damping given in Figure (3.4).

3.4 EVALUATION OF MATERIAL DAMPING

Unfortunately in much of the technical literature dealing with damping no distinction is made between (a). The properties of the system used to perform the damping test, (b), the damping properties of the test specimen or number of specimens on which the test is performed, and (c), the unit damping properties of the material itself [35]. Also, because of the variety of viewpoints and units used to designate damping properties, considerable difficulty is generally encountered in collecting, checking, and correlating damping data. It is, therefore, desirable to review the various damping units and expressions in current use and indicate their relationship to the present project.

The main expressions used to define the internal damping of materials are specific damping capacity and coefficient of attenuation. These two functions occur in the literature for evaluating of the internal damping in granular materials and soils [20].

For steady state conditions such as shown in Figure (3.5) the specific damping capacity is given by

$$\Delta C_{CS} = \frac{\Delta E_a}{E_a} \dots \dots \dots \dots \dots \dots \dots \dots \dots \quad (3.2)$$

The term E_a represents the strain energy described by the area under the hysteresis loop. For the condition of decaying vibrations, the relationship between the

logarithmic decrement and the specific damping capacity is

$$\Delta C_{cd} = 1 - \frac{K_{n+1}}{K_n} \text{Exp}(-2\delta) \quad \dots \quad \dots \quad \dots \quad \dots \quad (3.3)$$

in which K_n represents the proportionality factor between strain energy and the square of the displacement amplitude for the n th cycle of decaying vibration. For small values of δ , $\Delta C_s \approx \Delta C_d$ and the ratio of proportionality constants, K_{n+1}/K_n is approximately unity.

The decrease in amplitude of vibration with distance from a source caused by energy losses in soil is designated as "attenuation". This is measured in terms of the coefficient of attenuation and is related to the logarithmic decrement by

$$\delta = \frac{2\pi v \alpha}{\omega} = L \alpha \quad \dots \quad \dots \quad \dots \quad \dots \quad \dots \quad (3.4)$$

in which v is the velocity, ω denotes the circular frequency, and L is the wave length of the propagating wave. Attenuation should be distinguished from geometrical damping which occurs in elastic system because of the spreading out of wave energy from a source.

Internal damping in materials may also be evaluated by measuring the angle by which the strain lags the stress in a sample undergoing sinusoidal excitation. If the material is assumed to be a linear visco-elastic material,

the complex shear modulus G^* is considered to be composed of a real and imaginary component, each of which is a function of frequency, as

$$G^*(\omega) = G_1(\omega) + i G_2(\omega) \quad \dots \quad \dots \quad \dots \quad \dots \quad (3.5)$$

$G_1(\omega)$ is the elastic component and $G_2(\omega)$ is the viscos component. The loss angle SL is defined by

$$\text{Tan SL} = \frac{G_2}{G_1} \quad \dots \quad \dots \quad \dots \quad \dots \quad \dots \quad \dots \quad (3.6)$$

Logarithmic decrement δ is

$$\delta = \pi \tan SL \quad \dots \quad \dots \quad \dots \quad \dots \quad \dots \quad \dots \quad (3.7)$$

Damping in granular materials and soils increases with the amplitude of vibration and therefore, it may be convenient to use different methods for different ranges of amplitude. The use of a complex modulus may be valid for dynamic situations involving large-amplitude vibrations.

Little information exists regarding the damping properties of soil. Grapht and Johnson [36] summarized the results of measuring the damping capacity of mixtures of gravel, sand and silt in a modified triaxial compression apparatus. The soil samples were subjected in the method of testing used to a sinusoidal stress at frequency below that of resonance for the system. The stress-strain curves were recorded. The area of hysteresis loop was measured and

used in determining the damping capacity. The range of values obtained for specific damping capacity by some investigators is presented in Table (1) [20, 36]

TABLE 3.1 - SOME TYPICAL VALUES OF INTERNAL DAMPING IN SOILS [36]

Soil Type	Equivalent D_s
Dry Sand and Gravel	0.03 - 0.07
Dry and Saturated Sand	0.01 - 0.03
Dry Sand	0.03
Dry and Saturated Sand and Gravel	0.05 - 0.06
Clay	0.02 - 0.05
Silty Sand	0.03 - 0.10
Dry Sand	.01 - 0.03

3.5 INTERFACE EFFECTS IN DAMPING ANALYSIS OF STRUCTURES

The effect of the interface in multi-layered structures provides an additional damping mechanism for the propagating wave energy which must be considered in addition to the conventional material damping. The interfaces in pavement construction have different damping characteristics. In general, there are three types of interfaces, can be identified in structures, and are important in damping analysis.

- (a) a dry interface surface
- (b) a lubricated interface surface
- (c) adhesively bonded interfaces

The unjoined interfaces of (a) and (b) above are generally subjected to a wide range of loads and displacements in service. However, only two types of relative motions are generally important in damping analysis and these are:

- (a) a separation of mating surfaces (motion normal to interface)
- (b) interface shear effects (relative motion of mating surfaces in the plane of the interface)

For the case of dry interfaces, Coulomb friction provides an important mechanism for dissipating energy under cyclic shear displacements. Another different case is when the adhesive material has sufficient thickness to permit the relative shear motions between layer surfaces to be absorbed within the adhesive with no relative slip motion. For this case the adhesive layer is a component part of the structure. The stresses, strains and the damping effect of this adhesive layer can be analysed in the same manner as other component parts of the structure.

The above mentioned types of interfaces and their effect must be considered in the design of multi-layered structures subjected to impact loading. They occur

between pavement materials which possess different properties and characteristics. Figure (3.6) is a typical cross-section through the different layers of a flexible pavement. Numerical representation of the effect of interfaces on the response of the structure will be discussed in Chapter (4).

3.6 EXPERIMENTAL MEASUREMENT OF DAMPING

The basic energy-loss mechanisms in practical structures are seldom fully understood; and it is not feasible to determine the damping coefficient by means of the corresponding of generalized damping expressions [35]. For this reason, the damping in most structural systems must be evaluated directly by experimental methods.

In general the properties of a material are determined from the properties of a testing system. Unfortunately, in much of the literature dealing with damping no distinction is made between (a) the properties of the system used to perform damping test, (b) the damping properties of the test specimen or member on which the test is performed, and (c) the unit damping properties of the material itself.

The unit damping properties of the material may be generally determined directly from the properties of the entire specimen. The relationship between material and specimen properties were given by Lazan [35] for a specimen or a member made of macroscopically uniform

materials. Using these relations, the loss coefficient of the specimen (η_s). When the damping exponent is equal to 2 in the damping stress function (Equation (3.1)) η_m is equal to η_s . This case of linear materials has been considered in this research.

The damping coefficient of the structure can be measured by one of the following methods [37, 38]:

- (a) Free-vibration decay
- (b) Resonant amplification
- (c) Half-power (handwidth)
- (d) Impedance testing

Method (C) is the most preferable for establishing the damping coefficient experimentally in this project. This method of evaluating the damping ratio is discussed briefly in Chapter (6).

3.7 NUMERICAL FORMULATIONS FOR DAMPING ANALYSIS

The internal dissipation of energy in soils and granular materials is generally believed to be a hysteretic nature, but the loss of energy due to the propagation of waves is frequency dependent [19]. Both types of damping are present in the multi-layer half-space considered in this project. The continuum may be discretized as an N degree

of freedom system, thus producing equilibrium equations of the form

$$M \ddot{U} + C \dot{U} + K U = R(t) \quad \dots \quad \dots \quad \dots \quad (3.8)$$

where $[M]$, $[C]$ and $[K]$ are the $N \times N$ mass, damping and stiffness matrices respectively, and $\{U\}$ and $\{R(t)\}$ are the corresponding $N \times 1$ displacement and force vectors.

The difficulty in representing a continuum as an N degree of freedom, damped system is the determination of the form of the damping matrix $[C]$.

Linear viscous damping can be mathematically formulated by

$$- \eta \frac{\partial U_x}{\partial t} \quad , \quad - \eta \frac{\partial U_y}{\partial t} \quad , \quad - \eta \frac{\partial U_z}{\partial t}$$

η describes the energy loss and U_x , U_y and U_z are the displacements relative to the boundaries. The energy loss for each element is thus described by

$$\eta[N] \{\dot{q}\}$$

and is introduced into the equilibrium equations. The stiffness formulation then becomes

$$\delta\{q\}^T [K] \{q\} + \delta\{q\}^T [C] \{\dot{q}\} + \delta\{q\}^T [M] \{\ddot{q}\} = \delta\{q\}^T \{Q\}$$

... .. (3.9)

where $[C] = \eta \int_v [N]^T [N] dV$ (3.10)

which means that $[C]$ is proportional to $[M]$.

Alternatively and more reasonably, the damping could be related to the strain rates rather than the rates of displacement. This would give a loss of energy for each element of $[\eta] [\epsilon] \{\dot{q}\}$, in which $[\eta]$ is now a matrix of damping terms that accounts for the different component of strain. When this is introduced into the virtual-work expression it must be related to strains and not displacements. An equation similar to Equation (3.10) results, but $[C]$ is now defined by:

$$[C] = \int_v [\epsilon]^T [\eta] [\epsilon] dV \quad \dots \dots \dots (3.11)$$

This will be similar in form to the stiffness matrix if $[\eta]$ is proportional to the elastic stress-strain relations, $[C]$ will be proportional to $[K]$.

A generalization of these observations is that if $[C]$ can be related to $[M]$ and $[K]$ by.

$$[C] = \sum_r S[K] ([M]^{-1} [K])^r \quad \dots \quad \dots \quad \dots \quad \dots \quad (3.12)$$

Then

$$\beta_i = \sum_r \frac{S}{2} (\omega_i)^{2r+1} \quad \dots \quad \dots \quad \dots \quad \dots \quad \dots \quad \dots \quad (3.13)$$

This means that knowing the variation of β_i with modal frequency, computation of the corresponding $[C]$ can be achieved [19]. While the above procedure for evaluating the damping matrix is correct theoretically, serious numerical difficulties arise which make it impractical when the number of degrees of freedom is large.

A more general method was developed by Wilson and Penzin [39] since:

$$[\Phi]^T [C] [\Phi] = \begin{bmatrix} 2\beta_1 \omega_1 & & & & & & \\ & 2\beta_2 \omega_2 & & & & & \\ & & \dots & & & & \\ & & & 2\beta_i \omega_i & & & \\ & & & \dots & \dots & \dots & \\ & & & & & 2\beta_m \omega_m & \\ & & & & & & \dots \end{bmatrix} \quad \dots \quad (3.14)$$

which can be abbreviated as

$$[\Phi]^T [C] [\Phi] = [2\beta_i \omega_i] \quad \dots \quad \dots \quad \dots \quad \dots \quad \dots \quad (3.15)$$

and since

$$[\Phi]^T [M] [\Phi] = [I] \dots \dots \dots \dots \dots \dots \dots \quad (3.16)$$

it follows that

$$[\Phi]^T [C] [\Phi] = [\Phi]^T [M] [\Phi] [2\beta_i \omega_i] [\Phi]^T [M] [\Phi] \dots \dots \dots \dots \dots \dots \dots \quad (3.17)$$

Therefore

$$[C] = [M] [\Phi] [2\beta_i \omega_i] [\Phi]^T [M] \dots \dots \dots \quad (3.18)$$

The method required the knowledge of the damping ratios for each mode and this proves to be a difficulty. The damping is thus determined element by element rather than mode by mode. Three methods have evolved to evaluate the effects of damping when the damping is known as damping ratio for each element. These are Rayleigh damping, weighted modal damping and the complex formulation [19]. Rayleigh method has been adopted to evaluate the effect of damping in the numerical model and will be discussed in Section (3.8).

3.8 DAMPING IDEALIZATION AND DAMPING MODEL FOR PAVEMENT CONSTRUCTION

Soils and pavement constructions are built up using granular materials. The vibrating part of a pavement thus contains numerous distributed elements with their particular elastic, mass, and loss characteristics which all exert their constant values of M , C and K appears to give a good approximation [40].

In studying damping problems from a phenomenological viewpoint the idealization of properties is an important step. In pavement construction, both viscous and hysteretic damping exist which are dependent on the amount of asphalt in the mix. The published results by Heukelom and Klomb [40] show that the dissipation of energy depends on the velocity of motion. Also, the internal dissipation of energy in soil is generally of a hysteretic nature [19], but the loss of energy due to propagation of wave depends upon the frequency of the waves. The mathematical treatment of dissipation of energy in a flexible pavement as a linearly viscous damping offers close correspondence with the dynamic response of pavements.

An equivalent linearization procedure may also be used to evaluate the response of the granular materials (base and sub-base). The procedure involves the determination of an equivalent modulus G_{eq} and an equivalent viscous damping ratio η_s , for use in the linear elastic solution

[41, 42]. Considering these assumptions, it is vital to assess the most suitable numerical method to represent the damping. There are three numerical methods to represent the damping [19].

(1) The weighted modal damping which has been described by Roesset et al [43] is a method of obtaining the damping ratio β_i for different modes, when the individual elements have different damping ratios. The damping β_i in each element can be composed of a part which is independent of frequency to represent hysteretic effects and another part which is dependent of the frequency ω_j of an element j . This latter part represents viscous or radiation effects. This procedure allows the use of model decomposition and superposition. The method tends to underestimate the correct damping when there is a significant response at frequencies higher than the fundamental frequency. It is an excellent method, however, for cases in which the response is primarily in the lower frequencies [43].

(2) Complex formulation may be used to a particular frequency of impact. For more general input it can be used only in the frequency domain. For a system with both hysteretic and viscous damping, the complex stiffness would become

$$K^* = K(1 + 2i \beta_H + 2i \omega \beta_V) \dots \dots \dots (3.19)$$

where the subscript H and v indicate hysteretic and viscous damping respectively. The complex stiffness is computed by expressing the elastic coefficients in complex form when the system has more than one degree of freedom

$$[D]^* = [D](1 + 2i \beta_H + 2i \omega \beta_v) \quad \dots \quad (3.20)$$

where $[D]$ is the elasticity matrix.

- (3) The most commonly used relationship for expressing the damping phenomena that proposed by Rayleigh [19, 39] in which

$$C = \alpha[M] + \beta[K] \quad \dots \quad (3.21)$$

Figure (3.7) shows that the addition of mass damping and stiffness damping produces , a curve that is reasonably flat over a limited range of frequencies. The main disadvantage is that the damping becomes very large for higher frequencies because of the contribution of the β term. Idris and Seed [42] have extended the formulation by considering the damping to be strain-dependent. The damping value to be used in each element should be based on the strain development in that element.

It is important to use the appropriate method for the numerical representation of damping. The following main points are considered in choosing this method.

(a) The damping characteristics of pavements must be represented as accurately as possible.

(b) The damping properties of the granular materials must be linearized so that their response may be evaluated.

(c) A convenient method of solving the equations of motion must be employed.

The Rayleigh damping formulation was adopted in the current work since it was possible to include the three features mentioned above. Moreover, this form of damping needs no computer storage and no multiplications for a damping matrix. The mathematical formulation is given in Chapter (4) for this method.

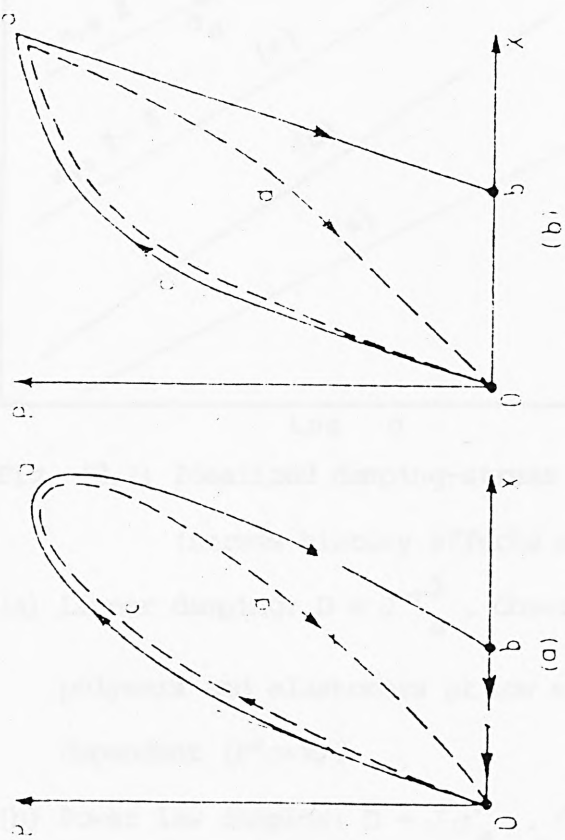


Fig. (3.1) Simplified hysteretic loops to illustrate rate-dependent, rate-independent, recoverable, and non-recoverable types of inelastic strain. O-c-a-d-O is "elastic hysteretic loop".

(a). Rate-dependent loops. (b). Rate-independent loops.

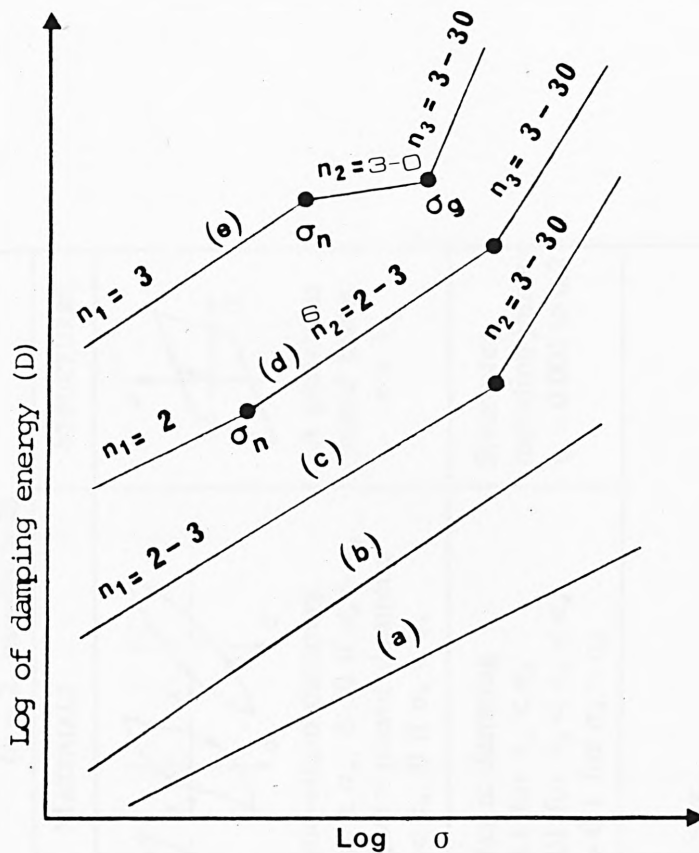
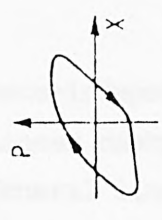
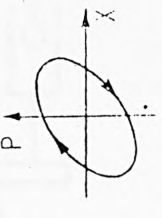
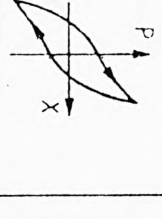
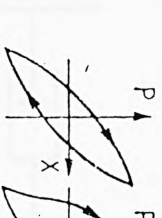


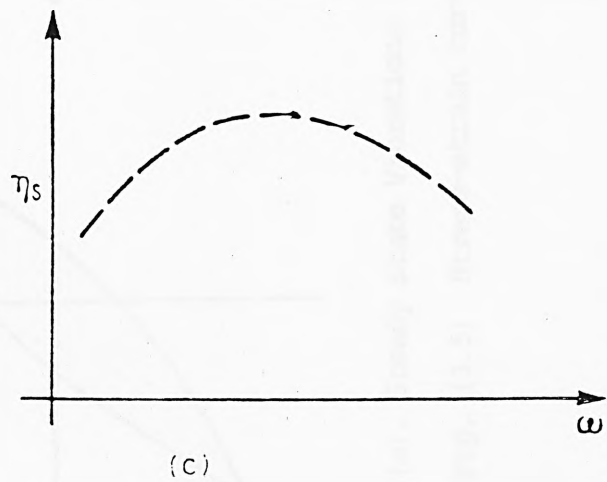
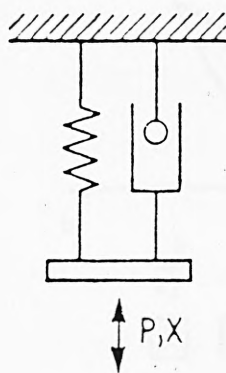
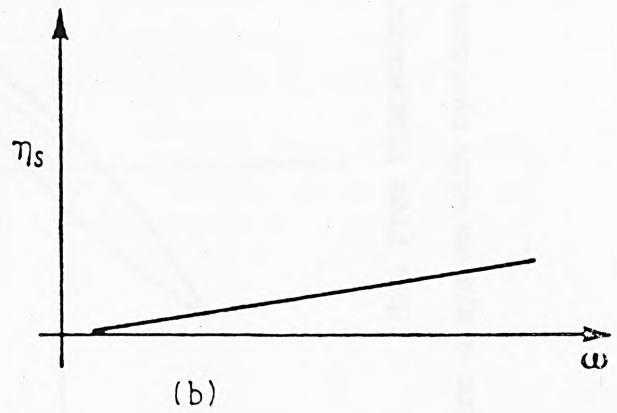
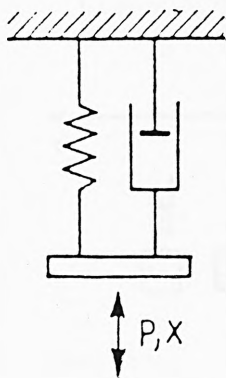
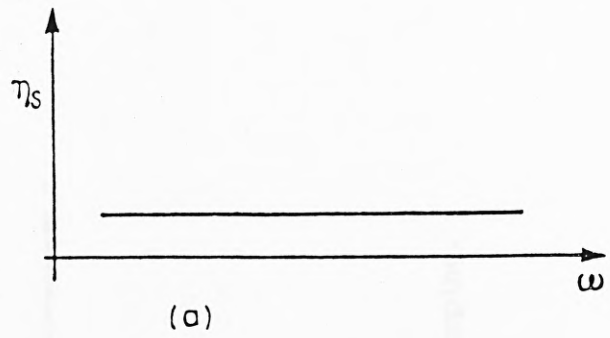
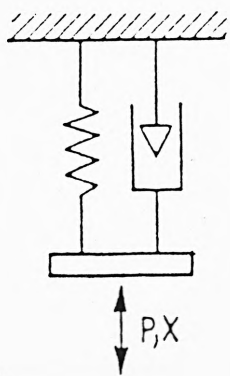
Fig. (3.2) Idealized damping-stress functions
(stress history effects not shown).

- (a) Linear damping: $D = J \frac{\sigma^2}{a}$. Observed in metals, polymers and elastomers at low stress. Usually rate dependent ($P'' \propto \dot{\kappa}$).
- (b) Power law damping: $D = J \frac{\sigma^n}{a}$. Often observed at intermediate stress. May be rate dependent or rate independent.
- (c) Idealized anelastic plastic (two-sequent curve)
- (d) Idealized anelastic plastic (three-sequent curve)
- (e) Idealized magnetoplastic damping.

Non-quadratic damping ($n \neq 2$)		Quadratic damping $n = 2$		Non-quadratic damping ($n \neq 2$, usually > 2)	
				MATERIALS	
<p>Non-quadratic damping ($n \neq 2$)</p>  <p>Loop has many shapes but with rounded ends</p>	<p>FOR LINEAR DAMPING: (a) $n = 2$ (b) Loop is ellipse</p> 			<p>A particular joined beam $n = 3$</p>	<p>Structures including joints. $\eta_s = 0.001$ to 0.2</p>
<p>Increases with increasing stress</p>	<p>Anelasticity $\eta = 0.001$ to 0.1 Viscoelasticity $\eta = 0.1$ to 1.5</p>	<p>Magneto-plastic damping 0.01 to 0.1 for $\sigma_a < \sigma_h$ 0.1 to 0.01 for $\sigma_h < \sigma_a < \sigma_g$ 0.01 to > 0.1 for $\sigma_a > \sigma_g$</p>	<p>Magneto-plastic damping 0.01 to 0.1 for $\sigma_a < \sigma_h$ 0.1 to 0.01 for $\sigma_h < \sigma_a < \sigma_g$ 0.01 to > 0.1 for $\sigma_a > \sigma_g$</p>		
<p>Anelasto-plastic damping. $\eta = 0.001$ to 0.5 if $\sigma_a < \sigma_g$.</p>	<p>$\eta = 0.01$ to > 0.5 if $\sigma_a > \sigma_g$.</p>				

P force, σ_h and σ_g are critical stress and x displacement.

Fig. (3.3) Classification of types of damping

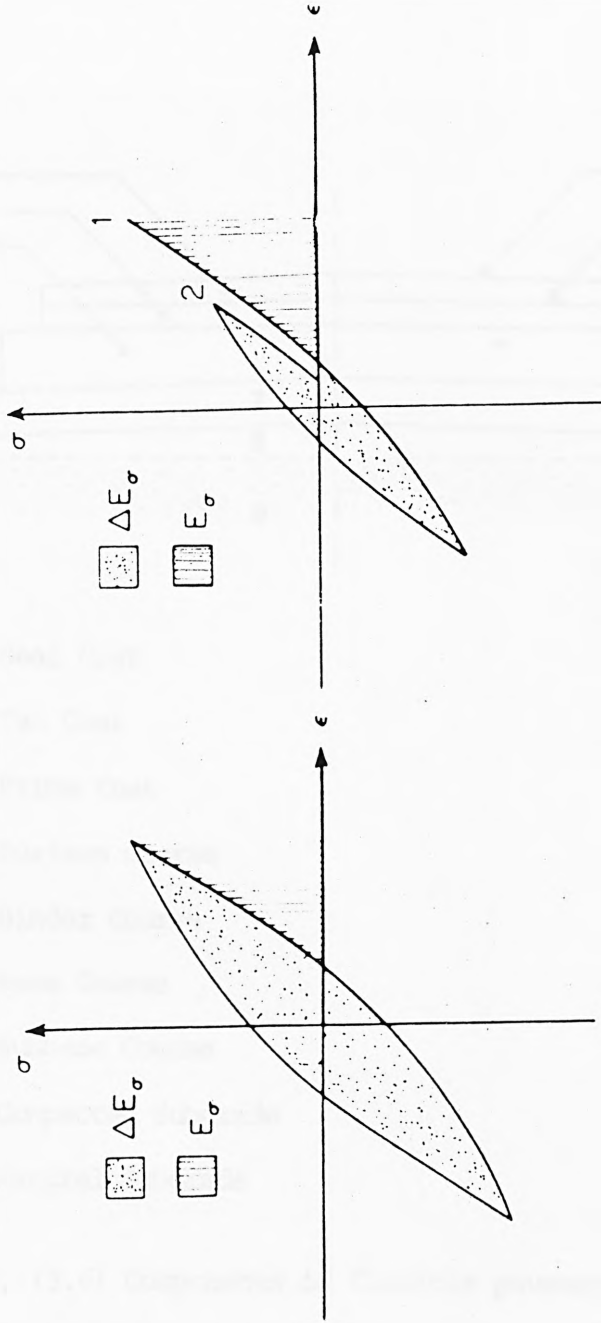


Case (a). Rate-independent linear damping.

Case (b). Linear dashpot damping.

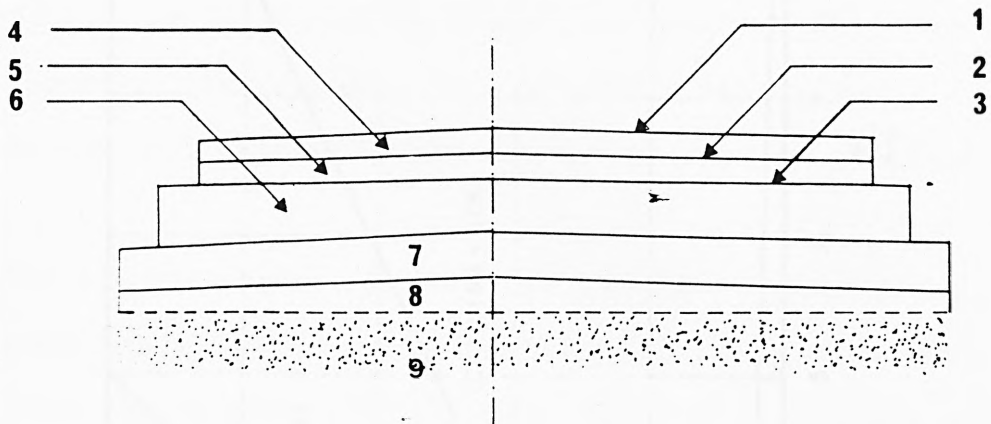
Case (c). General linear damping.

Fig. (3.4) Three classes of linear damping.



(a). Steady State Vibrations. (b). Free Vibrations.

Fig. (3.5) Stress-strain curves for a system with hysteresis damping.



- 1 Seal Coat
- 2 Tac Coat
- 3 Prime Coat
- 4 Surface Course
- 5 Binder Course
- 6 Base Course
- 7 Subbase Course
- 8 Compacted Subgrade
- 9 Natural Subgrade

Fig. (3.6) Components of flexible pavement.

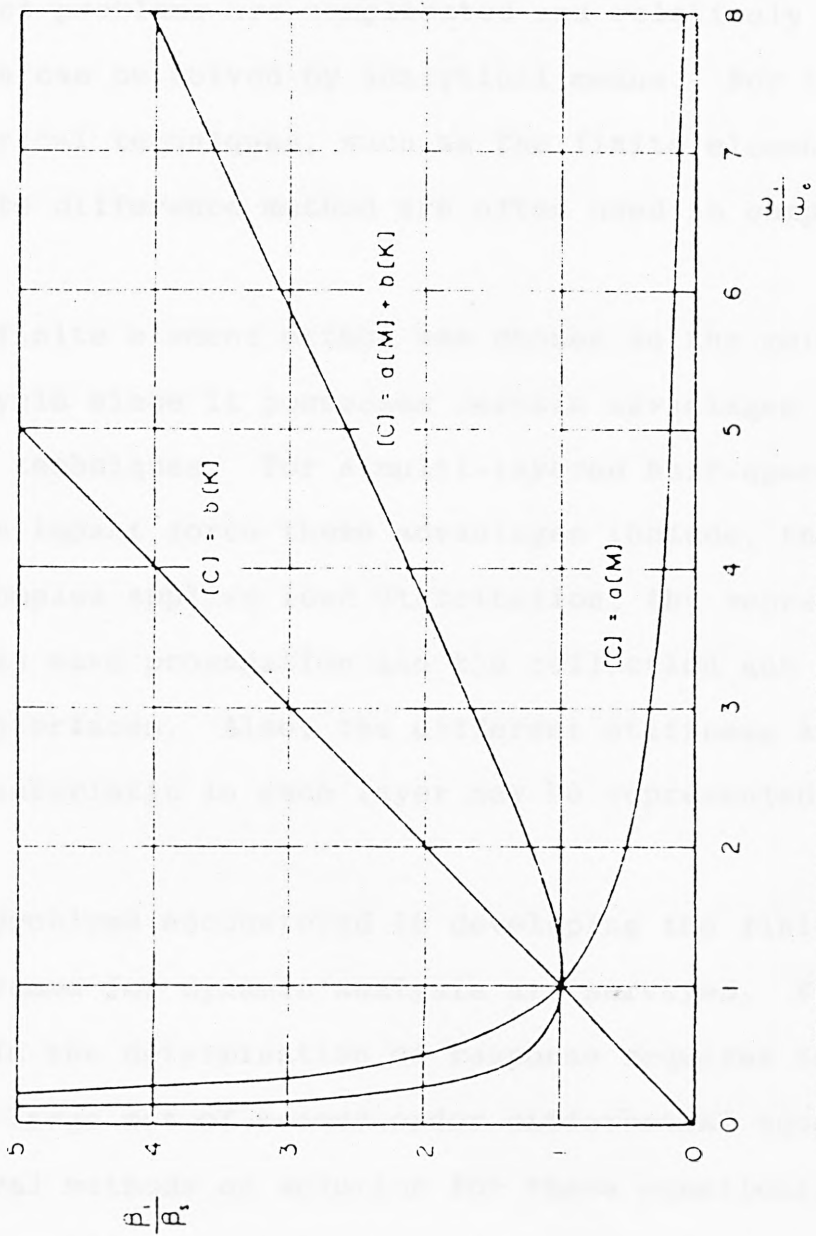


Fig. (3.7) Frequency-dependent damping.

CHAPTER 4

THE FINITE ELEMENT ANALYSIS NUMERICAL MODEL

4.1 INTRODUCTION

Impact problems are complicated and relatively few cases which can be solved by analytical means. For this reason numerical techniques, such as the finite element or the finite difference method are often used in complex cases [5].

The finite element method was chosen as the method of analysis since it possesses certain advantages over alternative techniques. For a multi-layered half-space subjected to an impact force these advantages include, the simulation of complex applied load distribution, the representation of stress wave propagation and the reflection and refraction at interfaces. Also, the different stiffness and damping characteristic in each layer may be represented.

The problems encountered in developing the finite element programme for dynamic analysis are surveyed. For these models the determination of response requires the solution of a large set of second order differential equations. General methods of solution for these equations, including factors affecting accuracy and economy of computation, are discussed. The Wilson- θ -Method has been used as the particular algorithm employed is summarized in Appendix II.

4.2 THE FINITE ELEMENT METHOD

The finite element method is a numerical technique for obtaining approximate solutions to complex boundary value problems. The development of the method in the field of structural mechanics began in the early 1950's with the work of Turner et al [44]. Since then the method has been developed extensively and is now widely used in structural and continuum mechanics. It has been also applied successfully to various other physical problems [45, 46, 47].

A published text by Zienkiewicz [48], describes in detail the application of the finite element method in structural and continuum mechanics. The text also contains an extensive list of references on the subject. The finite element method has been used very successfully in static and dynamic analysis of plane and axisymmetric problems [49, 50, 51]. It has also been applied to quasi-static and dynamic analysis of viscoelastic continua with considerable success.

Since the finite element method is well established only the principal steps involved in the particular application of the method to the analysis of impact problems and stress propagation in multi-layered media are summarized.

4.3 DISCRETIZATION OF "INFINITE" MEDIA AND MESH DESIGN

Applications of the finite element method to structures having well defined geometric and boundary conditions can be straightforward insofar as their subdivision and introduction of the boundary conditions are concerned. The situation in a multi-layered half-space, however, involves "infinite" media and the boundary conditions are not exactly defined.

Besides determining the significant zones to be included in the mesh, it is also necessary to arrive at elastic boundary conditions. The former is possible since the influence of the perturbations such as applied loads and potential diminish with increasing distance from the points of their applications. The significant distance of the boundaries are usually determined by trial-and-error procedures in which the boundary distances from the impact zone are varied and the resultant effects on the numerical solutions are examined.

Criteria for determination of discretized boundaries for stress-deformation problems are covered by many texts [19, 44, 48, 49]. Stress wave propagation problems represent a special case and were discussed in Chapter 2.

The finite element mesh design must produce accurate results and be computationally efficient. The internal geometry, e.g, zoning, layering, discontinuities and interfaces, are introduced, and planes of symmetry are sought. At this point the system is ready to be divided into finite elements. In general the smaller the element the more accurate the solution.

4.4 MATHEMATICAL FORMULATIONS

4.4.1 Linearly Elastic, Undamped Formulation

The equation of dynamic equilibrium for a linearly elastic, undamped continuous body are

$$\frac{\partial \sigma_{xx}}{\partial x} + \frac{\partial \sigma_{xy}}{\partial y} + \frac{\partial \sigma_{xz}}{\partial z} = \rho \frac{\partial^2 U_x}{\partial t^2} + P_x(t)$$

$$\frac{\partial \sigma_{xy}}{\partial x} + \frac{\partial \sigma_{yy}}{\partial y} + \frac{\partial \sigma_{yz}}{\partial z} = \rho \frac{\partial^2 U_y}{\partial t^2} + P_y(t)$$

$$\frac{\partial \sigma_{xz}}{\partial x} + \frac{\partial \sigma_{yz}}{\partial y} + \frac{\partial \sigma_{zz}}{\partial z} = \rho \frac{\partial^2 U_z}{\partial t^2} + P_z(t) \dots \dots \dots (4.1)$$

The right hand sides of these equations include both the products of mass density (ρ) and the corresponding accelerations and arbitrary, time-dependent forcing functions (p_x, p_y, p_z).

Many techniques can be used to obtain finite element formulations from Equations (4.1). The most straightforward is as follows.

First, the terms involving the product of the mass and acceleration are replaced by equivalent body forces as opposite sense, called d' Alembert forces

$$\begin{aligned}
 f_x &= -\rho \frac{\partial^2 u_x}{\partial t^2} \\
 f_y &= -\rho \frac{\partial^2 u_y}{\partial t^2} \\
 f_z &= -\rho \frac{\partial^2 u_z}{\partial t^2} \quad \dots \quad \dots \quad \dots \quad \dots \quad \dots \quad \dots \quad (4.2)
 \end{aligned}$$

where U_x , U_y and U_z are components of displacements in the x, y and z directions, respectively.

Then the equilibrium at a given instant of time must require satisfaction of the principle of virtual work.

$$\int_V \sigma_{ij} \delta E_{ij} dV = \int_V f_i \delta U_i dV + \int_V P_i \delta U_i dV + \int_S \bar{T}_i \delta U_i dS \quad \dots \quad \dots \quad \dots \quad \dots \quad \dots \quad (4.3)$$

where \bar{T}_i is the prescribed traction over the surface. If the interpolation functions are the same for displacement, velocity, and acceleration, then

$$\{U\} = [N] \{q\} \quad \dots \quad \dots \quad \dots \quad \dots \quad \dots \quad \dots \quad (4.4)$$

$$\{\dot{U}\} = [N] \{\dot{q}\} \quad \dots \quad \dots \quad \dots \quad \dots \quad \dots \quad \dots \quad (4.5)$$

$$\{\ddot{U}\} = [N] \{\ddot{q}\} \quad \dots \quad \dots \quad \dots \quad \dots \quad \dots \quad \dots \quad (4.6)$$

where $\{U\}$ = vector of displacement at point

$\{q\}$ = vector of nodal displacements

$[N]$ = matrix of interpolation functions

and the dots indicate differentiation with respect to time.

Substitution of these expressions into Equation (4.3)

together with the usual algebraic and variational operations leads to

$$\begin{aligned} \delta\{q\}^T [K] \{q\} = & - \delta\{q\}^T \left(\int_V \rho [N]^T [N] dV \right) \{\ddot{q}\} \\ & + \delta\{q\}^T \left(\int_V [N]^T \{P\} dV + \int_S [N]^T \{\bar{T}\} dS \right) \\ & \dots \quad \dots \quad \dots \quad \dots \quad \dots \quad \dots \quad (4.7) \end{aligned}$$

The first expression on the right hand side describes the inertial part of the system. It can be written in terms of the mass matrix $[m]$ as

$$- \delta\{q\}^T [m] \{\ddot{q}\}$$

The mass matrix for one element is

$$[m] = \int_V \rho [N]^T [N] dV \quad \dots \quad \dots \quad \dots \quad \dots \quad \dots \quad (4.8)$$

This is called the consistent mass matrix because its derivation is consistent with that of the stiffness matrix. An alternative approach is to assume that the mass is concentrated at the nodes, leading to a lumped mass matrix. "Roesset" [52] has demonstrated that for one-dimensional cases, the lumped mass matrix underestimates the resonant frequencies of the system and the consistent mass matrix overestimates them by nearly the same amount. Therefore, the most satisfactory procedure from the point of view of numerical accuracy is to use a mass matrix combining the lumped and consistent formulation in equal or nearly equal proportions.

The remaining terms on the right hand side of Equation (4.7) represent the contribution of externally applied loads. These can be combined in a nodal load vector $\{Q\}$, giving a term $\delta\{q\}^T \{Q\}$. The terms for all elements are added node by node in the usual manner of assembling finite element global equations. If $\{U\}$ is the global nodal displacements vector, $\{R\}$ the global nodal external load vector, $[K]$ the summation of the element $[k^*]$ matrices and $[M]$ the summation of the element $[m]$ matrices then

$$\delta\{U\}^T [K] \{U\} = - \delta\{U\}^T [M] [\ddot{U}] + \delta\{U\}^T \{R\} \dots \quad (4.9)$$

The vectors $\{U\}$, $\{\ddot{U}\}$ and $\{R\}$ are functions of time, but at any instant the principals of virtual work and equilibrium requires that the variation vanish.

Thus

$$[K] \{U\} + [M] \{\ddot{U}\} = \{R\} \quad \dots \quad \dots \quad \dots \quad \dots \quad (4.10)$$

This is the basic finite element formulation of the dynamic problems for linearly elastic undamped materials.

4.4.2 Formualtion of Damping Properties

The complete equations of motion for a discrete body or structure should include a term to account for energy dissipation. This problem has been discussed in Chapter 3, where it has been mentioned thus, that damping is linearly proportional to the velocity. Hence the equations of motion for the damped system are

$$[M] \{\ddot{U}\} + [C] \{\dot{U}\} + [K] \{U\} = \{R(t)\} \quad \dots \quad (4.11)$$

where $[C]$ is the damping matrix of the assemblage of elements.

There are a number of numerical methods for evaluating the $[C]$ matrix which have been considered in Chapter 3. From this discussion it has been shown that the method originally proposed by Rayleigh is particularly suitable [39, 41]. Therefore, the damping matrix $[C]$ can be assumed of the form

$$[C] = \alpha [M] + \beta [K] \quad \dots \quad \dots \quad \dots \quad \dots \quad (4.12)$$

Here α and β are proportionality constants which relate damping to the velocity of the nodes and the strain velocities, respectively. Most of the experimental data on damping properties of structures consist of modal damping ratios, that is, ratios of actual damping to critical damping for particular natural nodes of vibration. Therefore, it is useful if values of α and β in Equation (4.12) can be assigned from known values of modal damping. For this, the following relation between α and β and the damping ratio for the i th mode C_i are defined

$$C_i = \frac{\alpha}{2\omega_i} + \frac{\beta\omega_i}{2} \quad \dots \quad \dots \quad \dots \quad \dots \quad \dots \quad \dots \quad (4.13)$$

where ω_i is the natural frequency of the i th mode.

It has been found [41, 43, 53] that the use of a constant damping value for a multi-layered structure or the use of an overall weighted average can lead to inaccurate results. Accordingly, an analytical procedure that permits the use of different damping ratio for each individual element has been formulated. This formulation is also based on utilizing the Rayleigh damping expression, but instead of using Equation (4.12) for the entire system, the following relationship is used for each element q .

$$[\bar{c}]_q = \alpha_q [m]_q + \beta_q [k]_q \quad \dots \quad \dots \quad \dots \quad \dots \quad \dots \quad (4.14)$$

In which $[c]_q$, $[m]_q$, and $[k]_q$ are the damping, mass and stiffness submatrices respectively for element q and α_q and β_q

are parameters that are functions of the damping characteristics of element q. The parameters α_q and β_q are given by

$$\alpha_q = \lambda_q \omega_0 \dots \dots \dots \dots \dots \dots \dots \dots \dots \dots \quad (4.15)$$

$$\beta_q = \lambda_q / \omega_0 \dots \dots \dots \dots \dots \dots \dots \dots \dots \dots \quad (4.16)$$

The value of λ_q , which represents the damping ratio of element q depend upon the properties of the material of element q. The parameter ω_0 is equal to the fundamental frequency of the system and is obtained from the solution of the equation

$$[K] \{\phi^n\} = \omega_n^2 [M] \{\phi^n\} \dots \dots \dots \dots \dots \dots \dots \dots \quad (4.17)$$

For $n = 1$ this Equation (4.17) represents the eigen value problem from which the mode shapes and frequencies are determined [41]. It was found that the vibration frequencies, ω_i^2 and the corresponding mode shape vectors are required for solution of damping problems. It is the purpose of the next section to describe the solution procedures used to solve the eigenvalue problems of interest in order to obtain the vibration frequencies ω_i^2 .

4.5 SOLUTION OF EIGENVALUE PROBLEMS

It was stated in Section 4.4 that it is necessary to solve the eigenproblem and to obtain the eigenvalue $\lambda_1 \dots \lambda_n$ and the corresponding eigenvectors $\phi_1 \dots \phi_n$

$$K \phi = \lambda M \phi \quad \dots \quad \dots \quad \dots \quad \dots \quad \dots \quad \dots \quad (4.18)$$

A variety of eigensystem solution methods have been developed and are reported in the literature [44], [54], [55]. Most of the techniques have been devised for rather general matrices. The solution of the specific eigenproblem summarized above has been considered. The matrices have specific properties such as being banded and positive definite. The eigensystem solution algorithms should take advantage of these properties in order to make a more economical solution possible. The vector iteration method, in which the basic property used is that

$$[K] \{\phi_i\} = \{\lambda\} [M] \{\phi_i\} \quad \dots \quad \dots \quad \dots \quad \dots \quad (4.19)$$

The effectiveness of a solution method depends largely on two factors, firstly, the possibility of a reliable use of the procedure and secondly, the cost of solution. However, the real justification for using vector iteration derives from the fact that they did work and can be used economically by using the same solution algorithm for the equations

$$[K] \{U\} = \{R\} \quad \dots \quad \dots \quad \dots \quad \dots \quad \dots \quad \dots \quad (4.20)$$

Two techniques of vector iterations are used and these are the inverse and the forward iteration methods. A summary of the two techniques and the particular algorithms are given in Appendix II.

4.6 DYNAMIC ANALYSIS OF LAYERED SEMI-INFINITE MEDIA

For the analysis of multi-layered media Youder stated [2]:

- (1) The material properties of each layer are homogeneous
- (2) Each layer has a finite thickness, except for the lower layer and all are infinite in the lateral directions
- (3) Each layer is isotropic
- (4) Full friction is developed between layers at each interface.

These items are the basic importance assumptions in most theoretical procedures [3, 4]. However, the dynamic solution presented in this thesis assume all of the conditions previously mentioned. Moreover, it is necessary to consider not only the component materials of each layer and its effect on the reflection and refraction of stress wave, but also the energy dissipation caused by joint interface. The method of analysis developed in this project takes into account these factors.

Figure (7.8) shows the cross section of a typical plane problem in which the geometry, material properties and the external loads do not change in the direction

perpendicular to the cross section. The structure consist of horizontal layers which for pavements consist of the sub-base, base and mating surface. These three layers are constructed over a sub-grade. The particular characteristic of the multi-layered structure is the interfaces between layers figure (3.6).

4.6.1 Treatment of the Effect of a Wave Impinging upon an Interface

When a body wave travelling in an elastic medium encounters an interface with another elastic medium, some of the incident-wave energy will be reflected into the first medium and some energy will be transmitted into the second medium. Using the same approach as Sinitsyn [56] and Clough and Penzein [37], the dynamical conditions for the nodes on the interface boundary can be written in the form

$$M \ddot{U} + C \dot{U} + K U = \sigma_a + \sigma_b \dots \dots \dots \dots \quad (4.21)$$

where σ_a stress in incident wave
 σ_b stress in reflected wave

A continuity and equilibrium are imposed at the node of the interface and these are

$$U_1 = U_2$$

$$U_a + U_b = U_c \dots \dots \dots \dots \dots \dots \dots \dots \quad (4.22)$$

for the displacement, and

$$R_1 = R_2$$

$$R_a + R_b = R_c \quad \dots \quad \dots \quad \dots \quad \dots \quad \dots \quad (4.23)$$

for the forces

These conditions must be satisfied at all times. The time derivatives of the displacement conditions must be also satisfied, i.e.,

$$\frac{\partial U_a}{\partial t} + \frac{\partial U_b}{\partial t} = \frac{\partial U_c}{\partial t} \quad \dots \quad \dots \quad \dots \quad \dots \quad \dots \quad (4.24)$$

From which it is evident that the time and position derivatives are related by the velocity of wave propagation.

$$\frac{\partial U_o}{\partial t} = - C_1 \frac{\partial U_o}{\partial x} \quad \dots \quad \dots \quad \dots \quad \dots \quad \dots \quad (4.25)$$

Similar analysis for the reflected and refracted waves result in

$$\frac{\partial U_b}{\partial t} = + C_1 \frac{\partial U_b}{\partial x} \quad \dots \quad \dots \quad \dots \quad \dots \quad \dots \quad (4.26)$$

$$\frac{\partial U_c}{\partial t} = - C_2 \frac{\partial U_c}{\partial x} \quad \dots \quad \dots \quad \dots \quad \dots \quad \dots \quad (4.27)$$

where the positive sign in (4.26) is due to the negative direction of the reflected wave propagation using (4.25, 4.27) in (4.24) yields

$$- C_1 \frac{\partial U_a}{\partial x} + C_1 \frac{\partial U_b}{\partial x} = - C_2 \frac{\partial U_c}{\partial x} \dots \dots \dots \dots \quad (4.28)$$

but the strains $\frac{\partial U_a}{\partial x} = \epsilon_a$ can be expressed in terms of the forces acting at the node

$$\epsilon_a = \frac{\sigma_a}{E_1} = \frac{R_a}{A_1 E_1} \dots \dots \dots \dots \dots \dots \quad (4.29)$$

hence the compatibility condition of Equation (4.28) can be expressed in terms of force waves

$$- \frac{C_1}{A_1 E_1} R_a + \frac{C_1}{A_1 E_1} R_b = - \frac{C_2}{A_2 E_2} R_c \dots \dots \dots \quad (4.30)$$

i — e

$$R_c = Z(R_a - R_b) \dots \dots \dots \dots \dots \dots \quad (4.31)$$

where

$$Z = \frac{C_1}{C_2} \frac{A_2 E_2}{A_1 E_1} = \sqrt{\frac{m_2 E_2 A_2}{m_1 E_1 A_1}} \dots \dots \dots \dots \quad (4.32)$$

For special case of this project

$$Z = \sqrt{\frac{\rho_2 E_2}{\rho_1 E_1}} \dots \dots \dots \dots \dots \dots \quad (4.33)$$

Equation (4.31) can be introduced in the force equilibrium condition to express the refracted and reflected waves in terms of the incident wave

$$R_b = R_a \frac{Z-1}{Z+1} \quad \dots \quad \dots \quad \dots \quad \dots \quad \dots \quad \dots \quad (4.34)$$

$$R_c = R_a \frac{2Z}{Z+1} \quad \dots \quad \dots \quad \dots \quad \dots \quad \dots \quad \dots \quad (4.35)$$

Similar equations for the displacements

$$U_b = - U_a \frac{Z-1}{Z+1} \quad \dots \quad \dots \quad \dots \quad \dots \quad \dots \quad \dots \quad (4.36)$$

$$U_c = U_a \frac{2Z}{Z+1} \quad \dots \quad \dots \quad \dots \quad \dots \quad \dots \quad \dots \quad (4.37)$$

The factor Z defines the character of discontinuity between two different materials and controls the relative amplitudes of the reflected and refracted waves.

4.6.2 The Scheme for Numerical Analysis of Reflected, Refracted and Transmitted Waves

Numerical evaluation of stress wave propagation at an interface is conducted according to the theoretical considerations presented in (4.6.1). The scheme which is summarized in the following steps includes the load transfer method of Zeinkiewicz and Valliappan [57, 58, 59]

- (1) Solve the problem for the first increment of time Δt
- (2) Calculate \ddot{U} , \dot{U} , U after first increment of time
- (3) Read the elements and nodes of interface
- (4) Calculate the nodal forces

$$R_a = \int_v B^T \sigma dV$$

- (5) Calculate $R_b = R_a \frac{Z-1}{Z+1}$
- (6) Solve to obtain \ddot{U} , \dot{U} , U using these two forces
- (7) Add the effect of R_b by superposition, hence obtaining the final \ddot{U} , \dot{U} , U in which the effect of reflection and refraction is added
- (8) Repeat the calculation for each increment of time

This method of evaluation can be developed to include three kinds of interface. The method proposed appears to present few computational difficulties and resolves important questions regarding the behaviour of multi-layered structures.

4.7 SOLUTION OF THE EQUILIBRIUM EQUATIONS FOR THE DYNAMIC FINITE ELEMENT SYSTEM

In Section (4.4), the equations of equilibrium for a finite element system in motion are

$$[M] \{\ddot{U}\} + [C] \{\dot{U}\} + [K] \{U\} = \{R(t)\} \quad \dots \quad (4.38)$$

where M, C and K are the mass, damping and stiffness matrices; R(t) is the external load vector and U, \dot{U} , \ddot{U} are the displacement, velocity and acceleration vectors of the finite element assemblage.

Mathematically, Equation (4.38) represents a system of linear differential equations of second order and in principle the solution to the equation can be obtained by standard procedures for the solution of differential equations with constant coefficients [60]. However, the procedures proposed for the solution of general systems of differential equations can become very computationally inefficient if the order of the matrices is large, unless specific advantage is taken of the special characteristics of the coefficient matrices K, C and M [44, 46, 48, 49].

The procedures of solution are divided into two methods and these are the direct integration and mode superposition methods; Bathe and Wilson [44] have stated. Although the two techniques may at first sight appear to be quite

different, in fact, they are closely related and the choice for one method or the other is determined only by their numerical effectiveness.

The advantages of mode superposition are essentially, that frequencies and mode shapes are obtained and that a variety of response history and response spectrum analysis can be carried out with relatively small additional cost. Also, if the structure is slightly changed or more eigenvalues and vectors are required, i.e, the frequency domain to be considered can be extended, the eigensystem which has been already solved can be used to reduce the cost of the new eigensystem solution [44].

The direct step-by-step integration, however, is more effective, when many modes need be included in the analysis and the response is required over relatively few time steps, such as shock and impact problems.

CHAPTER 5

PROGRAM DESCRIPTION AND NUMERICAL EXAMPLES

5.1 INTRODUCTION

This chapter describes the main features of the computer program which has been developed during the course of the research work. The implementation of the ideas discussed in the previous chapters are represented in the program which has been compiled on a Honeywell computer and written in the Fortran IV language. The computer program represents the effective numerical model of the half-space and may be used to study the dynamic response and also important features such as the damping, reflection and refraction of stress waves.

It is particularly suitable for the analysis of multi-layered half-space subjected to an impact force. Although the program incorporates facilities for the analysis of the response to impulsive loading, other types of loading can be accommodated.

The following sections will describe in brief the various subroutines and the structure and organization of the main program. Information concerning the preparation of data and listing of the program is presented in Appendix (I).

In order to check the developed program, a number of dynamic problems have been solved and compared with published results. It should be noted that imperial units have been used in some examples instead of SI system to conform with published results.

5.2 BRIEF DESCRIPTION

The basic theoretical steps of the finite element procedure can be separated into several distinct phases. Each phase consists of a number of theoretical operations which are performed in separate subroutines. Figure 5.1 shows the main structure of the program together with the six primary subroutines. The order of calling the primary subroutines is controlled by a main or master segment. The function of each subroutine is described in the remainder of this section.

The solution of the equation of motion, Equation (4.1), was obtained by direct integration using the Wilson- θ -method. The algorithm which has been used for this method is summarized in Appendix II. It should be noted from Chapter 3 that Rayleigh damping within the half-space has been assumed. This form of damping is easily taken account of in the analysis, because no storage and no multiplications of a damping matrix are required to obtain the frequencies and vibration mode shapes. Solution routines are used which calculate the required eigen value and eigen vectors directly without a transformation of the structure stiffness matrix and mass matrix to a reduced form.

The program is based on the finite element displacement method. Parabolic plane isoparametric elements have been used for the analysis [61]. The method of solving the modified simultaneous equations is by a Gaussian Forward Elimination Technique which has the advantage of the banded form of the reduced stiffness matrix. The solution of the equation of motion in the first incremental of time is carried out by the subroutines SOLVE and BSUB. To complete the solution, the reduced form of equations are operated on by RESOLVE and BSUB which is of economic importance.

Although the program is not a general purpose computer program, additional options and new elements can easily be added. The analyses which are available are as follows:

1. Static analysis
2. Frequency calculation
3. Response history analysis by direct integration.

5.3 PROGRAM STRUCTURE

The structure of the program is shown in Figure (5.1). The primary subroutines or modules are described in relation to their general functions as follows

A INPUT MODULE

This is the first module entered and is controlled by the subroutine GDATA. it handles input data defining the geometry, boundaries and material properties. Some data is processed into a form compatible with later program requirements, and other constant data, such as Gaussian integration constants, are set up.

B STIF and MASS MODULE

This is the second module entered and organises the stiffness and mass calculations on the concept of numerical integration. Control of this phase is held within subroutine STIFM.

Evaluation of stiffness is made according to the stress state prevailing in the elements at the time of calculation. Stiffnesses are sorted with element identification on disc and ordered in the sequence required for assembly and solution.

This module also organises the calculation of lumped or consistent mass matrices and stored on disc and ordered in the same way as stiffness matrices.

A flow diagram of the program organisation for the calculation of the structure stiffness matrix and mass matrix is shown in Figure (5.2) . With the matrices stored in block form on tape either a static or a dynamic analysis can be carried out.

C LDATA MODULE

The flow of operations through this phase is governed by subroutine LDATA, It organises the calculation of nodal forces in case of static analysis. In case of a dynamic analysis, it organises the calculation of the modified effective load vector. Also, for frequency calculation it organises the calculation of modified vector of $[M] \{x\}$ for each iteration.

D SOLUTION MODULE

This module consists of the three subroutines SOLVE, RESOLVE AND BSUB[62 , 63] . The general purpose of this module is to assemble, reduce and solve the governing set of simultaneous equations

This module is controlled by the master segment because the flow of operations is dependent on the solution algorithm. If the new set of stiffness terms have been evaluated, SOLVE and BSUB is used to obtain the solution, whereas if there is only a new set of forces, RESOLVE and BSUB obtains the solution by using the reduced form of equations started during the previous entry into solve.

E STRESS MODULE

This module is controlled by the subroutine stress. It organises the calculation of incremental strains which are used in the evaluation of total stress and total strain. Computation and determination of the equivalent

nodal forces due to the total stresses are calculated by subroutine B-stress. All values of stress and strain are transferred to disc files for later use in output. This module is entered after every increment of time (in case of dynamic analysis) after calculation of node displacements in LDATA. Figure (5.1) shows the subroutines associated with this module.

OUTPUT MODULE

This phase represents the output of the results. Although there are no separate subroutines employed to output the results by using the subroutine GRAPH, results may be plotted automatically. Where a general purpose graphics package is available, such programs for output representation especially for dynamic problems are important to be devised.

5.4 NUMERICAL EXAMPLES

In the following, results of number of dynamic problems are represented and compared with the published results. Also problems of elastic waves propagation, for which its exact solutions are available, are considered. Numerical solution for these problems are calculated by means of the dynamic finite element program. The numerical results are compared either with exact or numerical published solution followed by remarks and discussion. According to the results obtained, a brief evaluation of finite element method accuracy for wave propagation problems is obtained

5.4.1 Cantilever Beam with Uniform Load

The linear response of a cantilever beam subjected to uniform pressure has been computed. The cantilever dimensions and material properties are given in Figure (5.3) . The finite element model of the cantilever is shown in Figure (5.3b) . Five (8-node) plane stress elements were used along the length with 2 x 2 Gauss integration points. A lumped and consistent mass idealization was used for the dynamic analysis. The computed dynamic response of the cantilever subjected to a step load is shown in Figure (5.4,6) . The computations were carried out using two different time steps, namely $\Delta t_1 = 45 \mu\text{secs}$ ($\sim T_0/120$) and $\Delta t_2 = 135 \mu\text{secs}$ ($\sim T_0/40$), where T_0 is the fundamental period of the cantilever. The results obtained for the linear analysis were compared with this in references [46 , 64] . It can be seen from Figure (5.4) that good agreement has been achieved.

5.4.2 Damping Effect

To check the accuracy of the program, the eigen-problem of the cantilever beam example has been solved. The natural frequency was found to be 1089.3638 radians per second which is very close to that published in reference [64] . Adopting Rayleigh damping, the constant α and β are calculated.

$$\alpha = \omega_1 \eta = 1089.3638 \eta$$

$$\beta = \omega_1^{-1} \cdot \eta = \eta / 1089.3638$$

assuming $\eta = .01$ $\alpha = 10.893$ $\beta = 0.0000091$.

The following figures (5.7a,b,c) represent the damped response of the system.

5.4.3 Dynamic Snap-Through of an Arch

The example is a dynamic analysis of a circular arch subjected to a uniform time varying pressure and was used by Wilson [65] to justify his solution procedure of solution to compare the result with Humphreys'.

The finite element and load idealizations are shown in Figure (5.8) and (5.9) respectively. The following data have been used in the example:

$$\beta = 30^\circ \quad \rho = 0.00625 \text{ lb m/in}^3$$

$$h = 2.0 \text{ in} \quad E = 3326.2 \text{ lb/in}^2$$

$$R = 72.95 \text{ in} \quad \Delta t = 0.025, .0125 \text{ and } 0.006255.$$

Figures (5.10,11) represent displacement, and the variation with time. Comparison of the dynamic response at node number (16) and static solution was given in Figure (5.11)

The comparison between the results obtained by Wilson [65] and those obtained using the program presented in this project show good agreement.

5.4.4 One-dimensional Wave Propagation Problems

The nature of the axial wave-propagation mechanism will be demonstrated by studying the stress wave propagation in two examples. In the first, a uniform prismatic bar is subjected to a force at the left hand side which travels undisturbed and undiminished down the bar. The second problem concerns the study of a stress wave generated by the impact of a pile-driving hammer at the top of a pile. For both, exact solutions are available.

(a) Bar Problem

The first problem considered was the one-dimensional (plane strain) stress wave problem, in which a step pulse is applied at the free end of the rod at a particular time Figure (5.12) . The dynamic response is shown in Figures (5.13—5.15).

Comparing the results of this problem with those obtained by Costantino [26] , Shipley et al[32] , and Yomada and Nagai[66] agree well with the predicted values.

(b) Pile-Driving Problem

For the purpose of this example, it will be assumed that the hammer generates a force pulse $P(t)$ equals $(2668920.0 \text{ N}) \sin(\pi t/0.005)$ and the stress distribution will be evaluated at the end of the pulse ($t_1 = 0.0055 \text{ sec}$) in both the steel and the concrete piles whose properties are shown in Figure (5.15).

Considering the steel pile first, in which the velocity of wave propagation $C_s = \sqrt{E/\rho}$ where (E) is Young's modulus and (ρ) is the density

$$C_s = \sqrt{E/\rho} = 513080 \text{ cm/sec.}$$

The stress at the origin generated by the hammer blow is

$$\sigma_o(t) = - \frac{P(t)}{A}$$

The solution of the one-dimensional wave propagation problem is written as

$$\sigma(x,t) = f_1(x - ct) + f_2(x + ct) \quad \dots \quad \dots \quad \dots$$

Evaluating at the origin and considering only the forward propagating wave

$$\sigma_o(t) = f_1(-ct) \quad \dots \quad \dots \quad \dots \quad \dots \quad \dots \quad \dots$$

Hence f_1 can be evaluated by equating these expressions giving

$$\sigma_s(t) = \left(\frac{-2668920.0}{193.548} \right) \sin \left(\frac{-\pi}{2560.32} \right) ct$$

Thus the general expression for the forward-propagating wave is

$$\sigma_s(x, t) = \left(\frac{-2668920.0}{193.548} \right) \sin \frac{\pi}{2560.32} (c_s t - x)$$

Evaluating at $t_1 = 0.005$ sec leads to

$$\sigma_s(x, 0.005) = \left(\frac{-2668920.0}{193.548} \right) \sin \pi \left(1 - \frac{x}{2560.32} \right)$$

which is plotted in Figure(5.15)

Following the same procedure for the concrete pile, the results were

$$C_c = 292608.0 \text{ cm/sec}$$

$$\sigma_c(x, 005) = \left(\frac{-2668920.0}{2580.6} \right) \sin \left(1 - \frac{x}{1463.04} \right)$$

Using the same data, the problems has been solved by the program, the results are compared and shown in Figure (5.16)

5.4.5 Two-Dimensional Wave Propagation

Numerical solutions are presented for certain examples of plane strain and axisymmetric problems to demonstrate the validity of the proposed formulation in obtaining the elastic dynamic response of multi-layered half-spaces. Rayleigh damping has been considered to be present. The problem of an axisymmetric uniform half-plane loaded by a radial surface pressure pulse fixed in space has been considered. The results have been compared with those obtained from a finite difference analysis [26].

The finite element mesh used in Figure (5.17) consists of 36 isoparametric elements. A comparison of the dynamic response of this problem is shown in Figure (5.19) which show reasonable agreement with those published by Constantino [26].

5.4.6 Response of Half-space Excited by Trapezoidal Pulse

Another problem of interest is shown in Figure (5.20) and consists of a perfectly elastic half-space with the mass density ρ and the elastic constants G and μ .

The constants were, $\rho = 0.00187 \text{ lb. S}^2/\text{in}^4$, $G = 3400 \text{ psi}$ and $\mu = 0.25$.

The half-space is excited by trapezoidal pulse, this pulse has the property of being constant, equal to 250,000 lb, for a period of 0.9 sec, which is considerably larger than the natural period of the system. A time interval of 0.5 ms was used. The displacement as a function of time

is also shown in Figure (5.20), and may be seen to converge on the static solution with increase in time. The computed results show good agreement with that published by Butterfield [67] as shown in Figures (5.21, 22, 23).

5.4.7 Dynamic Analysis of a Rubber Sheet with a Hole

The purpose of this example was to test the capability of predicting the dynamic response of rubber which has properties similar to the polyurethane rubber which has been used in the experimental investigations. Data for this problem are the same as that published by Bate, Ram and Wilson [46].

A dynamic plane stress analysis of the rubber sheet shown in Figure (5.28) was carried out. The specific material constants used for the material were $G_1 = 250$ PSI, $G_2 = 86$ PSI. These constants and the finite element mesh used in the analysis are presented in Figure (5.27).

The dynamic analysis was performed for the step load shown in Figure (5.27) using $\Delta t/T_f = 120$. Figure (5.28) compares the displacement response predicted with those published in reference [46].

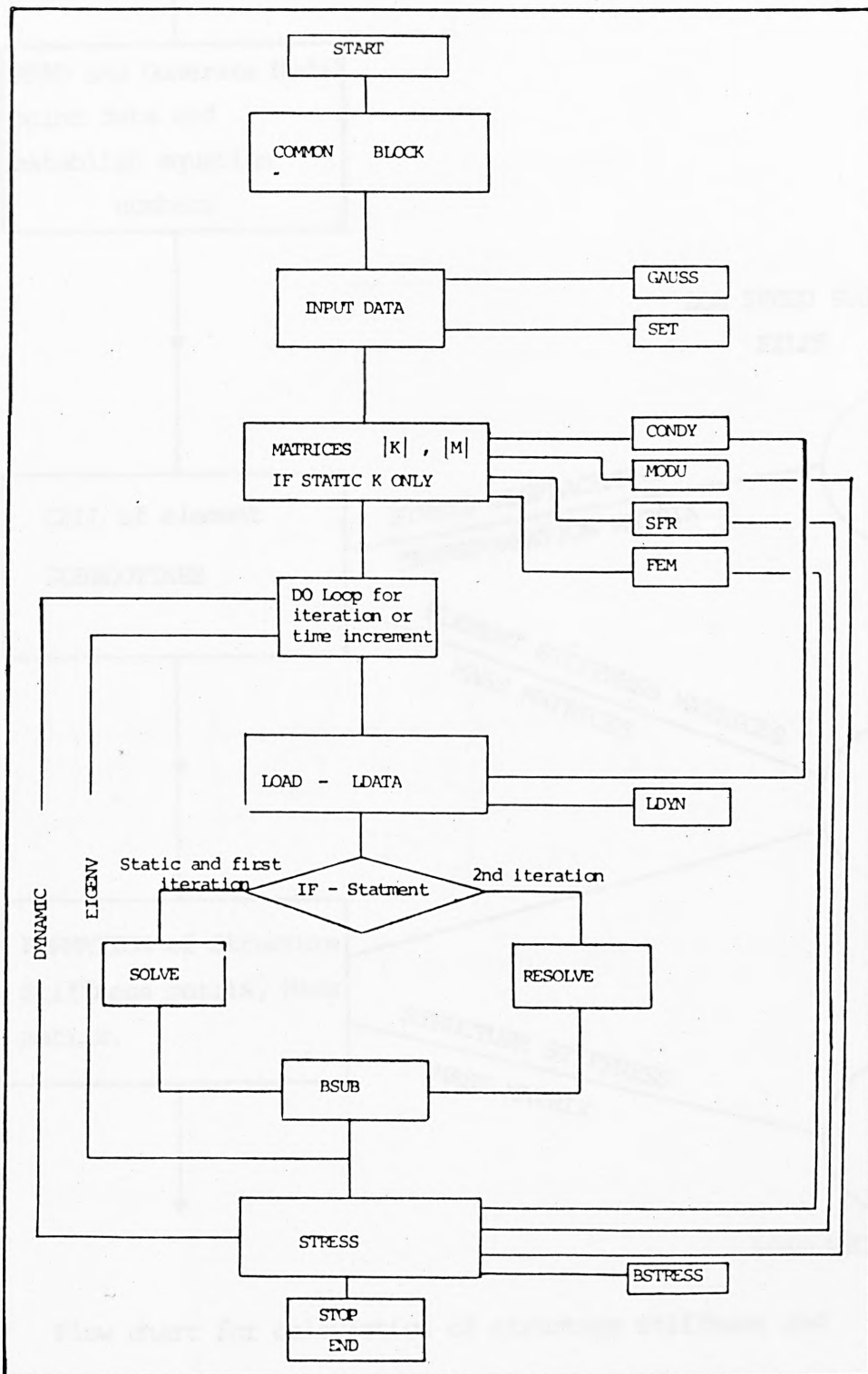
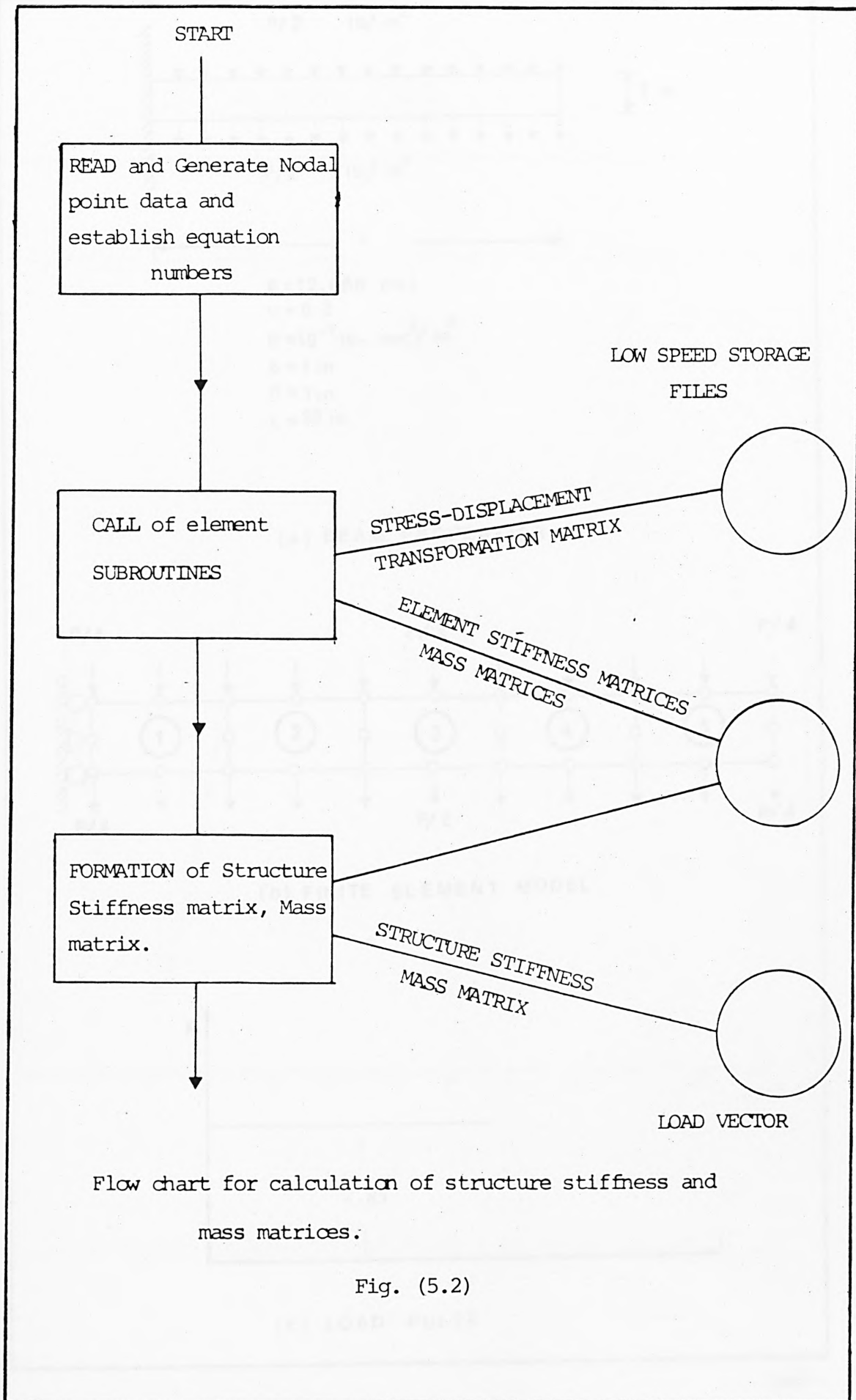
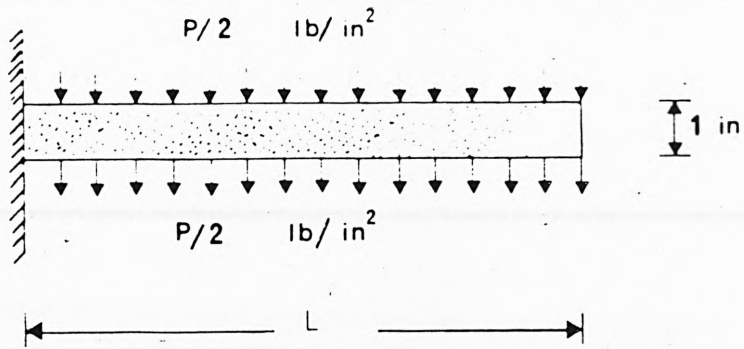


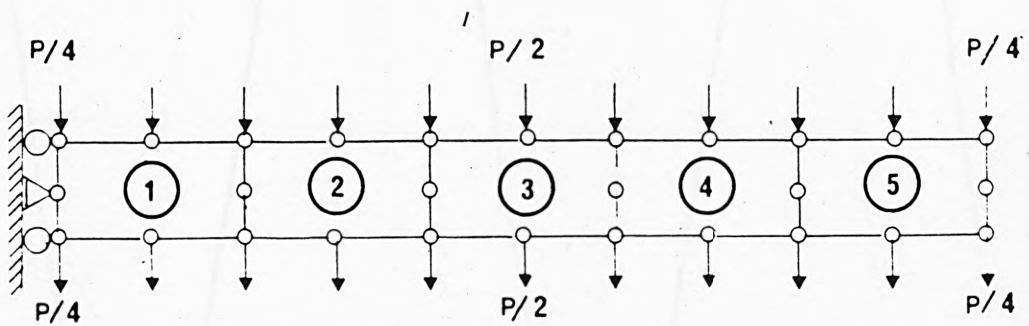
Fig. (5.1) Flow chart of DFEM programme



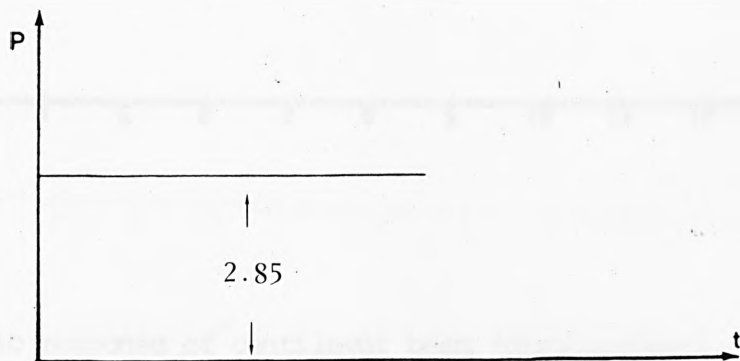


$E = 12,000 \text{ psi}$
 $\nu = 0.2$
 $\rho = 10^{-6} \text{ lb-sec}^2/\text{in}^4$
 $b = 1 \text{ in}$
 $d = 1 \text{ in}$
 $L = 10 \text{ in}$

(a) BEAM PROPERTIES



(b) FINITE ELEMENT MODEL



(c) LOAD PULSE

Fig. (5.3) CANTILEVER BEAM

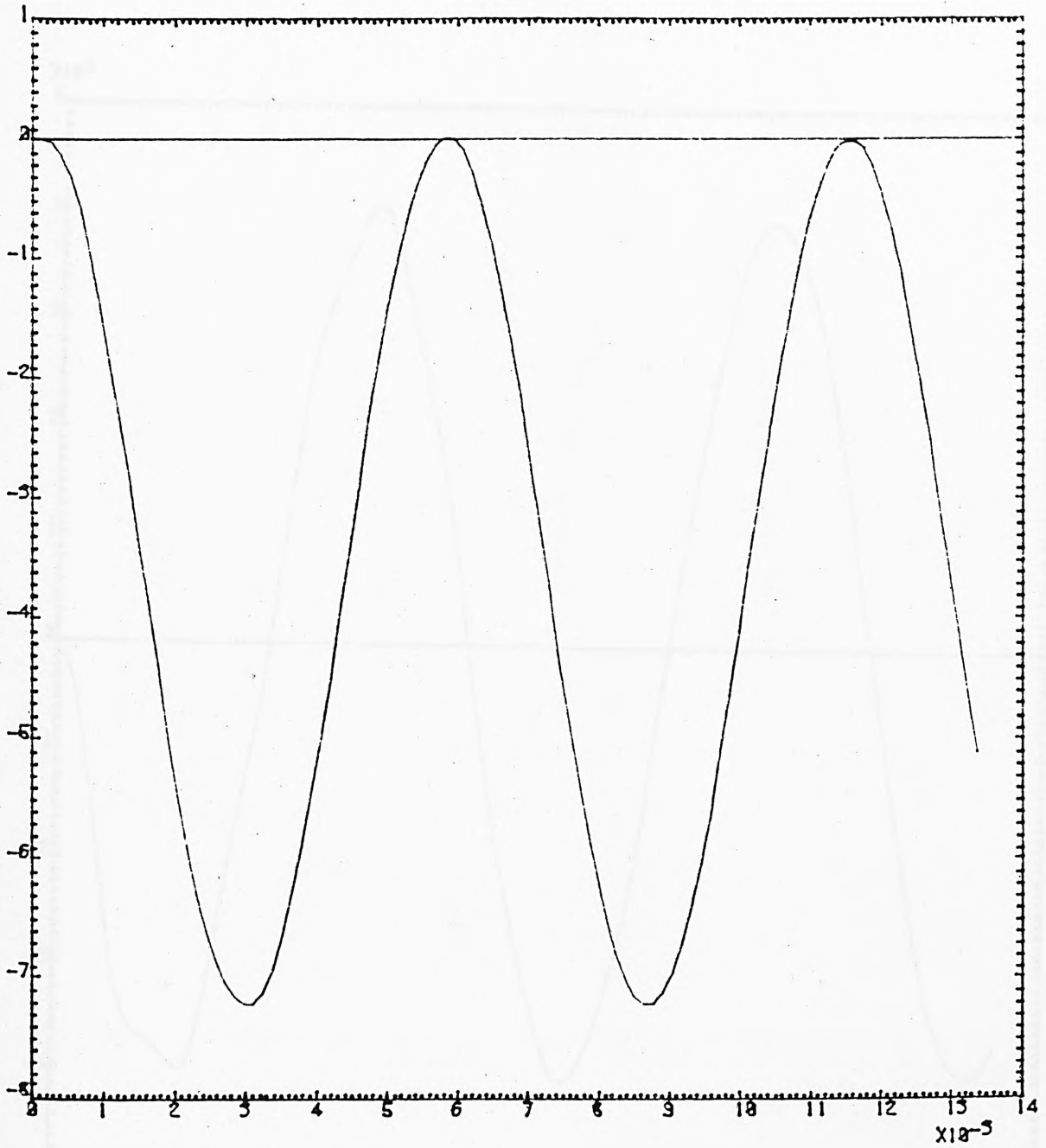


Fig. (5.4) Dynamic response of cantilever beam (displacement).

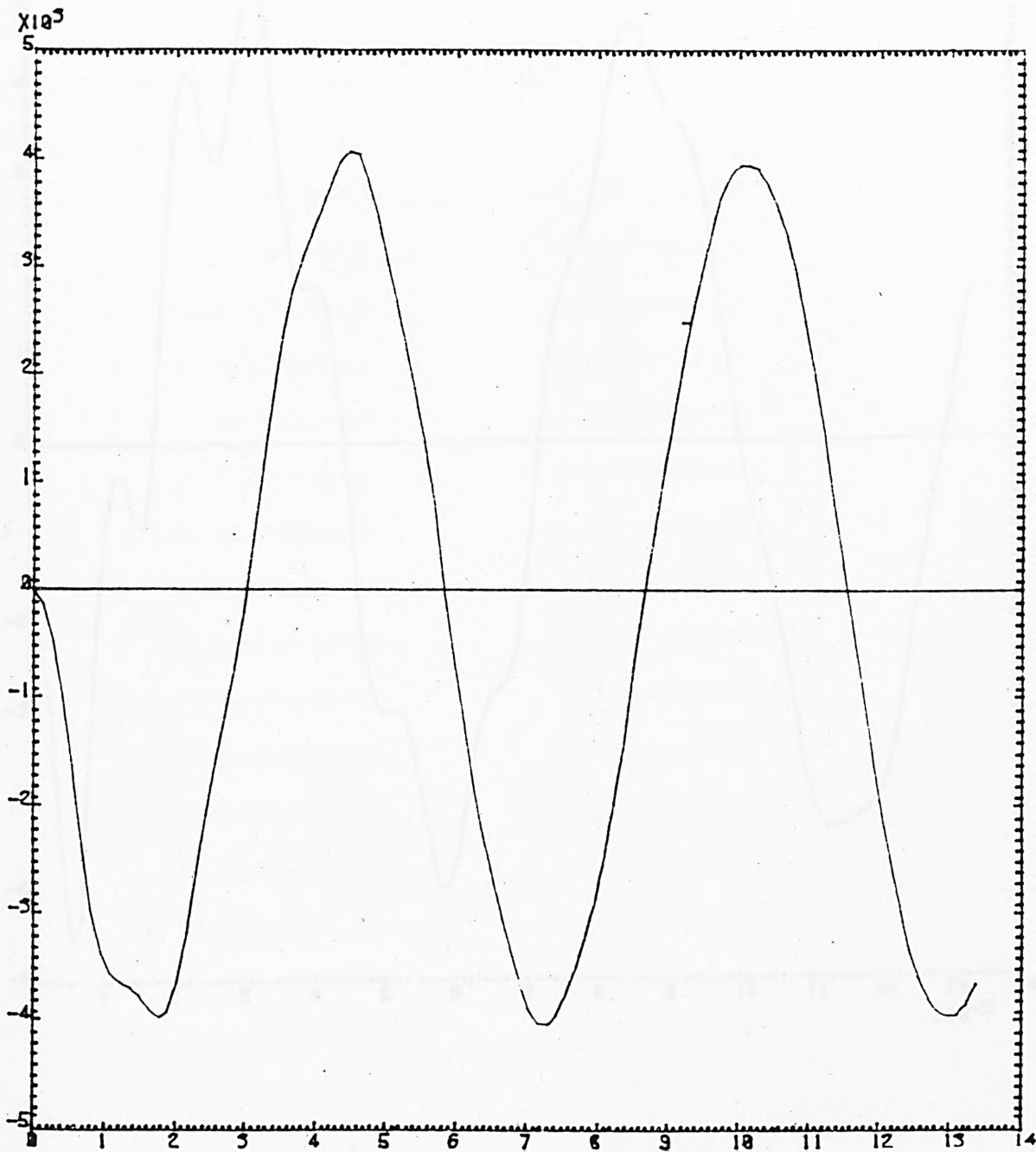


Fig. (5.5) Dynamic response of cantilever beam (velocity).

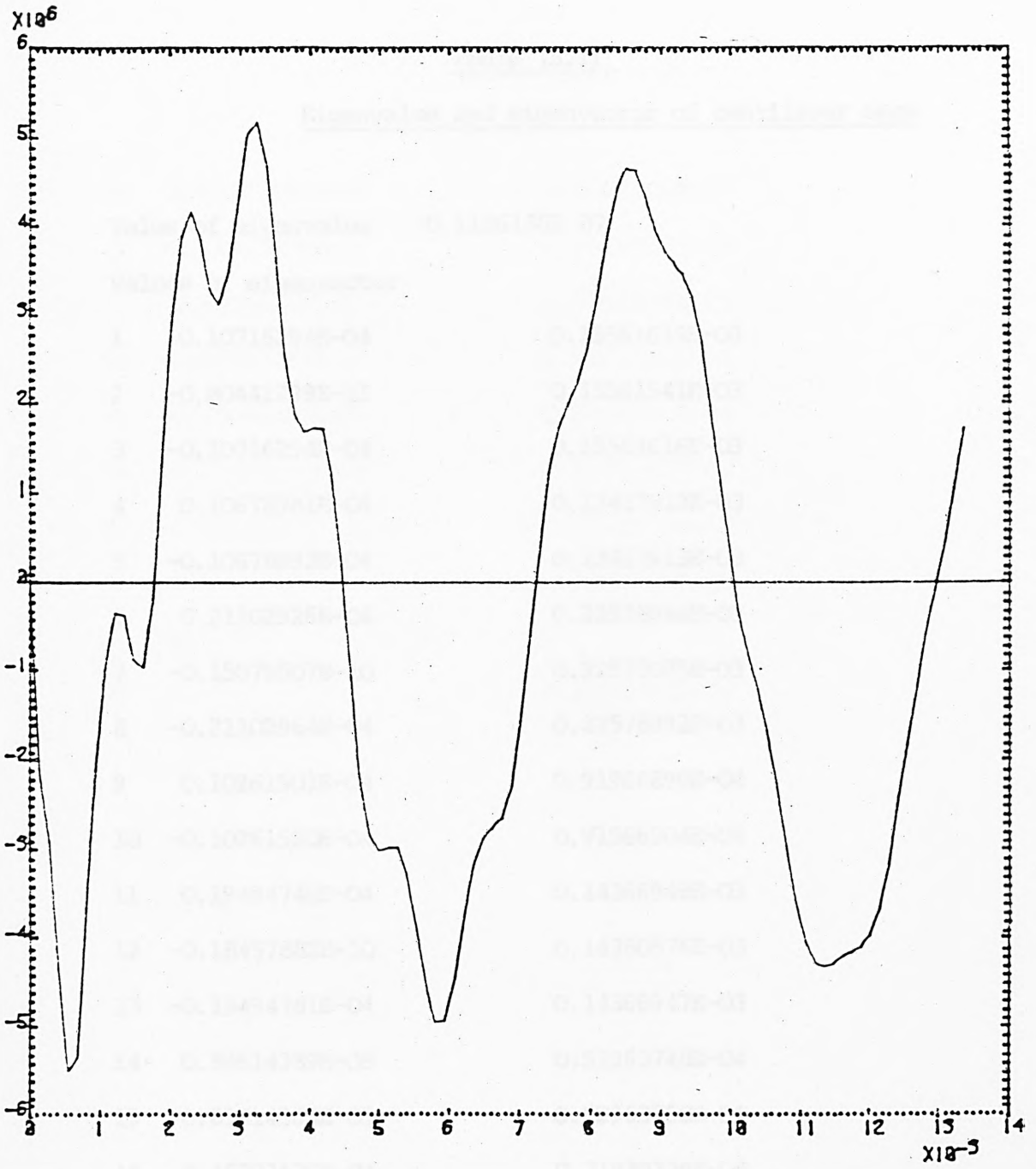


Fig. (5.6) Dynamic response of cantilever beam (acceleration).

Table (5.1)

Eigenvalue and eigenvector of cantilever beam

Value of eigenvalue	0.1186136E 07	
Values of eigenvector		
1	0.10716294E-04	0.15561619E-03
2	-0.80442299E-11	0.15561541E-03
3	-0.10716294E-04	0.15561616E-03
4	0.10678981E-04	0.13417912E-03
5	-0.10678993E-04	0.13417913E-03
6	0.21102926E-04	0.22578996E-03
7	-0.15076607E-10	0.22577075E-03
8	-0.21102964E-04	0.22578992E-03
9	0.10261501E-04	0.91966899E-04
10	-0.10261520E-04	0.91966904E-04
11	0.19494746E-04	0.14366948E-03
12	-0.18457882E-10	0.14360576E-03
13	-0.19494781E-04	0.14366947E-03
14	0.89614389E-05	0.52963748E-04
15	-0.89614564E-05	0.52963750E-04
16	0.15731620E-04	0.71939229E-04
17	-0.14944855E-10	0.71812543E-04
18	-0.15731651E-04	0.71939221E-04

Table (5.1) cont.

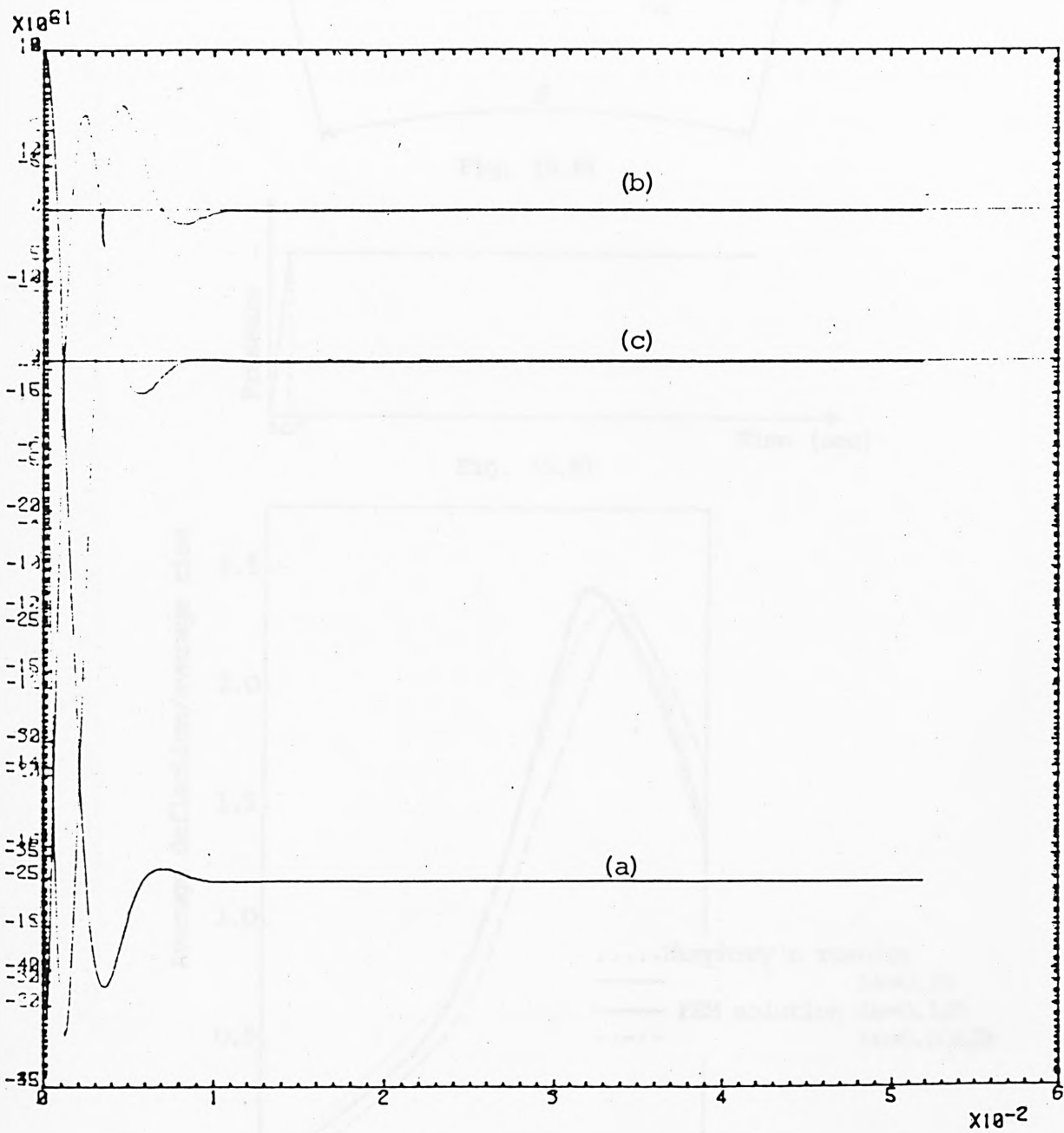
19	0.64357380E-05	0.21480832E-04
20	-0.64357498E-05	0.21480832E-04
21	0.93086819E-05	0.20403232E-04
22	-0.80507187E-11	0.20210630E-04
23	-0.93086970E-05	0.20403223E-04
24	0.25110585E-05	0.28442929E-05
25	-0.25110625E-05	0.28442948E-05
26	0.	0.14106748E-06
27	0.	0.
28	0.	0.14106502E-06

(a) Displacement

(b) Velocity

(c) Acceleration

Fig. (3.7) Exact response of single-degree-of-freedom system



(a) Displacement

(b) Velocity

(c) Acceleration

Fig. (5.7) Damped response of cantilever beam

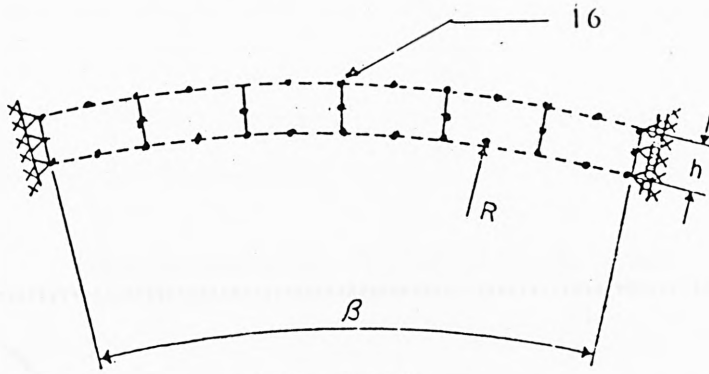


Fig. (5.8)

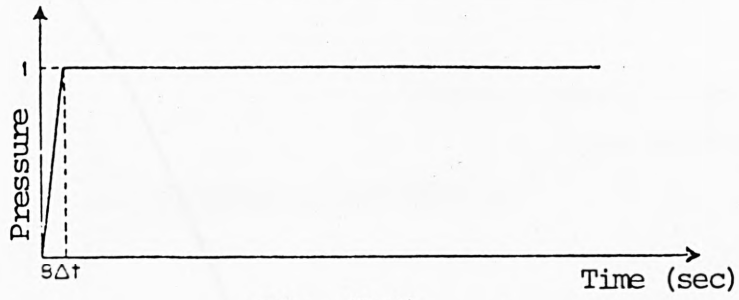


Fig. (5.9)

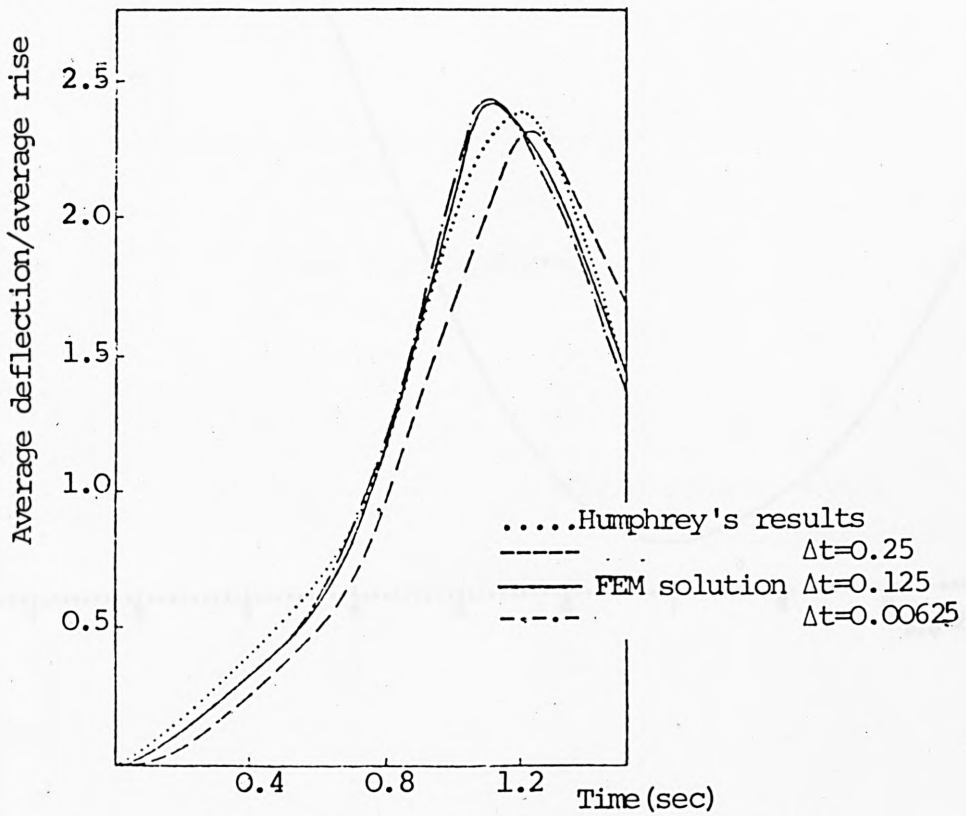


Fig. (5.10) Dynamic snap-through an arch [65]

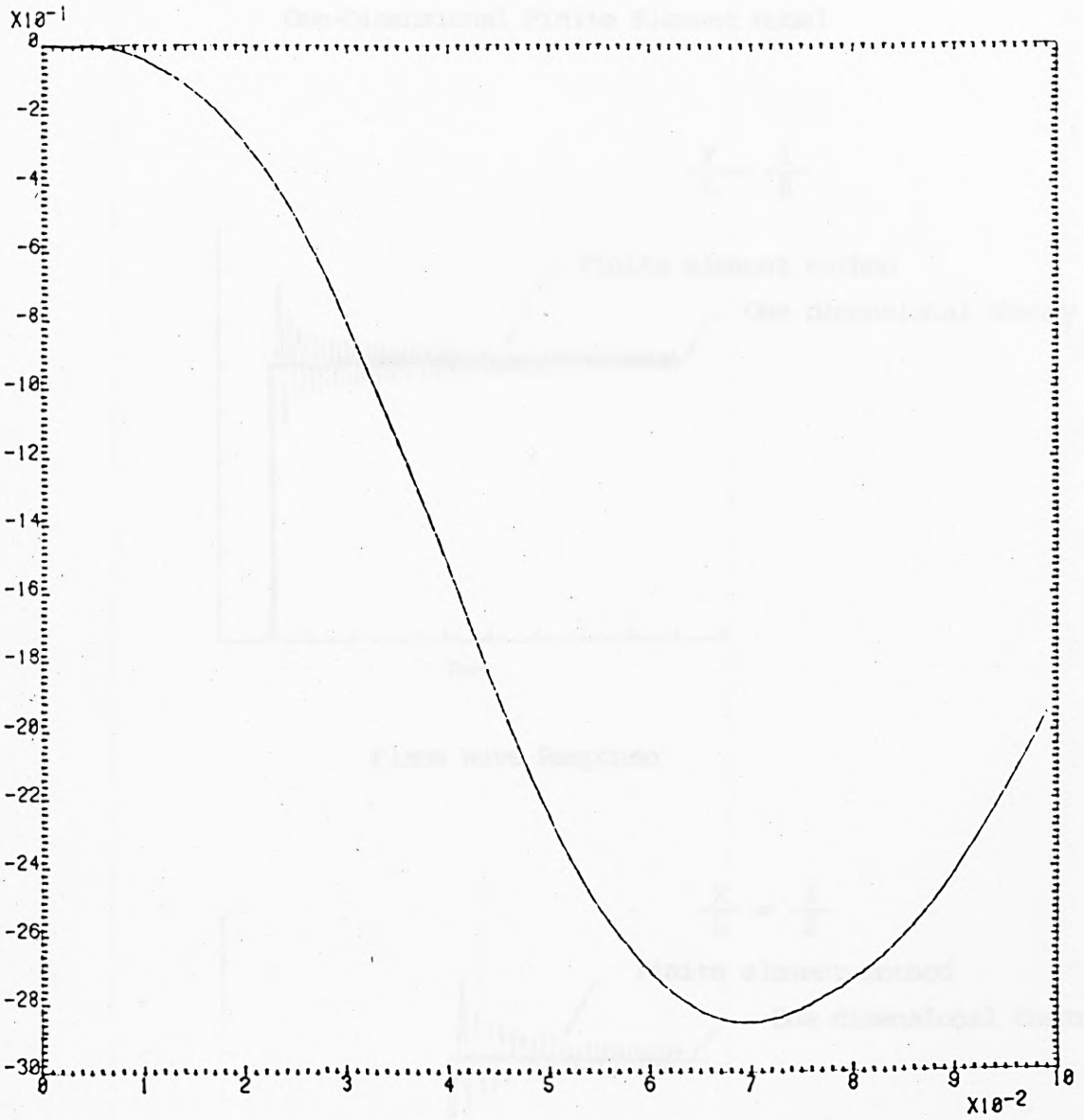
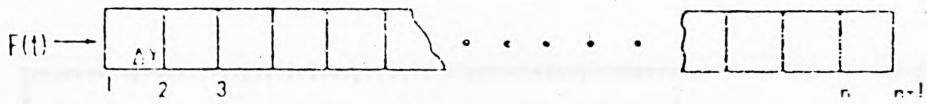
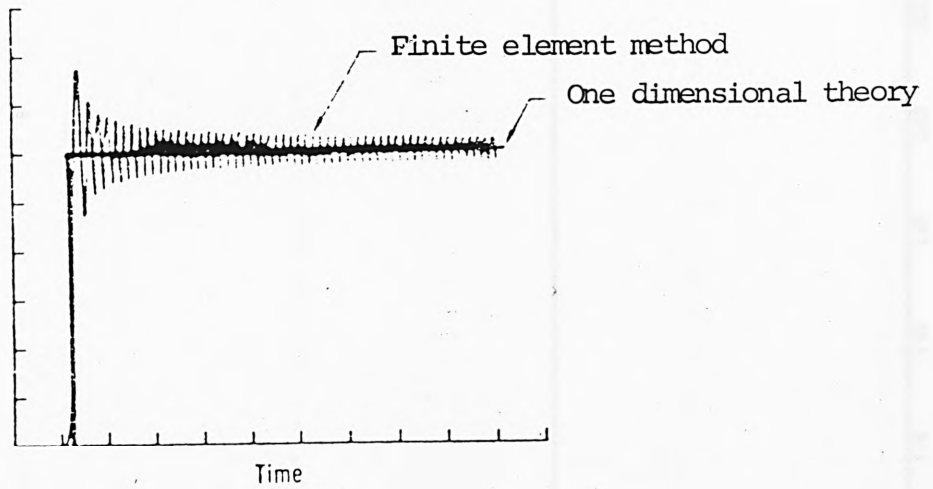


Fig. (5.11) Deflection of arch with time



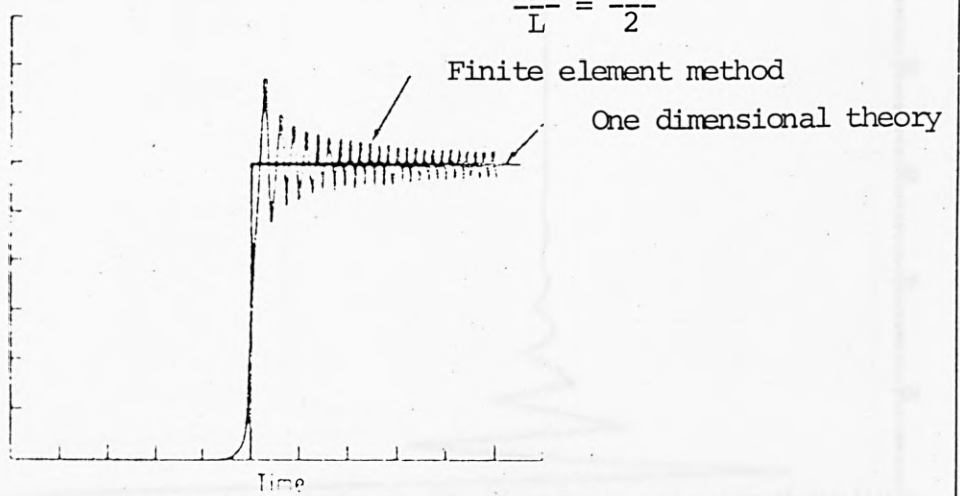
One-Dimensional Finite Element Model

$$\frac{X}{L} = \frac{1}{8}$$



Plane Wave Response

$$\frac{X}{L} = \frac{1}{2}$$



Plane Wave Response

Fig. (5.12)

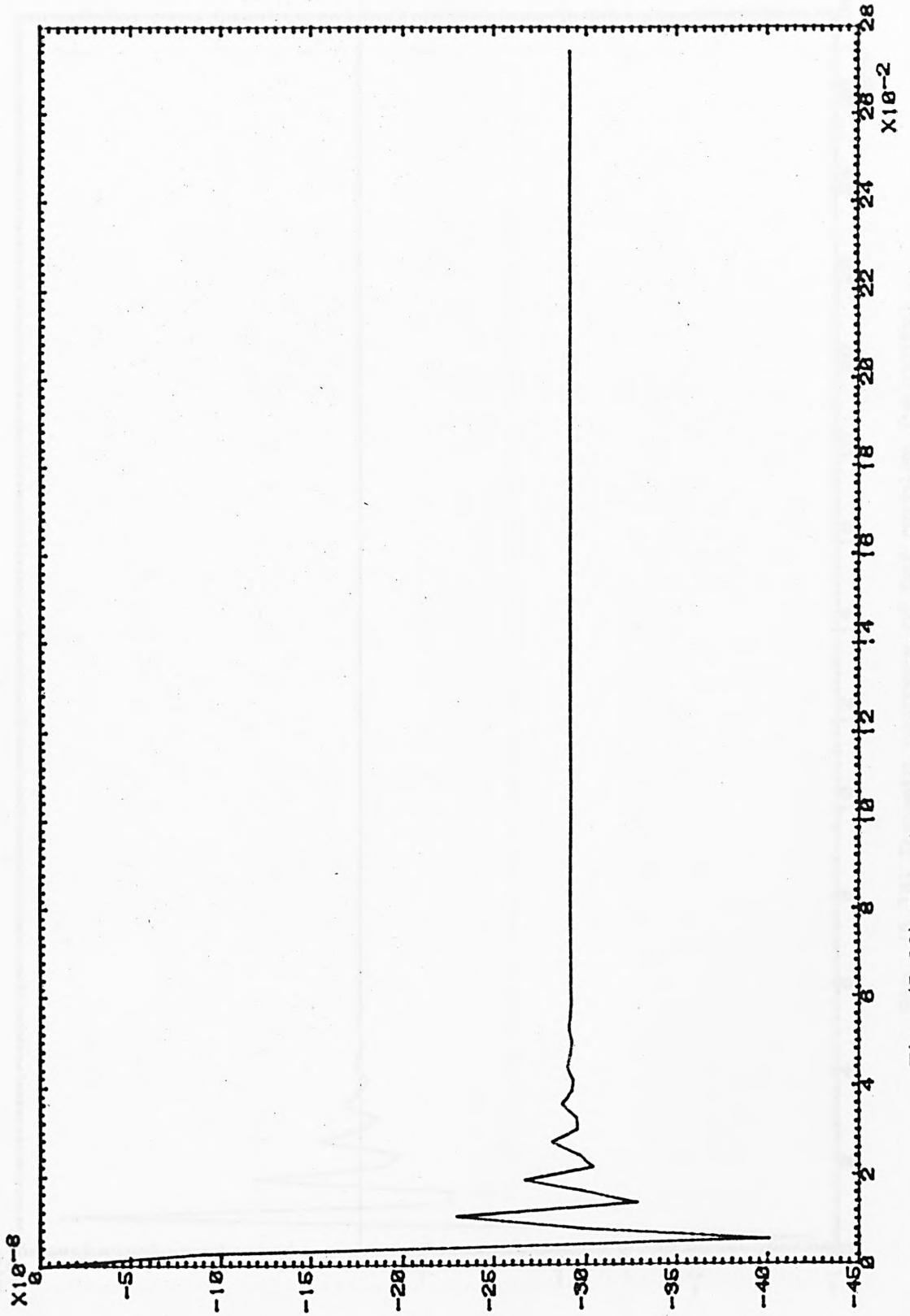


Fig. (5.13) Dynamic response of bar problem (displacement)

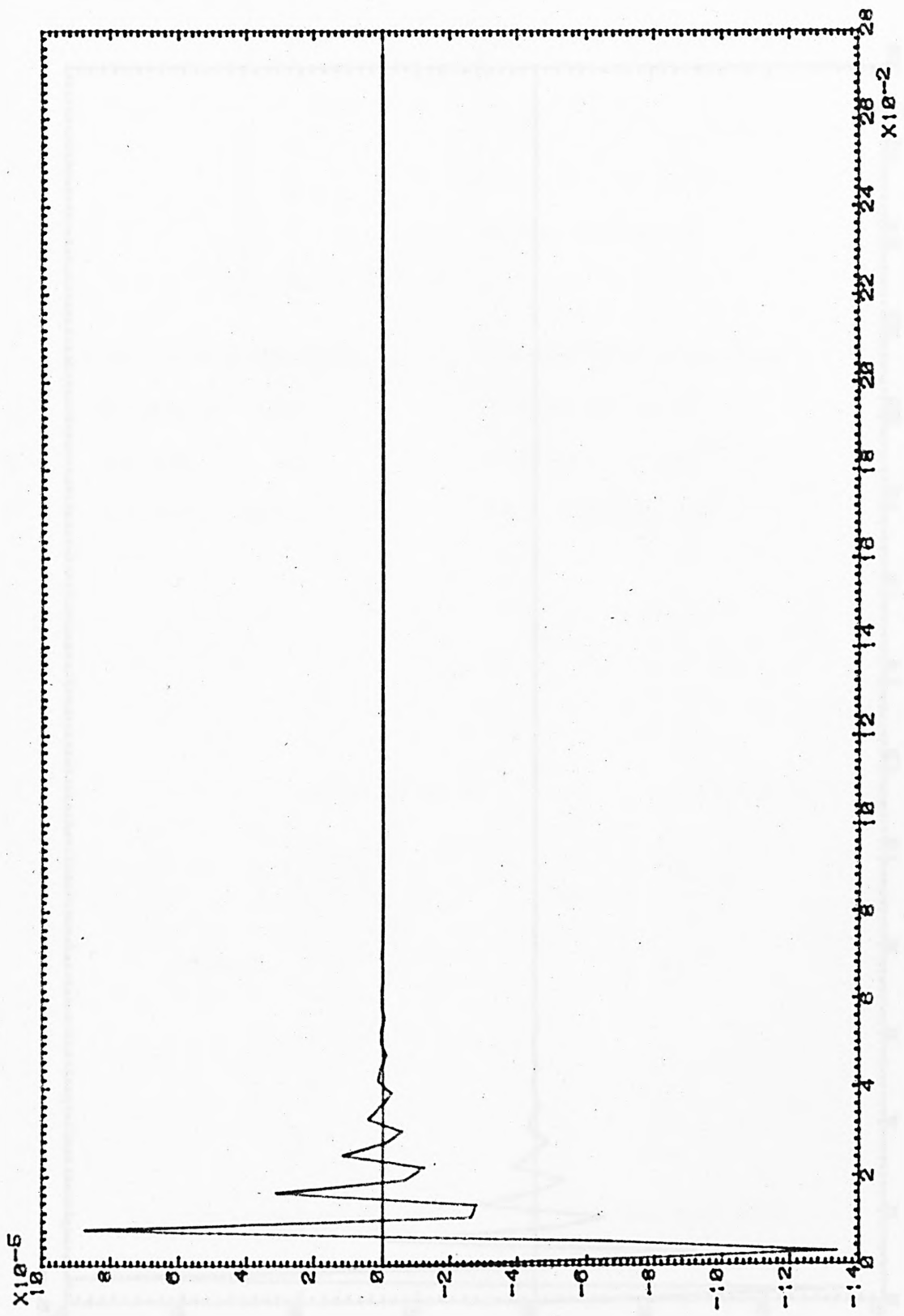


Fig. (5.14) Dynamic response of bar problem (velocity)

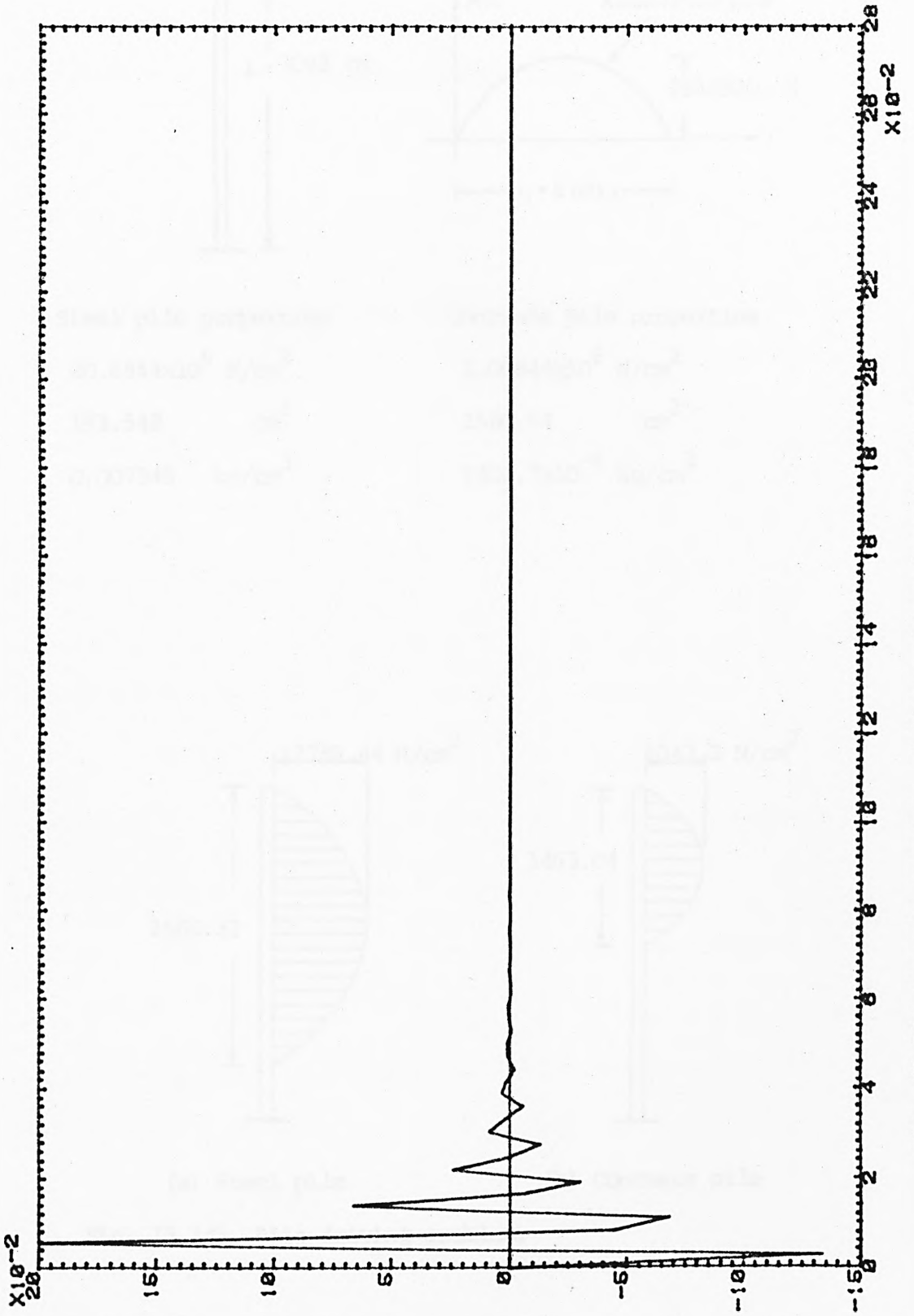
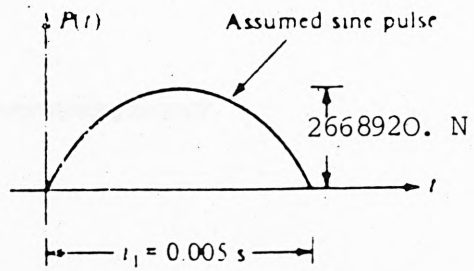
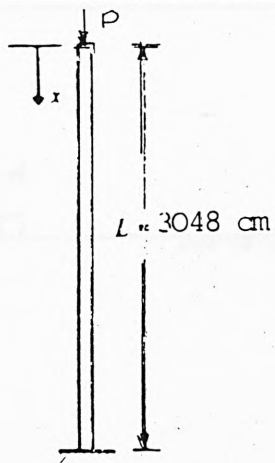


Fig. (5.15) Dynamic response of bar problem (acceleration)

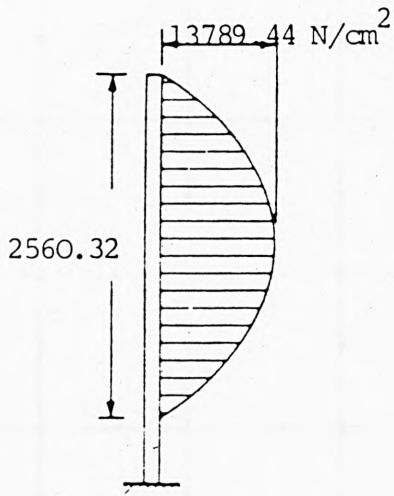


Steel pile properties

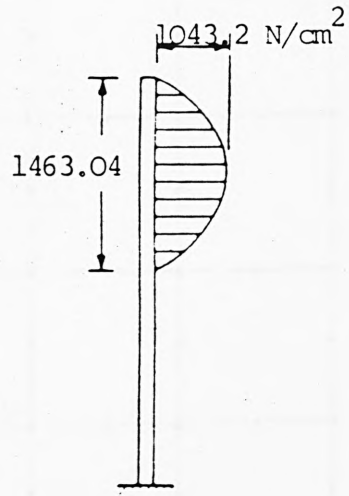
E	$20.6844 \times 10^6 \text{ N/cm}^2$
A	193.548 cm^2
ρ	0.007848 kg/cm^3

Concrete pile properties

E	$2.06844 \times 10^6 \text{ N/cm}^2$
A	2580.64 cm^2
ρ	$2402.7 \times 10^{-6} \text{ kg/cm}^3$

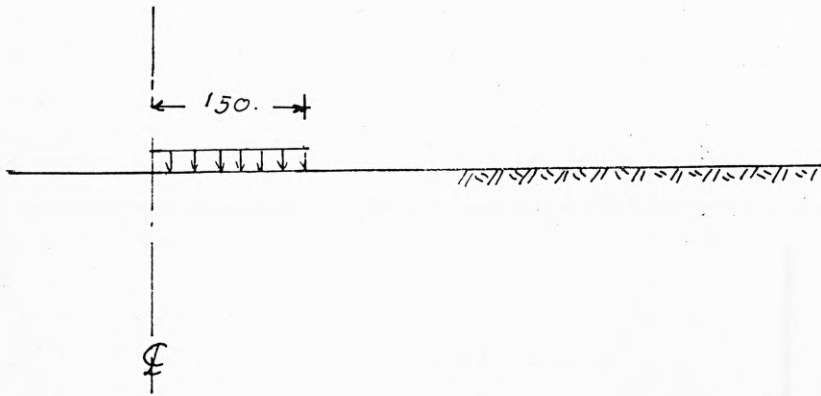


(a) Steel pile

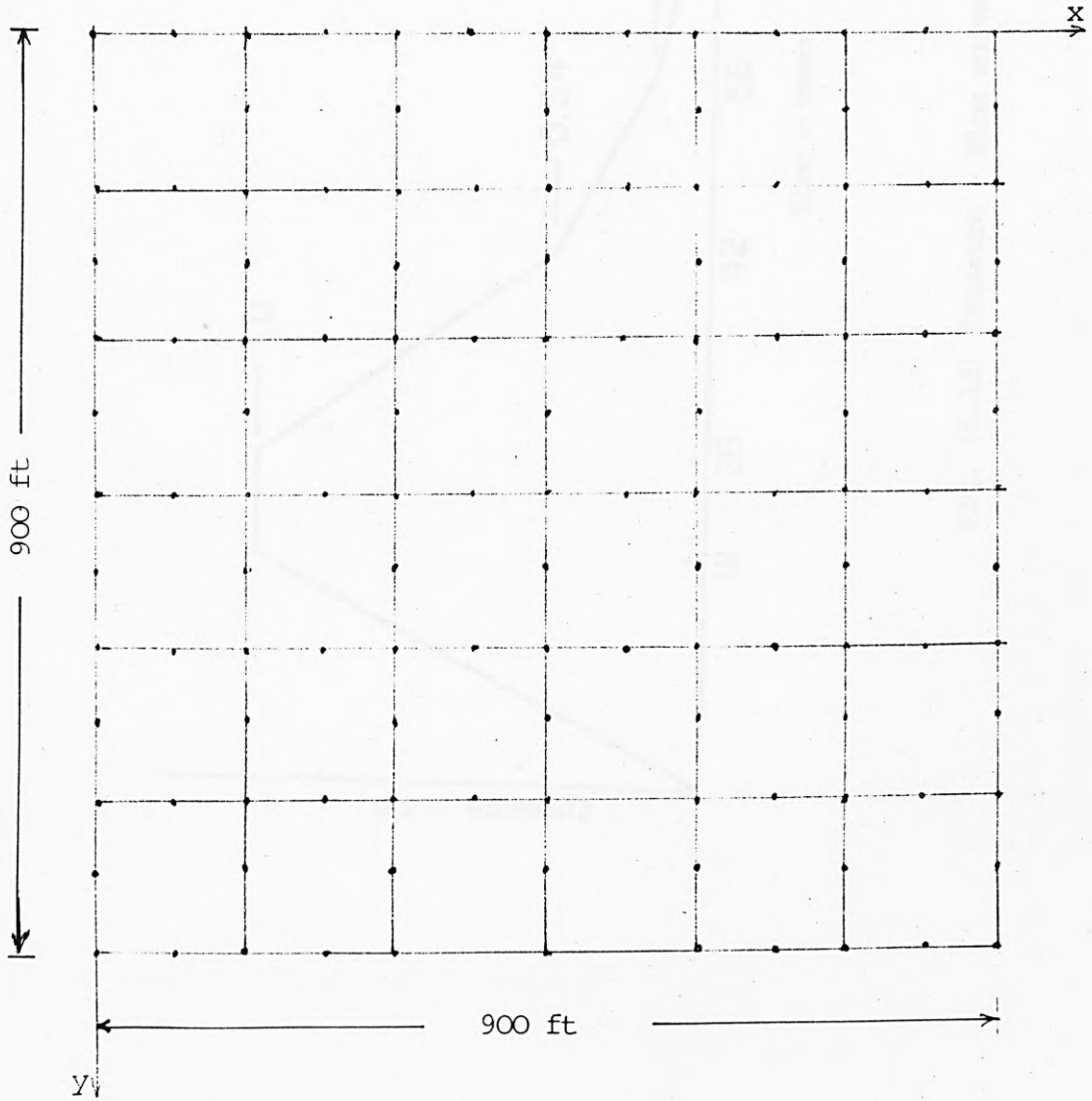


(b) Concrete pile

Fig. (5.16) . Pile driving problem.



(a) Half-space under vertical dynamic pressure



(b) Finite element idealization

Fig. (5.17)

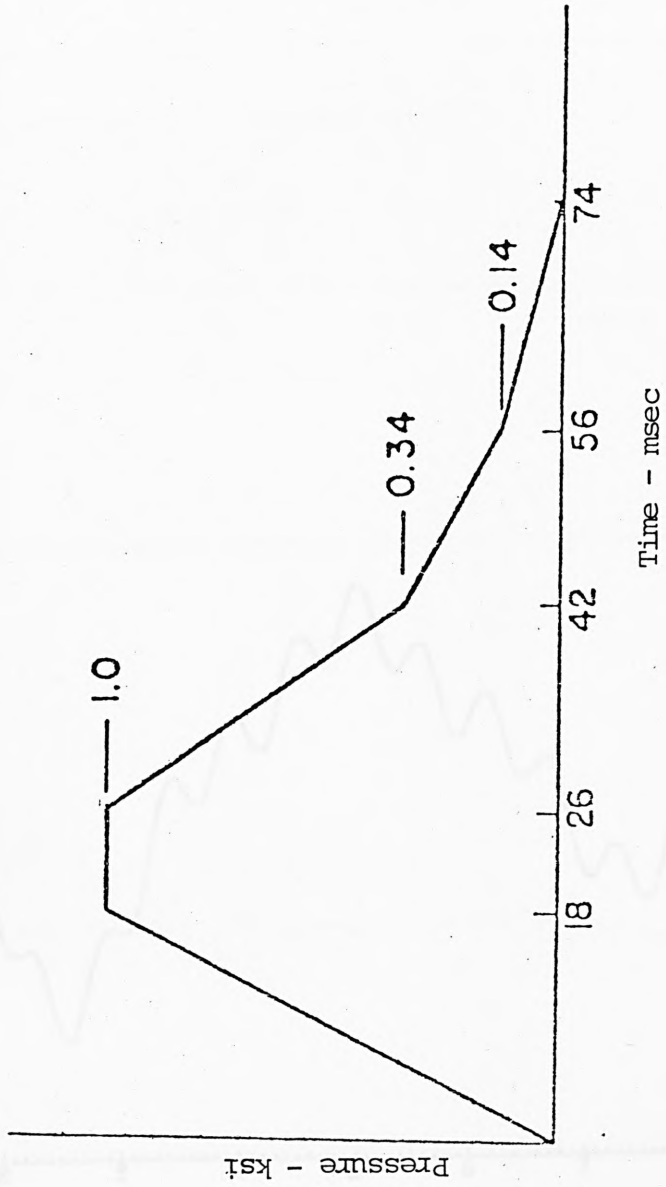


Fig. (5.18) Pressure - Time curve

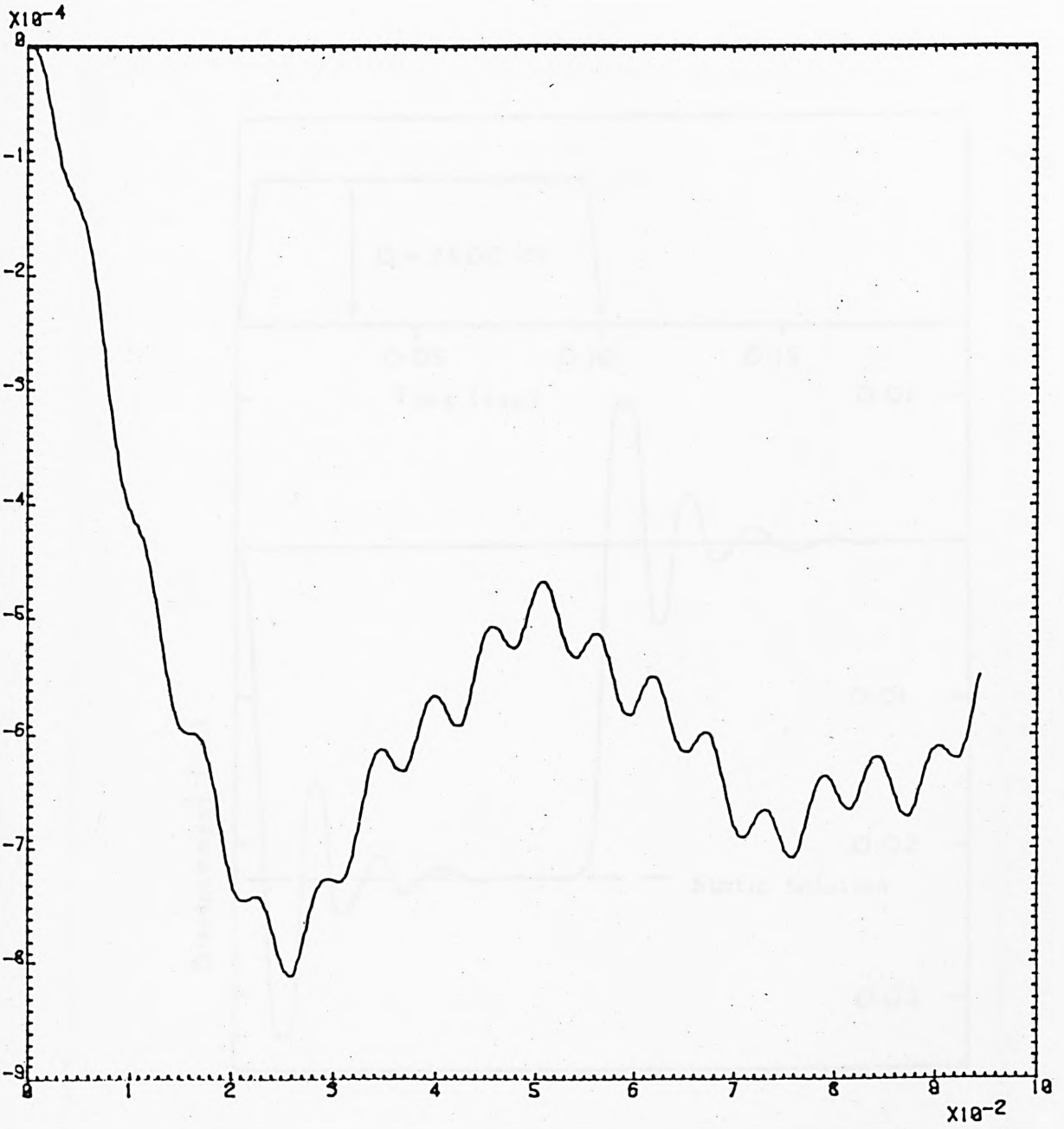


Fig. (5.19) Dynamic response of half-space

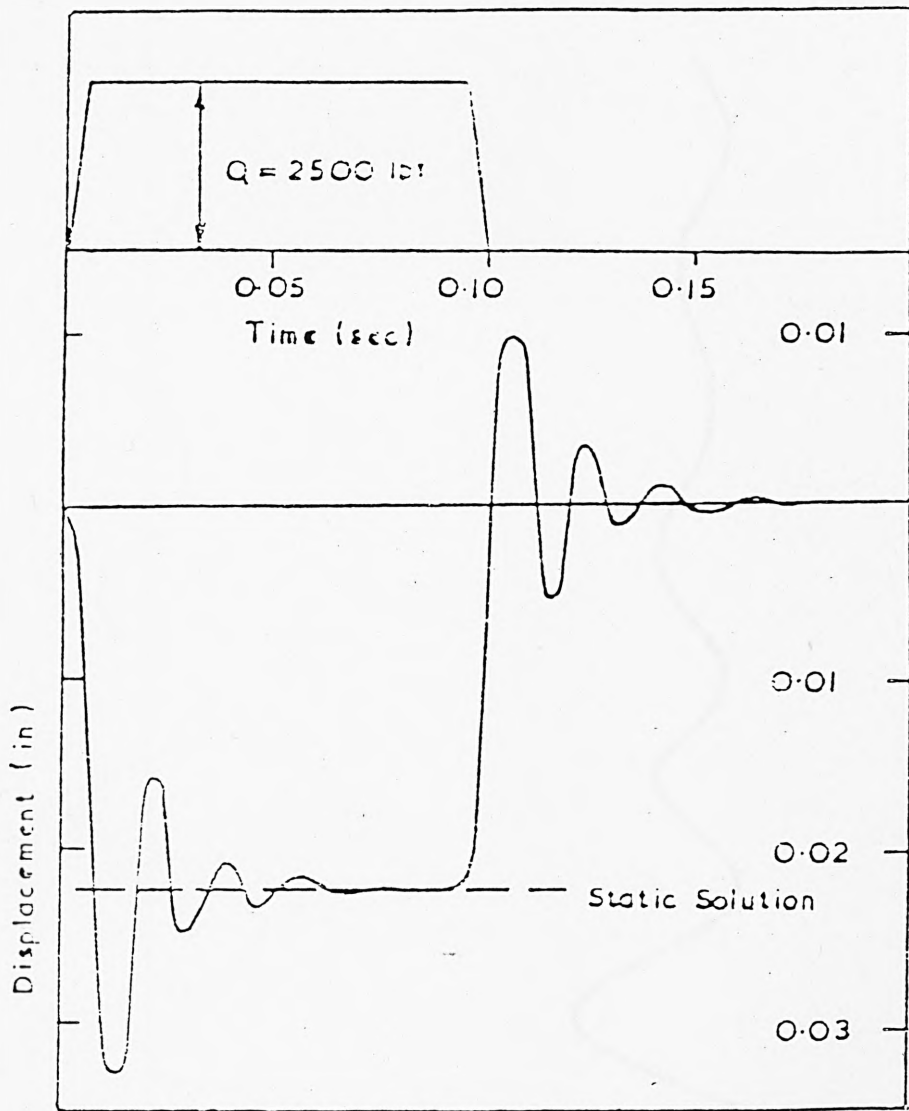


Fig. (5.20) Response under trapezoidal loading.

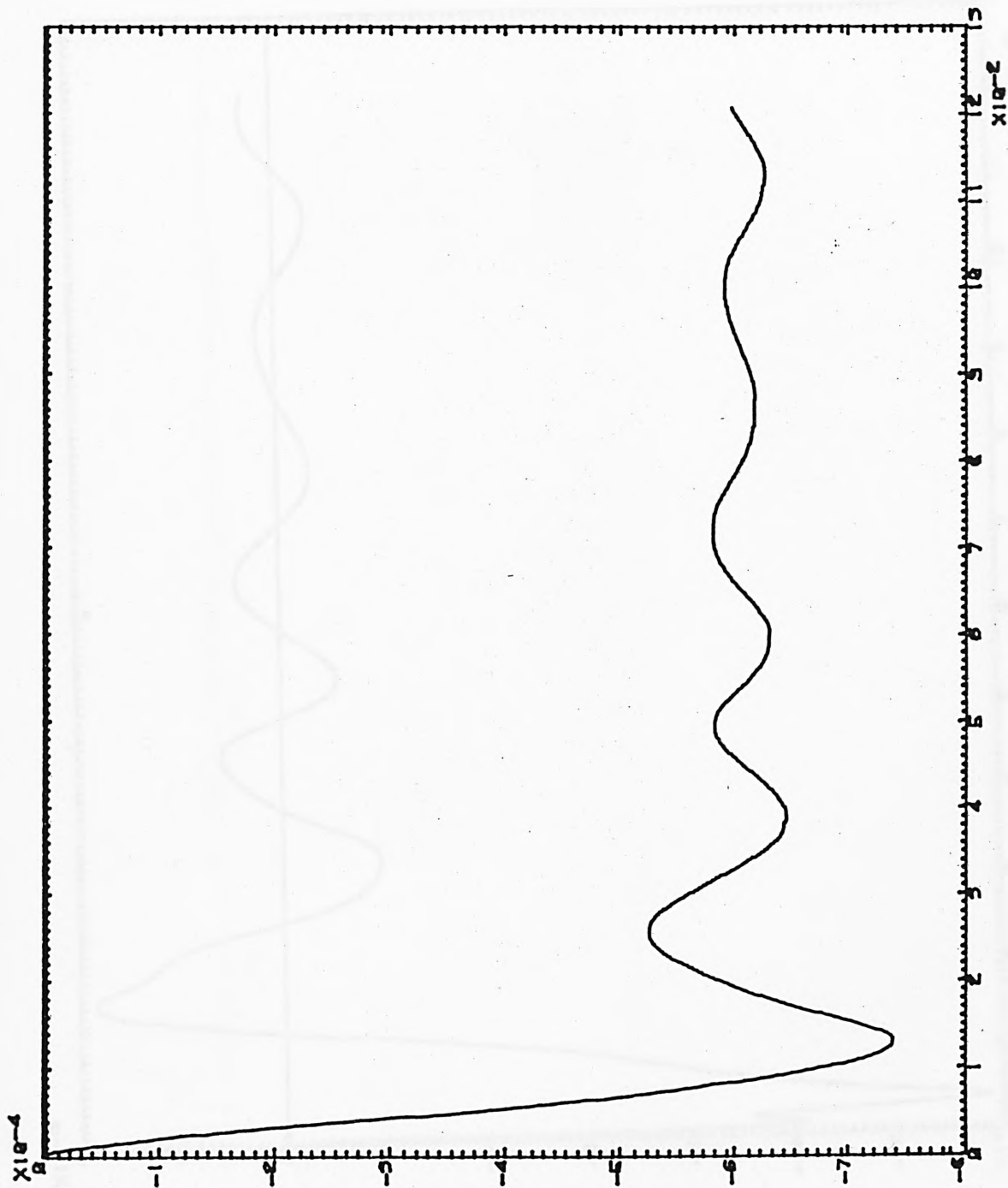


Fig. (5.21) (Dis.)

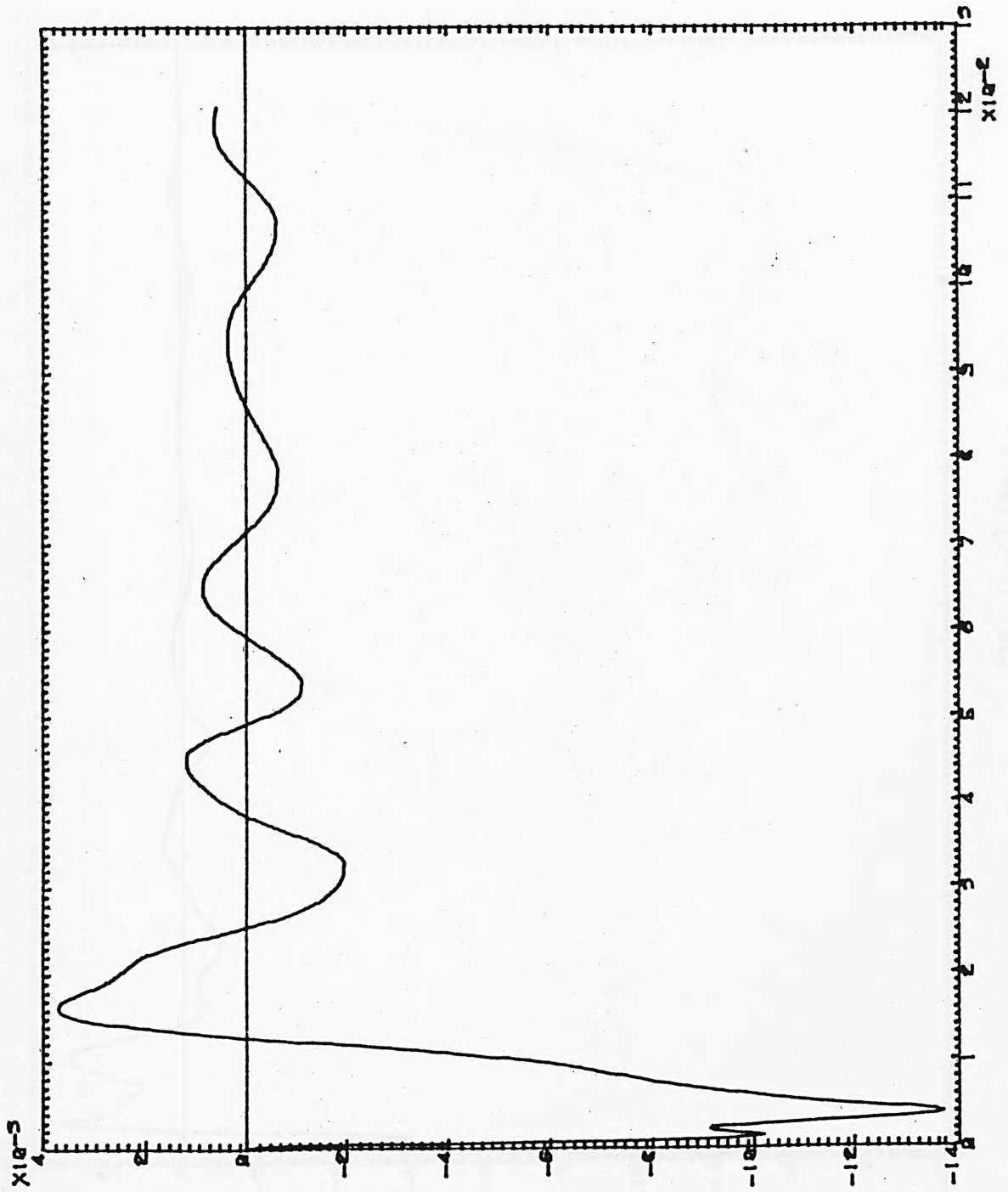


Fig. (5.22) (Vel.)

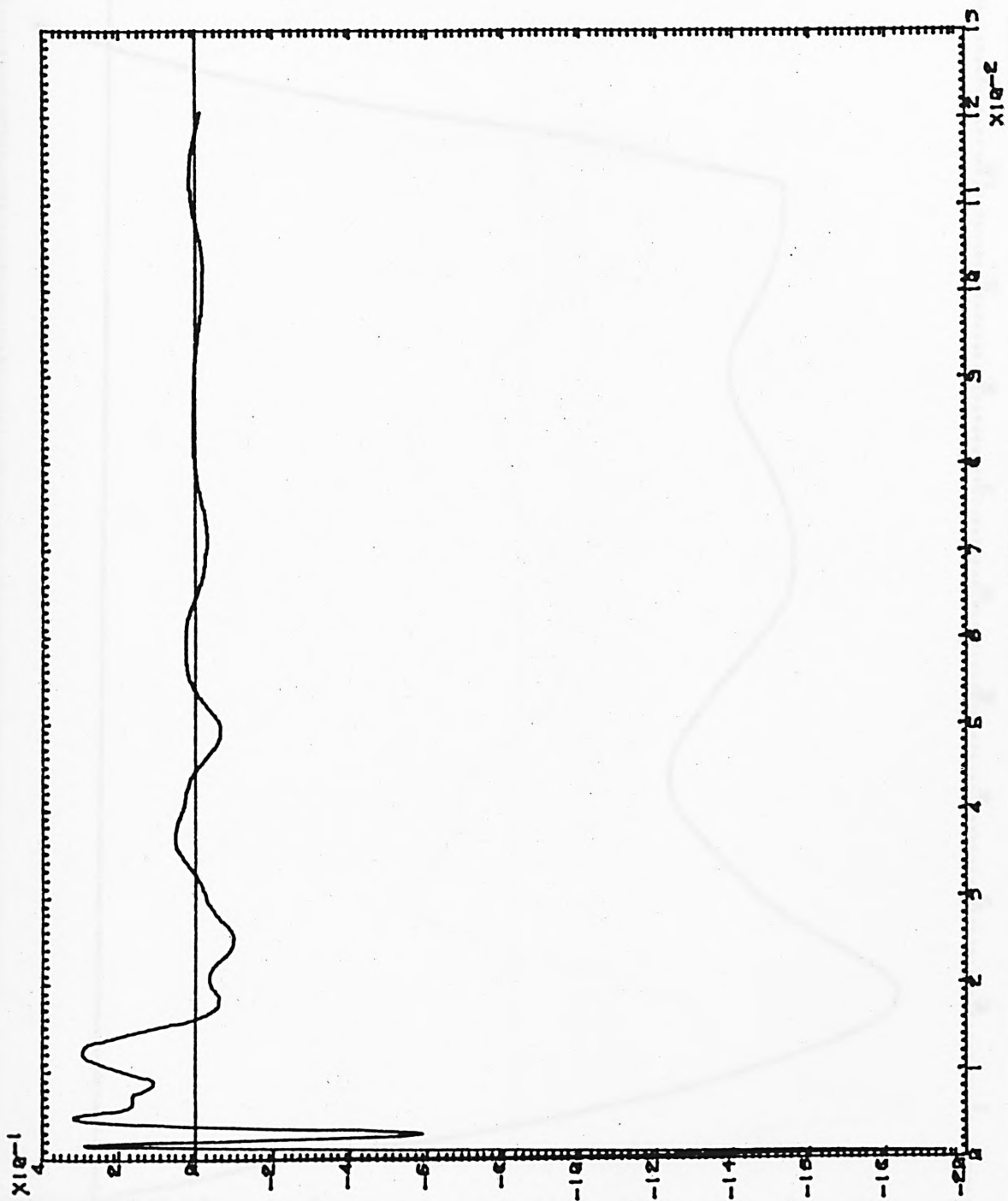


Fig. (5.23) (Acc.)

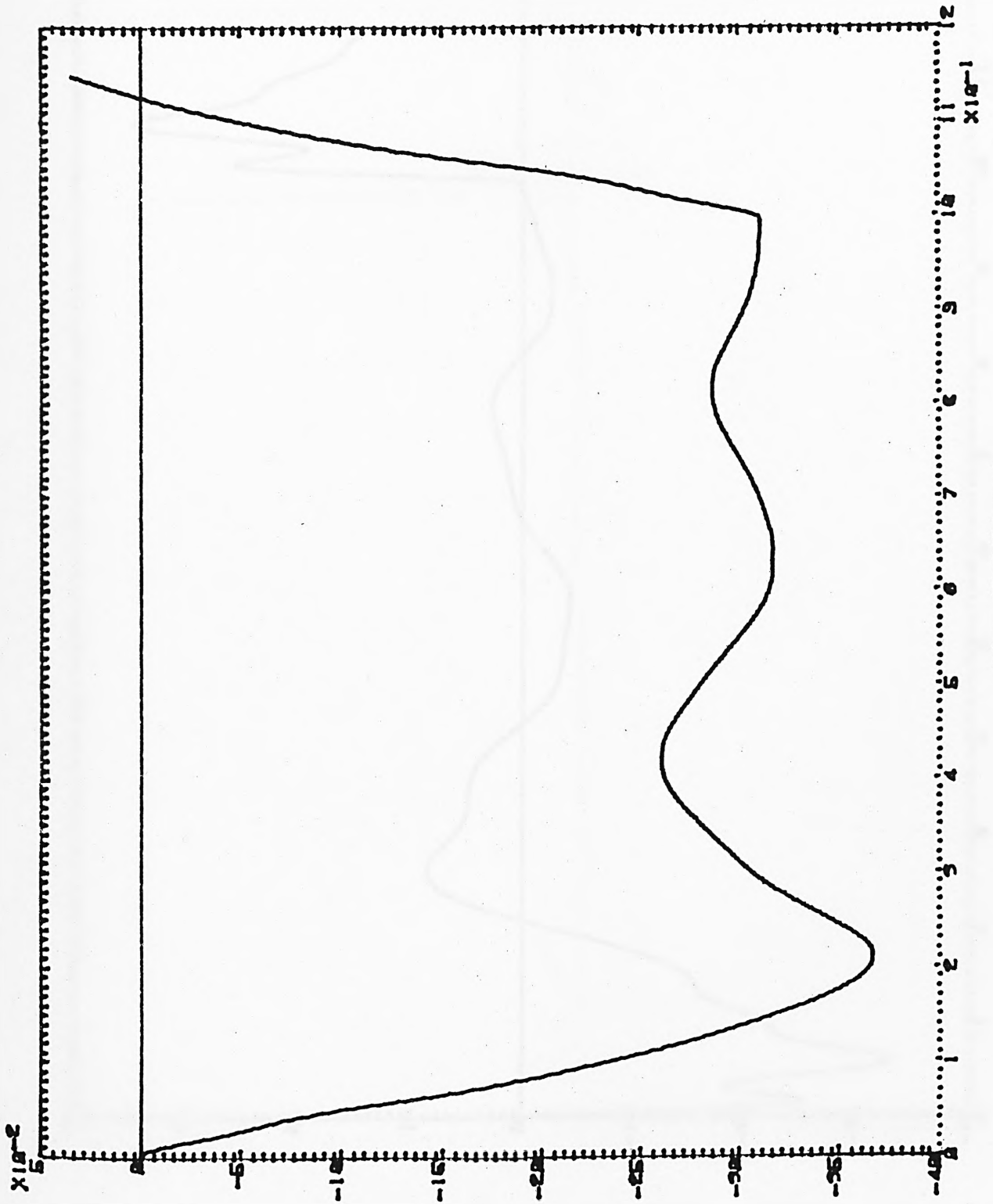


Fig. (5.24)(Dis.)

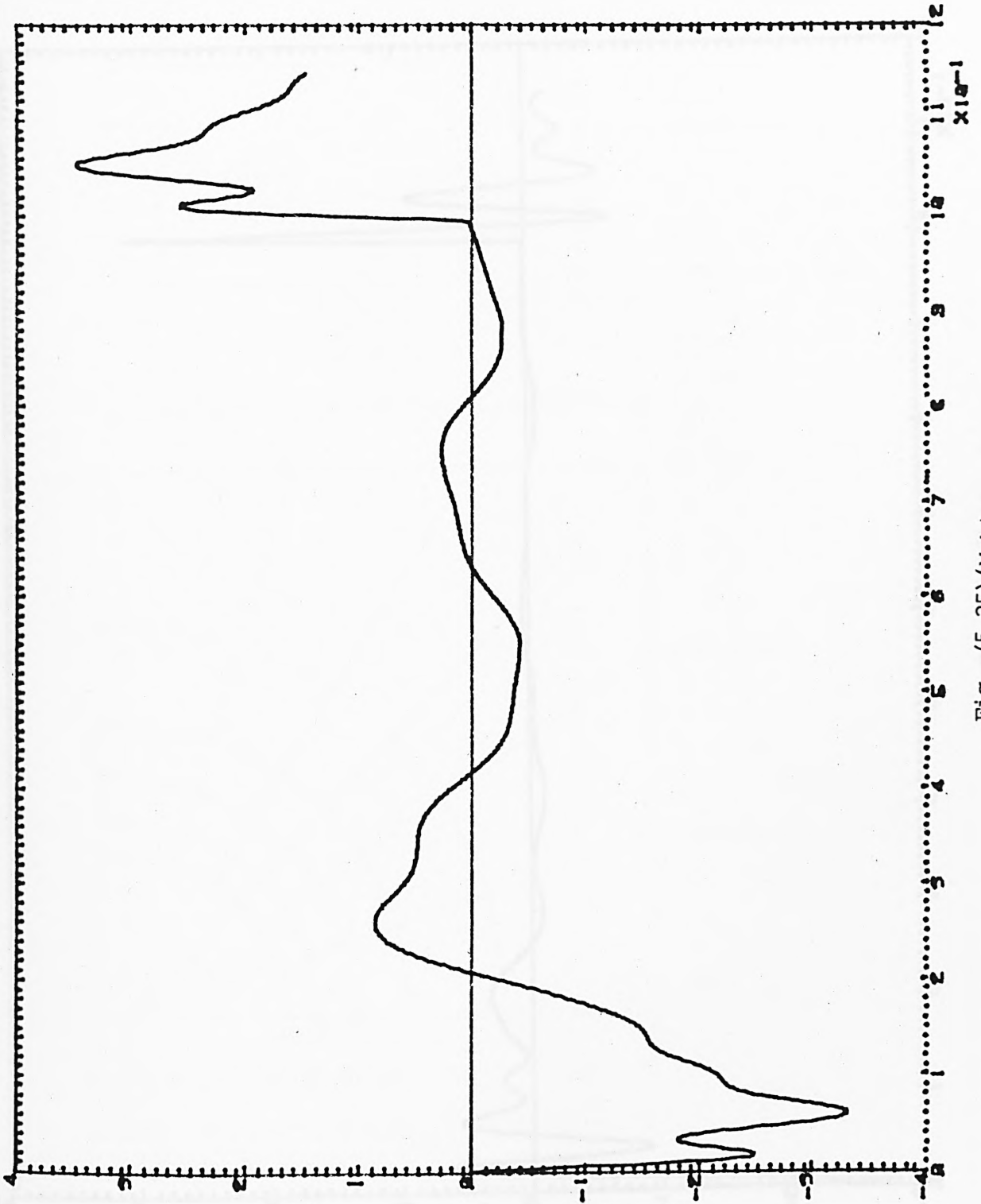


Fig. (5.25) (Vel.)

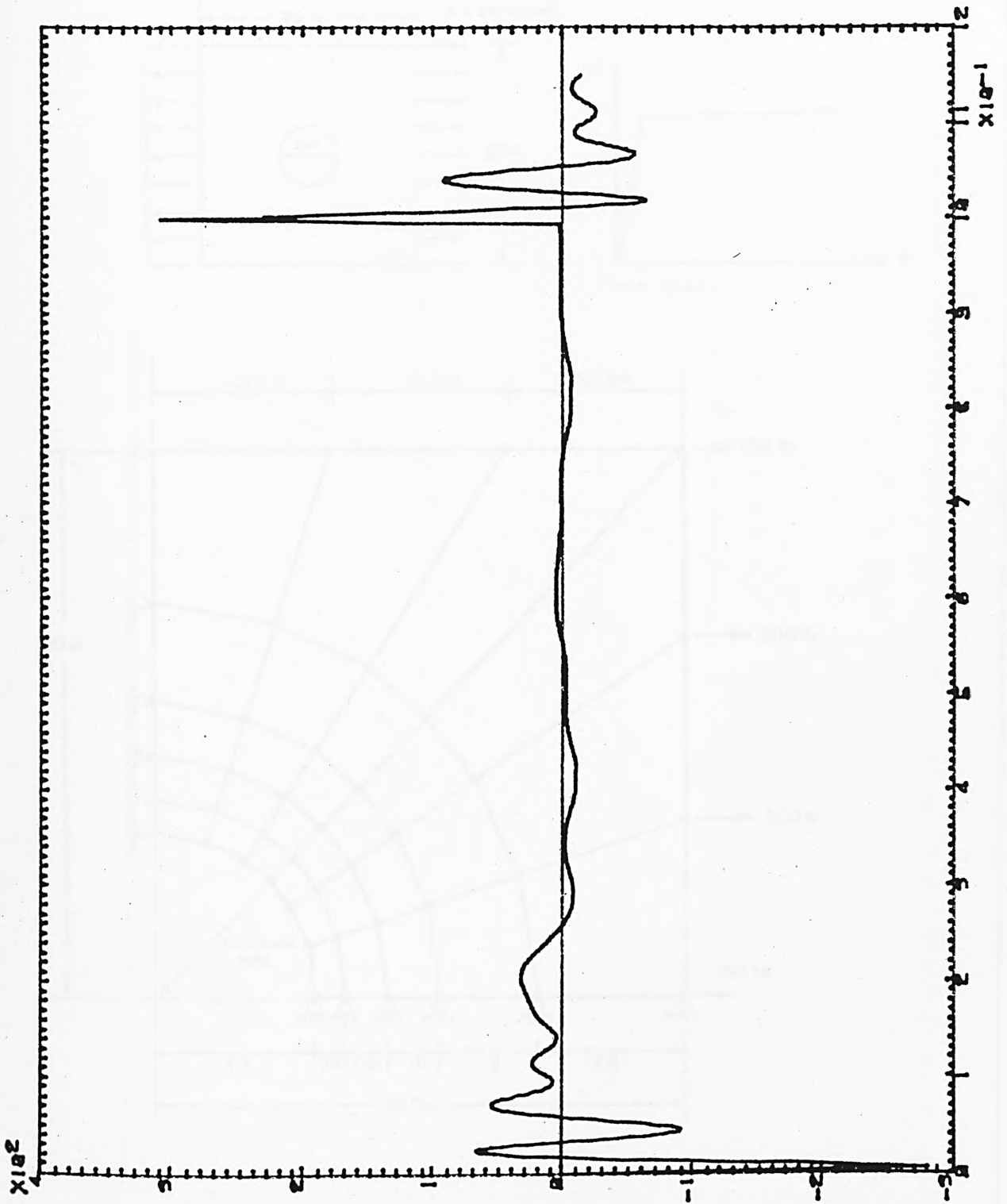


Fig. (5.26) (Acc.)

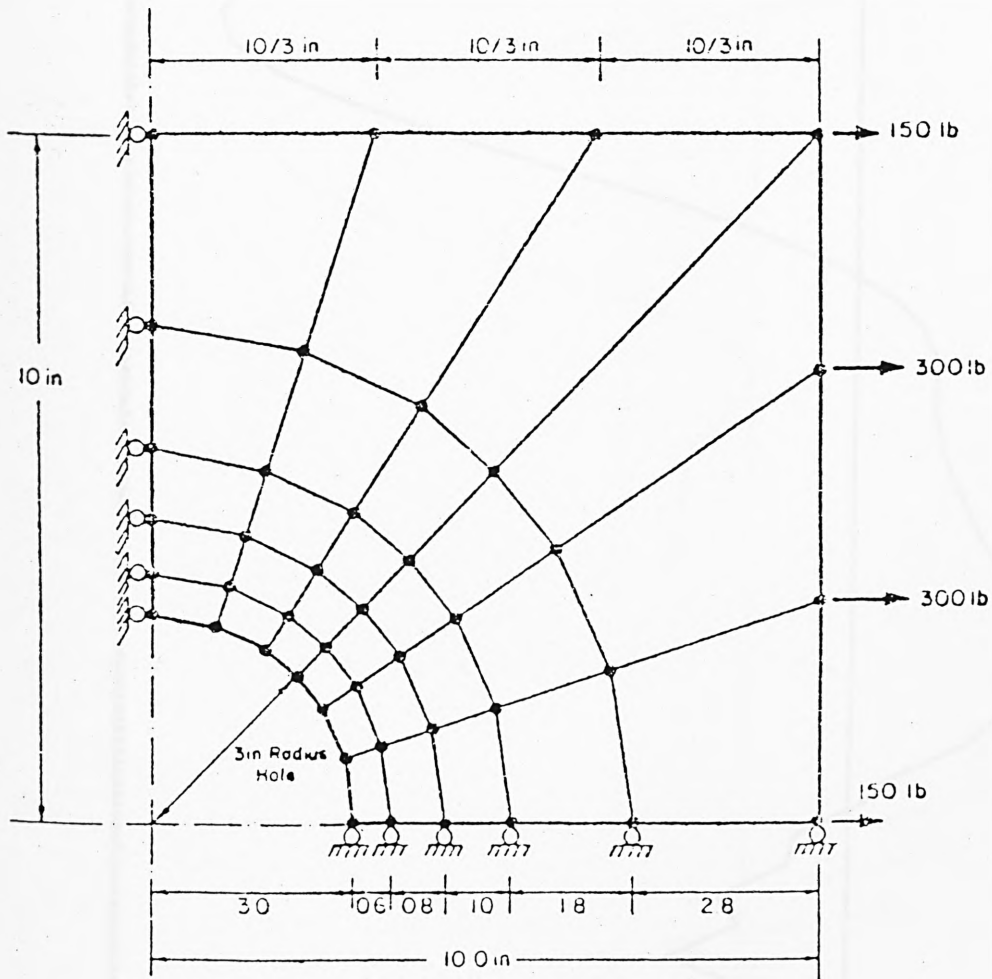
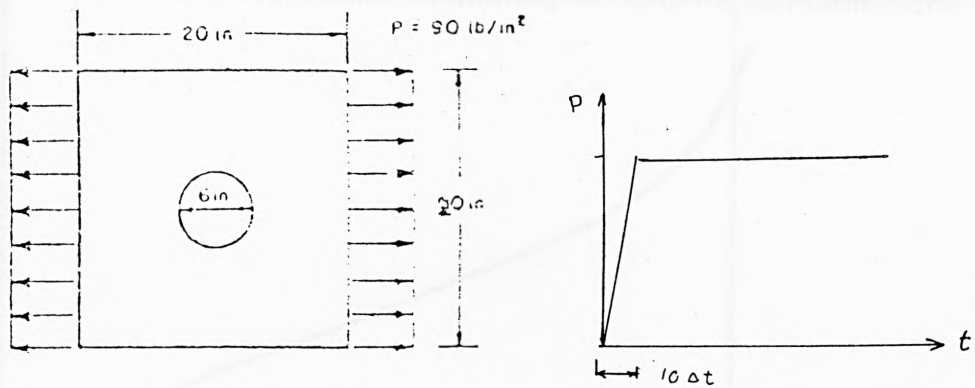
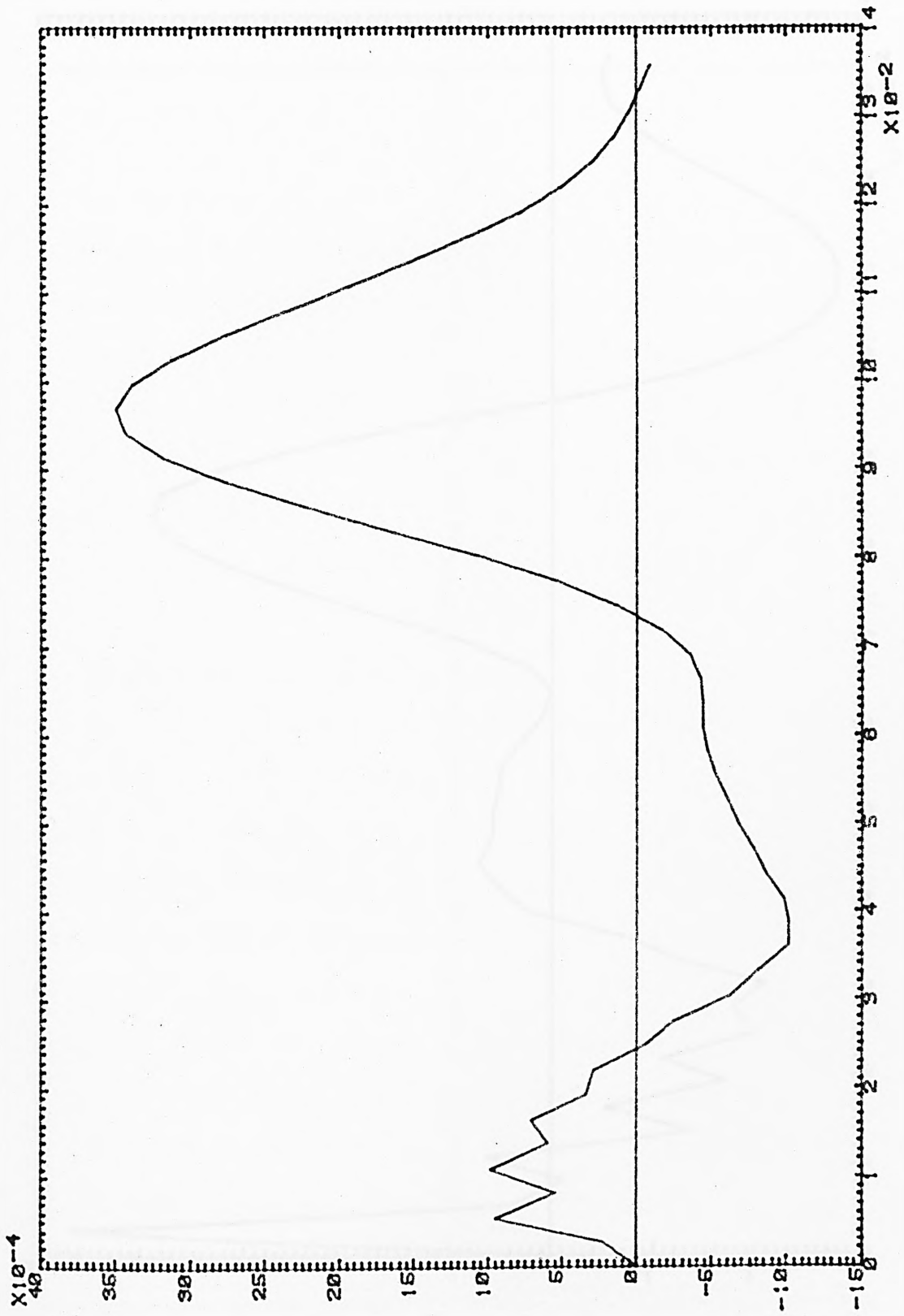


Fig. (5.27) Finite element mesh of rubber sheet with hole



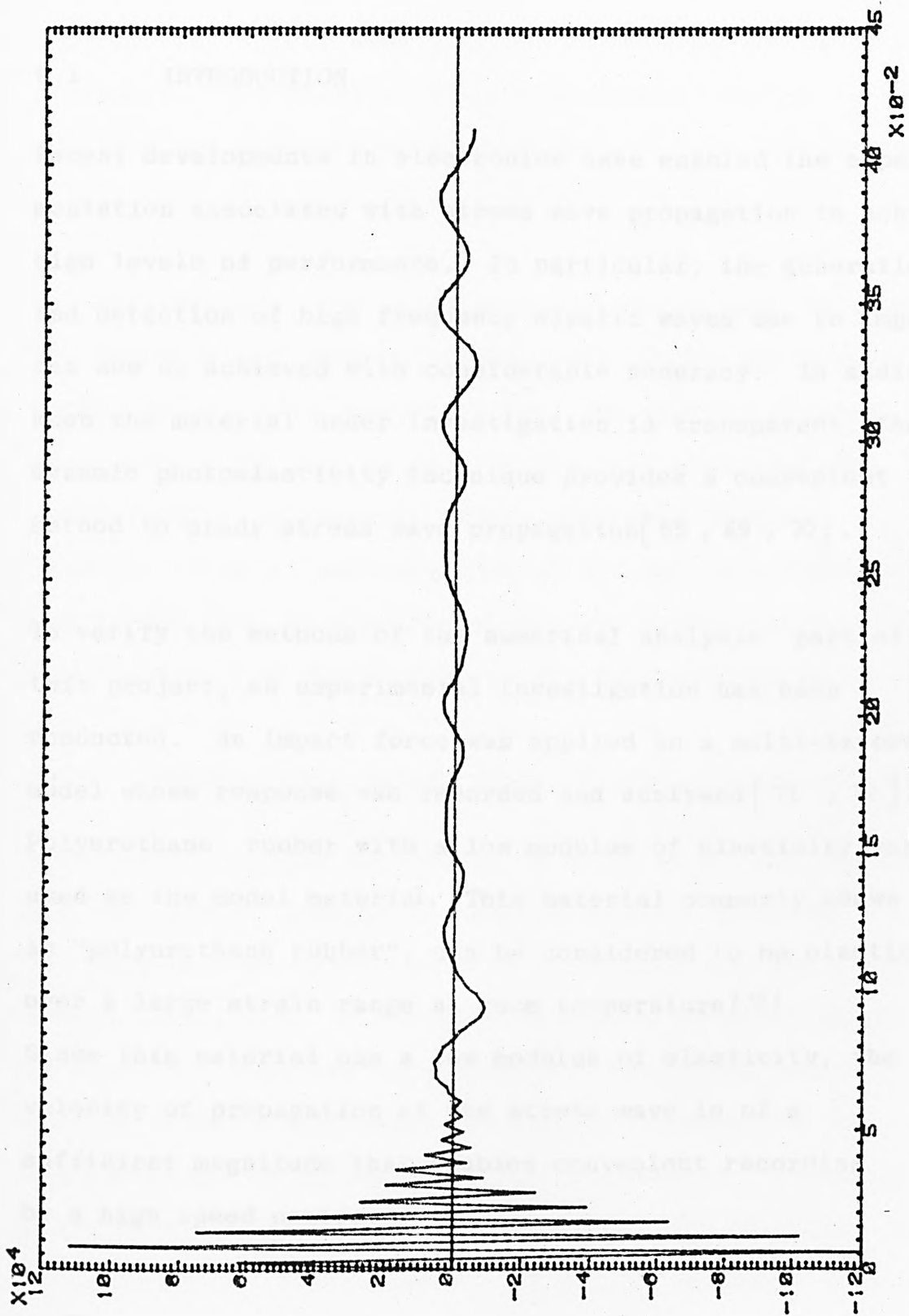
Dynamic response (displacement)

Fig. (5.28)



Dynamic response (velocity)

Fig. (5.29)



Dynamic response (acceleration)

Fig. (5.30)

CHAPTER 6

EXPERIMENTAL INVESTIGATION

6.1 INTRODUCTION

Recent developments in electronics have enabled the experimentation associated with stress wave propagation to achieve high levels of performance. In particular, the generation and detection of high frequency elastic waves due to impact can now be achieved with considerable accuracy. In addition, when the material under investigation is transparent, the dynamic photoelasticity technique provides a convenient method to study stress wave propagation [68 , 69 , 70] .

To verify the methods of the numerical analysis part of this project, an experimental investigation has been conducted. An impact force was applied to a multi-layered model whose response was recorded and analysed [71 , 72] . Polyurethane rubber with a low modulus of elasticity was used as the model material. This material commonly known as "polyurethane rubber", can be considered to be elastic over a large strain range at room temperature [72] . Since this material has a low modulus of elasticity, the velocity of propagation of the stress wave is of a sufficient magnitude that enables convenient recording by a high speed camera.

A brief description of photodynamics will be presented in this chapter since this was the basis of the experimentation scheme. This is followed by a description of the experimental method used in the current study and the test procedure. The results of the experimental work have been analysed and compared with those derived from the numerical solutions.

The objectives of the experimental research were to assess the validity and versatility of the proposed numerical method by means of comparison with the results of model tests and to be able to observe the real behaviour and response of multi-layered models subjected to impact loading. Thus an understanding of the impact phenomena and stress wave propagation action could be obtained, which would assist the development of the numerical model.

6.2 PHOTOELASTICITY AND APPLICATIONS TO ELASTODYNAMICS

Photoelasticity has been found to be an excellent technique for solution of appropriate stress analysis problems.

Not only can the method provide an overall assessment of stress conditions, it can also provide a detailed analysis at a point. Compared to mechanical, electrical and optical strain measurement methods, photomechanics has the advantage of giving an overall assessment of all stress distribution, rather than point-by-point information. This property allows a relatively easy determination of complete

stress fields (direction and magnitude of stress at every point).

In principle, photoelasticity is applicable to most states of stress, but it can be applied most conveniently in plane elasticity. Under these conditions the isochromatic fringes are loci of points of the same maximum shear stress in the plane of plate. By counting the fringes and multiplying their order by the proper calibration constant, the maximum shear stress distribution through the plate can be obtained.

Photoelasticity had been for many years a method limited to determination of static two-dimensional stress distribution. Recently, methods have been found to use the property of the birefringence to solve two-dimensional dynamic problems which may be both cyclic or transient [69 , 70 , 72 , 73]. A brief review of the application of dynamic photoelasticity to each of these areas is given by Dally [74].

6.3 DYNAMIC RECORDING SYSTEMS

Three different recording systems have been developed which give adequate results in dynamic photoelastic studies, the high-speed framing camera, the multiple-spark-gap assembly and the Q-switched laser system. The high-speed framing camera operates with constant-intensity source with an exposure time t_e which varies with framing rate (t_e is

approximately $\frac{1}{3}$ of the interframe interval). The spark gap light source provides an exponentially decaying intensity independent of framing rate with t_e established at the $\frac{1}{3}$ peak intensity points at typically 0.5 μ seconds. Q-switched lasers provide a triangular pulse of light also independent of framing rate; however, the value of t_e measured at the $\frac{1}{3}$ points is typically 0.10 μ sec. The ability of each of these systems to record accurately a dynamic fringe pattern depends upon the stress wave velocity and the stress distribution.

Since the magnitude of the modulus of elasticity of the material of the model was very low, the high-speed framing camera was used to record the dynamic fringe pattern. The type of the camera and its technical properties will be represented in the next section.

6.3.1 Rotating Prism High-Speed Camera

The HYCAM is a new concept of high-speed camera design. A single shaft carries the film transport sprocket and the rotating prism and segmented shutter produce good picture quality. The straight forward simplicity of the HYCAM design provides advanced technical performance at a reasonable cost. The important technical features concerning this camera are as follows:

Film sizes: 16 mm any pitch

Frame rates: 10-10,000 pictures per second full frame
20-20,000 pictures per second half frame
40-40,000 pictures per second ribbon frame
Stop/start operation to half speed

Film capacity: 100,400 and 2000 ft bodies

Lens mount: 'C' type standard lenses

Accessories: Timing light generator

Eastman 4-X negative film which is an extremely high speed negative material of medium graininess was used. A Gordon timing light generator was used to obtain time characteristics of each frame.

6.3.2 Timing Light Generator

A Gordon timing light generator was used to provide high resolution film marks with precise timing accuracy. This unit is portable and designed to operate using a mains supply or internal batteries. The technical specifications are as follows:

Accuracy: Timing channel $\pm 0.01\%$ (0-35°C)

Event operates within 1 milliseconds frame
initiation

Time marks : Switched choice of:

- a) One pulse every 10 ms (100 Hz)
- b) One pulse every 1 ms (1000 Hz)

- c) One pulse every 1 ms with one pulse every 0.1 ms between the ninth and tenth.

Event mark: Ten pulses of 0.1 ms separation to make an effective 1 ms mark

Film sensitivity suitable for use with 400-400 A.S.A

Power supply 220-250 V 50-60 Hz at 5 VA nom.

6.3.3 Fidelity of Dynamic Recording

The theory for dynamic exposure of a fringe pattern recorded in a polariscope was established by Dally, Henzi and Lewis [75] for a plane stress wave travelling with the velocity C in the x direction. The difference in the principal stresses in this plane stress wave was denoted as $\tau(x,t)$ and the instantaneous intensity of light emerging from the polariscope was identified as the transmission coefficient $T(x,t)$ given by

$$T(x, - Ct) = \frac{T_0}{2} \{1 + \cos[\frac{2\pi h}{f} \tau(x - Ct)]\} \dots \dots (6.1)$$

The record of the dynamic fringe pattern which is characterized by the transmission coefficient is strongly dependent on the light source and camera combination which also controls the recording intensity, $I(t)$. The exposure

of the film $E(x)$ is represented by the integral relation [70] given by

$$E(x) = \int_0^{\infty} I(t) T(x - ct) dt$$

6.4 EXPERIMENTAL SCHEME

The details of the experimental procedure are discussed after the following section.

6.4.1 The Impact Force

Basically, the apparatus consists of a means of releasing a steel cylinder from a predetermined height above the model. The release was accomplished by an electromagnetic device. This drop mechanism was carefully examined and tested to ensure that no significant rotation, initial velocity and acceleration were imparted to the impacting mass.

The impacted structure (model) was supported on a surface plate which could be levelled to significant accuracy to that of the cylinder (falling mass) would bounce perpendicular to the impact surface, Figure (6.1). The impact force was measured in every test using a quartz force transducer, Type (9203 Kistler), which has a very high resolution, high resonant frequency and small dimensions. Table (6.1) gives the technical properties of the force

transducer. The output of the force transducer was calibrated and recorded on a tape recorder and oscillograph by using a charge amplifier.

TABLE (6.1) - TECHNICAL DATA

Max, measuring range	KP	± 50
Resolution	P	0.1
Max force	KP	± 50
Sensitivity	PC/KP	480
Deformation at max load	μm	12
Resonant frequency	KHz	27
Rise-time	μs	15
Linearity	%	± 1
Weight	gm	13

6.4.2 Material Properties

Five materials with different moduli of elasticity were used in the manufacture of the models. Four of these have low moduli compared with the fifth. All of these materials were photoelastic and have high stress sensitivity. They were free from any measurable time-edge effects and did not exhibit viscous flow at room temperature [71].

The materials R-300, R-450, R-600 and R-Low.E have low moduli of elasticity and, therefore, the velocity of propagation of stress waves can be conveniently observed. The procedures followed for the determination of the

modulii of elasticity, Poisson's ratio and unit fringe value are presented in the following sections with the results for the five materials.

(a) Modulus of Elasticity and Poisson's Ratio

For the materials R-300, R-450, R-600 and R-Low.E, Young's modulus has been obtained from the standard tension test.

For the fifth material R-high.E the modulus of elasticity of the model specimen was measured by the flexure of a cantilever calibration beam and was calculated from the following expression

$$E = K \frac{P}{\delta} \quad \dots \quad \dots \quad \dots \quad \dots \quad \dots \quad \dots \quad (6.2)$$

where P is the concentrated load applied at the tip of the cantilever beam

δ is the measured deflection of the calibration beam

K is a proportionality factor depending on the dimension of the beam and the position of measurement.

The observed load-deflection curves are shown in Figure(6.3,4) . The optical properties and the characteristic acoustic velocities of the materials used for the models depend on an accurate knowledge of

the three quantities E , ρ and γ . These values were obtained accurately by the expedient methods with their variation with strain rate.

It was generally easier and more reliable to measure the wave velocities directly to determine the dynamic modulus of elasticity. At least two independent means were used to measure these velocities, (in bars or plates or both). The wave velocities were obtained by using an oscilloscope and by using a digital counter (PUNDET). The time required for a wave to pass between two strain gauges, or for a reflected wave to return to a single gauge, was measured. Although the variation between the dynamic and static moduli of elasticity is very small, the difference was used to obtain the dynamic unit fringe value of these materials Figure (6.5) .

The results of the tests conducted on the five different materials are shown in Table (6.2) . Poisson's ratio has also been deduced from these tests. The observed stress-strain curves for the five materials are shown in Figures (6.3,4).

(b) Unit Fringe Value

Two inch diameter disks were used in the standard diametral compression test to determine the unit fringe value. In the traditional point-matching approach, the fringe order at the centre of the specimen is compared with the theoretical value of the maximum shear stress at the same point. The value of the fringe constant required to match the two was then computed. The theoretical and the experimental distribution of the maximum shear stress is not particularly good at the centre of the specimen [76]. However, there is a good agreement between theoretical and experimental results in the region from 0.3 R to 0.5 R. Where R is the radius of the circular disc.

The tests have been performed by applying the load in increments and the standard specimen was marked with a surface grid marked grid. Photographs were taken of the results which have been analysed using the approach suggested by Robert [77].

The analysis of the results can be formulated mathematically as follows

$$N(x,y) = \frac{t}{f_a} G(x,y) + E(x,y) \quad \dots \quad \dots \quad \dots \quad (6.3)$$

where N = photoelastic fringe order
x,y = cartesian coordinates
t = model thickness

$\bar{G}(x,y)$ = the theoretical solution for the difference of the principal stresses in cartesian coordinates

$E(x,y)$ = an error term included to account for any residual birefringence field.

$$\text{Assume } E(x,y) = Ax + By + C \quad \dots \quad \dots \quad \dots \quad \dots \quad (6.4)$$

It has been stated by Frocht [68] for a disc in diametral compression

$$t \times \bar{G}(x,y) = \frac{4PR}{\pi} \times \frac{R^2 - (x^2 + y^2)}{(x^2 + y^2 + R^2) - 4y^2R^2} \quad \dots \quad (6.5)$$

that is for any point having coordinates (x_i, y_i)

Equation (6.3) can be written as

$$N_i(x_i, y_i) = \frac{1}{f_a} G_i(x_i, y_i) + Ax_i + By_i + C \quad \dots \quad (6.6)$$

For M points which are arbitrarily selected over the field (M , 4), an over-determined system of linear equations of the following forms result

$$N_1 = \left(\frac{1}{f_a}\right)G_1 + Ax_1 + By_1 + C$$

$$N_2 = \left(\frac{1}{f_a}\right)G_2 + Ax_2 + By_2 + C$$

.....

.....

.....

$$N_m = \left(\frac{1}{f_a}\right)G_m + Ax_m + By_m + C \quad \dots \quad \dots \quad \dots \quad \dots \quad (6.7)$$

In matrix notation

$$[N] = [a] [Z] \quad \dots \quad \dots \quad \dots \quad \dots \quad \dots \quad \dots \quad (6.8)$$

Multiplication of the last equation from the left by the transpose of the coefficient matrix, i.e, $[a]^T$ gives

$$[a]^T [N] = [a]^T [a] [Z] \quad \dots \quad \dots \quad \dots \quad \dots \quad \dots \quad (6.9)$$

$$[a]^T [N] = [C] [Z] \quad \dots \quad \dots \quad \dots \quad \dots \quad \dots \quad (6.10)$$

If matrix $[C]$ has an inverse, the solution of Equation (6.10) is given by

$$[Z] = [C]^{-1} [a]^T [N] \quad \dots \quad \dots \quad \dots \quad \dots \quad \dots \quad (6.11)$$

In the classical least-squares approach an expression for the cumulative error E has the form

$$E = \sum_{i=1}^M \left[\left(\frac{1}{f_a} \right) G(x_i, y_i) + Ax_i + Bx_i + C \dots N_i \right]^2 \quad (6.12)$$

The least-square criteria requires that

$$\frac{\partial E}{\partial \left(\frac{1}{f_a} \right)} = \frac{\partial E}{\partial A} = \frac{\partial E}{\partial B} = \frac{\partial E}{\partial C} = 0 \quad \dots \quad \dots \quad \dots \quad \dots \quad (6.13)$$

Many results have been obtained using the stereocomparator to read every photo at each increment of load. A computer program has been written to analyse these data using the

algorithm which is equivalent to the determination of the solution of equations (6.7) in the least squares method. A flow chart of the computer program is given in Figure (6.17) and the calibration disc results are given in Table (6.2) for the five materials.

(b) Damping Properties

The half-power method was used to investigate the values of damping ratio of identical specimens as well as the model. This and the other methods were discussed in Chapter 3. The major advantage of this free vibration method is that equipment and instrumentation requirements are minimal.

The results of these tests are given in Figure (6.18) and Table (6.2). From these results it was expected that the damping ratio of the model is higher than those of the materials. According to the results of experiment the difference is insignificant.

6.5 THE INVESTIGATION OF THE ISOCLINICS

An isoclinic is the locus of points along which the principal stresses have parallel directions, as shown in figure (6.6). The parameter is measured from the positive end of the x axis in a counterclockwise direction to the nearer principal stress. Further, since at a given point there exists in general only one definite set of principal stresses, it follows that only one isoclinic can pass through a given point, unless the particular point happens to be an isotropic point.

By removing the two $\frac{1}{4}$ wave plates from the field of view, the circular polariscope was converted to a plane polariscope. A suitable dead load was used so that isoclinics would not be obscured by isochromatic fringes. A dark field was maintained and the polarizer and analyzer elements coupled. With the rotation of this unit, relative to a reference, the isoclinics were obtained at various values of isoclinic parameter.

Photographs were taken to the model at the various values of isoclinic parameters as shown in Figure (6.6). Using the stereocomparator to read every photo, the results have been obtained and recorded. Isoclinic parameters at certain points on the model have been obtained using the procedure discussed in Section (6.8).

6.6 MODEL MANUFACTURING AND ITS PROPERTIES

The material which was used in manufacturing the model is polyurethane rubber, commonly known as urethane [71]. The material, which is cast from a mix forming a low modulus photoelastic medium having good clarity, high fringe/stress sensitivity and is free from time-edge and machining stresses. The fringe/strain sensitivity is, however, poor. More information about the material is given in reference [73 & 74]. The speed of the camera 10,000 frames/sec required materials of moduli of elasticity ranging between 200 - 600 N/cm².

Five models were manufactured of dimensions 15.24 x 15.24 cm. Precautions have been taken to minimize any residual stresses by applying the correct method of machining and by using the suitable adhesive material.

Each model was mounted in a frame and it was noted that plane lateral deflection normal to the impact force did not occur. Thus, plane sections remained plane.

6.7 EXPERIMENTAL PROCEDURE

In accordance with the objectives of the research, the response of the model was determined by applying an impact load. The shapes of the impact pulses which were applied to the models are shown in figure (6.7).

The properties of the materials which have been used were determined. The calibration tests of the equipments were conducted. Certain precautions were adopted to ensure the impact event and the photographic recording coincided. The test procedure adopted for each of the five models was similar. Preliminary tests were carried out on each model to check the operation of the loading system and instrumentation. Five high speed films were taken and processed by specialists. The high speed was ranged between 8000 to 10000 frames per second, which is the maximum speed of the available camera. This film speed is sufficient to record the velocity of the propagating wave. Overall views of the models, layout of the instrumentation and loading system can be seen in figure(6.1).

The models were instrumented with surface strain gauges in a specified points after the photoelasticity investigation to check the shape of the response by using the same impact force, the response of the points in which the gauges were bonded was obtained at 12 points and recorded on a tape recorder. A check has been done for the shape of the response, as well as the damping coefficient at those points. The arrangements of the strain gauges of the model tests is shown in figure (6.15). The impact load and the response of the strain gauges are shown in figures (6.15,16).

6.8 Processing of Photoelastic Results

High speed films were processed and then examined using a stereocomparator. This technique was chosen to provide accurate results and a convenient method to record results for further analysis. Control points on each film were recorded for transformation of axes and for calculating the scale factor. The coordinates of reasonable number points at centre line of each fringe were recorded for each frame. A computer program was written to analyse the recorded results. This program is to be discussed later.

6.9 Interpretation of Photoelastic Results

The interpretation of photoelastic data can be difficult and time consuming. This section is concerned with the assessment of isoclinics and isochromatics. The results of these experiments are compared with those of the numerical analysis. The following stages have been considered.

- (a) The definition of the area to be analyzed and the sub-division of this area into boundary zones.
- (b) The selection and spacing of lines along which data was to be collected.
- (c) The collection of isoclinics data.

(d) The collection of isochromatic data.

(e) The choice of points for which solution was required.

(f) The computer solution.

The information obtained using the photoelastic method consists of the principal stress difference ($\sigma_1 - \sigma_2$) and the direction of the principal stresses (isoclinic). Usually, separation of stresses refers to the individual determination of σ_1 and σ_2 and their respective directions or the determination of the stress components σ_x, σ_y and τ_{xy} referred to a given system of coordinates. There are several methods for the separation of stresses [78 & 79]. The method used in this project is based on the integration of the differential equations of equilibrium which, for zero body forces and two-dimensional problems are:

$$\frac{\partial \sigma_x}{\partial x} + \frac{\partial \tau_{yx}}{\partial y} = 0 \quad \dots \quad \dots \quad \dots \quad \dots \quad \dots \quad \dots \quad (6.14)$$

$$\frac{\partial \tau_{xy}}{\partial x} + \frac{\partial \sigma_y}{\partial y} = 0 \quad \dots \quad \dots \quad \dots \quad \dots \quad \dots \quad \dots \quad (6.15)$$

Integration gives

$$\sigma_x = - \int_{x_0}^x \frac{\partial \tau_{yx}}{\partial y} dx \quad \dots \quad \dots \quad \dots \quad \dots \quad \dots \quad (6.16)$$

$$\sigma_y = - \int_{y_0}^y \frac{\partial \tau_{xy}}{\partial x} dy \quad \dots \quad \dots \quad \dots \quad \dots \quad \dots \quad (6.17)$$

OR in finite difference form

$$\sigma_x = (\sigma_x)_o - \sum_{x_o}^x \Delta\tau_{yx} \frac{\Delta x}{\Delta y} \quad \dots \quad \dots \quad \dots \quad \dots (6.18)$$

$$\sigma_y = (\sigma_y)_o - \sum_{y_o}^y \Delta\tau_{xy} \frac{\Delta y}{\Delta x} \quad \dots \quad \dots \quad \dots \quad \dots (6.19)$$

From Mohr's circle, if θ_1 is the angle measured from the axis to the σ_1 direction in the counterclockwise direction

$$\tau_{xy} = \frac{\sigma_1 - \sigma_2}{2} \sin 2\theta_1 \quad \dots \quad \dots \quad \dots \quad \dots (6.20)$$

$$\sigma_x = \sigma_y + (\sigma_1 - \sigma_2) \cos 2\theta_1 \quad \dots \quad \dots \quad \dots \quad \dots (6.21)$$

Also, the values of σ_1 and σ_2 are given by

$$\sigma_1 = \frac{\sigma_x + \sigma_y}{2} + \frac{(\sigma_1 - \sigma_2)}{2} \quad \dots \quad \dots \quad \dots \quad \dots (6.22)$$

$$\sigma_2 = \frac{\sigma_x + \sigma_y}{2} - \frac{(\sigma_1 - \sigma_2)}{2} \quad \dots \quad \dots \quad \dots \quad \dots (6.23)$$

The inclination of maximum shear stress directions to the positive axis θ_x , θ_y as follows

$$\theta_x = \theta_1 + \left(\frac{\pi}{4}\right) \quad \dots \quad \dots \quad \dots \quad \dots \quad \dots (6.24)$$

$$\theta_y = \theta_1 + \left(\frac{-\pi}{4}\right) \quad \dots \quad \dots \quad \dots \quad \dots \quad \dots (6.25)$$

where θ_1 is the angle which related to the isoclinic parameter; and $(\sigma_1 - \sigma_2)$ is the difference in principal stresses and is related to the fringe order by the calibration constant.

6.10 THEORY OF COMPUTER DATA ANALYSIS OF EXPERIMENTS AND THE ANALYSIS OF EXPERIMENTAL RESULTS

A computer program was written to calculate the stresses at a specified number of points on the model. A flow chart of the program is given in figure(6.19) . The theory of this program has been discussed in section (6.9).

Further explanation will be given to show how the analysis has been conducted.

Figure (6.20a) shows a photo of frame for which information has been obtained concerning the isoclinic and isochromatic values. The computer program initially forms a polynomial $f(\text{isoch.}, y)$ along the centre line of each frame of the film. The coefficients of the polynomial are obtained at points $(0, y_1)$, $(0, y_2)$... $(0, y_n)$ which represents the isochromatic values at those points. The same procedure was followed for isoclinic values.

Noting that at two points E and F which are symmetrically located with respect to the axis of symmetry, figure (6.20a) the shear stresses are equal numerically but are of opposite signs. Hence, the difference $\Delta\tau_{yx}$ between the vertical shear stresses at F and E is

$$\tau_{yx} = (\tau_{yx})_f - (\tau_{yx})_e = 2(\tau_{yx})_f \quad \dots \quad \dots \quad \dots (6.26)$$

In order to determine $\Delta\tau_{yx}$ therefore, it is necessary to determine only the vertical shear stresses at one section parallel to the axis of symmetry. The steps essential to the solution of this problems are

$$(1) \quad \frac{\sigma_1 - \sigma_2}{2} \quad \text{across Section AB}$$

$$(2) \quad \tau_{yx} \quad \text{at Section AB}$$

$$(3) \quad \Delta\tau_{yx} = 2\tau_{yx}$$

$$(4) \quad (\sigma_y)_i = (\sigma_y)_o - \int_0^i \Delta\tau_{yx} \left(\frac{\Delta y}{\Delta x}\right)$$

$$(5) \quad \sigma_x = (\sigma_1 - \sigma_2) + \sigma_y$$

The normal stresses across horizontal lines can be deduced from the results for σ_x and σ_y at the centre line using the following formulae.

$$(\sigma_x)_i = (\sigma_x)_o - \int_0^i \Delta\tau_{xy} \left(\frac{\Delta x}{\Delta y}\right)$$

$$(\sigma_y)_i = \sigma_x - \sqrt{(\sigma_1 - \sigma_2)^2 - 4\tau_{xy}^2}$$

6.11 THEORETICAL SOLUTIONS

The models were analysed by the finite element method of analysis using the DFEM program. The general theory has been derived and discussed in previous chapters.

For each impact test, the response of the model was recorded by high speed film and the impact force was recorded on an oscillograph and also on a tape recorder. The recorded pulses were used as the impact forces for the computed analysis of the models. The output of the computer program provides the dynamic response of the model at each node.

The computed results for the shear stresses at selected nodes have been compared with those obtained from the experimental investigation.

6.12 DISCUSSION OF EXPERIMENTAL RESULTS

The preliminary test concerning the recording of the impact force and intensity of light showed perfect results. The models which have the same configuration are shown in Figure (6.9). Impact forces recorded by the method discussed in Section (6.4.1) are given in Figure (6.7).

The material of model 1 was R-300. The results indicate good correspondence between the measured and calculated stresses. The dimensions of the model showed that wave reflection from the free edges would not interfere with

the waves at the instant they were being photographed. In practice, the time of the impact of aircraft landing is greater than the experiment impact time.

In test number 2, the model had a nominal thickness of 0.61 cm. The materials were R-300, R-450 and R-600 with the low-modulus material as the top, Figure (6.9)). These results can be sharpened by photographic techniques related to equidensity methods [80, 81].

The models numbers 3 and 4 were tested to show the effect of the interface. Figure (6.9), shows the two models. The results of these two tests will be compared and discussed in the next section. Test number 5 was conducted by the model of R-300, R-600 and R-450 with R-300 as the top layer.

6.13 COMPARISON OF THE THEORETICAL AND EXPERIMENTAL RESULTS

The values obtained from the experimental test on the models numbers 3 and 4 will now be compared with those predicted numerically by the DFEM program. Samples from the experimental results are given in Appendix IV. Shear stresses at nodes numbers 7, 17, 27, 37, 47, 57 and 67 on the centre line of the model and nodes numbers 9, 18, 29, 38, 49, 58 and 69 at a distance of 2.54 cm from the centre line were obtained numerically and are shown in Figures (6. 24 - 6 . 37).

In the comparison of results obtained from the test on model 3, the shear stresses at the specified points were located on the corresponding graphs obtained from the numerical solutions.

In test number 4, the differences between the experimental and theoretical results was expected. These differences ave been discussed in Chapter (3) and are caused by the interface between the layers Tables (6.3,4).

The observed results of model 3 indicate good correspondence between the experimental and calculated stresses. The finite element solution provides a better correlation with the experimental results when the transmitted and reflected stresses have been considered in the numerical analysis.

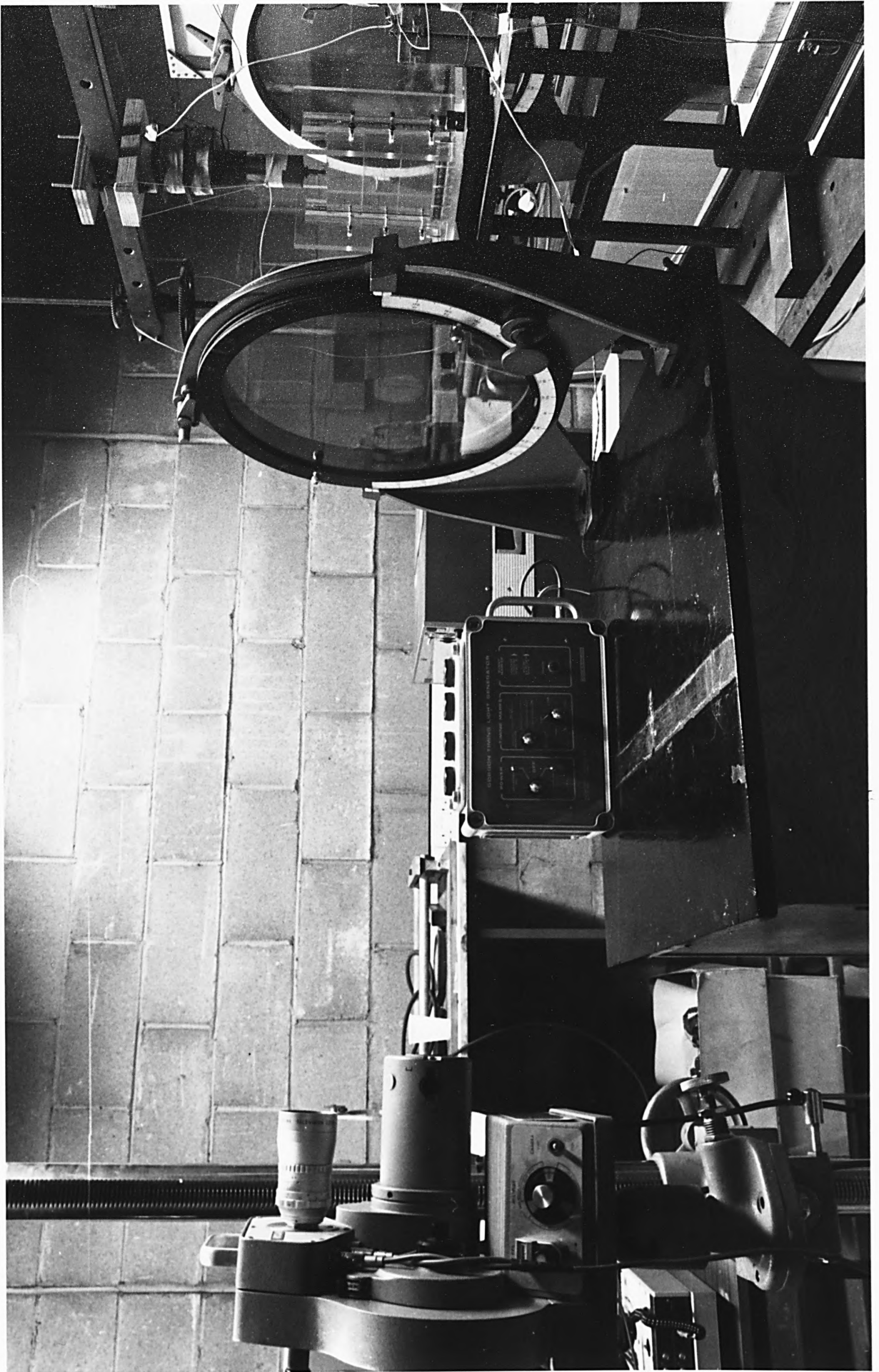


Fig. (6.1) Layout

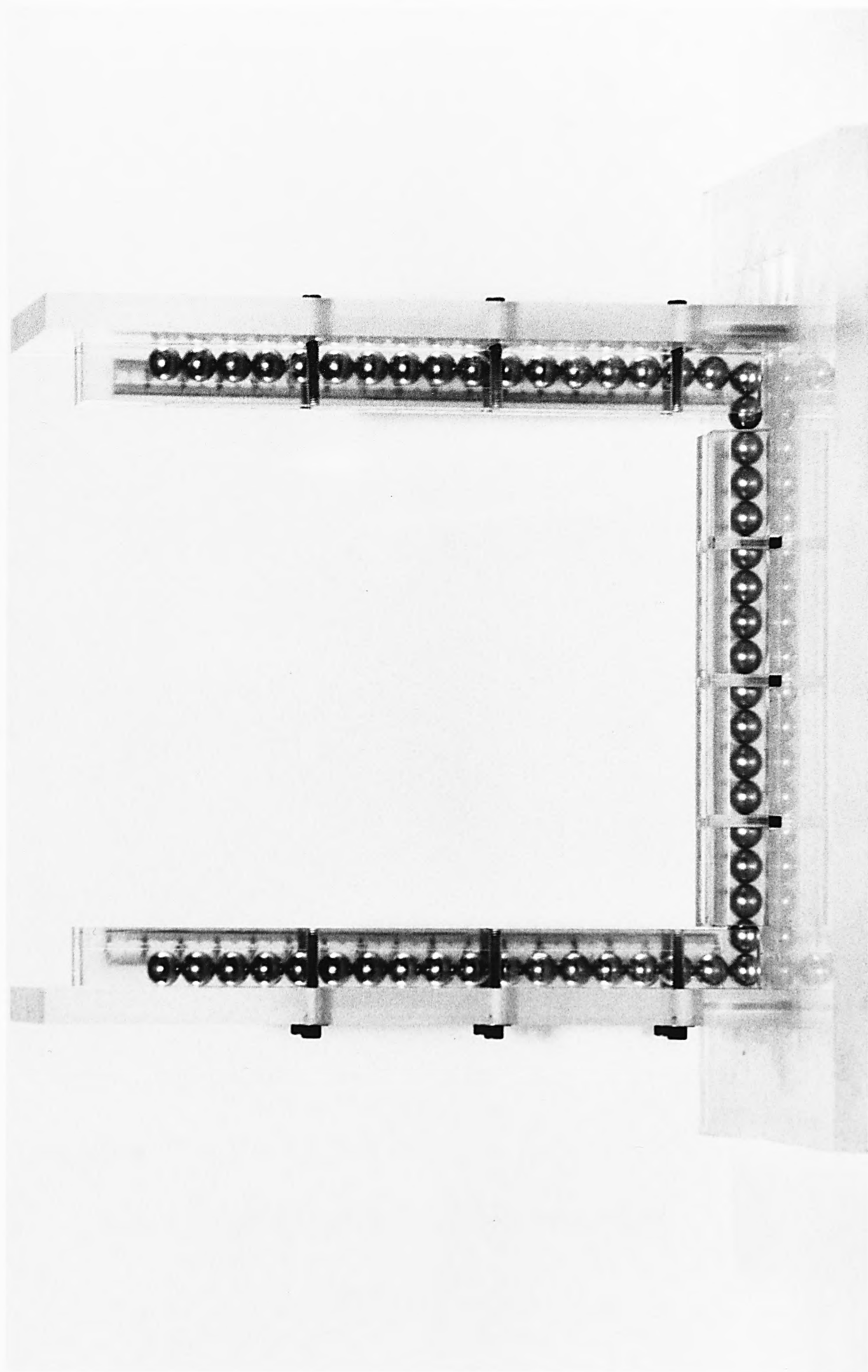


Fig. (6.2) Model 1

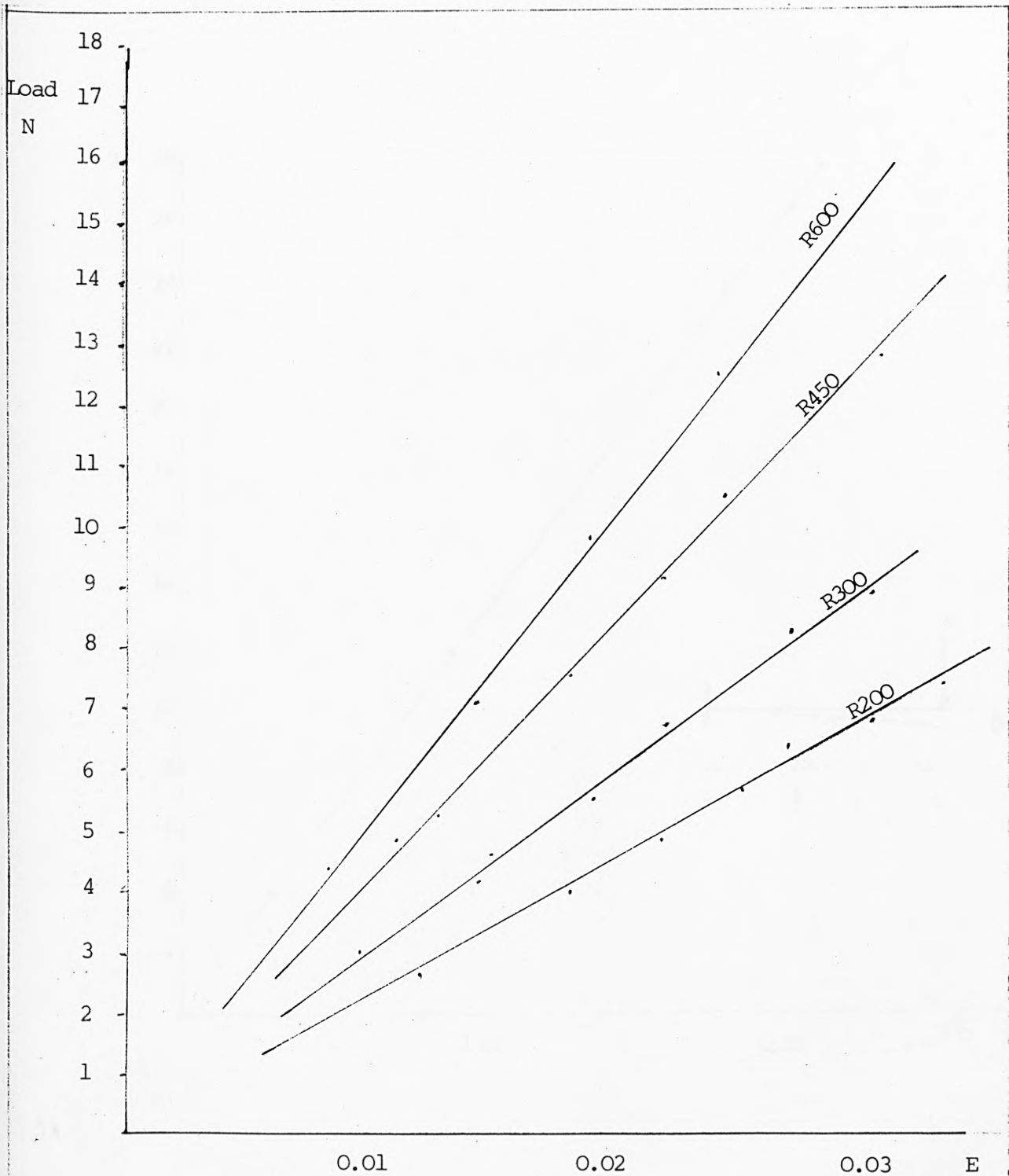
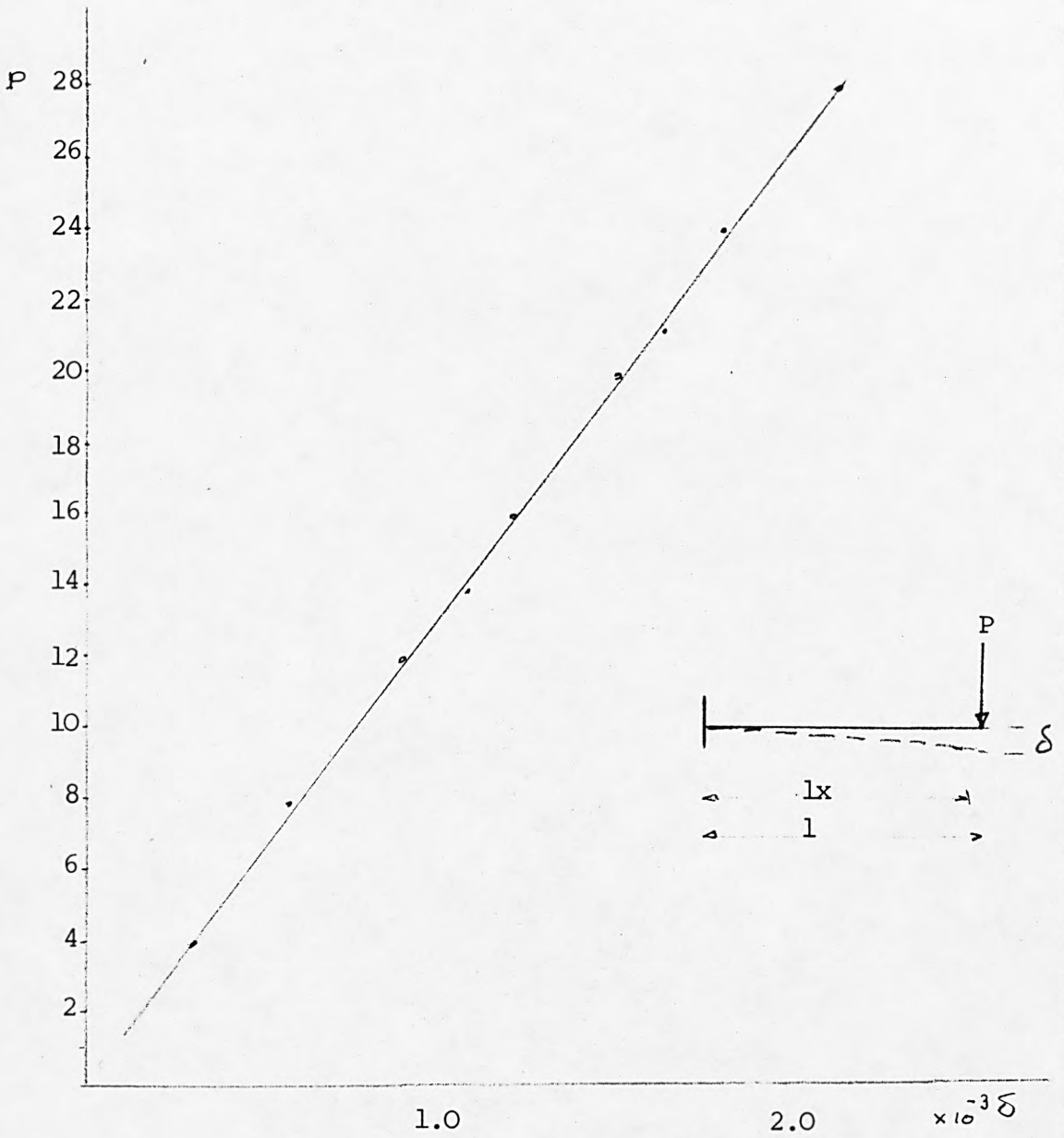


Fig. (6.3) Young's Modulus of low-modulus material



$$E = 2839.918 \text{ N/cm}^2$$

Fig. (6.4) Load deflection model R-high modulus material

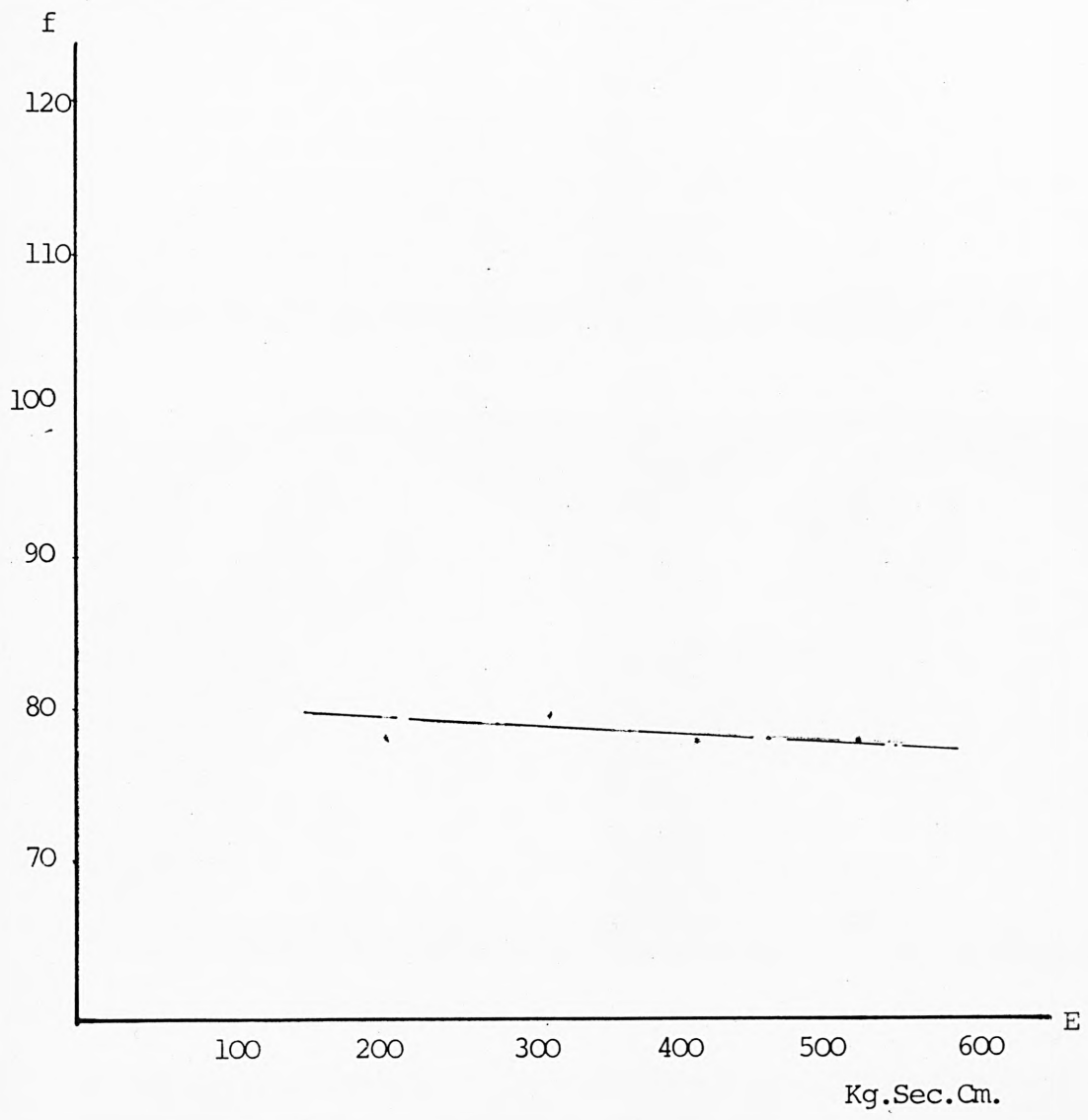


Fig. (6.5) Dynamic fringe constant, f for low-modulus materials.

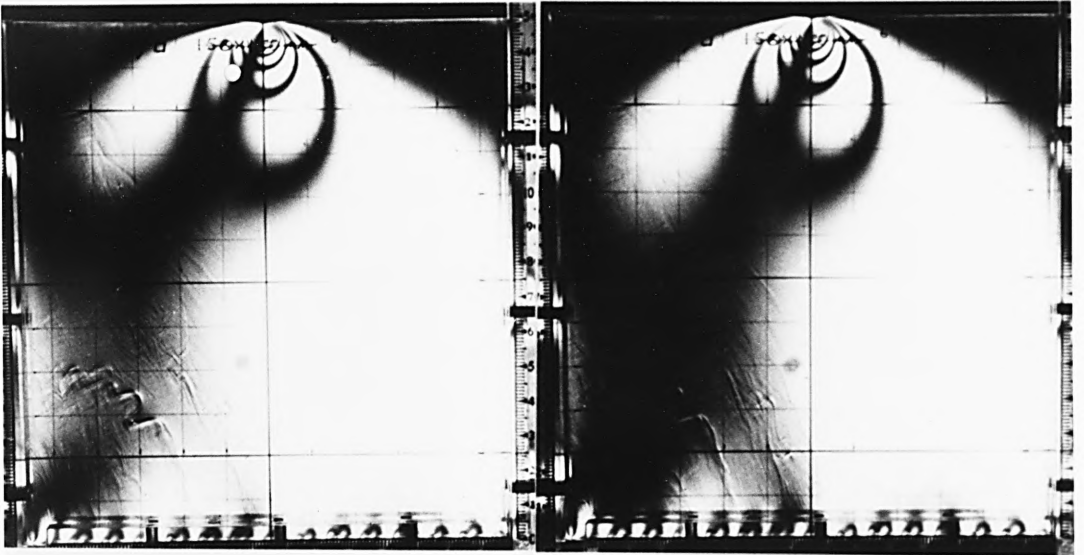
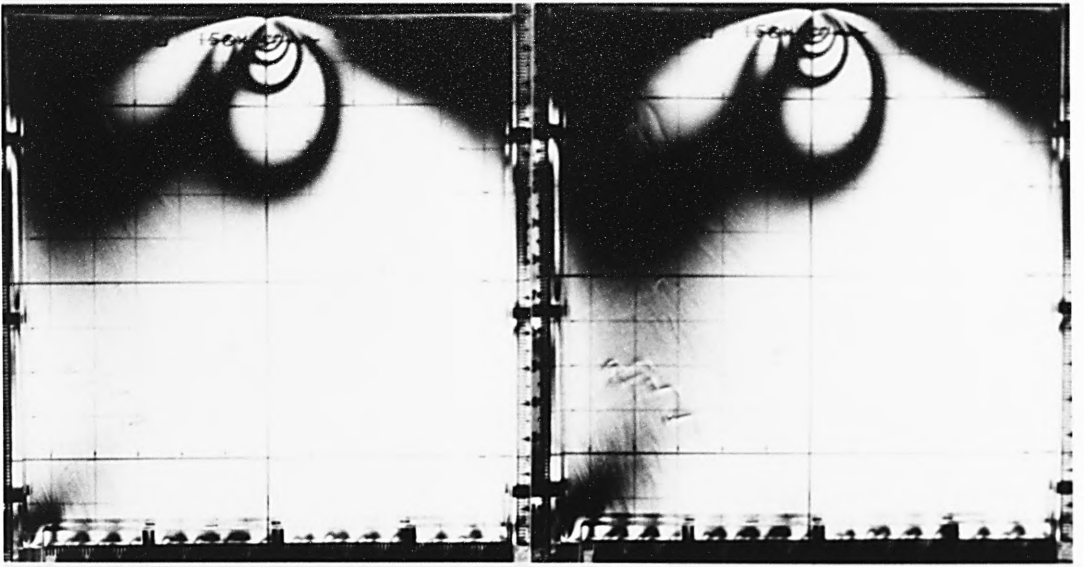


Fig. (6.6) Isoclinic values (sample)

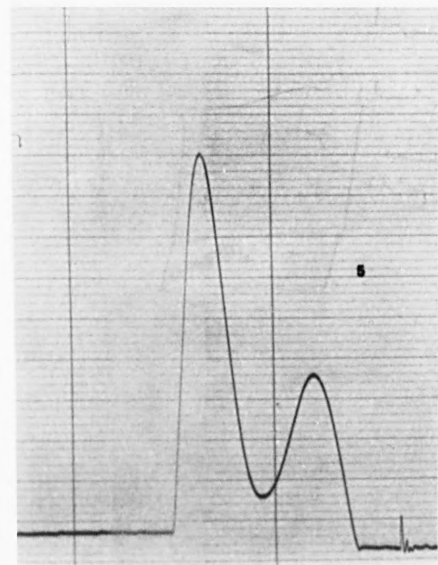
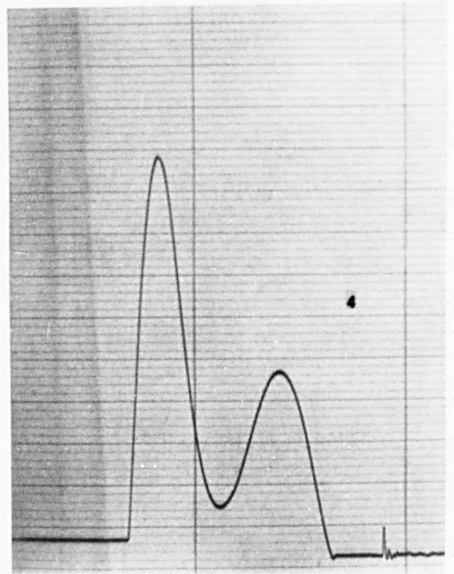
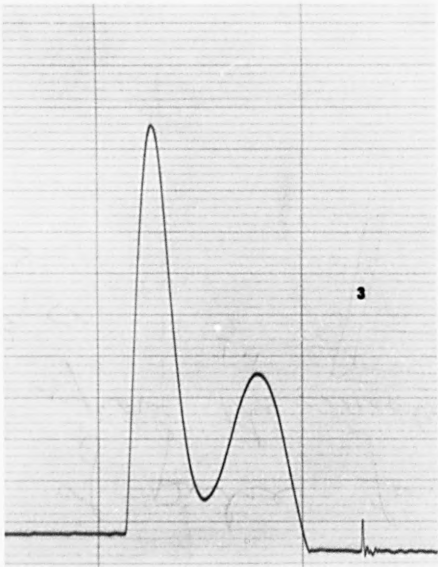
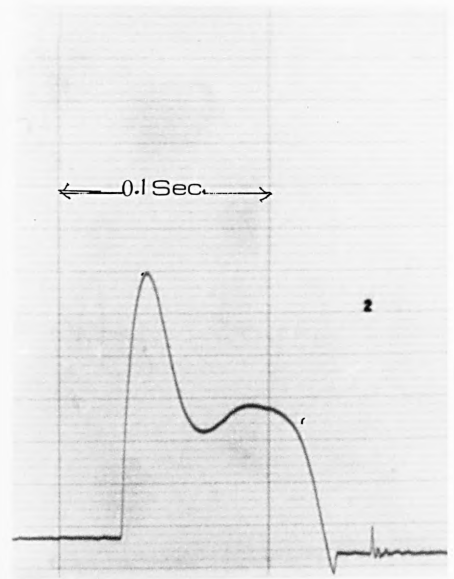
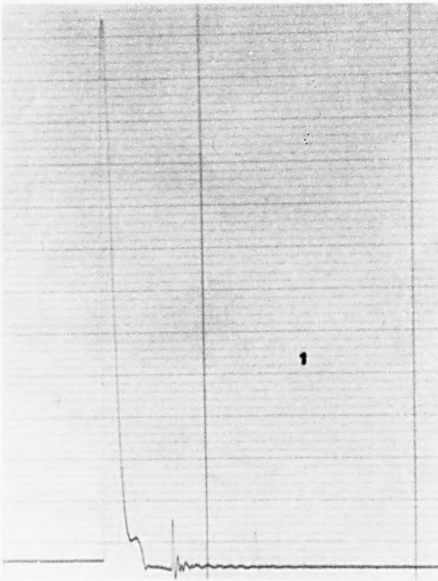


Fig. (6.7)
The impact force
for the five models

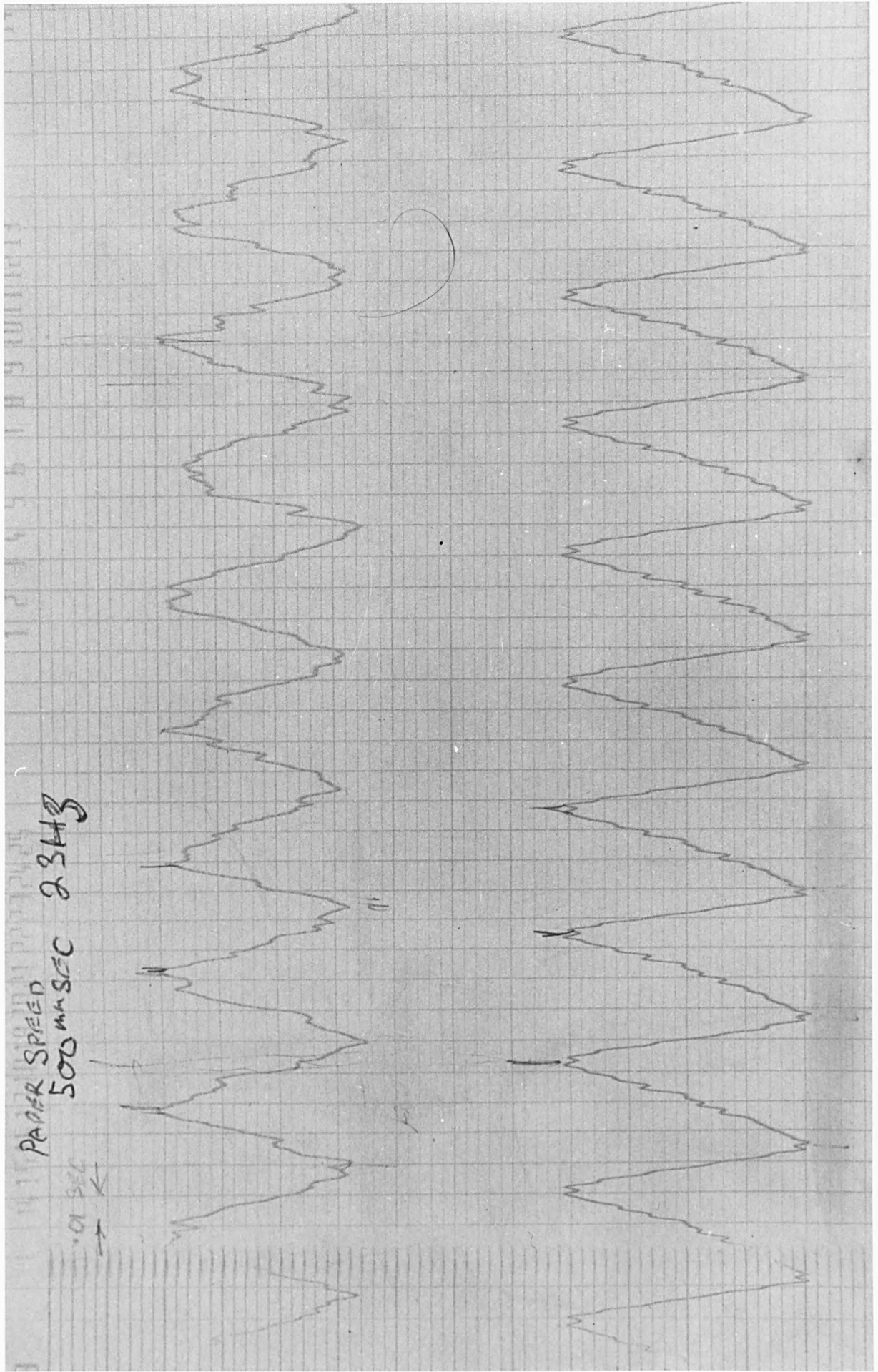
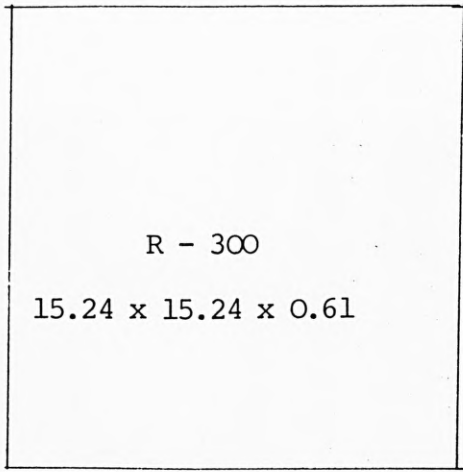
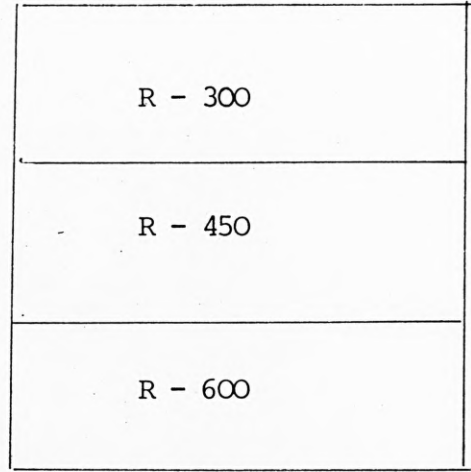


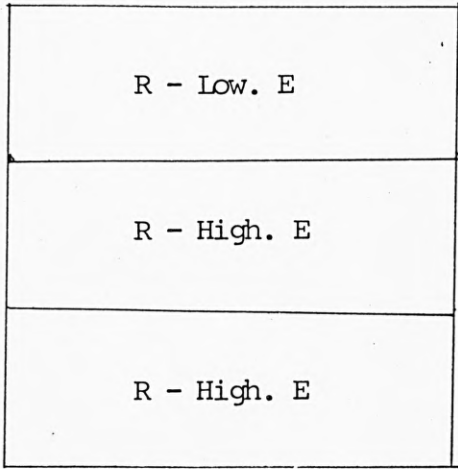
Fig. (6.8) Dynamic modulus of elasticity (sample result)



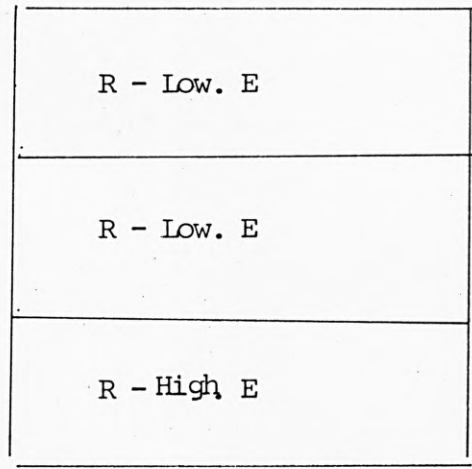
Model 1



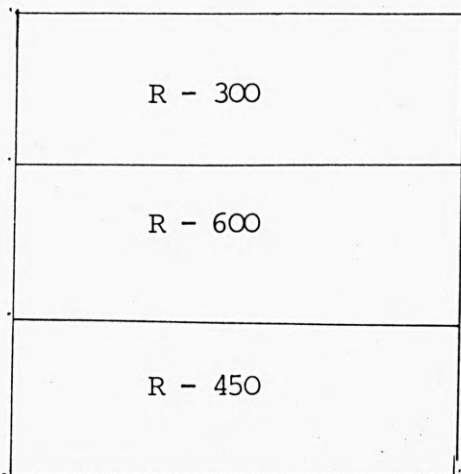
Model 2



Model 3



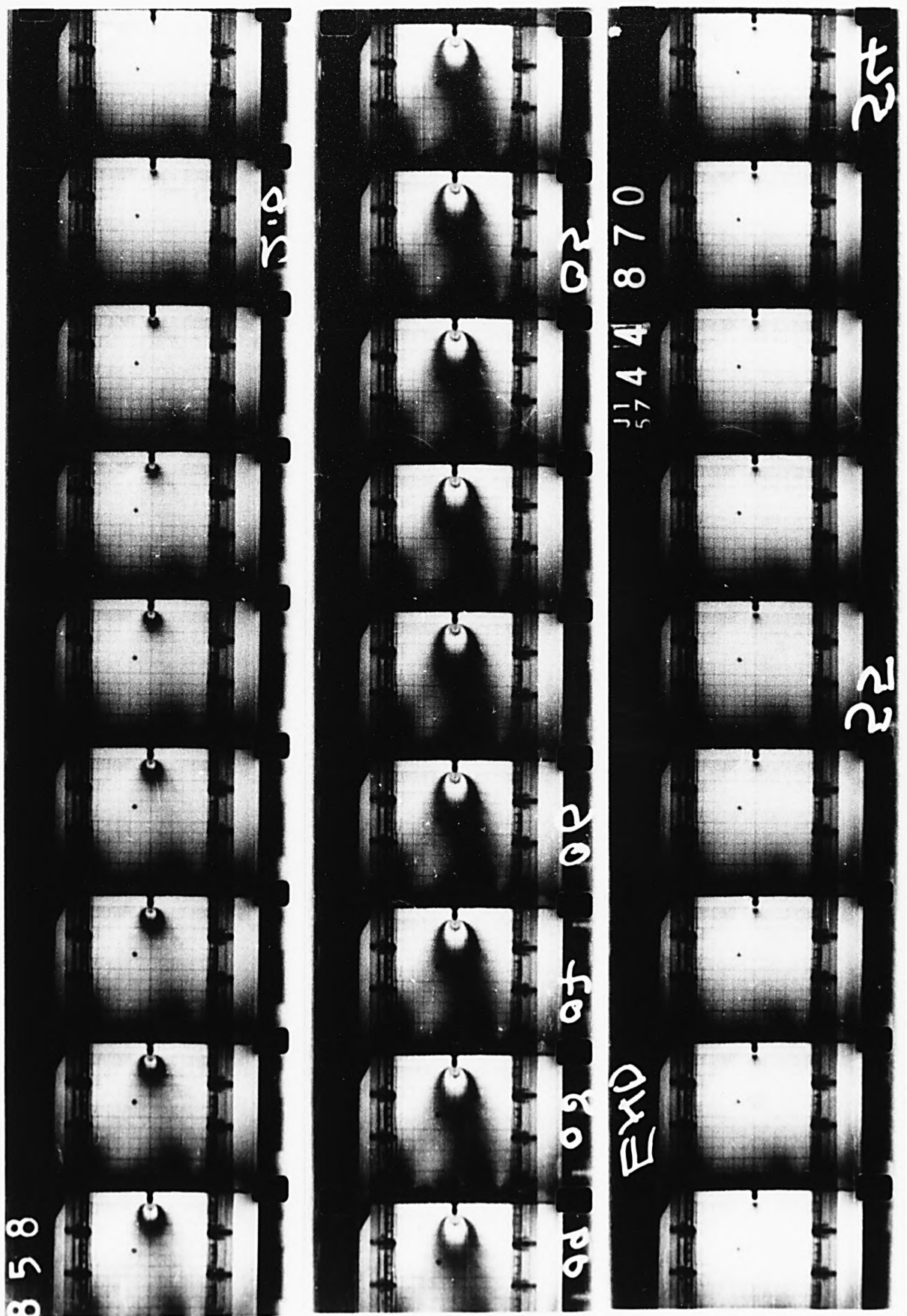
Model 4



Model 5

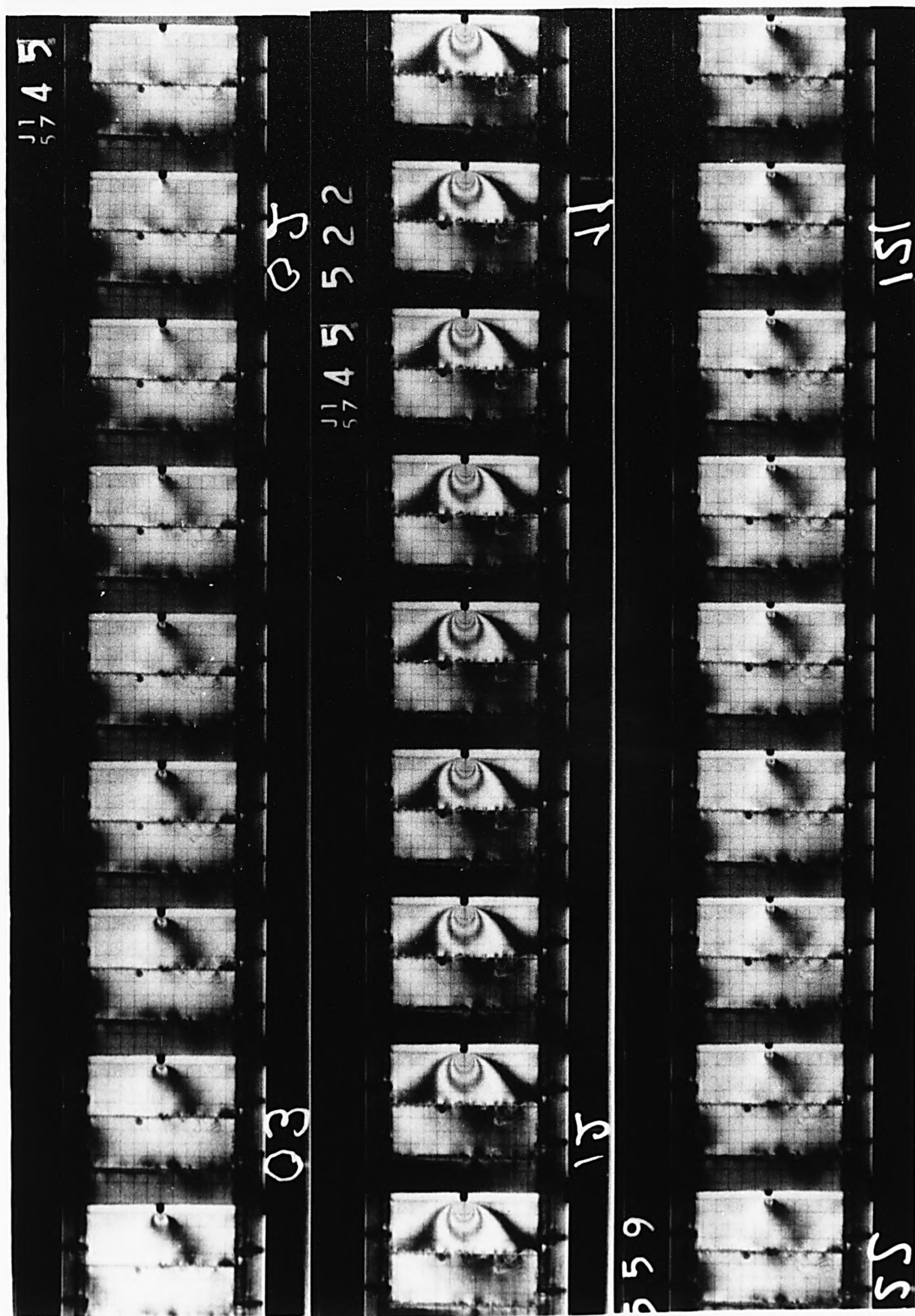
Model	Length	Width	Thickness
1	15.24	15.24	0.61 cm
2	15.24	15.24	0.61 cm
3	15.24	15.24	1.27 cm
4	15.24	15.24	1.27 cm
5	15.24	15.24	0.61 cm

Fig. (6.9)



1

Fig. (6.10) Sample from high speed film No. 1.

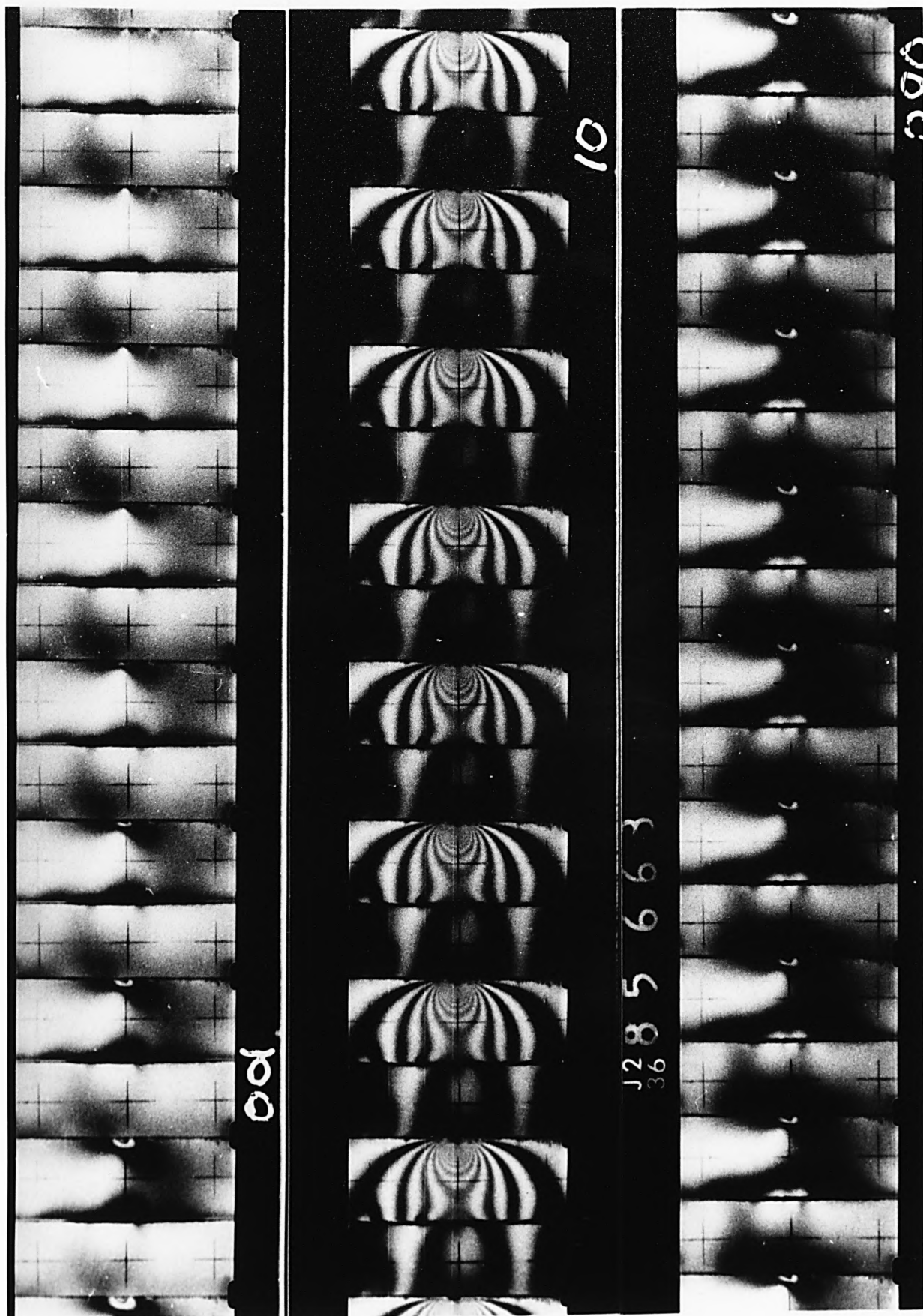


2

Fig. (6.11) Sample from high speed film No. 2.



Fig. (6.12) Sample from high speed film No. 3.



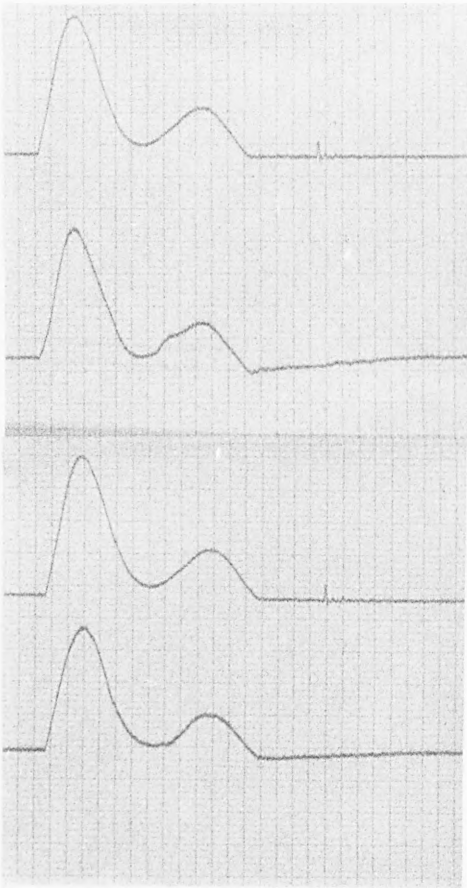
4

Fig. (6.13) Sample from high speed film No. 4.



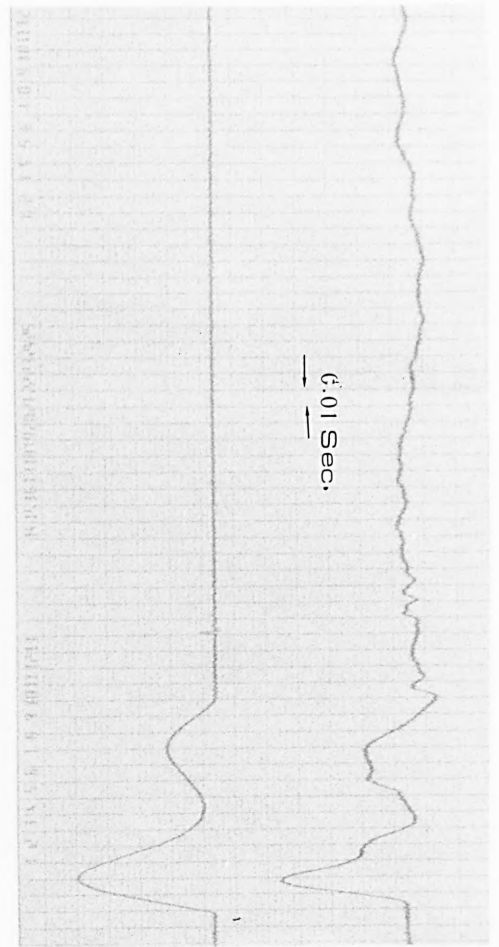
Fig. (6.14) Sample from high speed film No. 5.

1-3



1-4

1-2



1-7



1-10

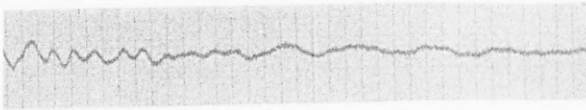
	<u>2</u>	<u>3</u>	<u>4</u>	<u>5</u>
A	+	6 7 8	+	
B	+	9 10 11	+	
C	+	.	+	

A R-300

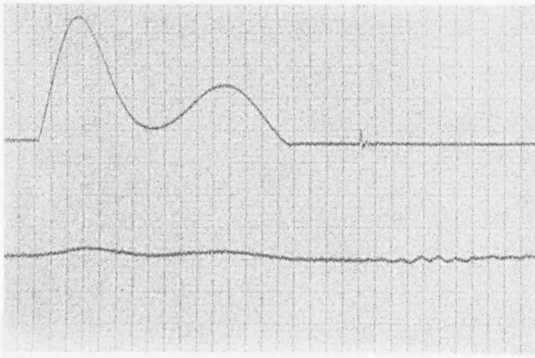
B R-450

C R-600

Fig. (6.15) Dynamic response of strain gauges on model 3.



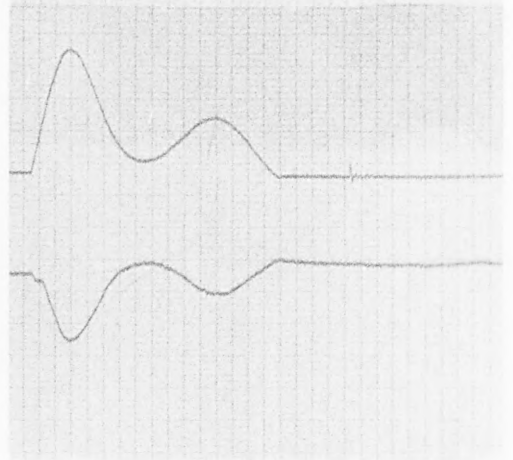
2.6



2.7

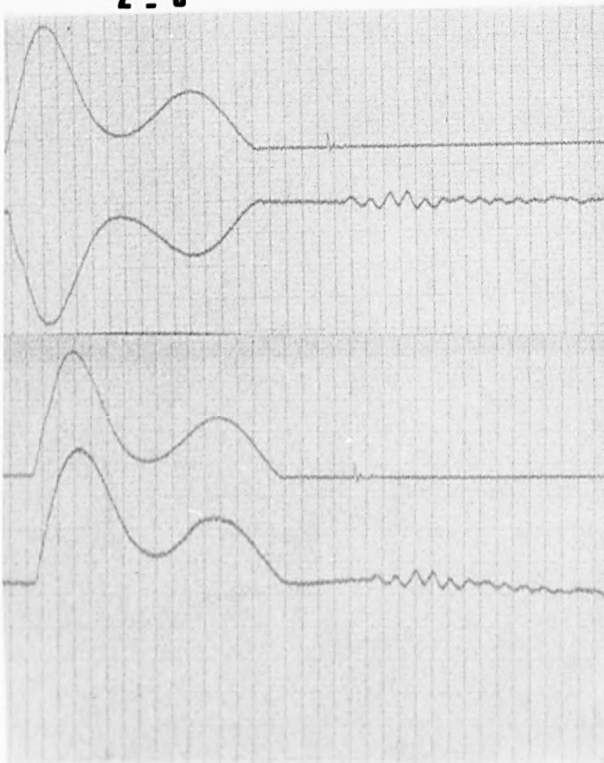


2.4

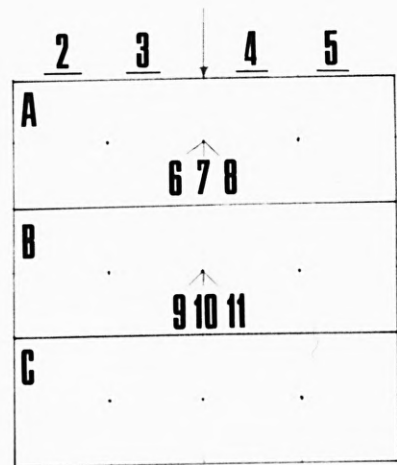


2.3

2.9



2.10



A-R - LOW.M
 B-R - HIGH.M
 C-R - HIGH.M

Fig. (6.16) Dynamic response of strain gauges on model 4.

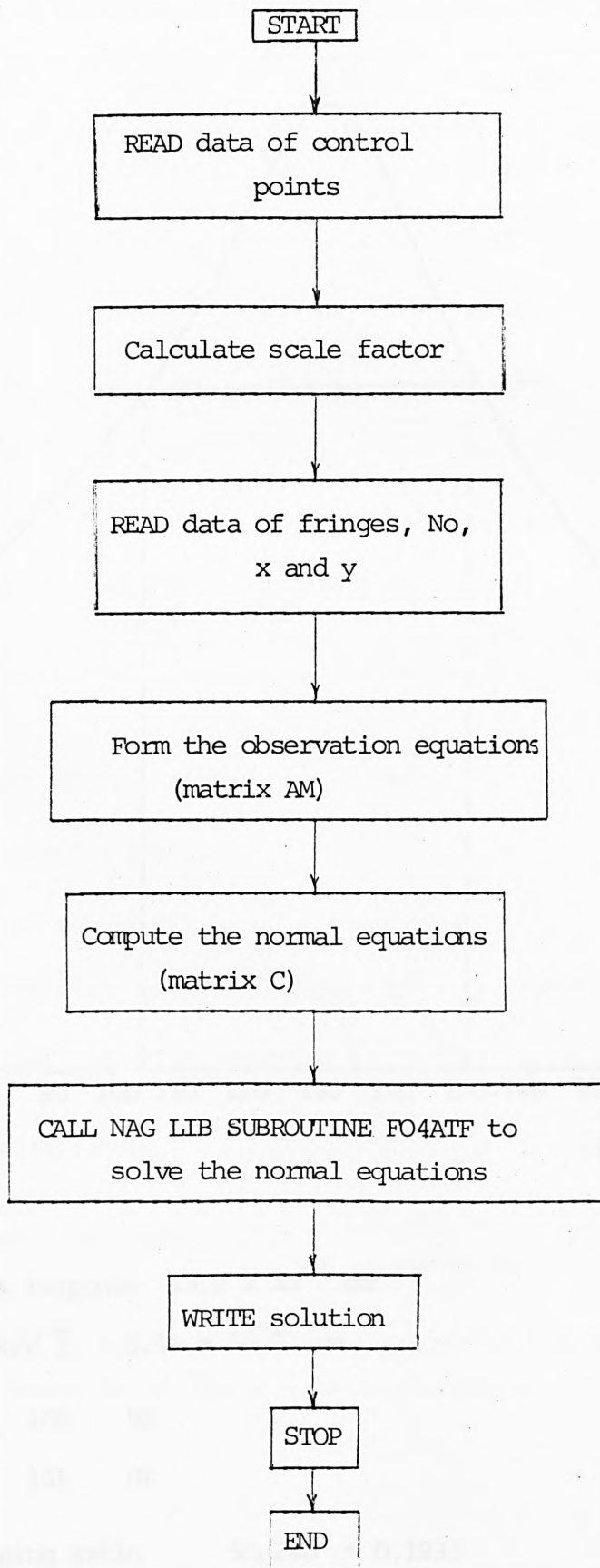
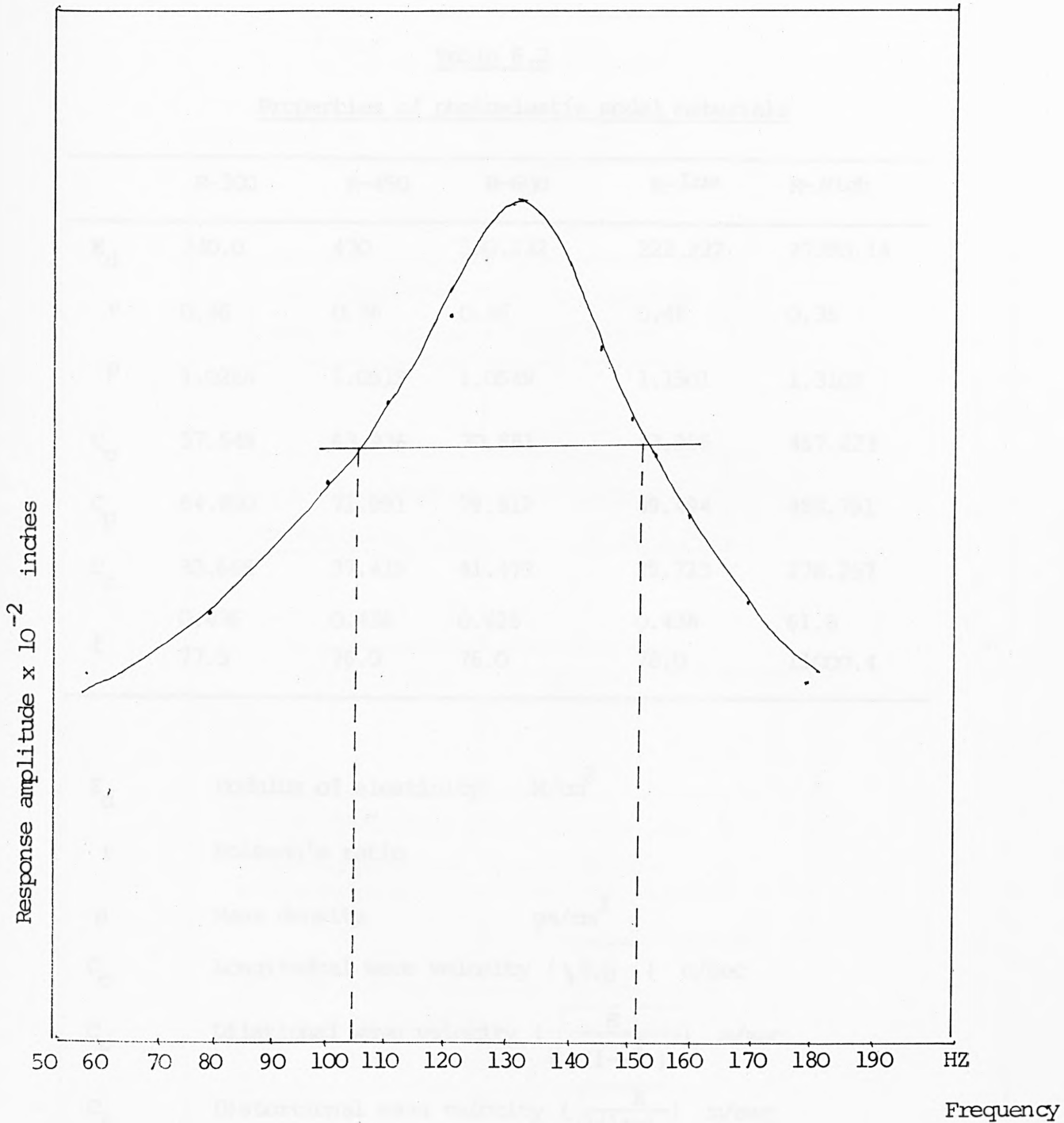


Fig. (6.17)



Peak response 13.8×10^{-2} cm

Peak/ $\sqrt{2}$ 9.75×10^{-2} cm

f_1 105 HZ

f_2 155 HZ

Damping ratio $50/260 = 0.1923$

Fig. (6.18)

Table 6.2

Properties of photoelastic model materials

	R-300	R-450	R-600	R-Low	R-High
E_d	340.0	430	530.232	222.222	27390.14
ν	0.46	0.46	0.46	0.46	0.35
ρ	1.0266	1.0519	1.0549	1.1501	1.3102
C_o	57.549	63.936	70.881	43.956	457.223
C_p	64.800	71.991	79.812	49.494	488.791
C_s	33.666	37.415	41.479	25.723	278.257
f	0.436	0.436	0.426	0.438	61.8
	77.5	76.0	76.0	78.0	11000.4

E_d Modulus of elasticity N/cm^2

ν Poisson's ratio

ρ Mass density gm/cm^3

C_o Longitudinal wave velocity ($\sqrt{E/\rho}$) m/sec

C_p Dilational wave velocity ($\sqrt{\frac{E}{2(1-\nu^2)}}$) m/sec

C_s Distortional wave velocity ($\sqrt{\frac{E}{2(1+\nu)}}$) m/sec

f Material fringe value $lb\ in^2/in$
 $g\ sec\ cm/cm$

η_s Damping ratio for low modulus material 0.192.
Damping ratio for high modulus material 0.01.

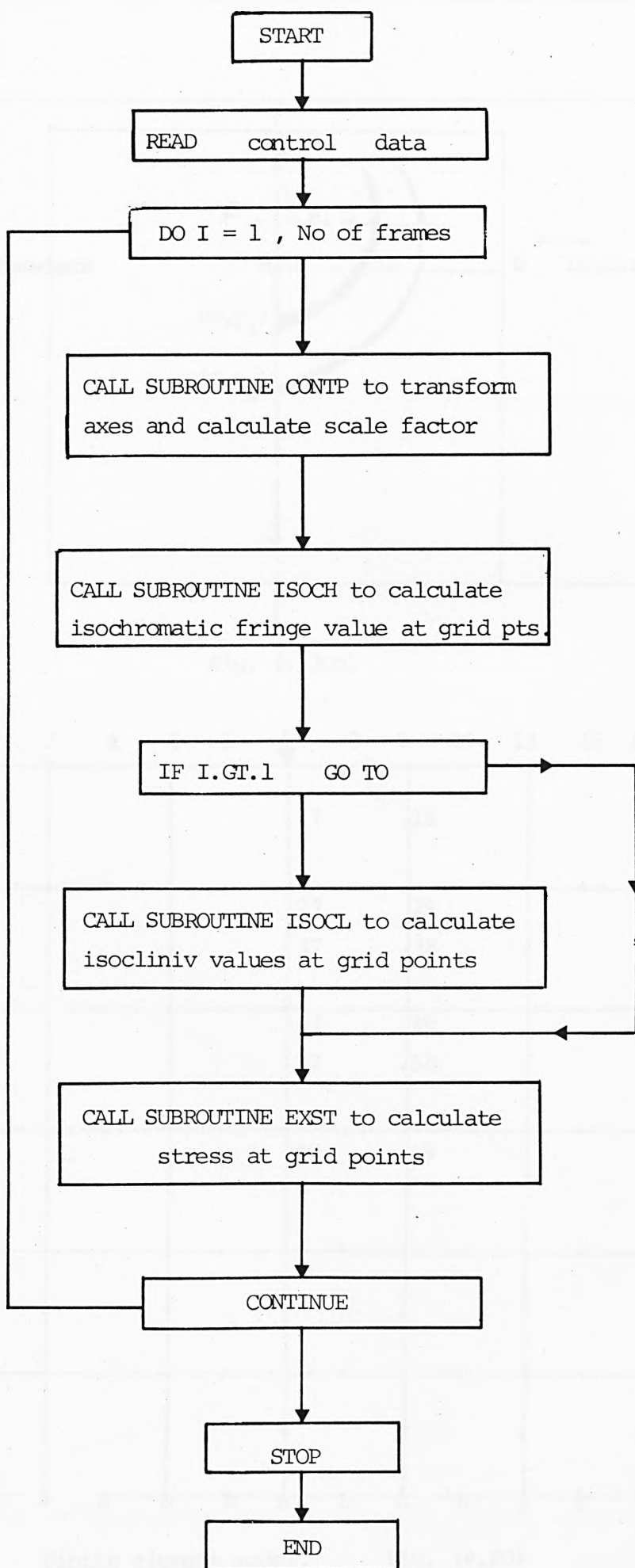


Fig. (6.19) Flow chart for the programme of analysis of experimental results.

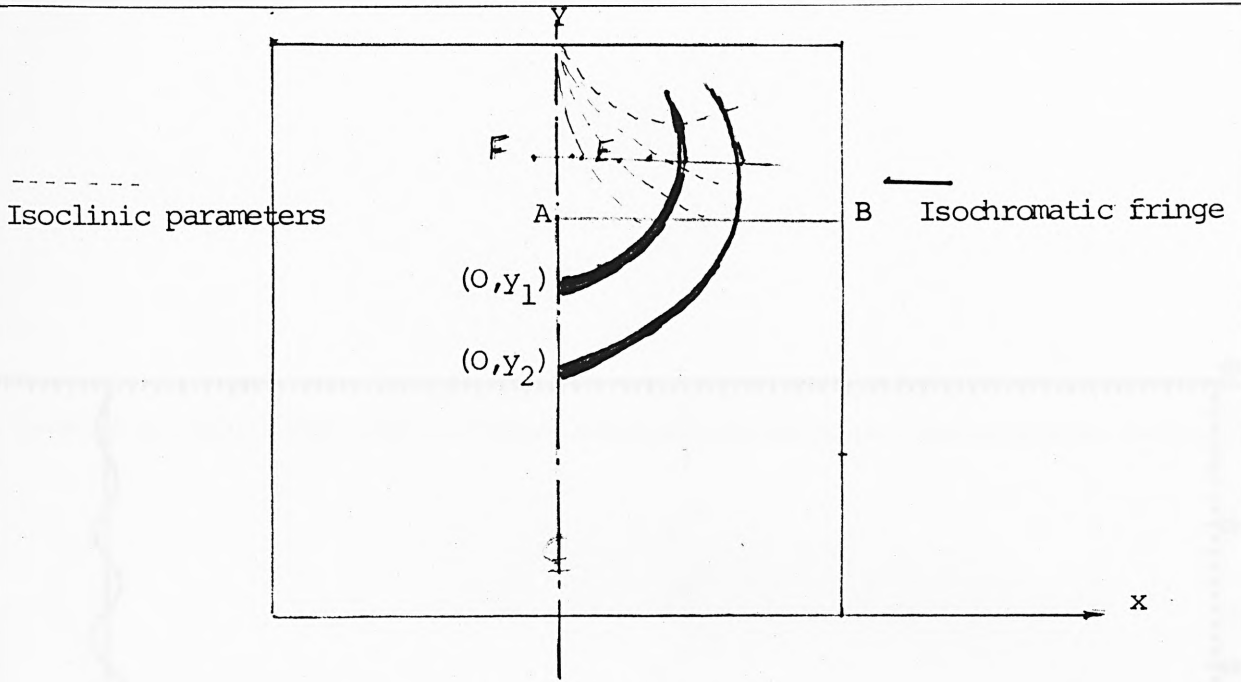
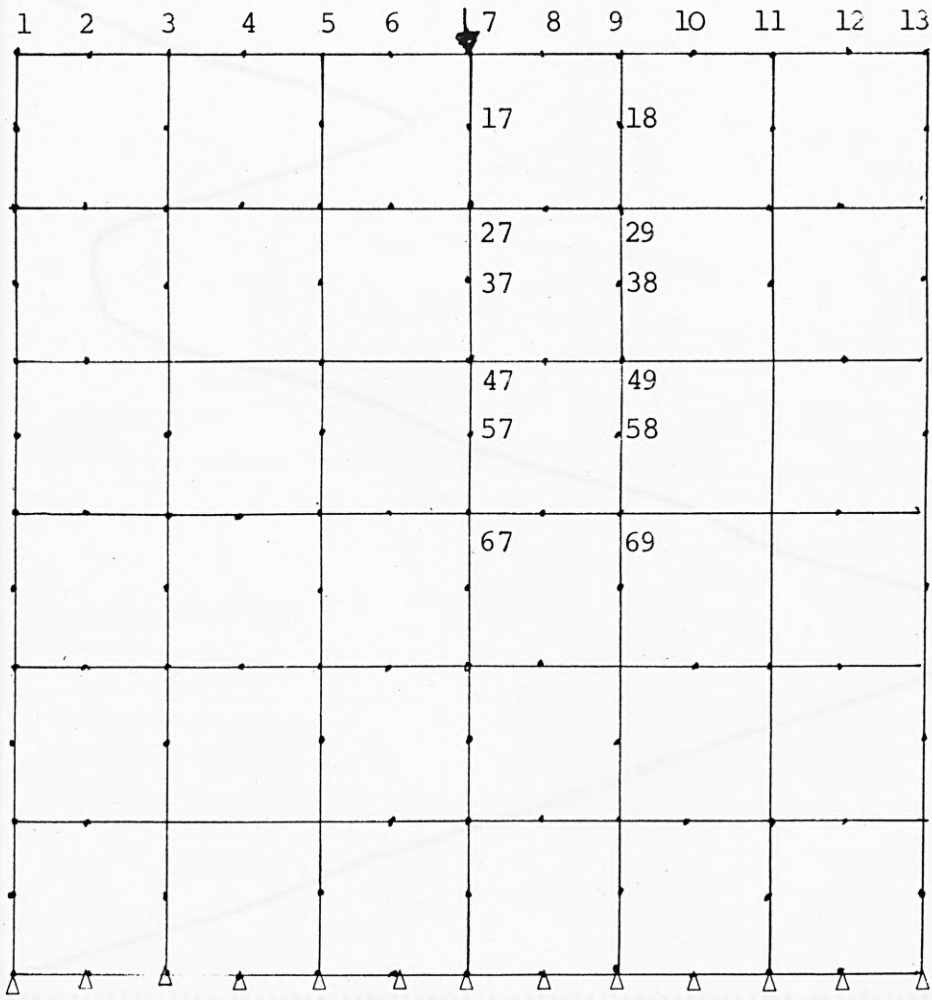


Fig. (6.20a)



Finite element model.

Fig. (6.20)

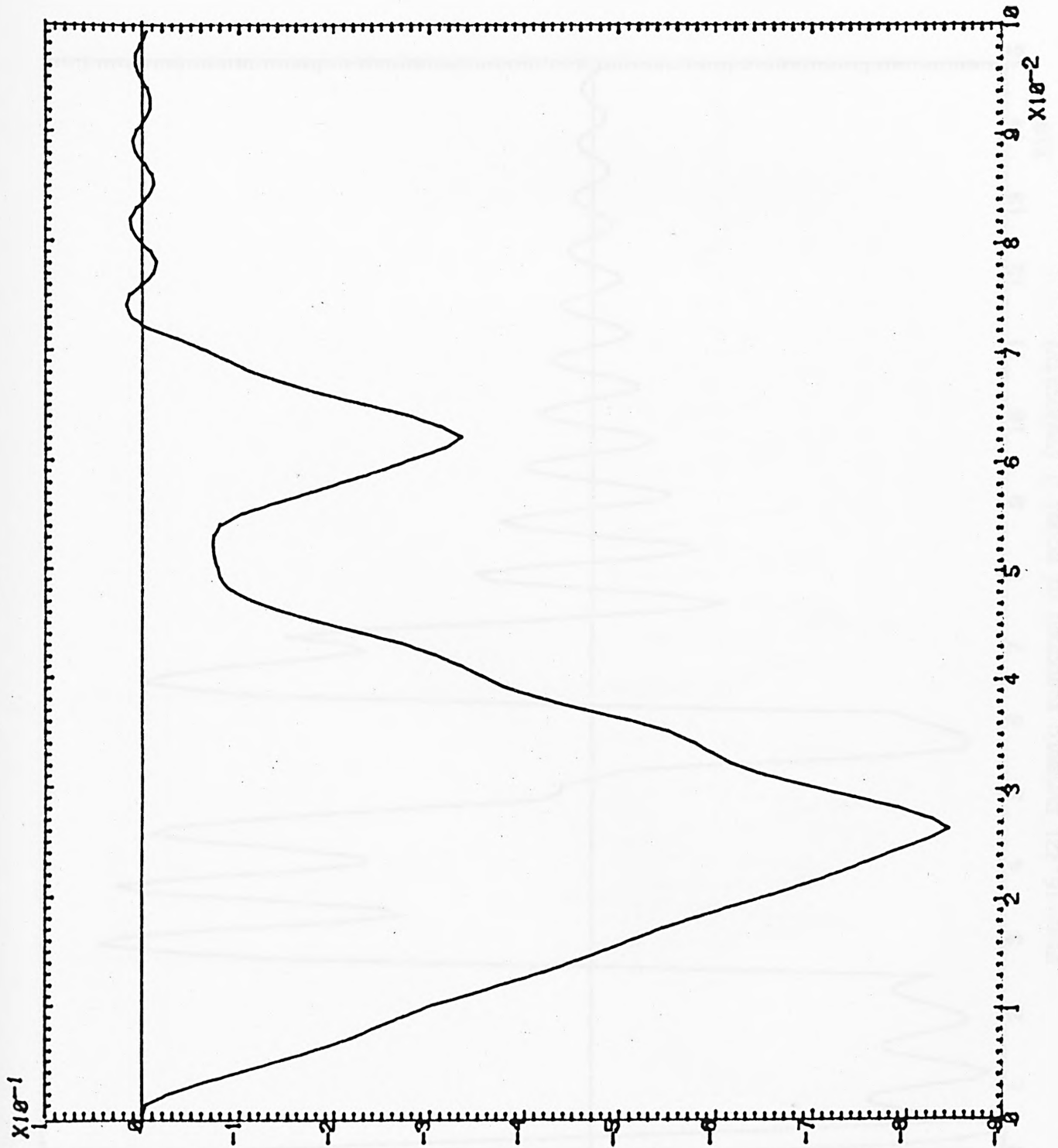


Fig. (6.21) Dynamic response of model 3 (displacement)

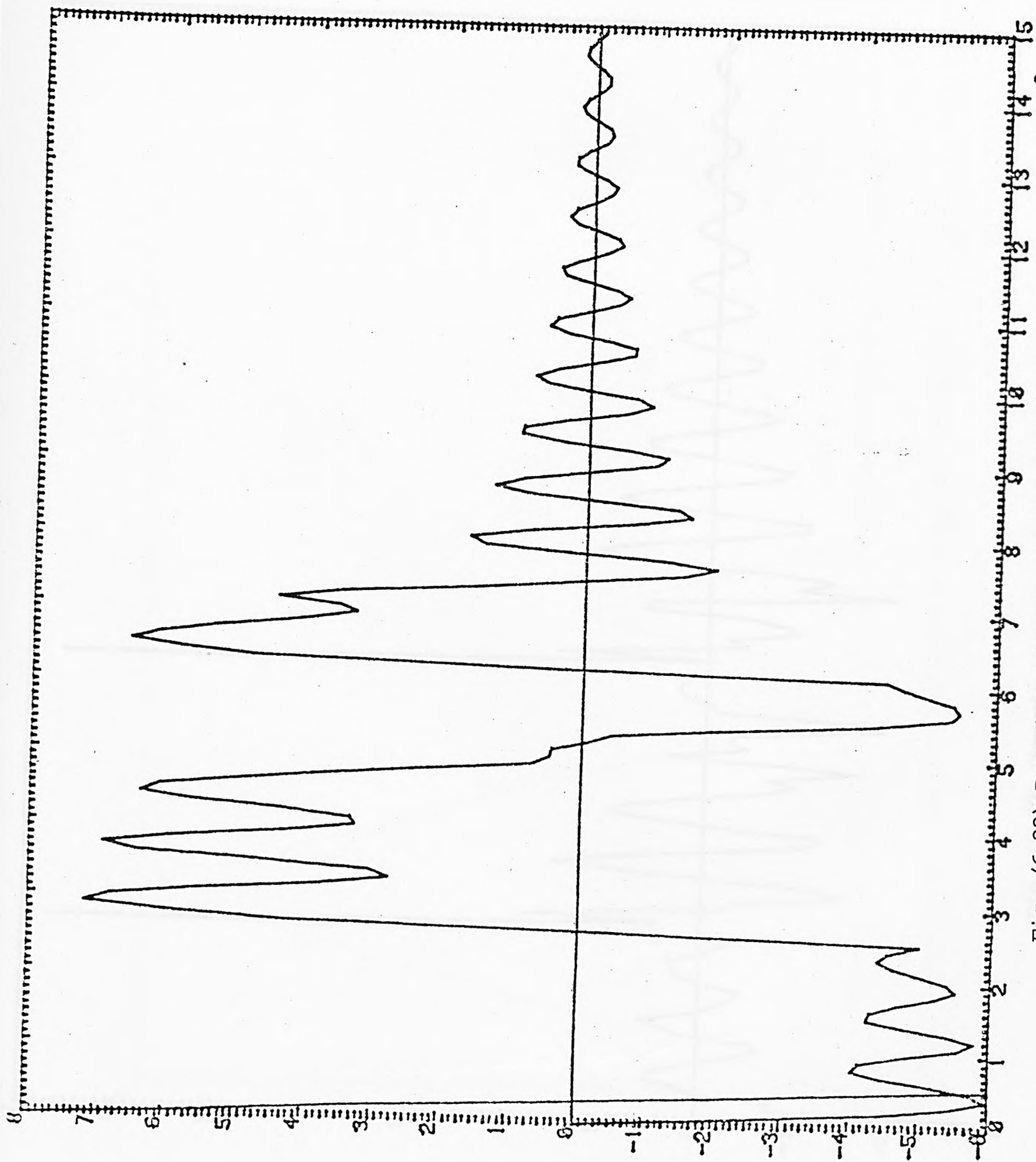


Fig. (6.22) Dynamic response of model 3 (velocity) $\times 10^{-2}$

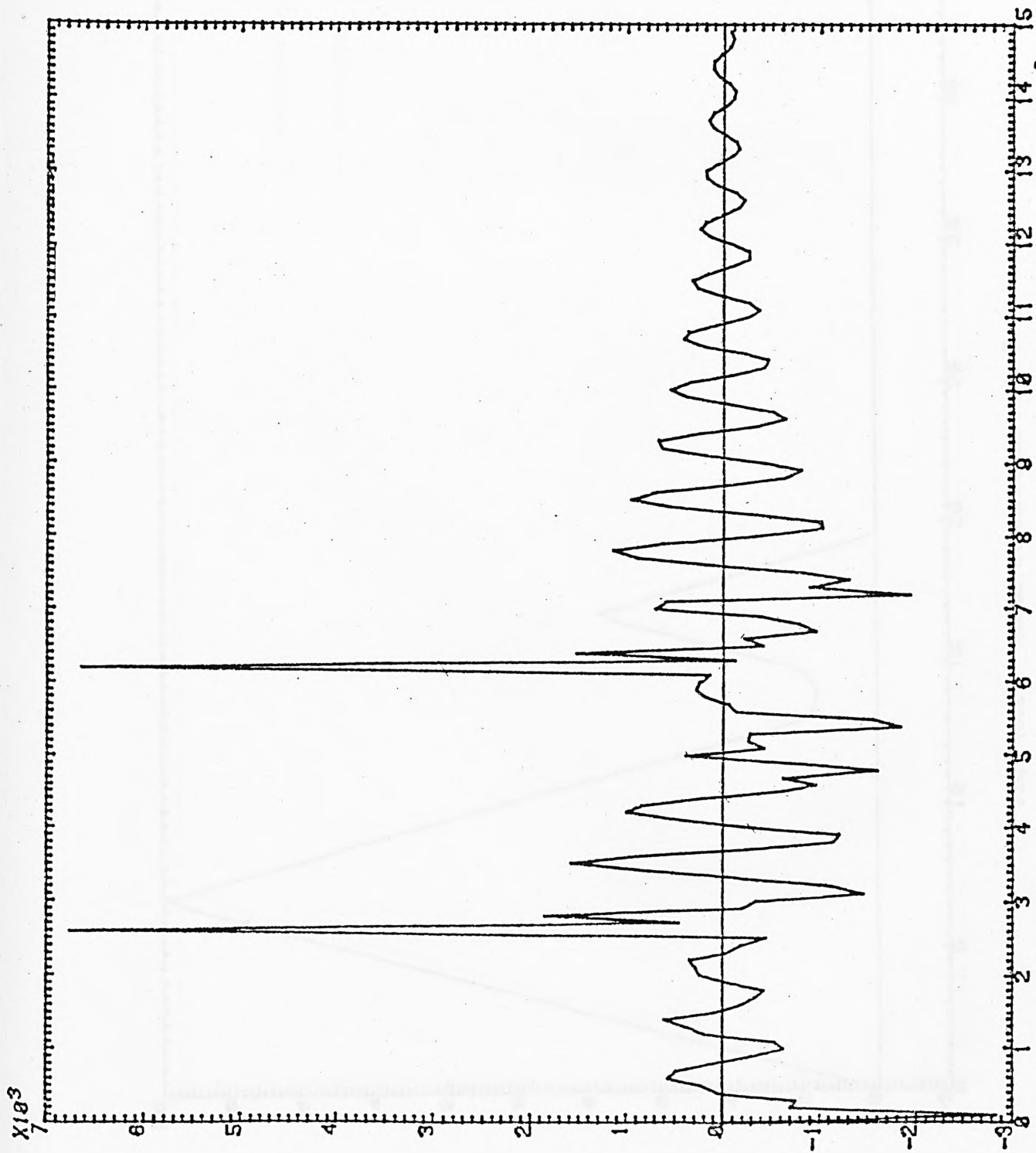


Fig. (6.23) Dynamic response of model 3 (acceleration)

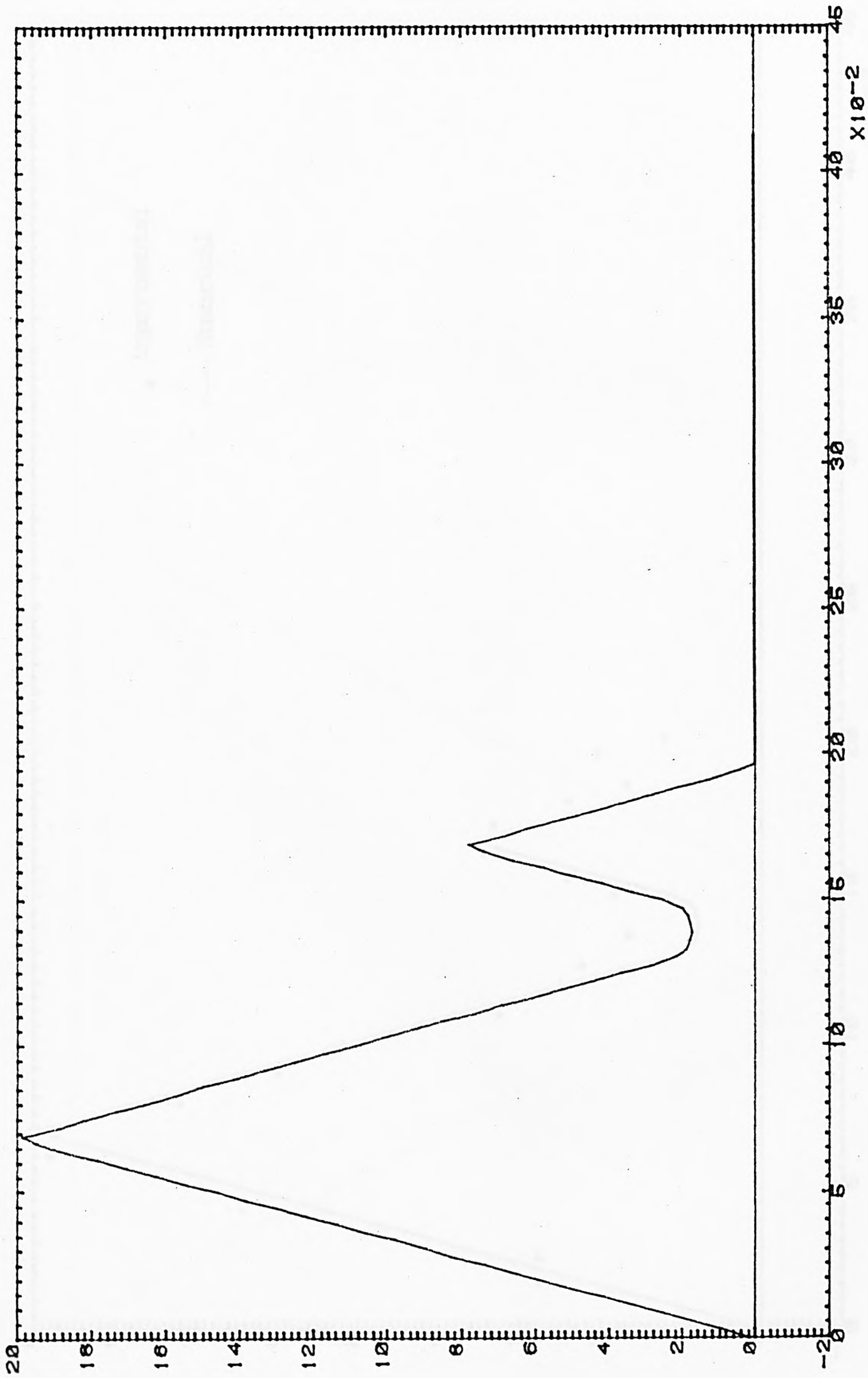


Fig. (6.24) Shear stresses at node 7.

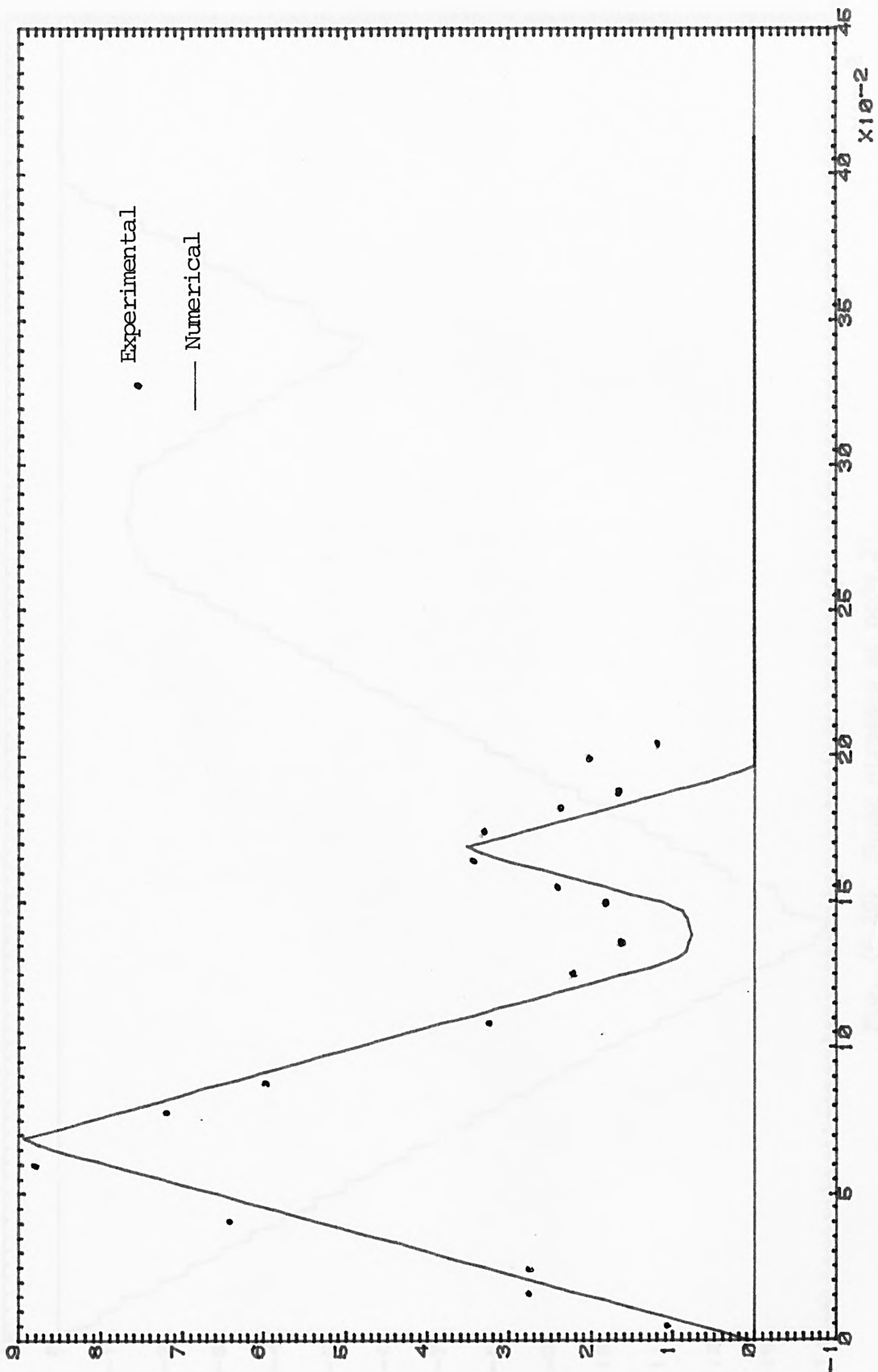


Fig. (6.25) Shear stresses at node 17.

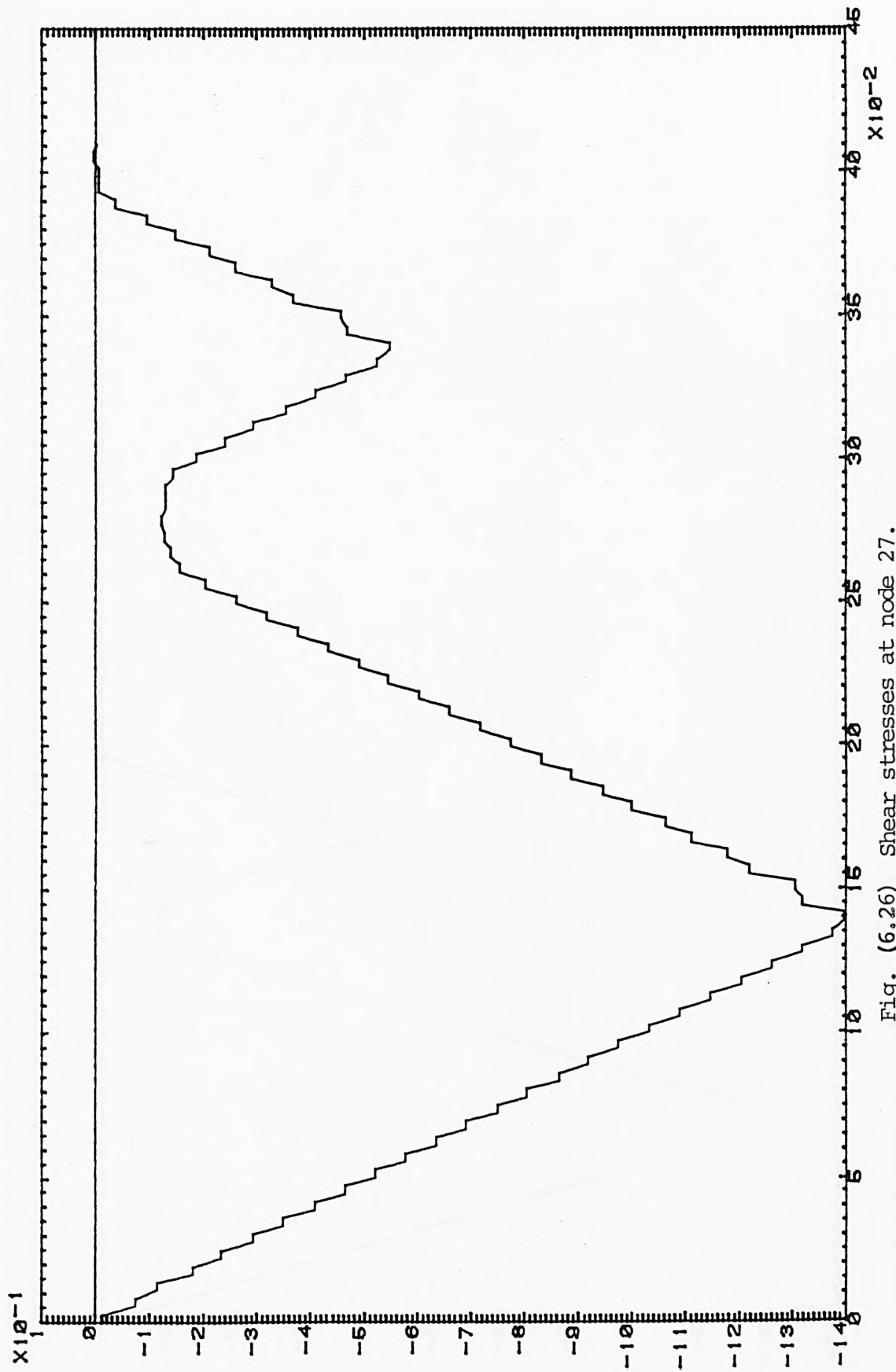


Fig. (6.26) Shear stresses at node 27.

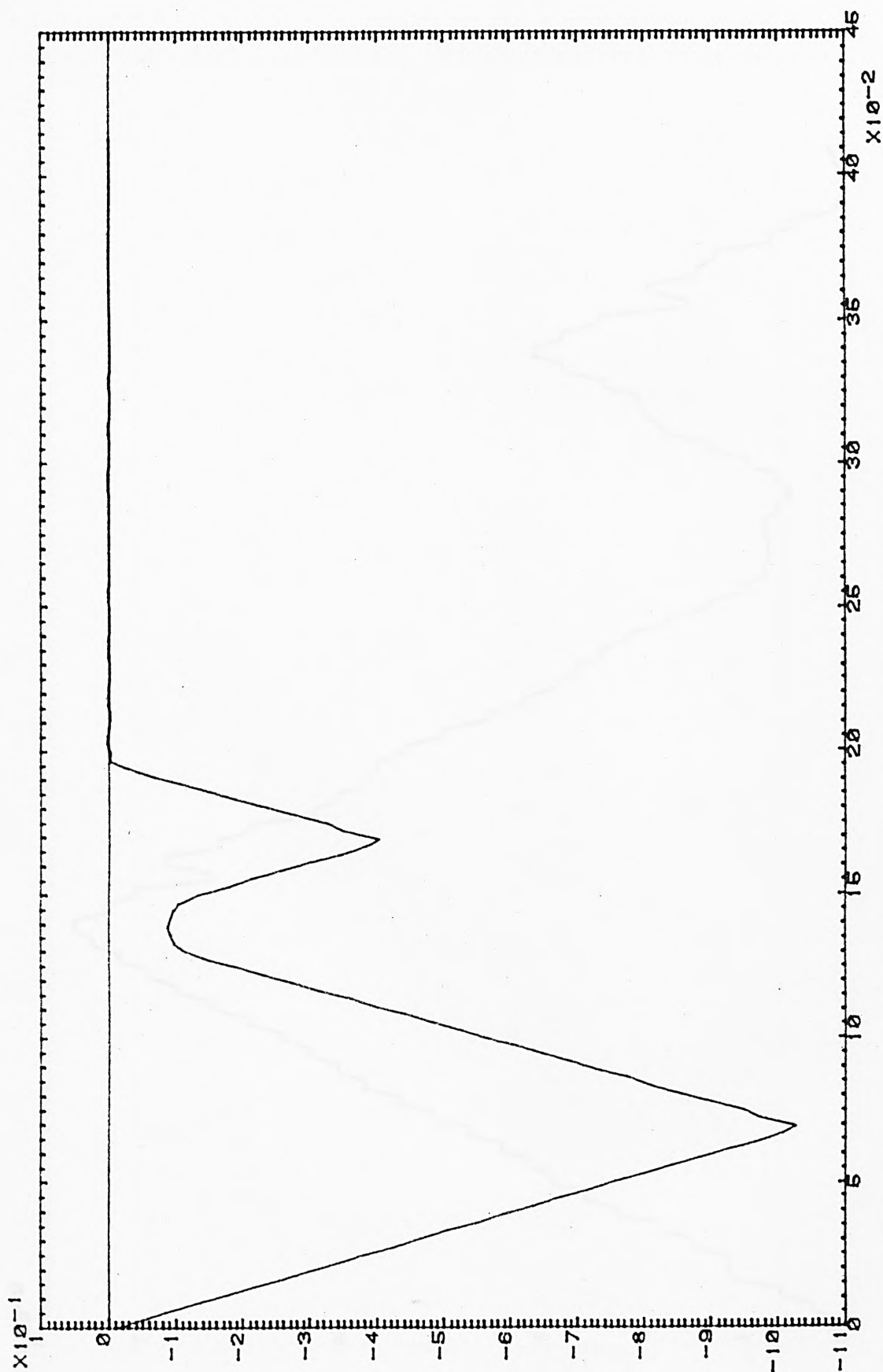


Fig. (6.27) Shear stresses at node 37.

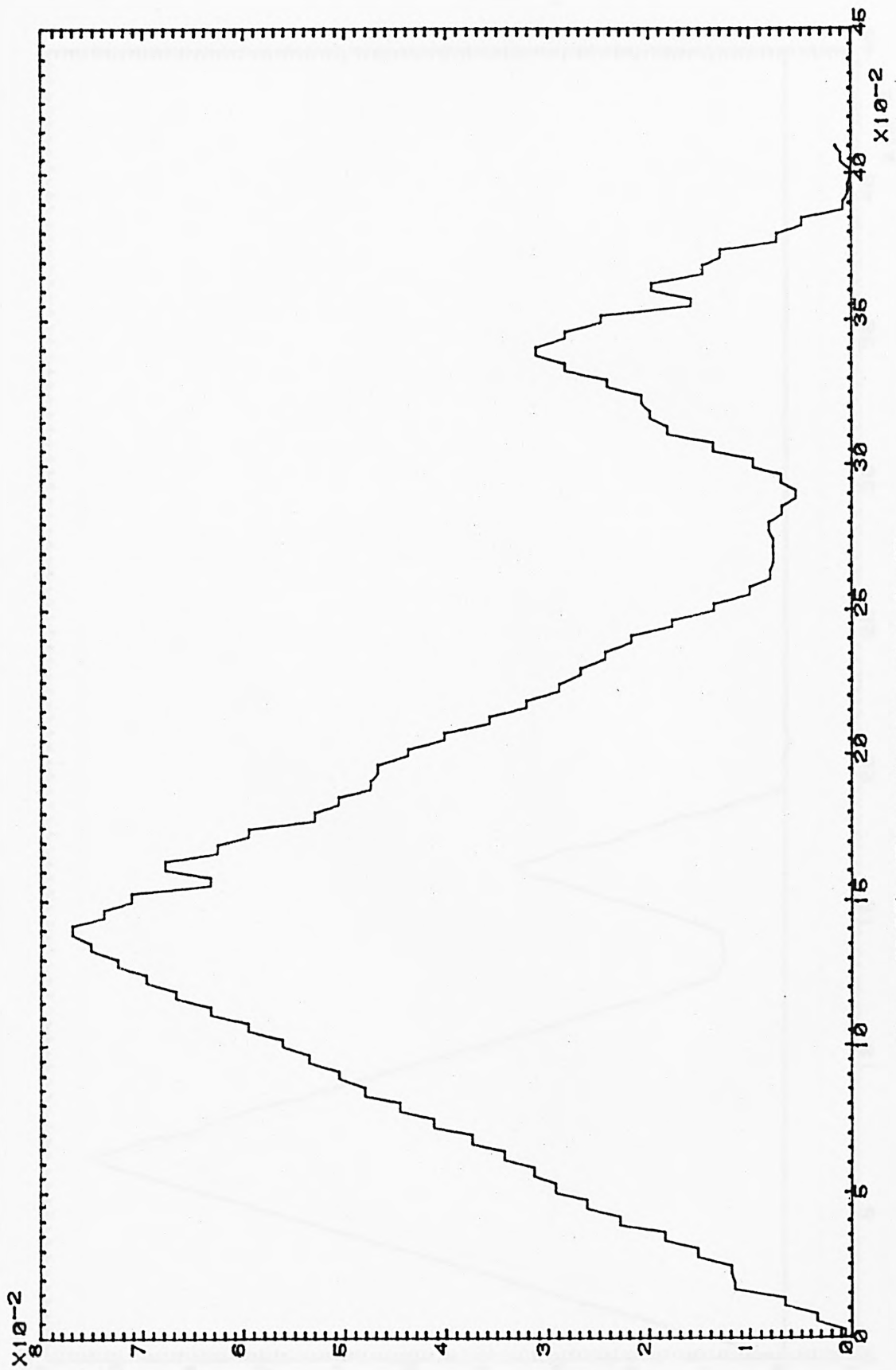


Fig. (6.28) Shear stresses at node 47.

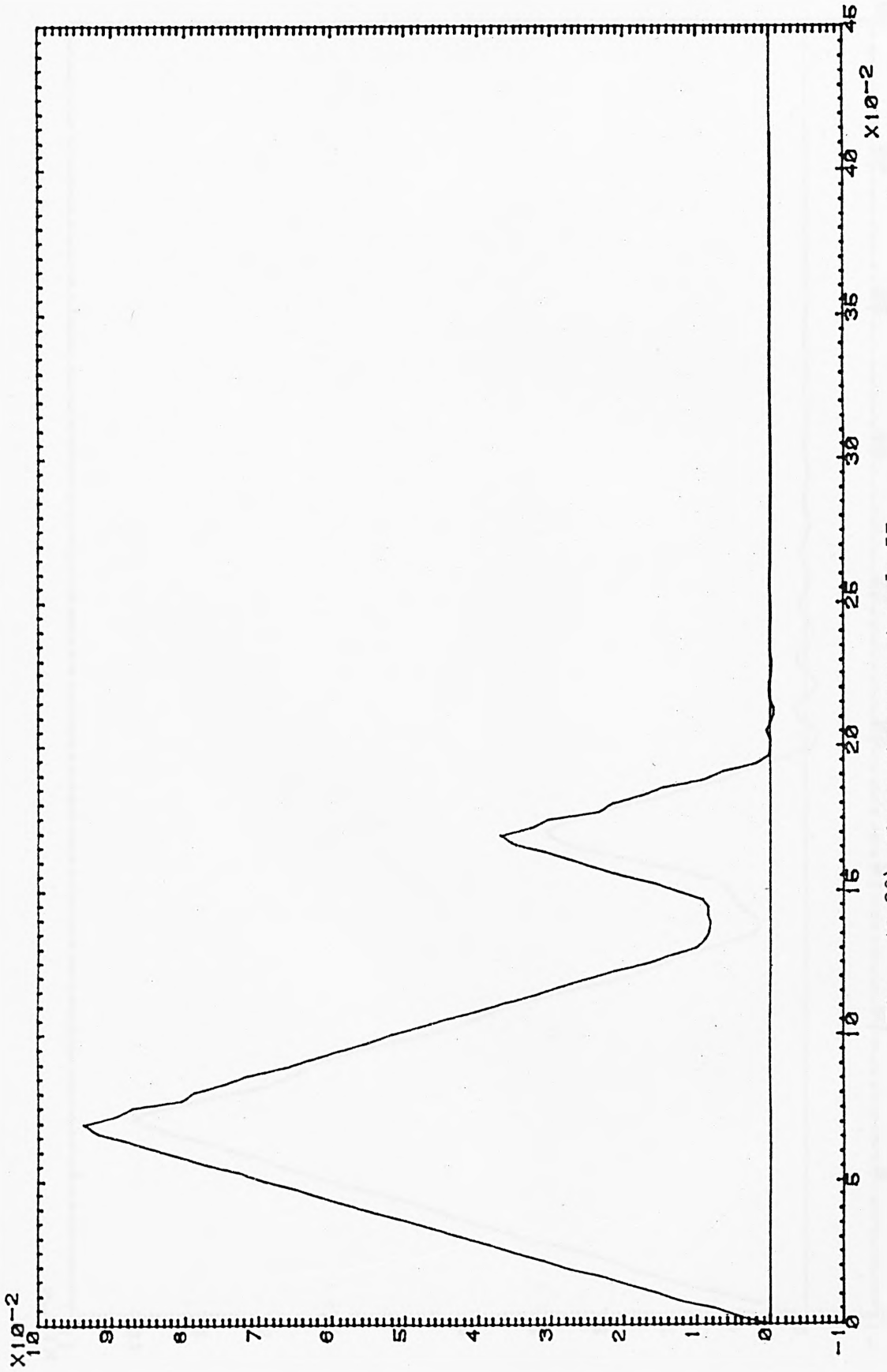


Fig. (6.29) Shear stresses at node 57.

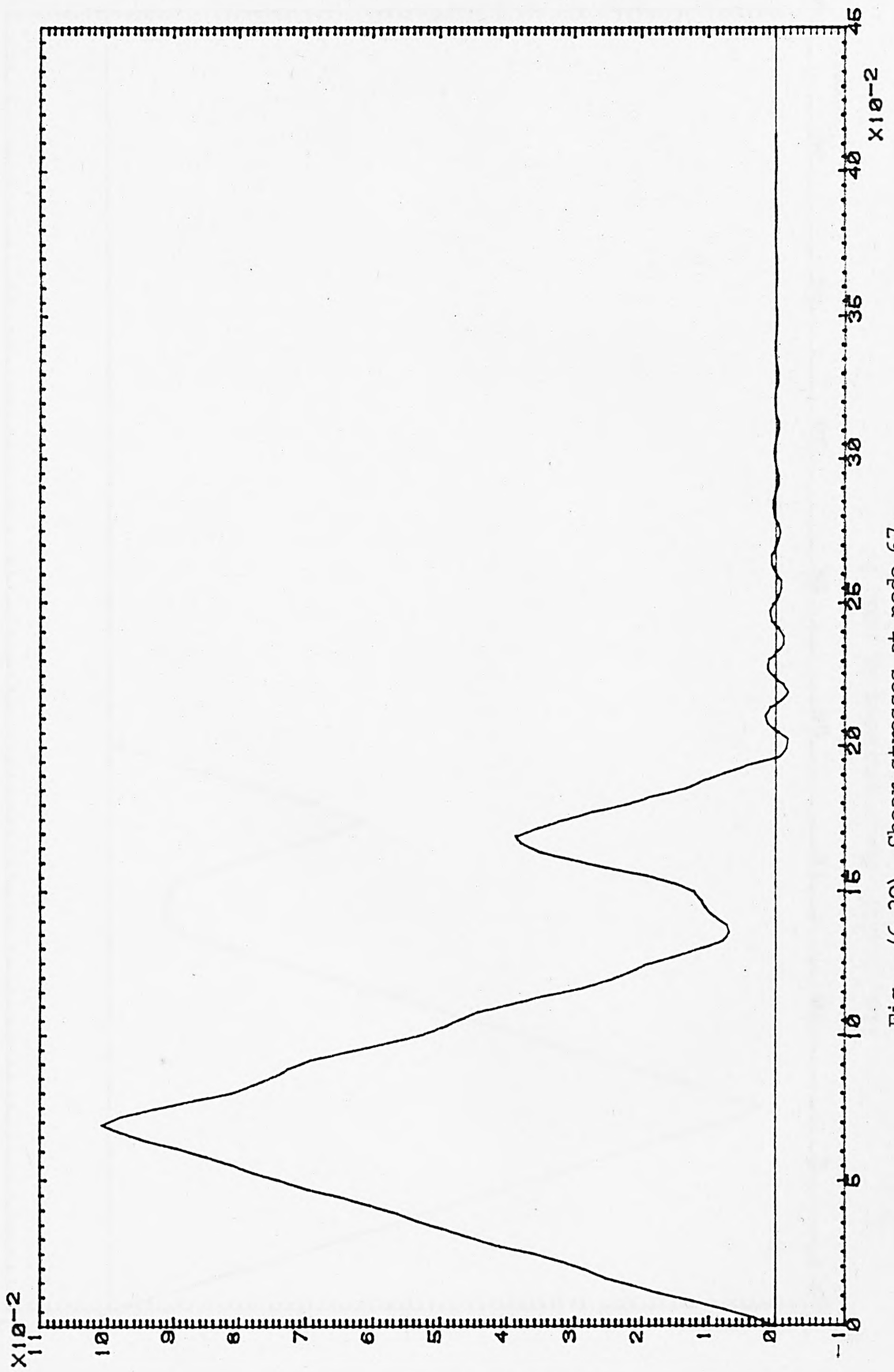


Fig. (6.30) Shear stresses at node 67.

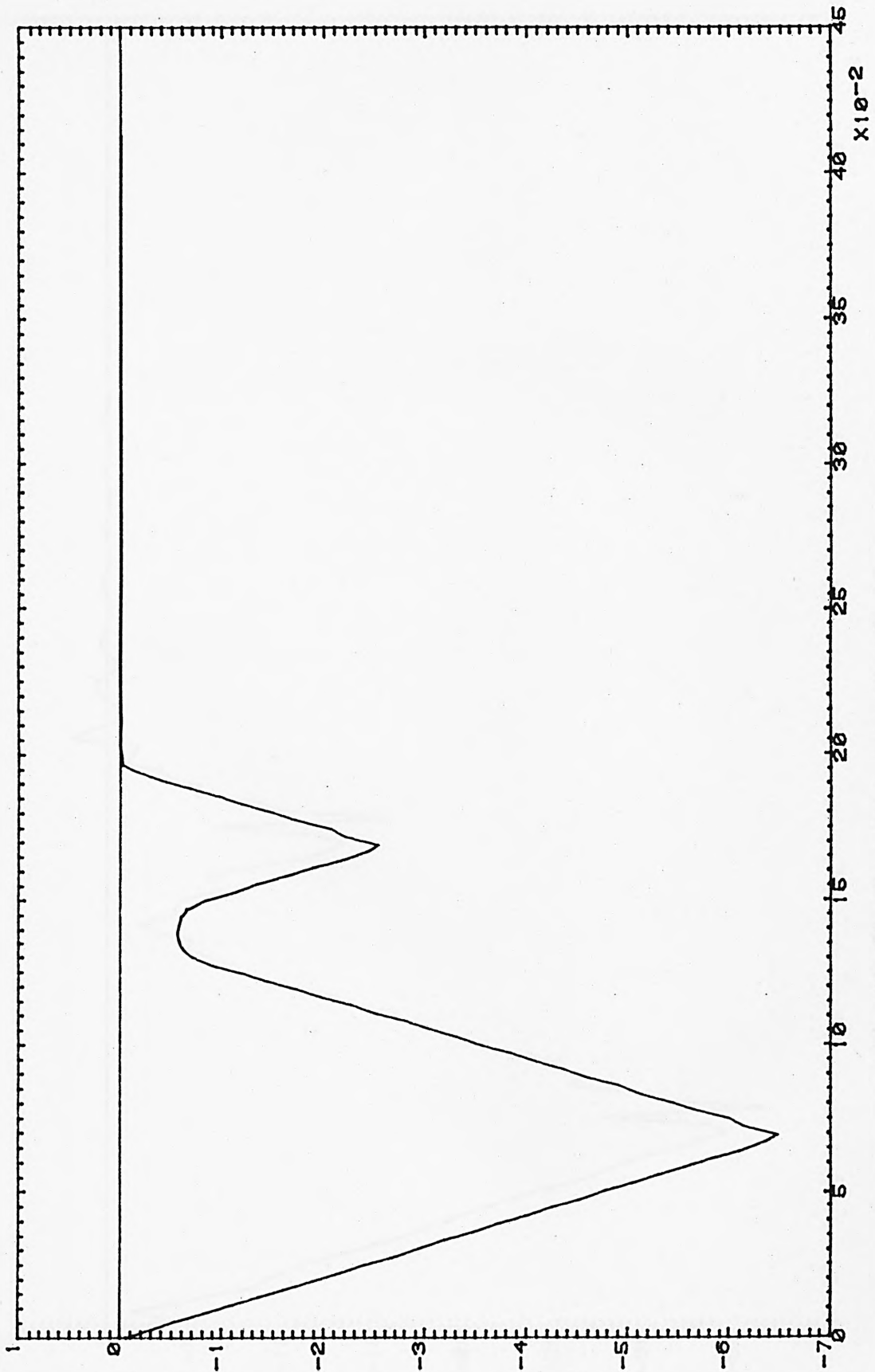


Fig. (6.31) Shear stresses at node 9.

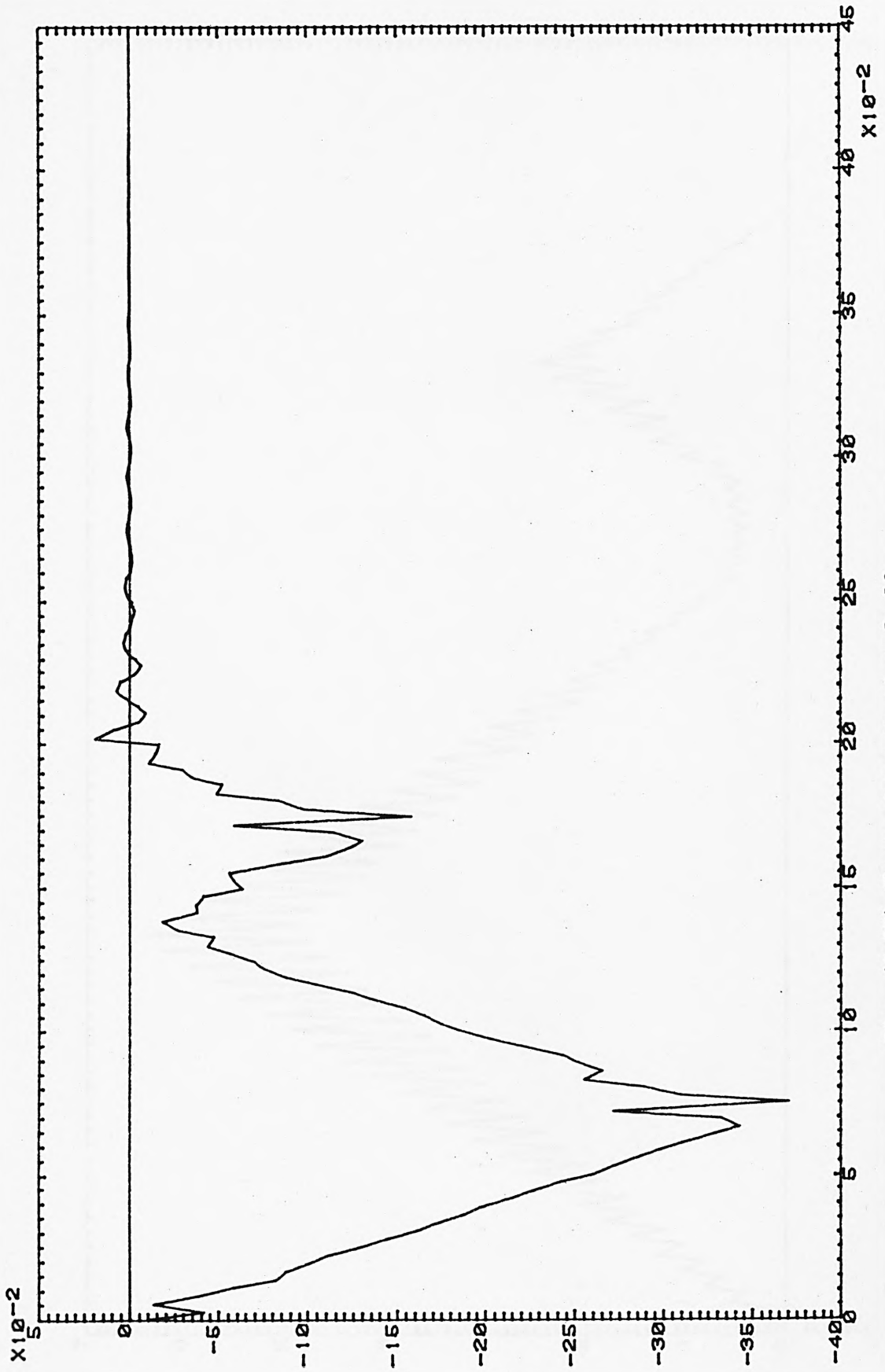


Fig. (6.32) Shear stresses at node 18.

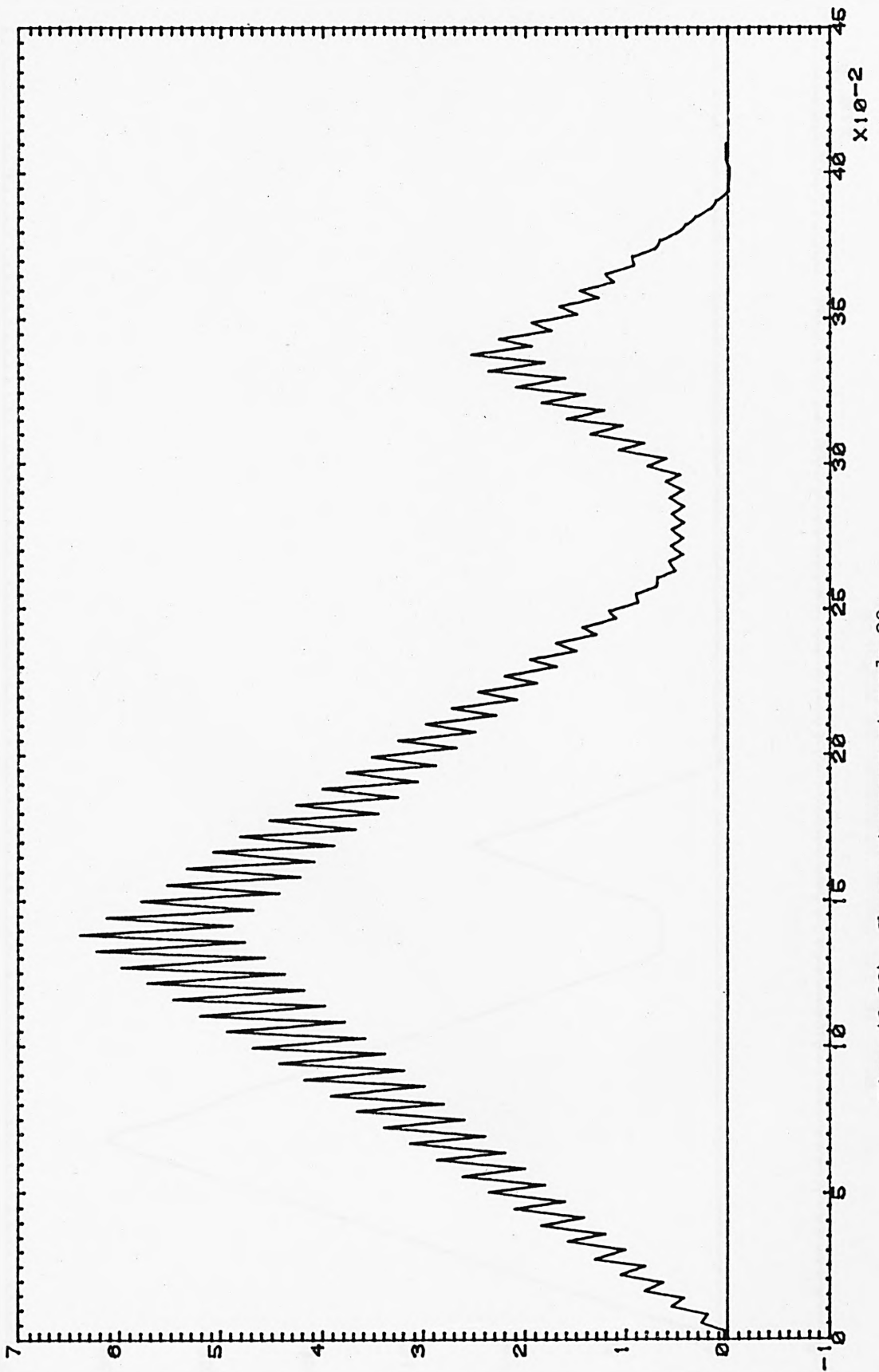


Fig. (6.33) Shear stresses at node 29.

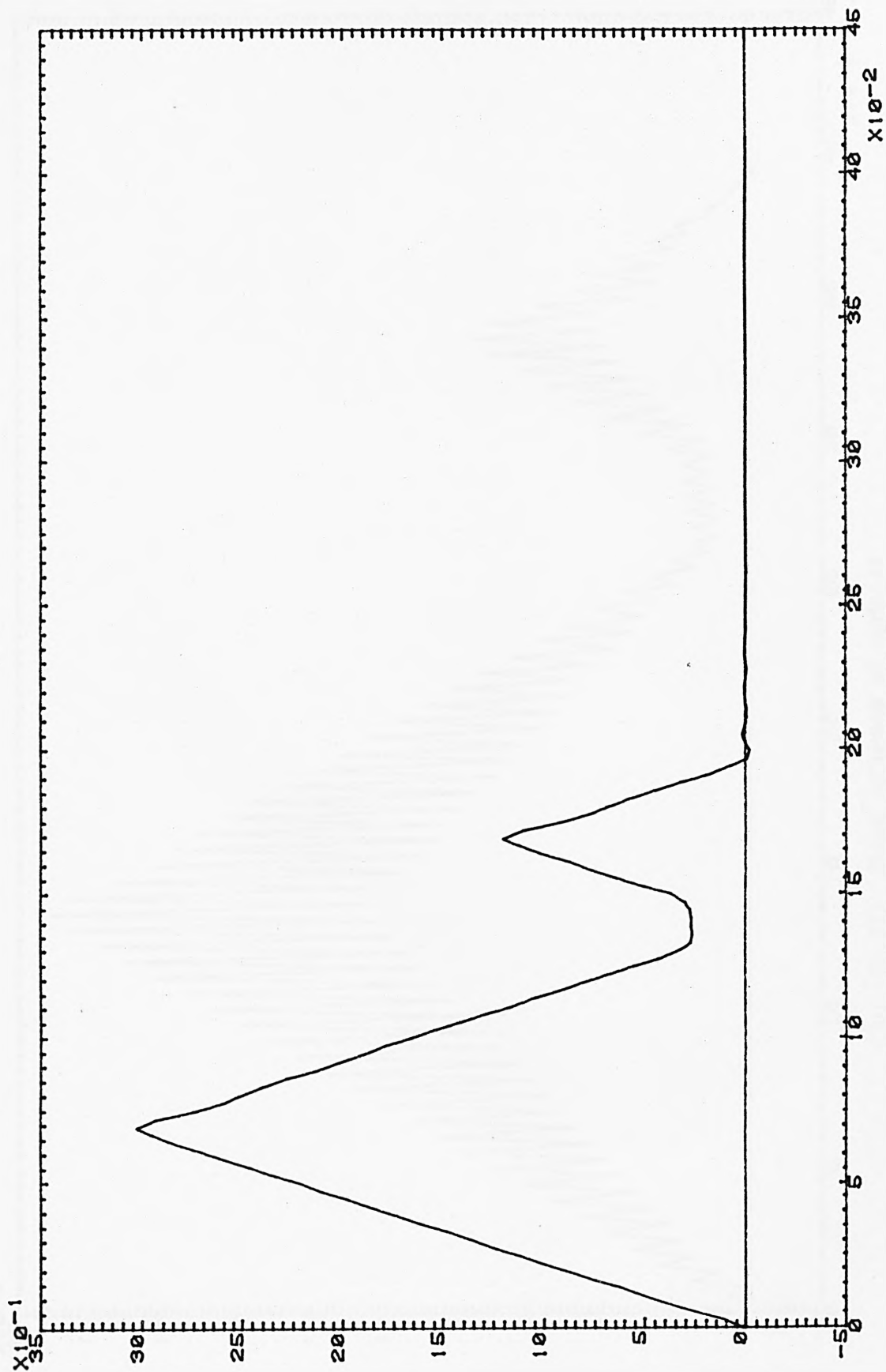


Fig. (6.34) Shear stresses at node 38.

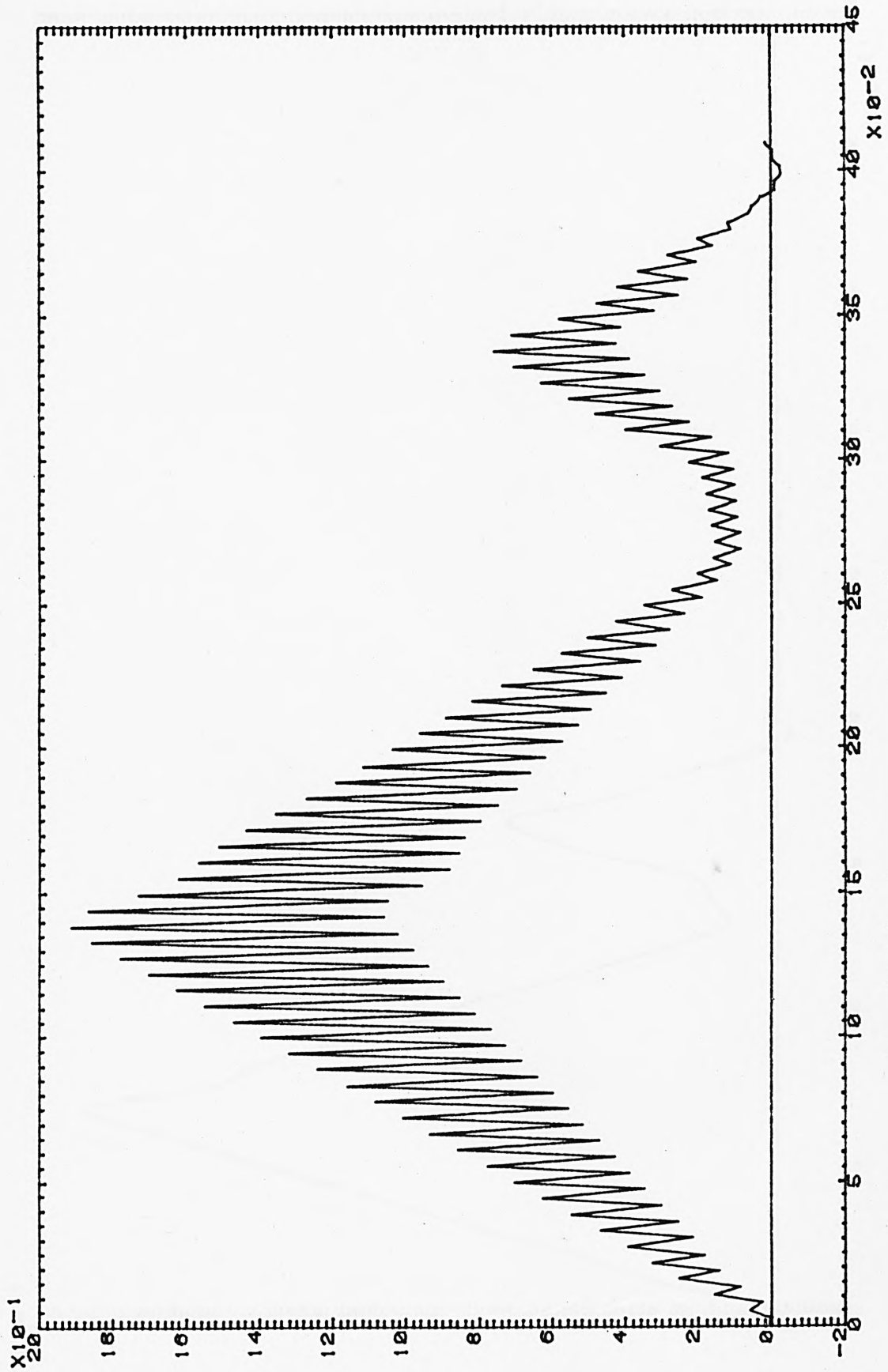


Fig. (6.35) Shear stresses at node 49.

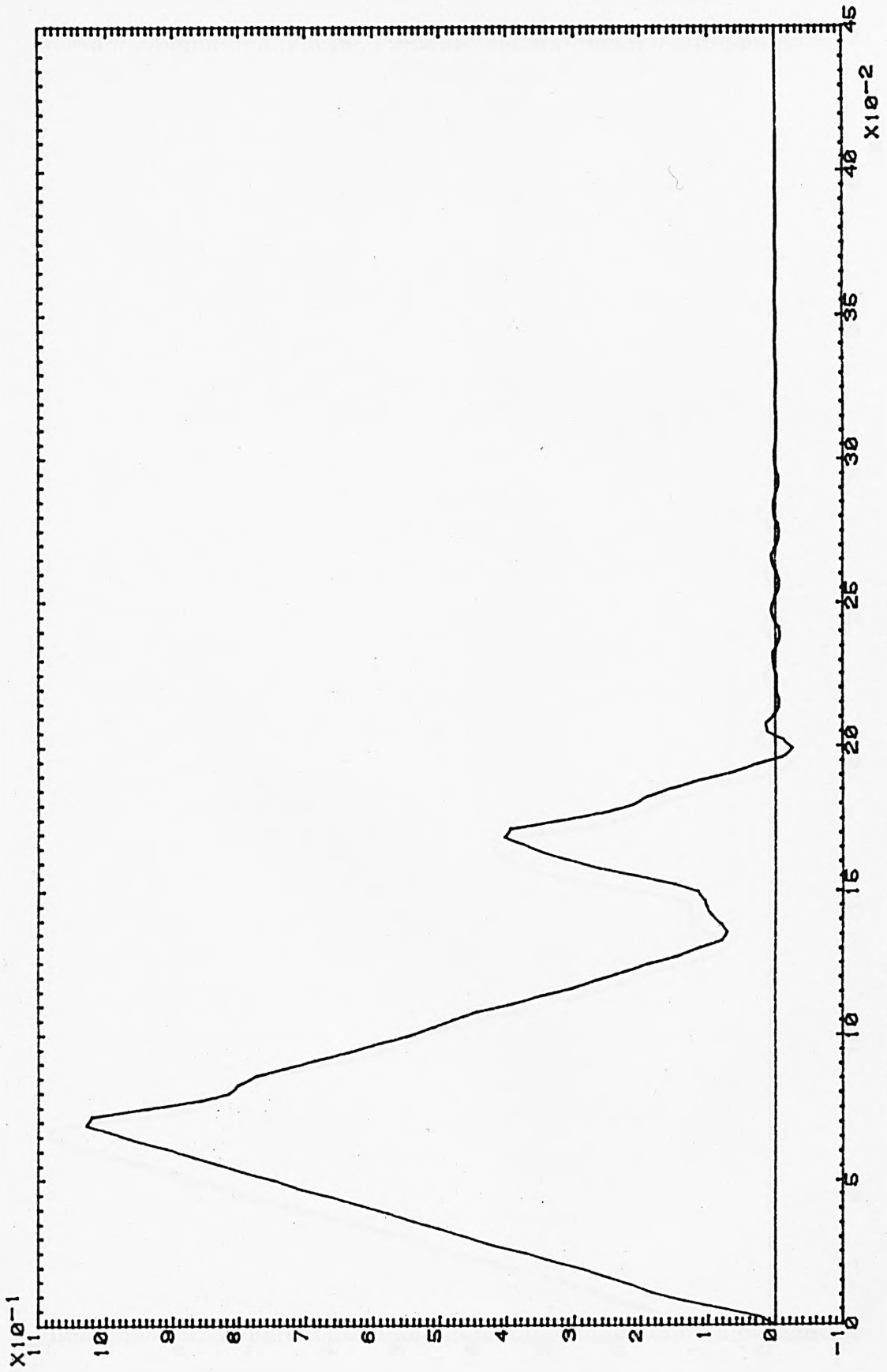


Fig. (6.36) Shear stresses at node 58.

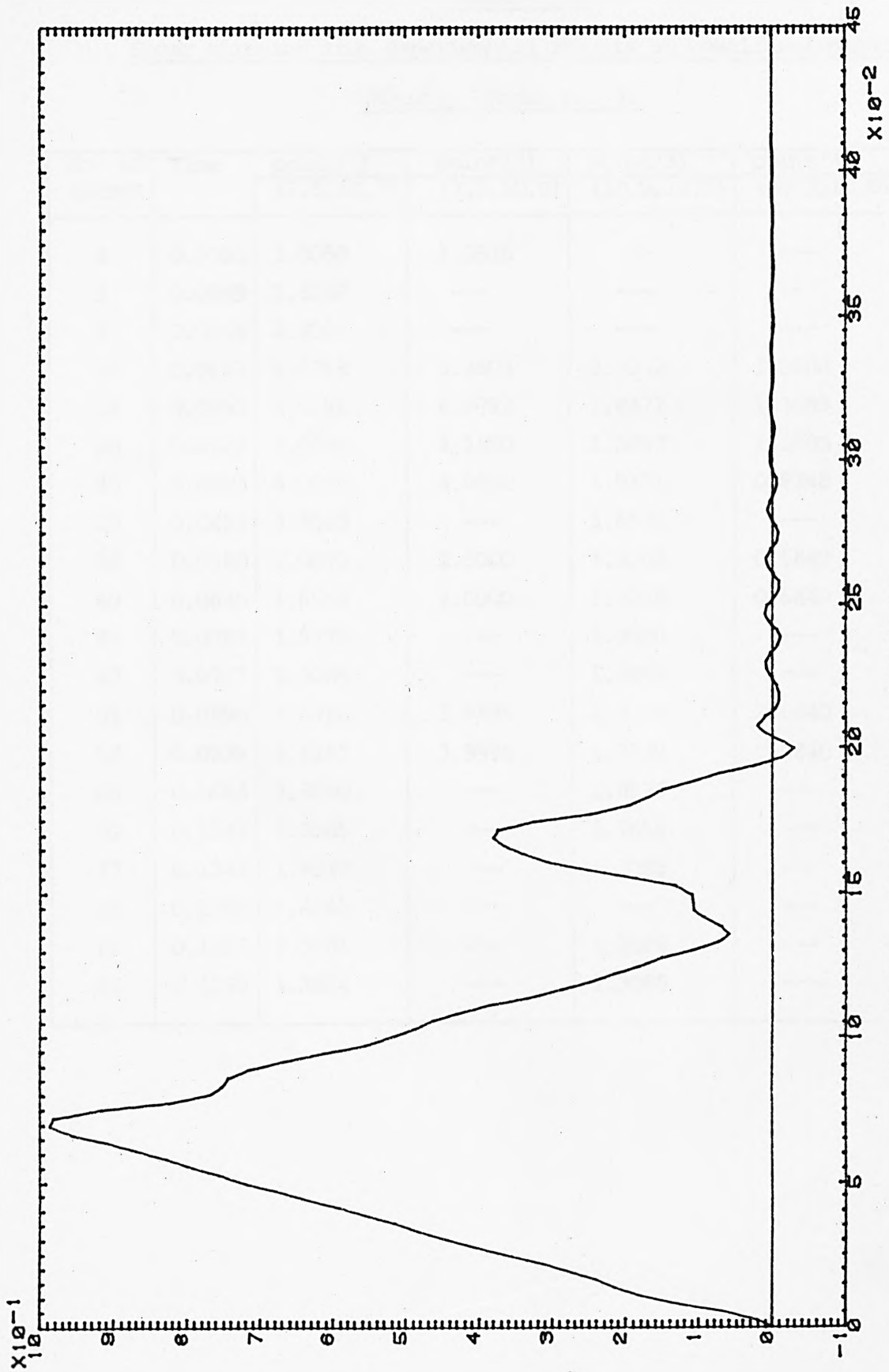


Fig. (6.37) Shear stresses at node 69.

Table (6.3)

Shear stresses from experimental results at specificel points

(N/cm²). Model No. 3.

No. of frames	Time	point (1)	point (2)	point (3)	point (4)
		(7.5,12.5)	(7.5,10.0)	(10.0,12.5)	(10.0,10.0)
2	0.0033	1.0059	1.3516	---	---
3	0.0049	2.8287	---	---	---
4	0.0065	2.8010	---	---	---
10	0.0161	6.6718	3.4603	2.7032	1.3680
15	0.0250	8.7591	4.9792	2.8477	1.3680
20	0.0323	7.0084	4.1850	2.5703	1.3680
25	0.0404	6.0700	4.0000	1.9151	0.9248
28	0.0453	3.8523	---	1.6935	---
36	0.0580	2.0672	2.0000	1.3088	0.6840
40	0.0640	1.6964	2.0000	1.3088	0.6840
45	0.0728	1.5775	---	1.3088	---
48	0.0777	2.3086	---	1.3088	---
55	0.0890	3.6726	1.9849	1.4755	0.6840
58	0.0939	3.5287	3.9999	1.7539	0.6840
66	0.1668	3.8990	---	1.8576	---
70	0.1133	3.7085	---	1.7656	---
77	0.1246	1.9030	---	1.3088	---
80	0.1290	1.4142	---	---	---
82	0.1327	2.0181	---	1.3088	---
84	0.1359	1.2824	---	1.3088	---

Table (6.4)

Shear stresses at points of interface (N/cm²) . Model No.4.

No. of frames	Time	Shear stresses at centre line (7.5,12.5)	
		Above interface	Below interface
1	0.0015	1.7021	---
2	0.0030	0.6878	---
3	0.0045	4.0948	---
4	0.0060	4.7373	2.1151
5	0.0076	6.8970	3.2129
7	0.0106	8.6320	4.3217
10	0.0152	9.8350	4.5312
15	0.0228	12.2532	6.1262
20	0.0304	4.1470	2.0702
25	0.0380	3.3505	1.9033
35	0.0533	3.2301	1.5171
45	0.0685	6.8307	2.3213
50	0.0761	7.2923	3.4318
55	0.0825	5.4718	2.9027
57	0.0868	4.2102	2.4038
60	0.0913	3.1055	2.1025
65	0.0989	3.8362	1.8342
70	0.1066	3.1057	1.5373
80	0.1218	2.6724	1.0224
85	0.1294	1.3678	---
90	0.1370	2.0153	---
95	0.1446	1.0519	---

CHAPTER 7

THE INFLUENCE OF IMPACT LOADING UPON THE DESIGN OF AIRFIELD PAVEMENTS

7.1 INTRODUCTION

The critical areas for consideration in the design of aircraft pavements are the primary taxiway and runway ends. The introduction of jet aircraft and the possibility of greater dynamic response have resulted in the re-evaluation of the design principles to examine what is the critical airfield area and critical type of load to be considered[82,83,84]

Several methods of design for airport pavements are available. Although there is no one method for flexible pavement design accepted by all agencies, there are five basic methods which have been briefly summarized[1,2,4,85].

The value of the applied load and its description are important factors which affect the design of pavements for jet aircraft. In this chapter the dynamic and impact loads caused by aircraft landing gear are discussed and their effect on pavement design evaluated. Procedures for design of asphalt pavements, which treat the structure as a layered elastic half space, which have been developed by the Shell Company and by the Asphalt Institute were used to evaluate the impact loading factor. By using the DFEP program, a comparison has been made between the method

developed by the Shell Company and that presented in this thesis. Numerical examples have been given which assess the impact factor and the structural pavement design. Since the overlay of pavements is considered to be an important aspect of airfield operation in the future, recommendation for dynamic and impact loading is discussed.

This thesis is primarily concerned with the study of impact forces on multi-layered half space and their effect on the design of runway ends. The objective of the study, therefore, is to assess the dynamic factor and to demonstrate its use in the structural design of pavement.

7.2 DESIGN OF AIRCRAFT PAVEMENTS

Pavement design has been approached from two broad and different points of view. First, the engineer often approaches the problem solely from the standpoint of pavement performance. In contrast, researchers approach the problem largely from theoretical concepts[2,3].

There are five basic methods which deal with the design of flexible airfield pavements. These are:

- (a) The Corps of Engineers method (CBR)analysis
- (b) The Federal Aviation Administration (FAA) method
- (c) The Canadian Department of Transportation (CDOT) procedure
- (d) The Asphalt Institute method
- (e) The Shell method

(a) Corps of Engineers (CBR) Method

The CBR method of design was first used by the California Division of Highway as a result of surveys made during the years 1928 and 1929[2] . The investigations showed that the principal types of pavement failure were, lateral displacement of the subgrade material as a result of the pavement absorbing water, differential settlement of materials underneath the pavement and the excessive deflection of the materials under the pavement. The CBR test was devised in 1929 to predict the behaviour of paving materials. Tests were performed on a large number of typical crusher-run materials which were considered representative of base-course materials. The average of these test results was designated CBR100 percent. The CBR test is a penetration test and is expressed as a percentage of the penetration resistance to that of a standard value for crushed stone. The test is valid only when a major portion of the penetration of the piston is caused by shear deformation. Since the CBR is a percent of standard load, it is possible in some cases to measure CBR values in excess of 100 percent. Generally, the CBR at 0.1 inch penetration is used for design purposes. However, if a bearing ratio of 0.2 inch penetration is greater, then this value is used.

The Corps of Engineers in the US made an extensive survey of the different methods of flexible-pavement design[3] . As a result of these investigations the CBR method was

adopted. The thickness of the different elements comprising a pavement is determined by the CBR values.

This method has some advantages and disadvantages, one of the advantages is the simplicity with which the design test can be performed. A disadvantage of the procedure is that the test is empirical and, therefore, the design is based upon correlations. However, much research has been carried out which permits extrapolation of the data from one wheel load and gear configuration to another.

(b) The Federal Aviation Administration (FAA) Method
Civilian airports within the United States are designed in accordance with FAA advisory circular standards[2,3]. Although subgrade CBR tests may be used to evaluate the design of subgrade conditions, the FAA design procedure uses its own soil classification groups, subsurface drainage conditions, and the presence or absence of frost problems. Major airfield pavements may be designed solely upon soil classification and a quantitative assessment of the environmental conditions existing at the site.

The general design procedure involves a knowledge of the characterization of the pavement materials (subgrade as well as pavement components), the effect of the critical aircraft load, design repetitions and the condition for frost.

(c) Canadian Department of Transportation (CDOT)

Method

This method, for determining the required thickness of flexible airfield pavements, was developed from an investigation into the load-carrying capacity of the runways at Canadian airports by means of plate bearing tests. Tests were made on the surface, base course, and subgrade at a large number of test locations. In addition, cone-bearing, penetrometer, CBR, and triaxial compression tests were performed on the subgrade at each test location and were correlated with the corresponding subgrade plate-bearing tests. From this original investigation, one empirical thickness and design equation are developed[2].

The thickness design procedure is based upon the selection of a critical design aircraft for each new pavement facility. The original procedure assumes that the thickness obtained is adequate for "capacity" operations at the airfield. This is generally acknowledged to be equivalent to about 5000 coverages of the design aircraft. Since cold weather is predominant in Canada, the effects of frost upon design thickness is included in the analysis. This include a reduction in strength and allowance for heave due to frost penetration.

(d) The Asphalt Institute Method

The Asphalt Institute published its airfield pavement design manual (MS-11) in 1973 with a computer program

solution manual[3,86] . The method is applicable to the design of pavements having asphalt mixtures employed for all courses above the subgrade or improved subgrade intended for air carrier (generally greater than 60 kip gross weight) aircraft. In contrast to most other present airfield pavement design methods, the design utilizes the concepts of a mixed traffic analysis rather than the selection of a critical or design aircraft. This procedure is conceptually identical to the traffic analysis frequently used in highway design. The standard aircraft used is a 358 kip gross weight DC-8-63F and the relative destructive effects of 22 major aircraft types are given in the manual. The design is based on the theory that a full-depth asphalt pavement is a multi-layered elastic system and that the application of a load to the pavement produces two critical elastic strains. These strains are the horizontal tensile strain ϵ_t at the bottom of the asphalt-concrete-layer and vertical compressive strain ϵ_c at the top of the subgrade layer. Each strain must be examined separately in the design analysis. Design criteria, in terms of maximum allowable values for both critical strains, evaluated at a critical asphalt concrete modulus E_1 , have been established and are used as the basis for selection of the design thickness. The failure criteria for fatigue cracking of the asphaltic concrete is based primarily upon the work of Kingham [87]. The compressive subgrade strain criteria was developed from a multilayered analysis of pavement structures designed

in accordance with the Corps of Engineers Design equation for CBR analysis

Since the modulus of asphalt concrete is temperature dependent, the period of the year for greatest potential damage to the pavement varies with the temperature condition peculiar to each geographical location. The ϵ_0 value which is an indicator of permanent deformation, is greater when the pavement temperature is high and the asphalt modulus is low.

Conversely, during cool conditions when the asphalt modulus is high, the horizontal tensile strain ϵ_t at the bottom of the asphalt bound layre are critical for repetitive cracking. Design thickness required to overcome a particular type of distress, therefore, vary with different environmental conditions.

The Asphalt Institute method provides a detailed analysis which relates the mean annual air temperature and pavement thickness (T_A). As the annual average air temperature increases, the T_A increases to satisfy deformation requirements. On the other hand, thicker pavements are required in cooler environments to satisfy the fatigue cracking criteria.

This method contains a number of innovative concepts for design. It permits an airfield pavement to be designed for mixed traffic conditions which is representative for most large civil airports. In addition, environmental

influences are considered for asphalt-bound layers since the influence of temperature on asphalt concrete stiffness is significant.

The theoretical design method advocated by the Asphalt Institute is a departure from the empirically oriented designs of the Corps, FAA and CDOT.

(e) Shell Method

This method of design is applicable for pavement structures consisting of asphalt concrete, untreated granular base and prepared subgrade or asphalt concrete resting directly on subgrade. The structure is represented by a three-layer elastic system which assumes full friction between the layer interfaces [3].

The critical conditions for design are:

1. Horizontal Tensile Strain on the Underside of the Asphalt-Bound Layer (ϵ_h , Layer 1, Figure 7.8)

Cracking may occur in the asphalt layer if ϵ_h is large. The value of tensile strain is dependent on the fatigue characteristics of the asphalt mixture with an allowable strain value of 2.3×10^{-4} associated with 10^6 cycles of strain .

2. Vertical Compressive Strain in the Surface of the Subgrade (ϵ_v , Layer n, Figure 7.8)

If this value exceeds a specific limit, depending on traffic, permanent deformation may occur at the top of the subgrade leading to further permanent deformation (rutting) at the surface of the pavement. The limiting value of vertical compressive strain, which is also dependent on the number of load applications, has been established as 10.3×10^{-4} at 10^6 repetitions.

The fatigue characteristics of asphalt concrete mixtures can be represented by an equation of the form

$$N_f = K \left(\frac{1}{\epsilon_t} \right)^n$$

where N_f = applications to failure

ϵ_t = tensile strain

k, n = experimentally determined coefficients dependent on mixtures characteristics.

Materials of the layers are assumed to exhibit linear elastic behaviour. For asphalt concrete the time of loading and temperature dependency are recognized.

Tensile strains in the asphalt concrete are determined at a stiffness (E_1) of 900000 lb/in^2 (this corresponds to a temperature of 50°F and a time of loading of 0.2 s).

For the determination of subgrade strain, the air temperature is assumed to be 95°F and an effective stiffness

modulus in the range 100,000 to 200,000 lb/in² (depending on thickness of asphalt concrete) is selected. The modulus of the untreated granular base is a function of the subgrade modulus (E_3) and is dependent on the thickness of this layer (h_2) ranging from two to three times E_3 . The modulus of the subgrade soil has been related to the CBR based on dynamic vibratory tests in situ by the relation.

$$E_3 = 1500 \text{ CBR}(\text{lb}\cdot\text{in}^2)$$

Poisson's ratio, γ , for all layers has been assumed to be 0.35.

7.3 DYNAMIC PHENOMENA IN AIRFIELD PAVEMENTS

Consideration of dynamic effects under high-rate loading is becoming increasingly important both to the aircraft landing gear designers and the civil engineer responsible for preparation of soil and airfield surfaces. Airfield construction engineers are primarily concerned with preventing pavement distresses and frequent repairs. The dynamic response effects of gear loads on the surface due to manor roughness can increase pressure in the pavement sufficiently to aggravate the roughness. There is also some evidence that these dynamic effects are causing break up of runways under conditions where conventional flotation formulas indicate that no problems should occur[14].

The mode of aircraft operation is primarily concerned with the style and speed at which the aircraft operates on the design pavement area. It should be noted that there are two major but independent considerations in defining the total response due to dynamic load. First, the variation in operational speeds may affect the response of the various pavement component materials. Secondly, the dynamic response effects of gear loads on the surface due to minor roughness which increase pressures in pavement [88]. The roughness may create extreme stresses in the aircraft as the result of resonant frequencies caused by combinations of speed and gear configuration of the aircraft and the wavelength of the surface. One obvious means of recording runway roughness is by use of the profilometer. This is a device that is mounted on a vehicle and measures and records the profile of the pavement surface. Periodic use of this instrument would present a historical picture of the increasing need for maintenance to a runway.

Surface irregularities present a problem peculiar to the bicycle type landing gear. Bicycle gear aircraft have an inherent rocking tendency, called "porpoising", that is increased by the rough surface. This presents an operational hazard to the pilot while increasing the impact loading on the pavement [1].

Heukelom [40] , discussed the factor which governs the movement under a rolling load against those under sustained vibration. He suggested the dynamic tests of soil and pavements due to their close correspondence with the dynamic character of moving traffic. Figure(7,9) represents mechanical elements governing the movements of the pavement construction under dynamic loading conditions. Much research has also been undertaken to define the dynamic aircraft effects for the design of pavements and their resistance to deformation [89,90,91,92] .

In the case of Helicopters the strength requirements for the landing and take off area are determined by considering the helicopter's dynamic and static wheel loads and the landing gear configuration. Especially, on roofs, dynamic or impact loads must be considered to ensure that the structure will not fail if a helicopter makes a hard landing [3] .

From a broad engineering standpoint, both the response of aeroplane to runway and the response of runway to aeroplane as well as their interaction are of interest [88] . In this investigation the response of runways to aeroplanes was considered in the dynamic analysis. Since the types of landing gears and wheel configuration represent a major factor in dynamic response of runway pavement, more information and discussion is given in the next section.

7.4 LANDING GEAR AND DYNAMIC RESPONSE PREDICTION

An aeroplane can land safely with the airplane in various altitudes at the instant of ground contact. Figure (7.13) illustrates the three altitudes of the aeroplane that were specified by the government aviation agencies for the design of landing gear [93,94,99]. In addition to these symmetrical unbraked landing, special landing such as a braked condition, landing on one wheel condition and side load may occur. These cases must be taken into consideration for the design of landing gear and of runways.

The design of landing gear for present day aircraft reduces the impact forces involved in landing or in taxiing over rough pavements. A special energy absorption unit in the landing gear beyond, absorbs the forces.

A diagram for an aeroplane model in which tyres are represented by linear elastic springs is shown in Figures (7.4) and (7.11). The impact force during landing can be determined. Figure (7.12) shows a runway profile and explains how the dynamic forces during aircraft ground motion and take-off may be obtained.

It will be possible to determine the energy absorption required for the impact during landing when the characteristics of the shock absorber in the landing gear leg are known. The maximum dynamic load can then be calculated.

The maximum kinetic energy of the aircraft to be absorbed normal to the runway during touch down is

$$E = \frac{W}{2g} v^2 \quad \dots \quad \dots \quad \dots \quad \dots \quad \dots \quad \dots \quad \dots \quad (7.1)$$

where v is the ultimate velocity of descent. Assuming that this energy will have to be absorbed completely by the main undercarriage, thus ignoring the energy transmitted to the atmosphere, the required stroke of each shock absorber is derived from

$$E = N_S P_S \lambda (\eta_t \delta_t + \eta_s S) \quad \dots \quad \dots \quad \dots \quad \dots \quad \dots \quad (7.2)$$

where N_S is the number of main gear shock absorbers

P_S is the static load per leg

λ is a reaction factor, or ratio of maximum load to static load per leg

δ_t is the maximum tyre deflection

S is the stroke of the shock absorber, and

η is an efficiency factor, equal to the energy absorbed by the tyre or the absorber divided by the product of P and the maximum deflection or stroke respectively

The reaction factor λ may be assumed equal to 2.0 to 2.5 for transport aircraft and 3.0 for light aircraft. The maximum tyre deflection can be obtained from the tyre handbook, or alternatively from the approximation [94]

$$\delta_t = \text{constant} \frac{\lambda L_w}{P \sqrt{D_t b_t}}$$

where L_w is the static load per wheel and D_t and b_t are the tyre diameter and maximum width respectively. The constant is equal to 5.0. A similar assumption is to take δ_t equal to three times the static deflection of the tyre.

From the above investigation, it is justifiable to assume that the dynamic load during landing will be adapted to the energy which the tyre is able to absorb at maximum deflection. Table (7.2) represents the tyre characteristics and the variation in the contact area due to the dynamic loading factor. These data were used in the analysis of airfield pavements to evaluate the effect on the response of pavements.

7.5 THE ANALYSIS OF THE DYNAMIC RESPONSE OF AN AIRFIELD PAVEMENT

For this analysis a finite element model has been used to simulate the actual pavement behaviour [95 96 97] Duncan, J. M, Monismith, C. L, and Wilson, E. L, described an application of the finite element technique to the analysis of systems representative of pavement structures [96] . They presented the results of the response systems with linear material properties. Comparisons between displacements and stresses computed during the finite element technique and those computed using elastic half-space and layered system analysis were made to establish criteria for boundary conditions in the finite element procedure. For the elastic half-space subjected to a uniform circular load the displacements and stresses computed by the finite element technique compared favourably with those determined from the Boussinesq solution, where the nodal points in the finite element procedure fixed at a depth of 18 radii for the bottom boundary and constrained from moving radially on the vertical boundary at a distance of about 12 radii from the centre. For a three layered system, however, it was necessary to move the fixed boundary in the finite element procedure to a depth of about 50 radii while maintaining the same radial constraints as the single layered half-space analysis [96] . A recent finite element analysis for heavily loaded airfield pavements

was presented by Barker [97] . The computed deflections compared favourably with field measurements and it was concluded that finite element method may be used as a basis of the design of such pavements.

In the present study the results obtained by the former investigators are extended and the response of a pavement subjected to a given impulse was considered. By using the dynamic finite element program which has been developed during the course of this research, a number of examples have been solved and compared with those computed using multi-layered static solutions [2, 97] .

Conventional data for an airfield pavement system has been used as input for the dynamic analysis. Three cases of loading have been considered, Table (7.2). The mesh shown in Figure (7.14) was used for the finite element analysis. Normal stresses at varying depths on the centre line of the model were compared with those calculated using static assumptions. Figure (7.15) shows how the impact force can create higher stresses than those predicted by the elastic layer theory. It is these higher stresses which contribute to the accumulated damages which is known to occur in certain circumstances in runway ends.

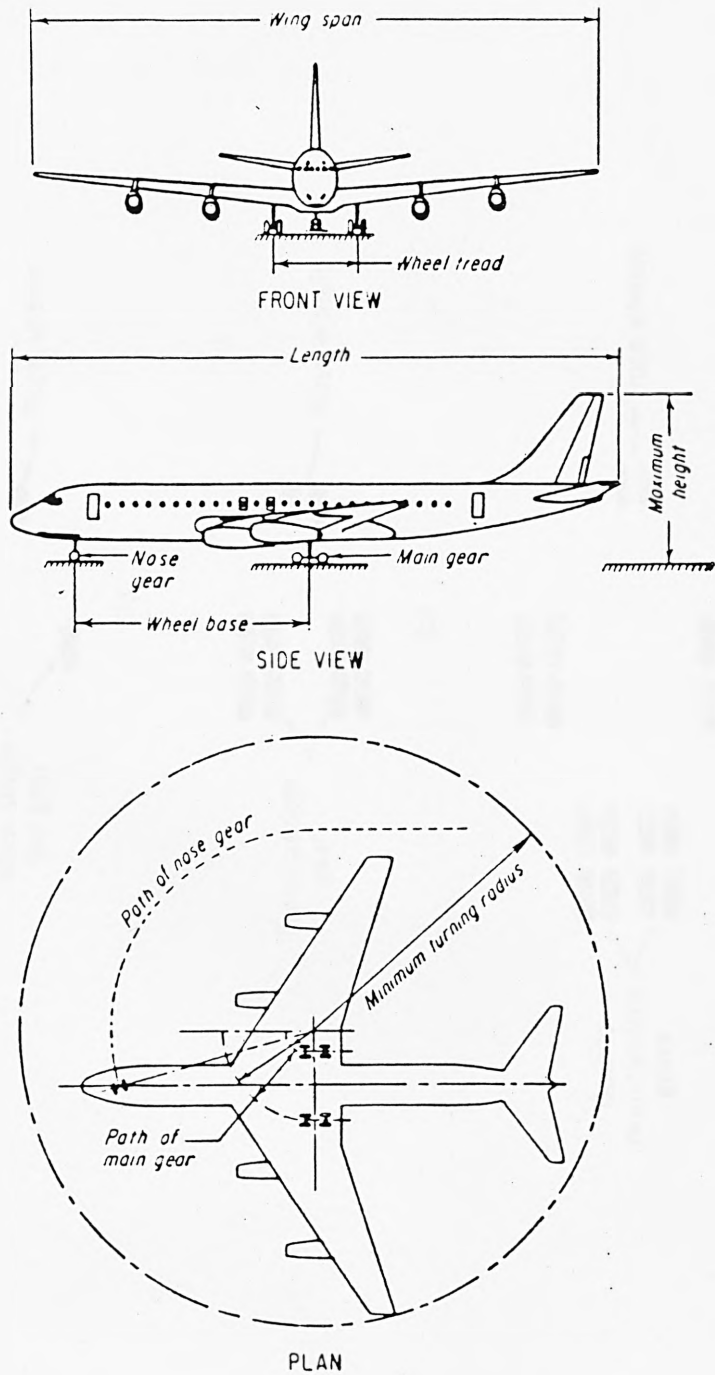


Fig. (7.1)

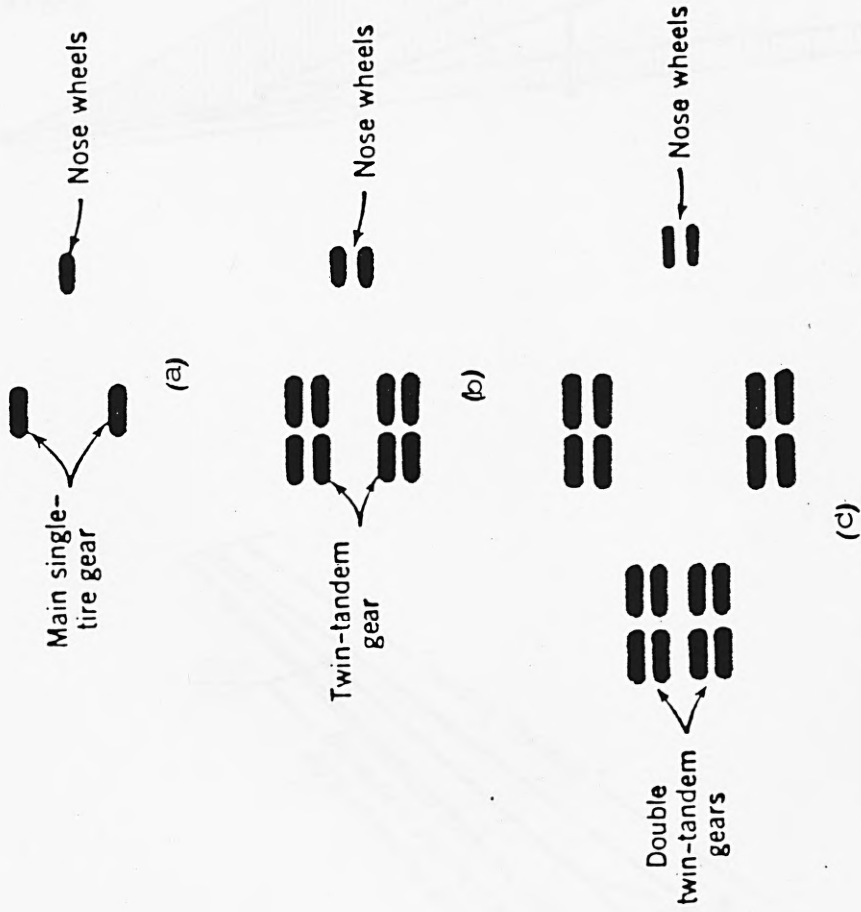


Fig. (7.2) Plan view of several basic types of wheel configuration.
 (a) tricycle landing gear with single tires, (b) twin-tandem landing gear, (c) double twin-tandem gear. (note: not to scale).

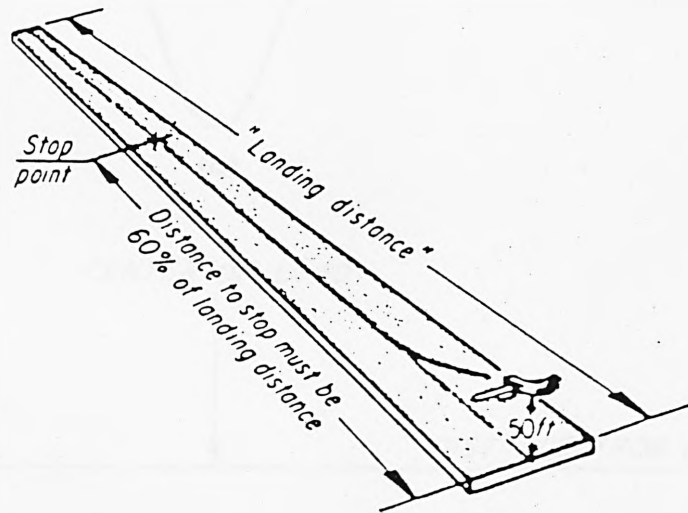
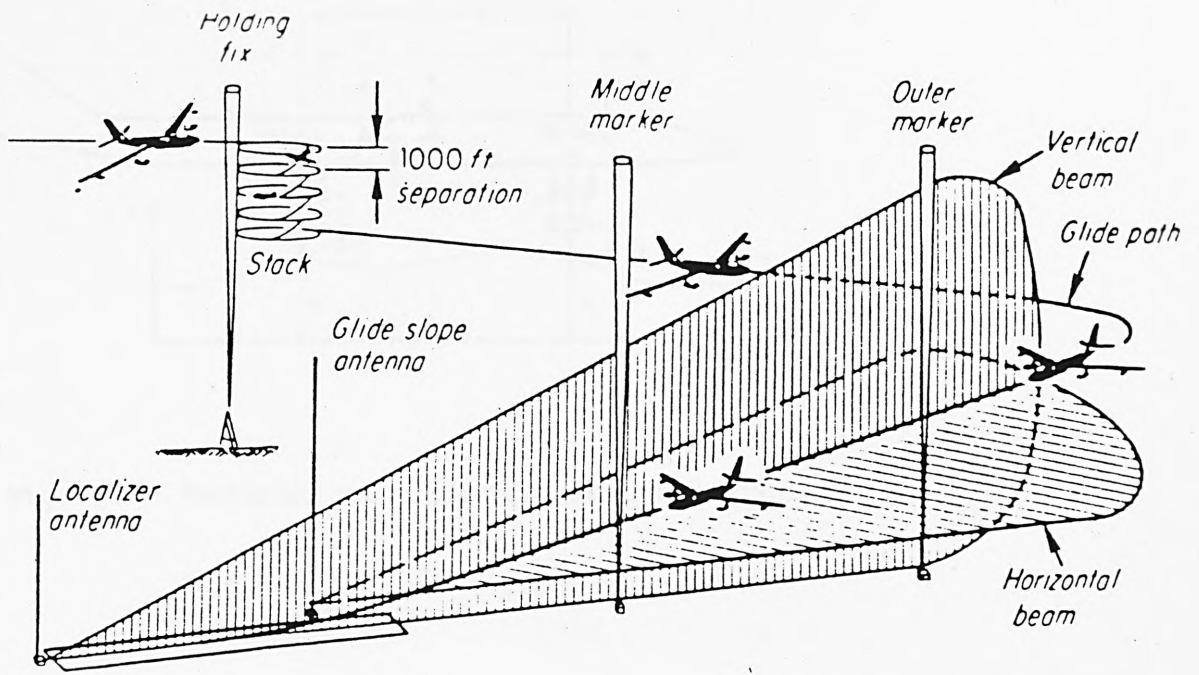


Fig. (7.3) Landing system. (Scientific American Magazine).

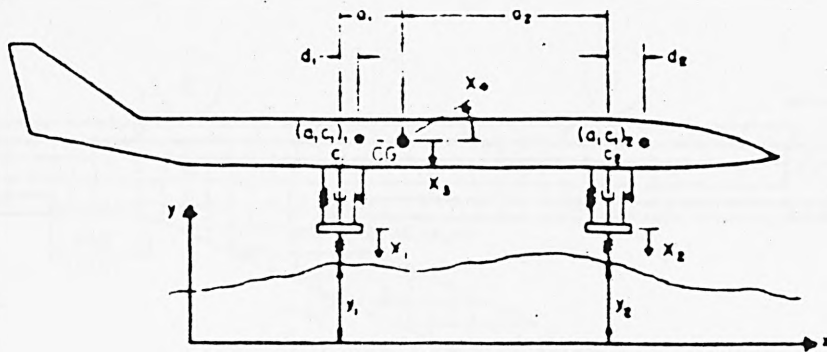


Fig. (7.4) Mathematical model for airplane structures [88].

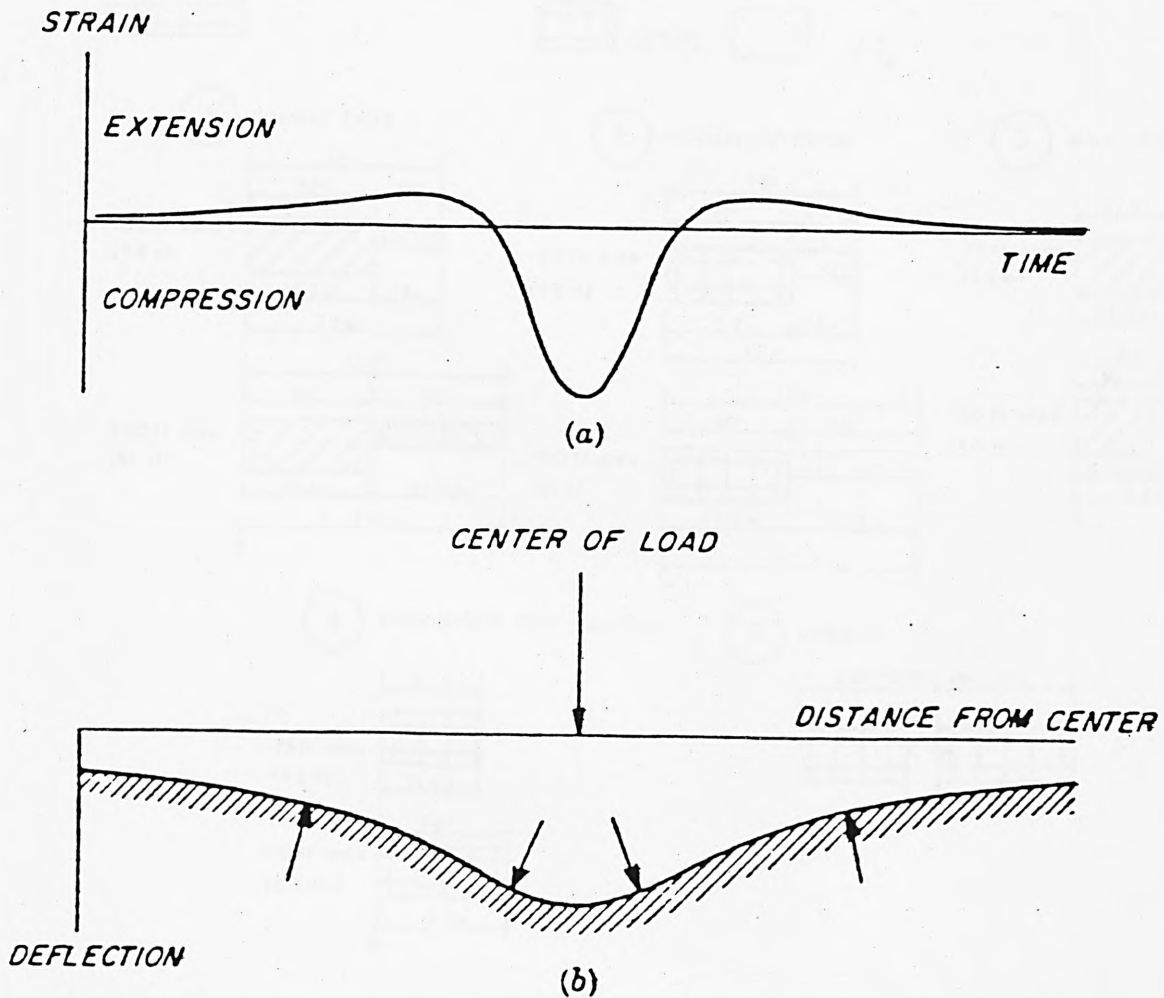


Fig. (7.5) Recorded strain in comparison with deflection of a pavement.

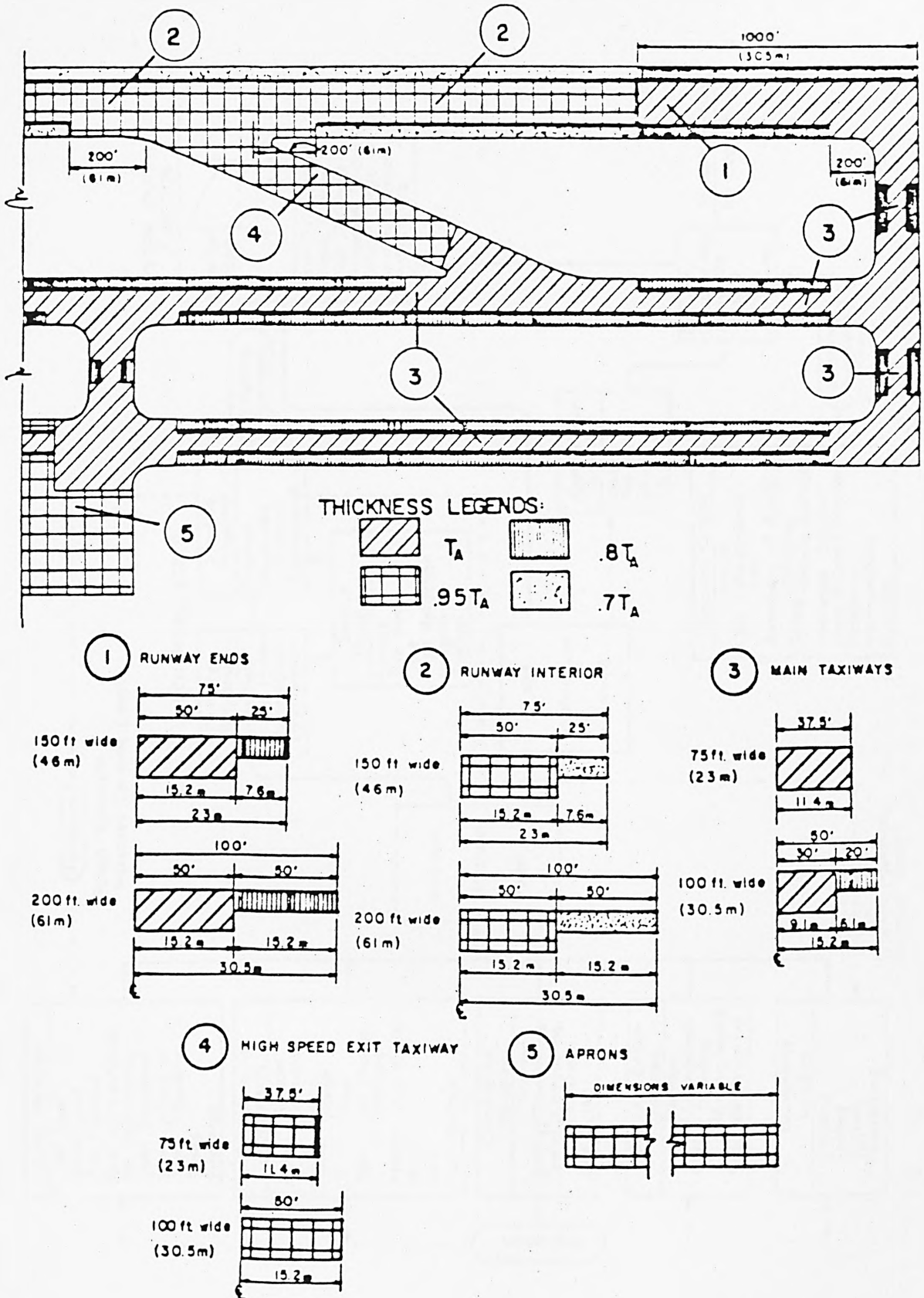


Fig. (7.6) Recommendations for design and cross section thicknesses.

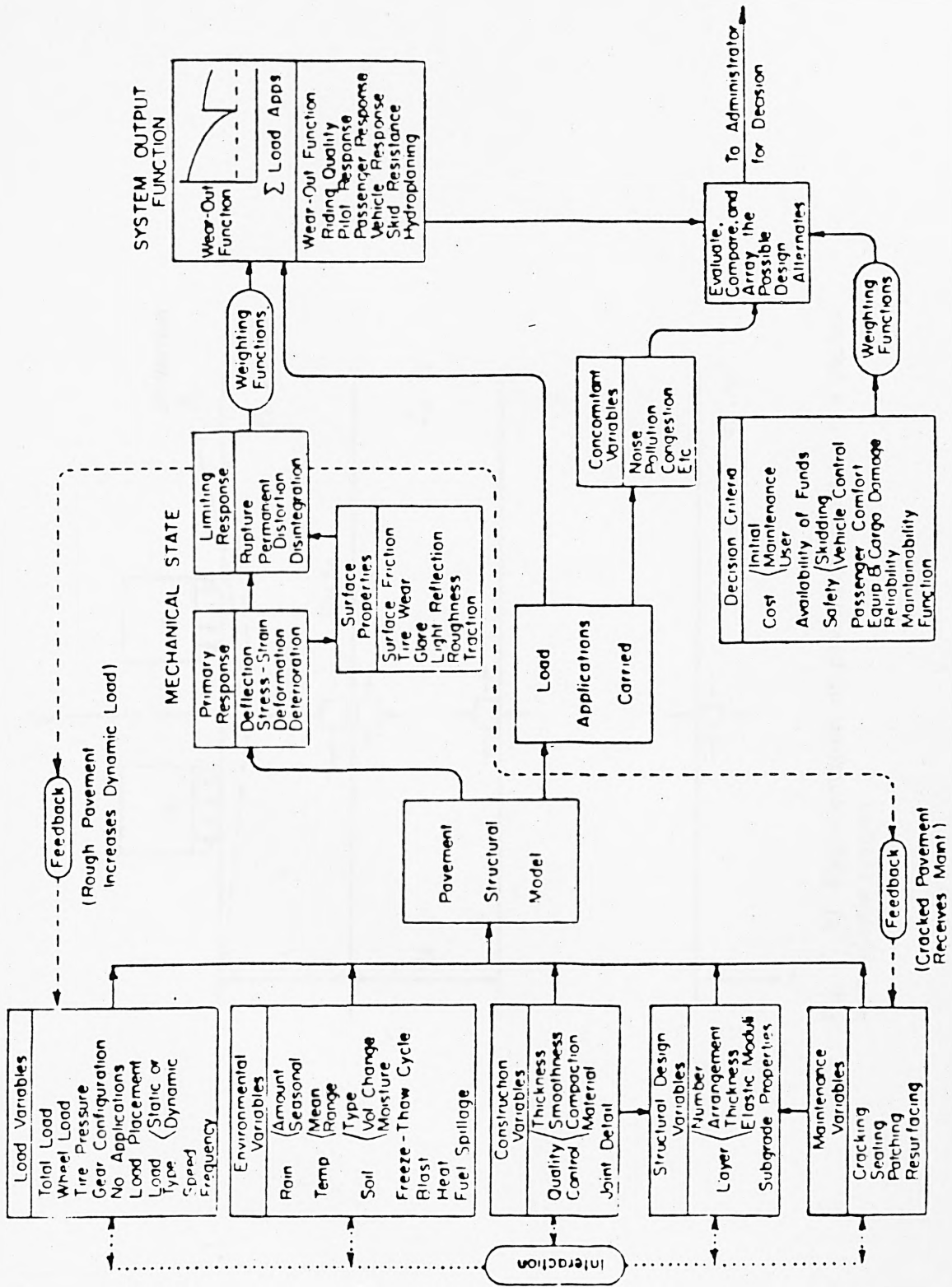


Fig. (7.7) Airfield pavement system [1].

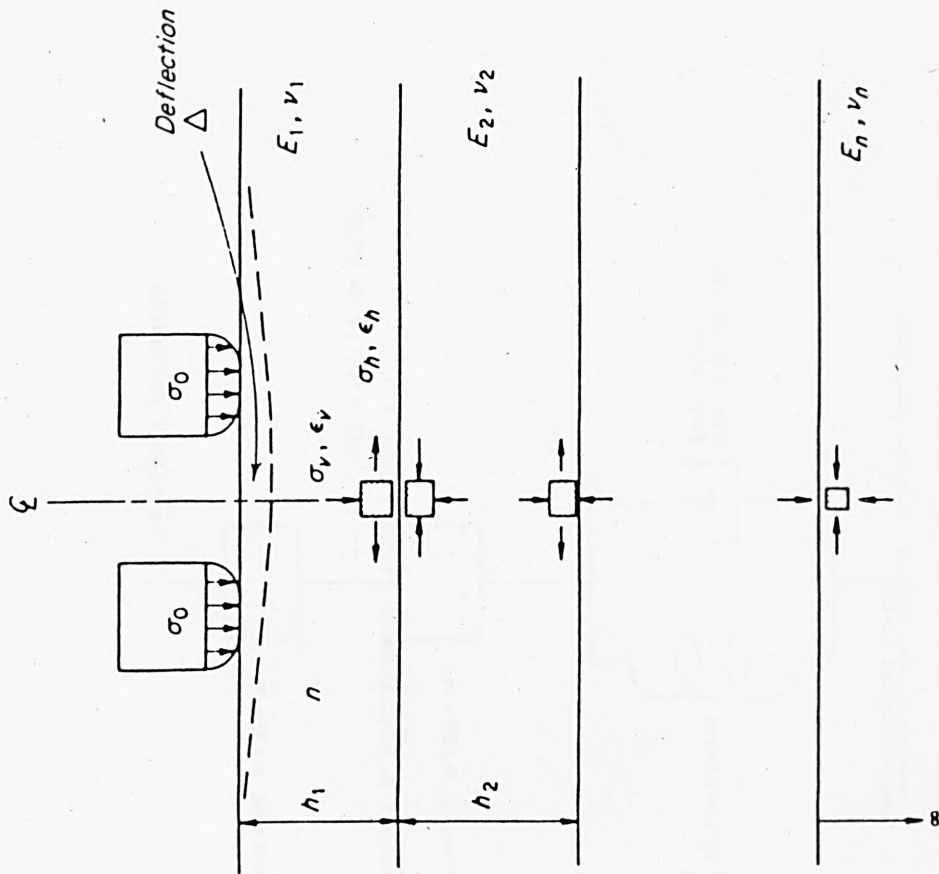


Fig. (7.8) Representation of pavement structure as a multi-layer elastic system.

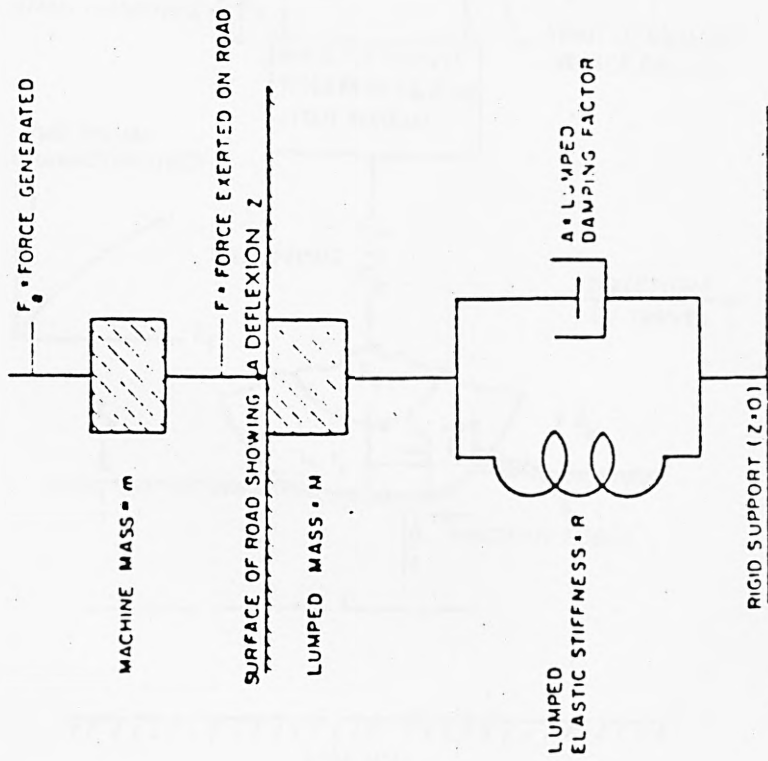
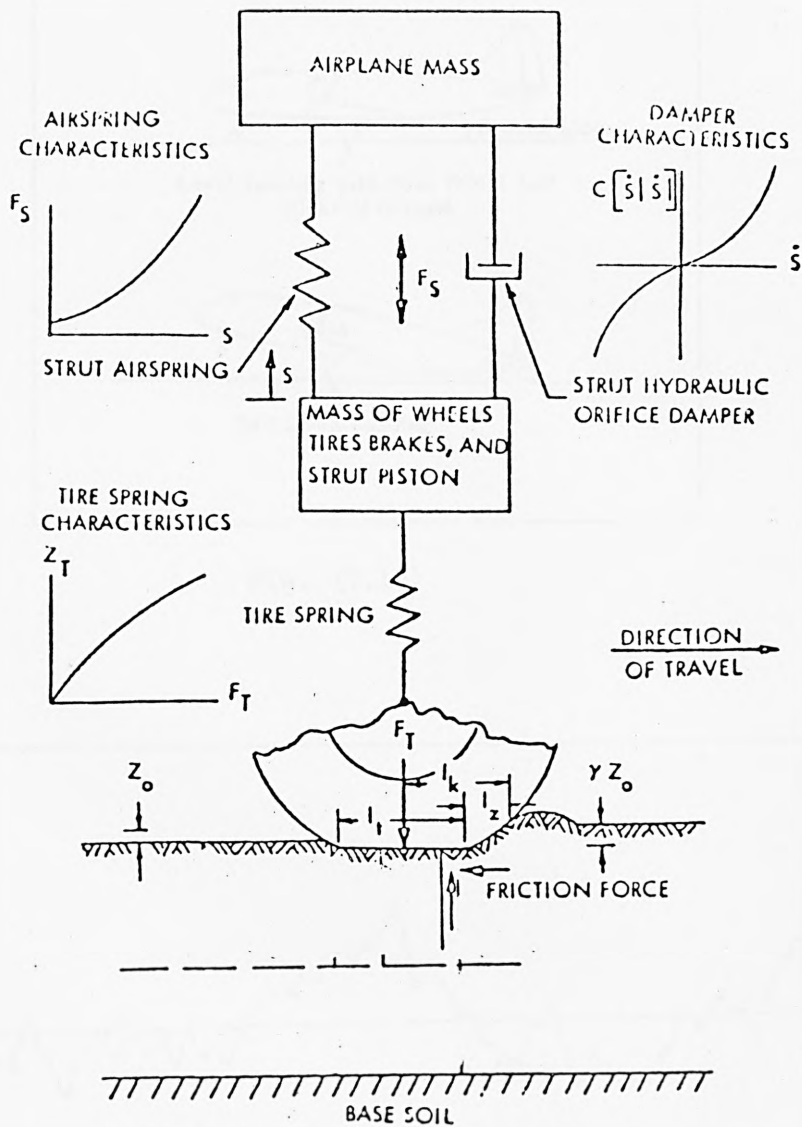


Fig. (7.9) Simplest representation of mechanical elements governing the movements of pavement constructions under dynamic loading conditions [40]



Figure(7.11)Model for Determining Landing Gear Dynamic Characteristics

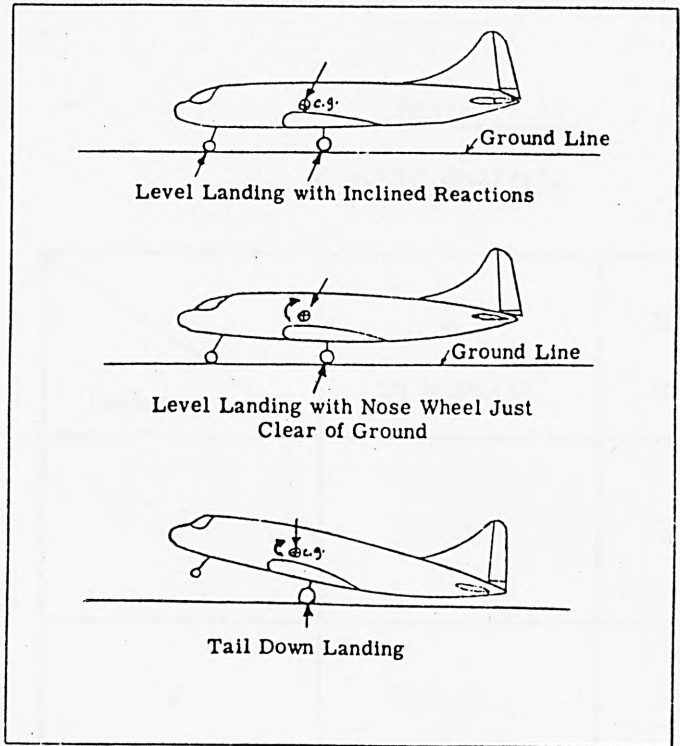


Fig. (7.13)

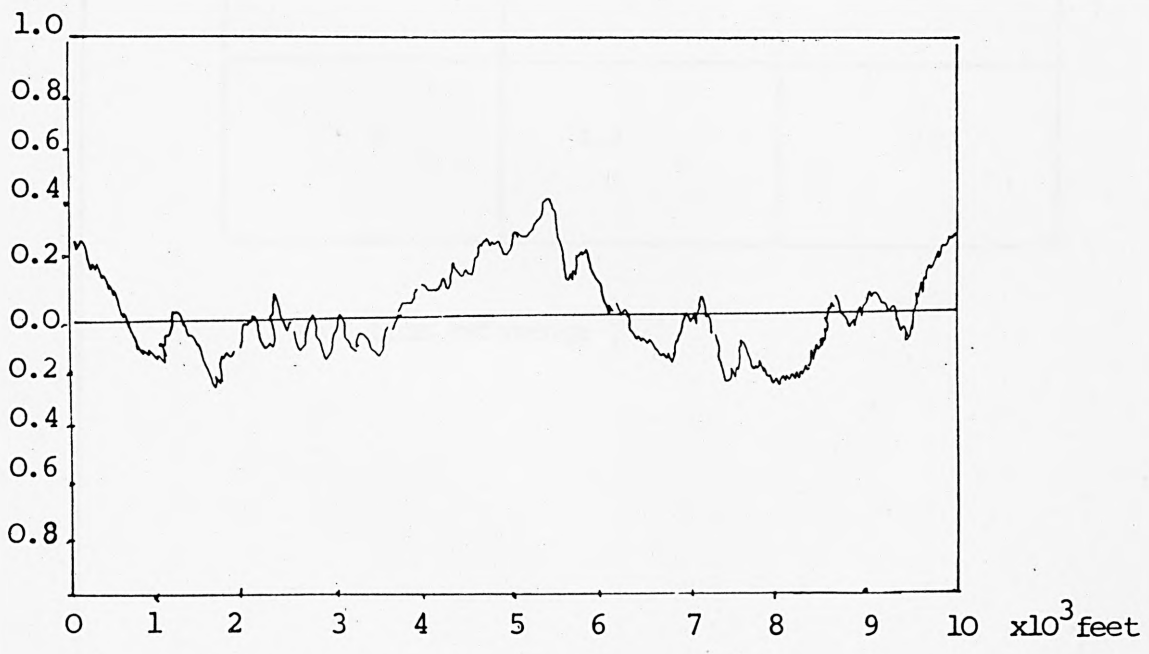


Fig. (7.12) Simulated runway profile (1 ft = 0.305 m)

Table (7.1)
Elastic analysis

Layer	E in kips/in ²	Thickness in inches
1	150.0	3
2	108.0	6
3	22.5	24
4	4.4	INF

Data from reference |97| .

Table (7.2) Tyre Characteristics*

Load in kips $\lambda = 1$	Tyre pressure in pounds per square inch $\lambda = 1$	Contact area in square inches $\lambda = 1$	Contact pressure in pounds per square inch $\lambda = 1$	Equivalent Radius		
				$\lambda = 1$	$\lambda = 2$	$\lambda = 3$
15	45	285	52.65	9.5246	$\sqrt{2} \times 9.5246$	$\sqrt{3} \times 9.5246$
30	100	285	105.27	9.5246	$\sqrt{2} \times 9.5246$	$\sqrt{3} \times 9.5246$
50	165	285	175.44	9.5246	$\sqrt{2} \times 9.5246$	$\sqrt{3} \times 9.5246$
75	290	270	277.78	9.5246	$\sqrt{2} \times 9.5246$	$\sqrt{3} \times 9.5246$

* 49x17 , 26 - ply rating tyres $\lambda =$ Dynamic loading factor

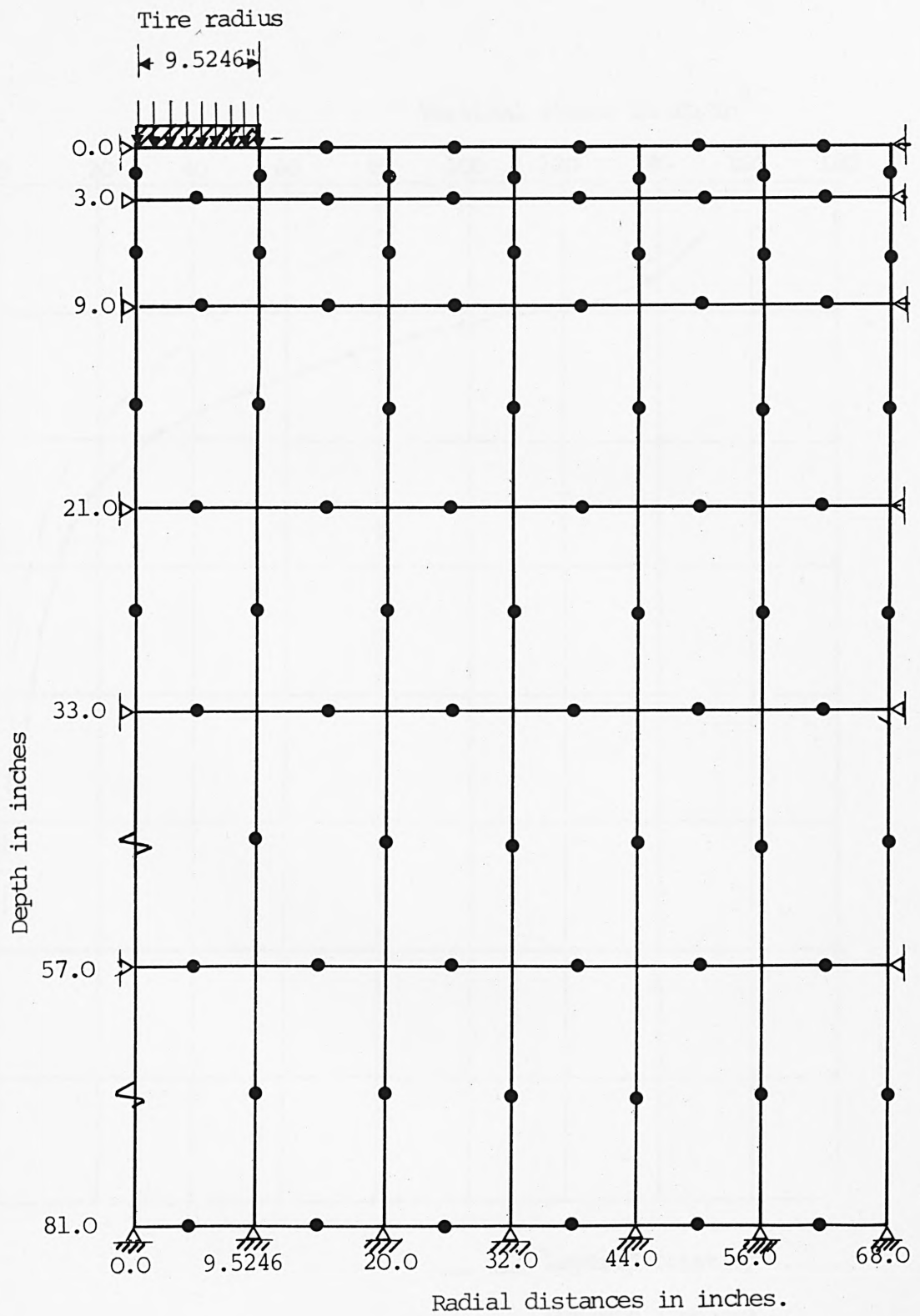
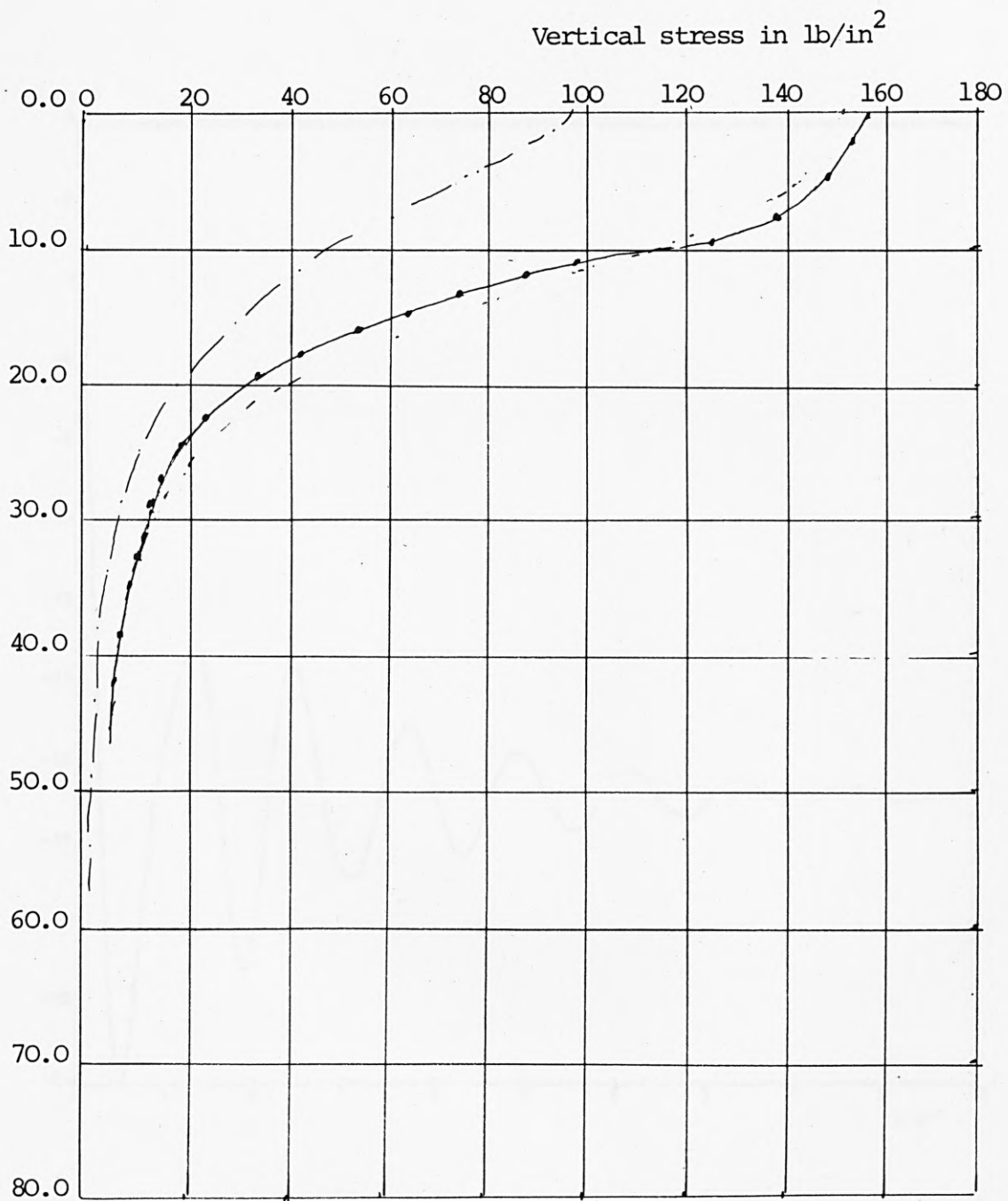


Fig. (7.14) Mesh used for finite element analysis



— — Layered (static)

—●— Dynamic (impact)

$\lambda = 3$

Time of impact 0.2 sec

Fig. (7.15) Vertical stresses versus depth in dynamic (impact) and atatic solution.

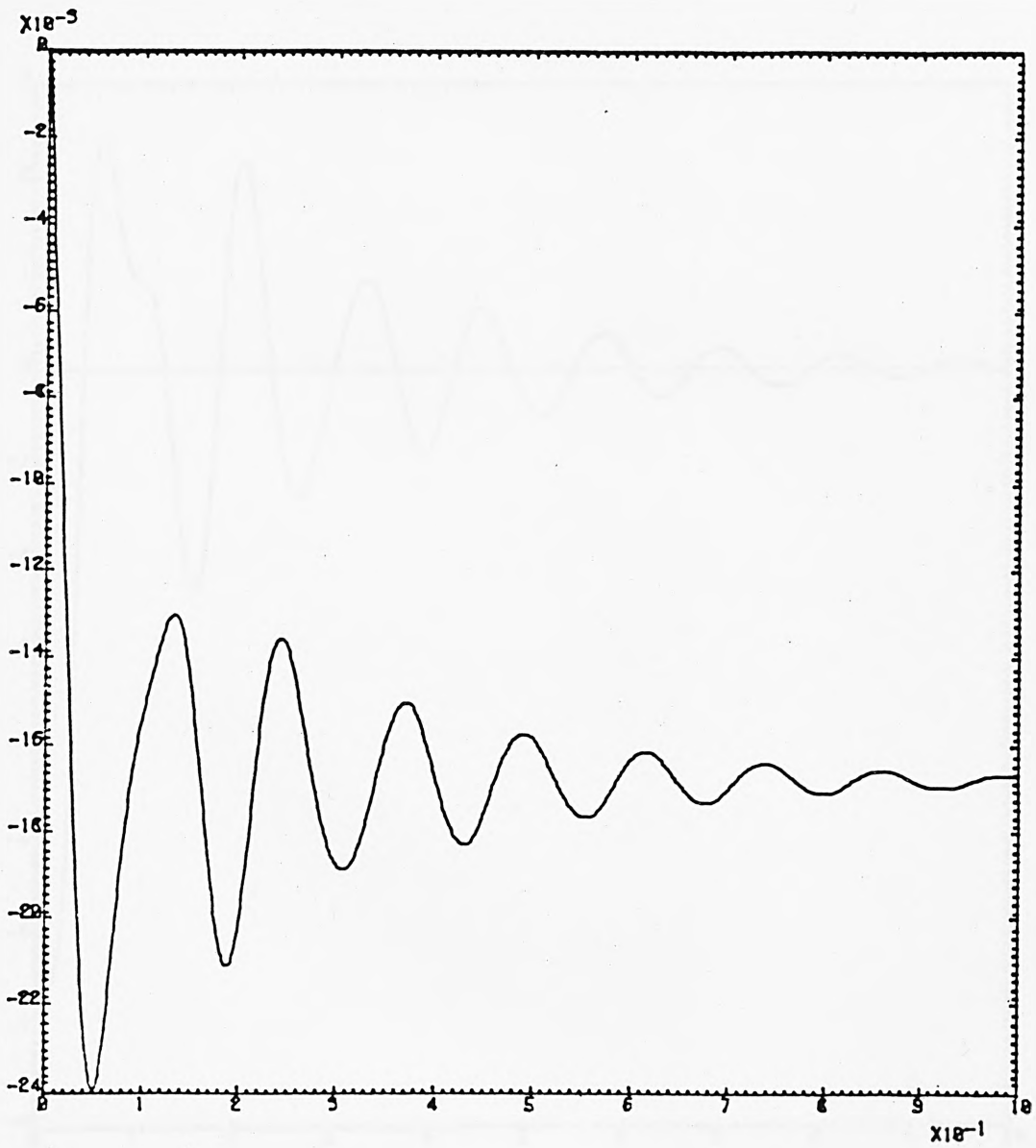


Fig. (7.16)

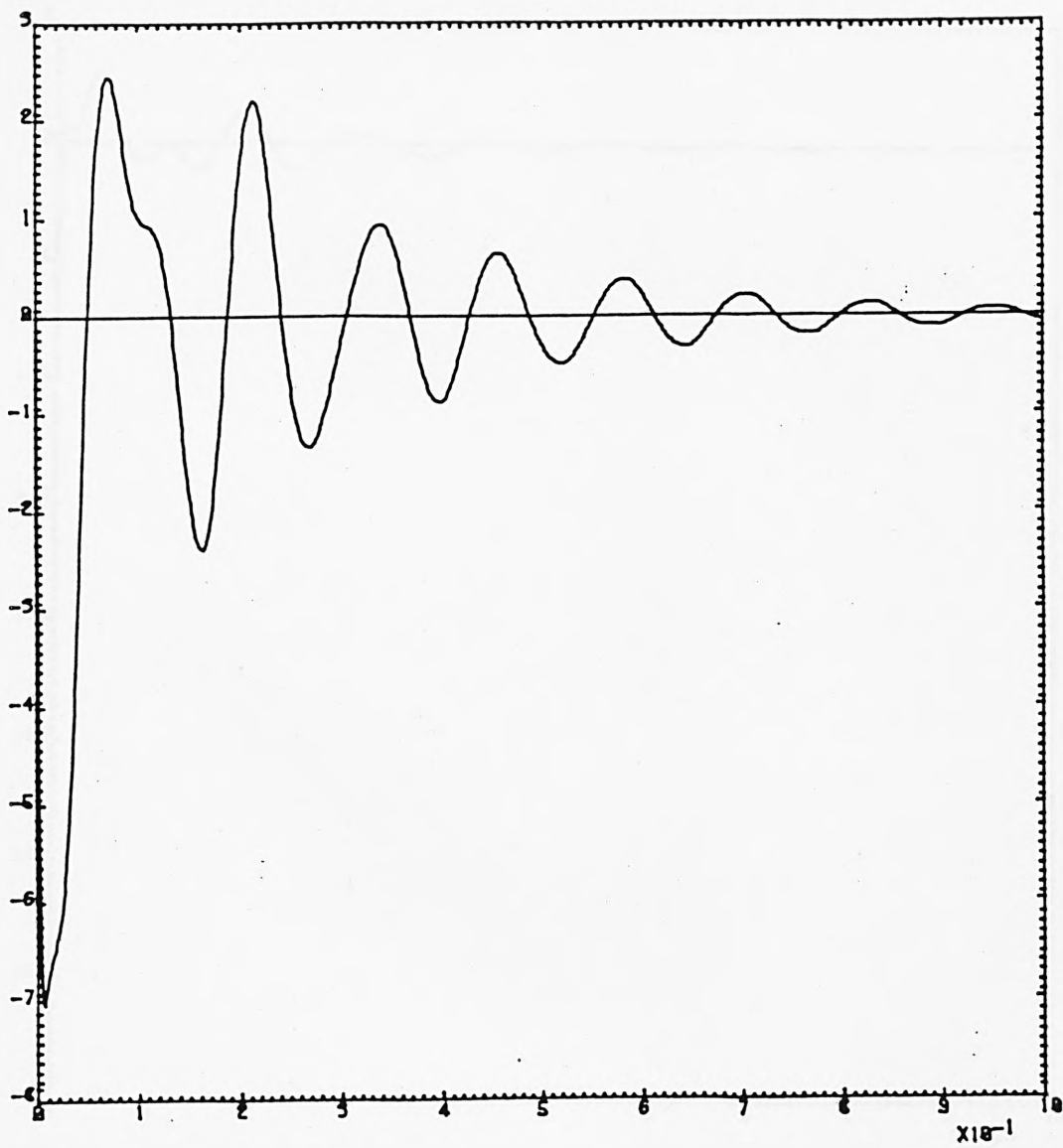


Fig. (7.17)

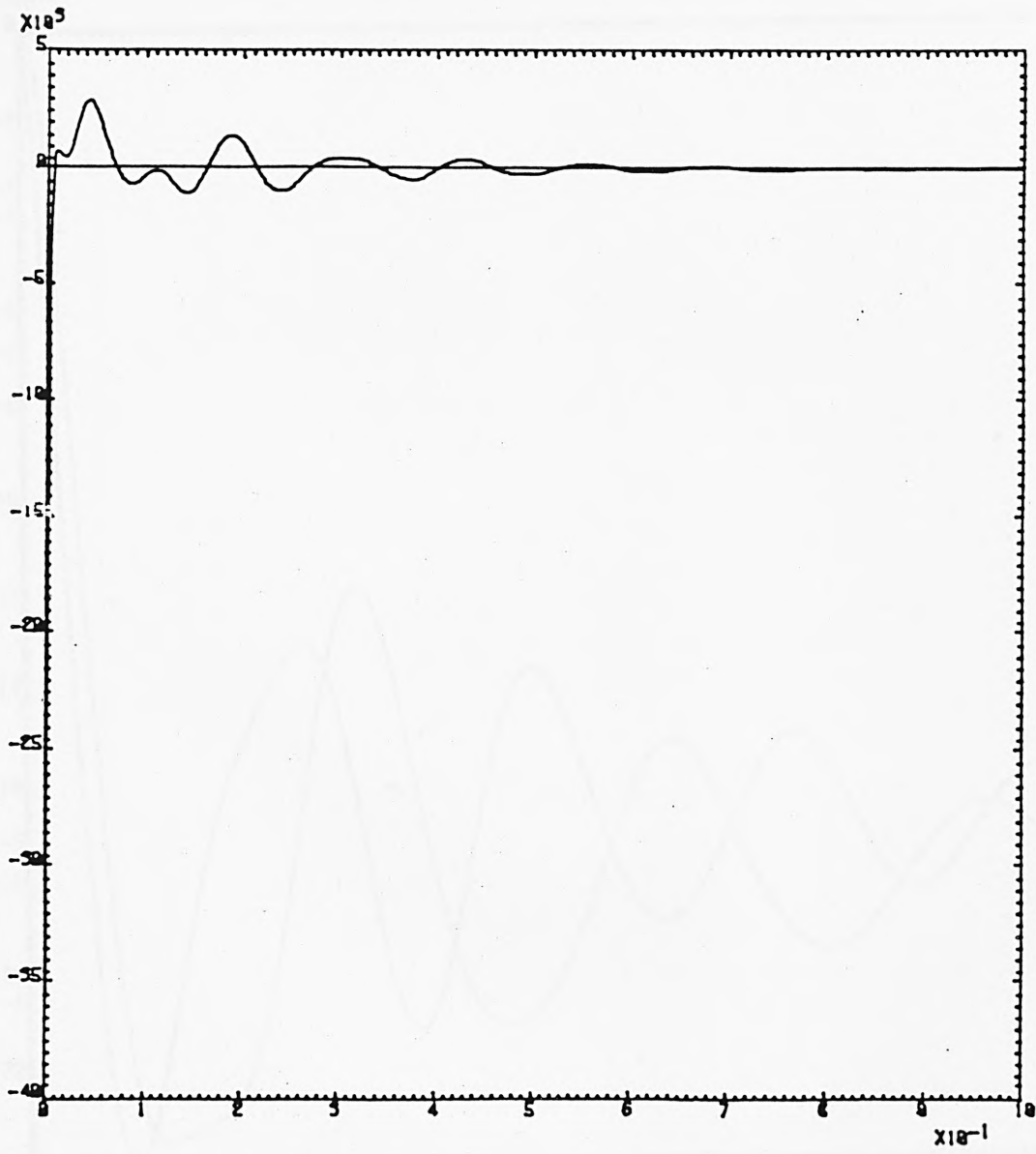


Fig. (7.18)

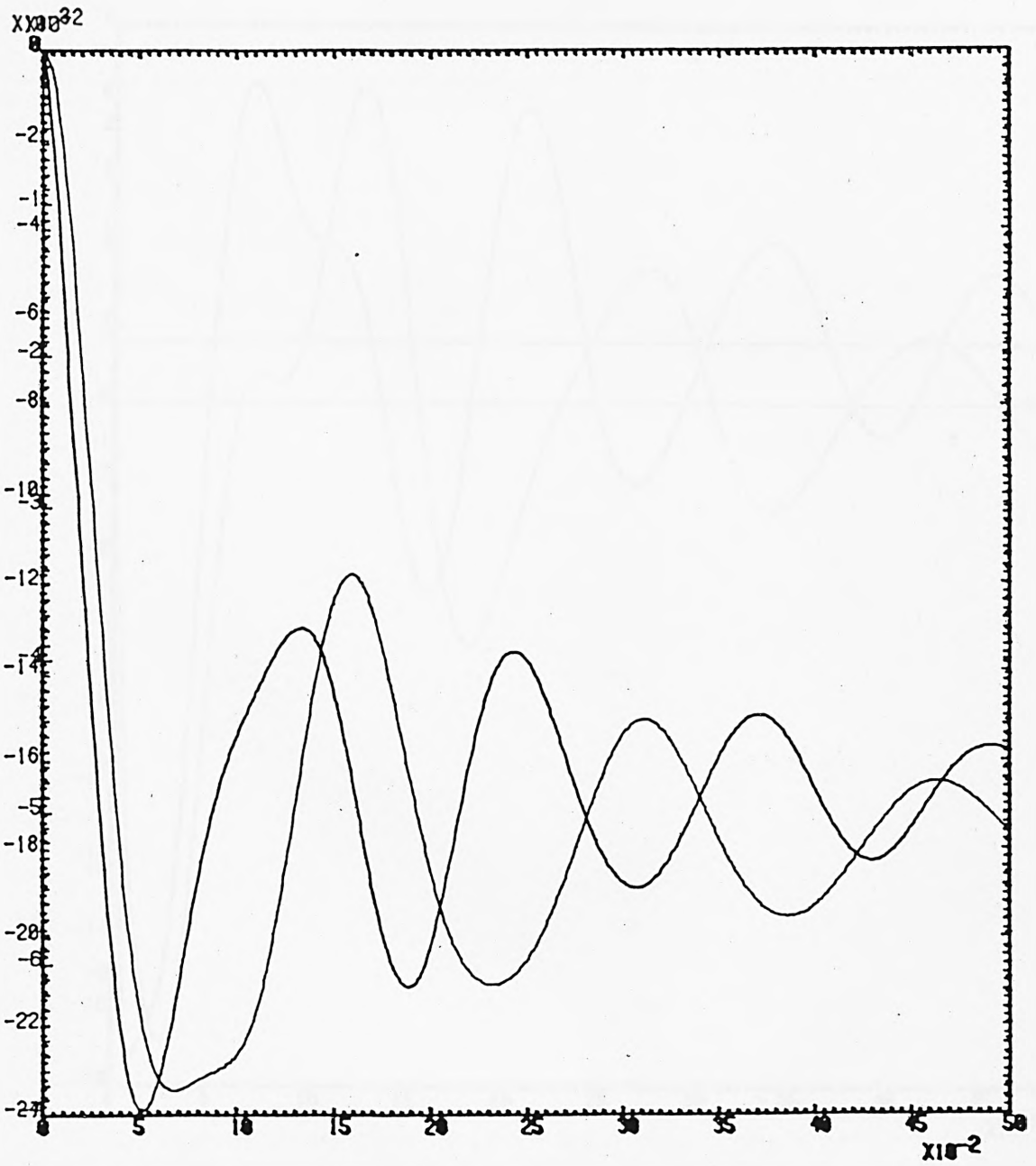


Fig. (7.19) Dynamic response of pavement with and without interface effect (Displacement)

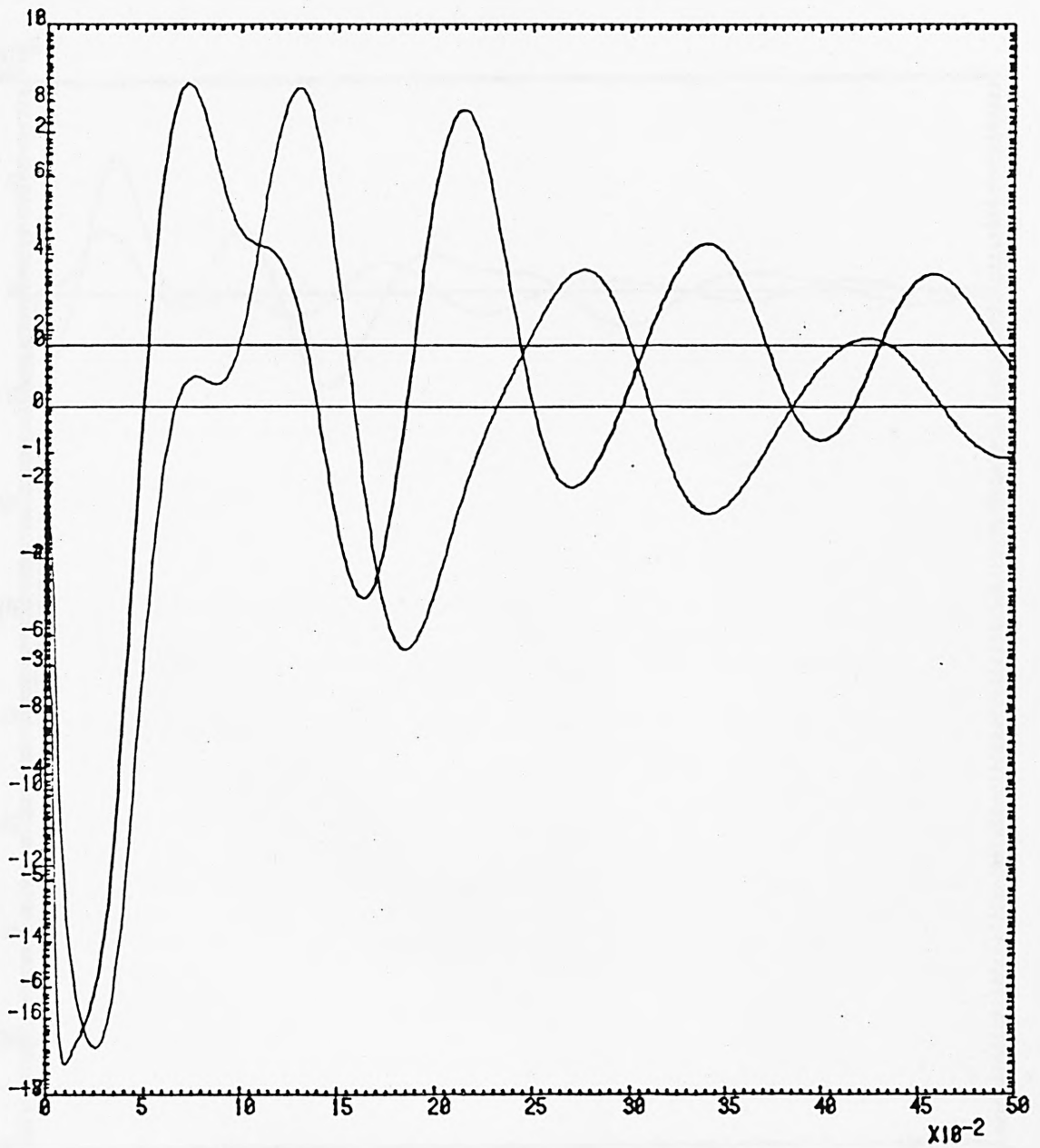


Fig. (7.20) Dynamic response of pavement with and without interface effect (Velocity)

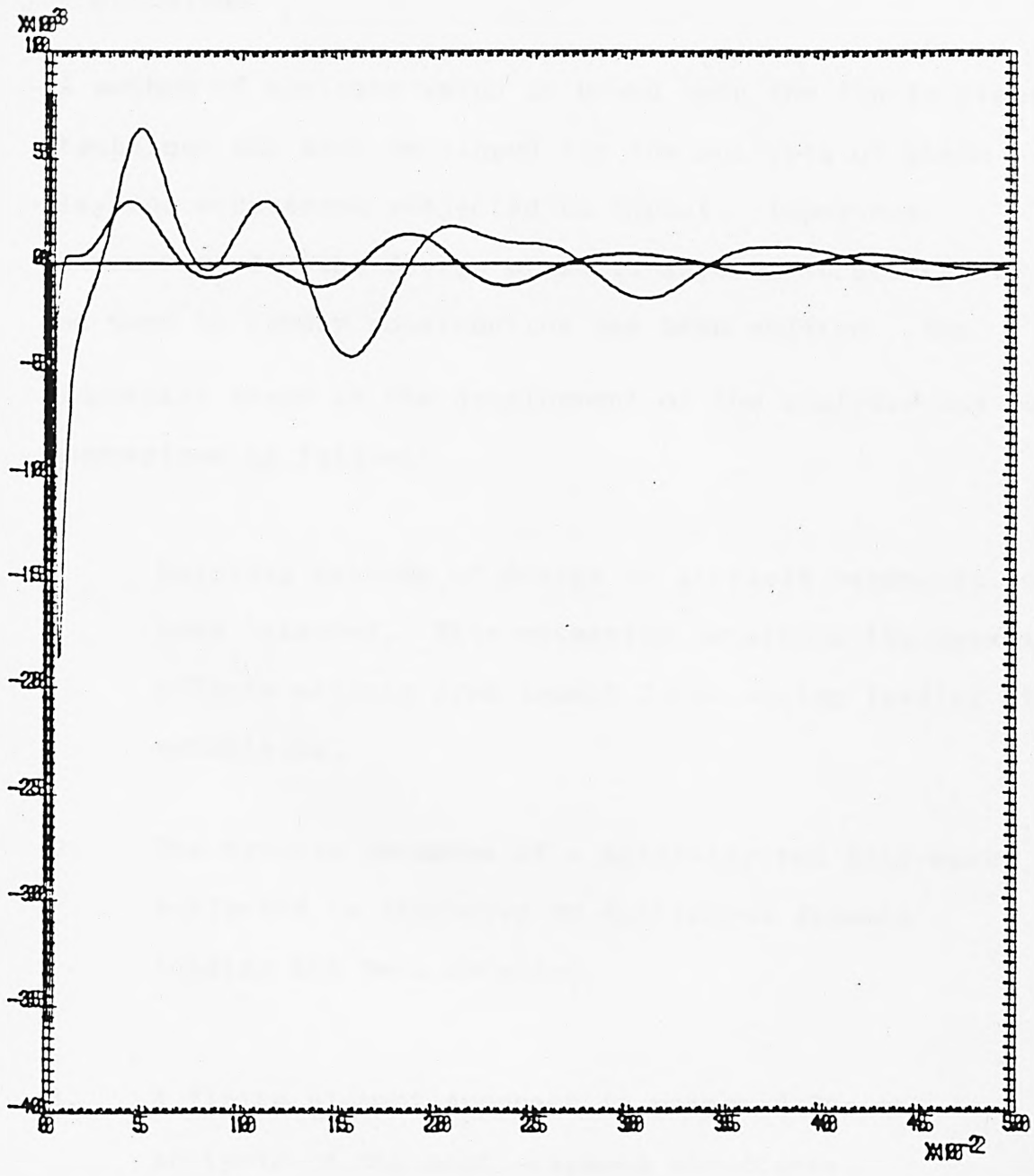


Fig. (7.21) Dynamic response of pavement with and without interface effect (Acceleration)

CHAPTER 8

CONCLUSIONS AND RECOMMENDATION FOR FURTHER WORK

CONCLUSIONS

A method of analysis which is based upon the finite element technique has been developed for the analysis of plane layered structures subjected to impact. Important parameters for the design of multi-layered structures to be used in runway construction has been studied. The important steps in the development of the analysis may be summarized as follows:

1. Existing methods of design of airfield pavements has been extended. This extension considers the dynamic effects arising from impact force during landing of aeroplanes.
2. The dynamic response of a multi-layered half-space subjected to impulsive or continuous dynamic loading has been obtained.
3. A finite element approach is proposed for the analysis of the multi-layered structures.

Also, the developed dynamic finite element program included a means by which a wide variety of boundary conditions, damping, wave reflection and wave refraction can be considered.

The above theoretical work has been incorporated into a computer program called DFEM which is also applicable to structures or structural components which may be considered to act as plane or axisymmetric systems subjected to dynamic forces.

A number of dynamic problems were solved by the DFEM program. The numerical results were compared either with exact or other numerical results. The comparison of the results of the developed program DFEM and the published results shows good agreement. An effective numerical evaluation of stress wave propagation at an interface was obtained.

The computer program can be modified to incorporate new parameters such as material nonlinearity or new element types.

Extensive photodynamic tests have been conducted. The experimental tests enabled the real behaviour of multi-layered structures to be observed. Thus an understanding of the stress wave propagation action was obtained which effectively assisted the development of the theory.

Comparison of the experimental results with those obtained from the developed program shows that the effectiveness of the numerical model indicates good correspondence.

Since the practical application of this research is to the study of the effect of significant impact loading upon the analysis and design of aircraft runways, the author suggests the following recommendations:

1. The impact force must be taken into consideration as a loading case in the design of runway ends.
2. Flexible overlays over rigid pavements are not recommended. Higher stresses will result in the flexible pavement due to the reflection of the stress wave.

RECOMMENDATION FOR FURTHER RESEARCH

1. A field study to assess the time of impact and impact forces of an aeroplane during landing.
2. It should be recognised that the application of charts and tables for the design of pavement may have limitations. It is suggested that for appropriate cases the pavements be directly designed to resist dynamic forces.

3. Recent developments in digital computers provide a good facility which can be applied to the optimal design of pavements.

REFERENCES AND BIBLIOGRAPHY

1. McCullough, B.F, and Pearson, M. W, "Air Force Pavement Design System Concepts," Proceedings of ASCE, Transportation Engineering Journal, Vol. 100, No. TE4, Nov. 1974, pp 921-932.
2. Yoder, E. J, and Witzak, M. W, "Principles of Pavement Design," John Wiley & Sons, Inc, 1975, 2nd Edn.
3. Robert Horonjeff, "Planning and Design of Airports," McGraw-Hill, Inc, 1975, 2nd Edn.
4. Monismith, C. L, and Finn, F. N, "Flexible Pavement Design: State-Of-The-Art-1975," Proceedings, ASCE, Transportation Engineering Journal, Vol. 103, No. TE1, Jan. 1977, pp 1-53.
5. Sahlin, S, and Nilsson, L, "Theoretical Analysis of Stress and Strain Propagation During Impact," Materiaux et Construction, Vol. 8, Part 44, 1978, pp 88-101.
6. Caudle, W. N, Pope, A. Y, McNeill, R. L, and Margaso, B. E, "The Feasibility of Rapid Soil Investigations Using High-Speed, Earth-Penetration Projectiles," International Symposium on Wave Propagation and Dynamic Properties of Earth Materials, University of New Mexico Press, Aug. 1967.

7. Chen, W. T, and Engel, P. A, "Impact and Contact Stress Analysis in Multilayer Media," Int. J. Solids Structures, Vol. 8, 1972, pp 1257-1281.
8. Goldsmith, W, "Impact," Arnold Ltd, London, 1960.
9. Johnson, W, "Impact Strength of Materials," Edward Arnold Ltd, 1972.
10. Phillips, J. W, and Calvit, H. H, "Impact of a Rigid Sphere on a Viscoelastic Plate," Journal of Applied Mechanics, Dec. 1967, pp 873-878.
11. Abramson, H. N, Plass, H. J, and Ripperger, E. A, "Stress Wave Propagation in Rods and Beams," Advance in Applied Mechanics, Vol. 5, 1958, pp pp 111-194.
12. Brown, I. C, and Perry, S. H, "Transverse Impact on Beams and Slabs," BOSS '79, Second International Conference on Behaviour of Off-shore Structures, Held at Imperial College, London, 28-31 Aug. 1979.
13. "Design Manual for Airport Pavements for Classes 3, 4 and 5 Airports," Dept. of the Airforce, Washington, Order - N6, Nov. 4, 1947.

14. Theisen, J. G, Boyd, W. C, Crenshaw, B. M, and Haisler, J. B, "Analysis and Modeling of Soils Subjected to Dynamic Loading by Aircraft Landing Gear," International Symposium on Wave Propagation, University of New Mexico, 23-25 Aug. 1967.
15. Gunter Waas, "Linear Two-Dimensional Analysis of Soil, Dynamics Problems in Semi-Infinite Layered Media," Ph.D. Thesis, University of California, Berkely, 1972.
16. Liang, V. C, Roesset, J. M, and Waas, G, "Dynamic Response of Structures in Layered Soils," MIT, Dept. of Civil Engineering, Cambridge, Mass, Jan. 1974.
17. Kolsky, H, "Stress Waves in Solids," Dover Publications, Inc. 1963.
18. Ewing, W. M, Jardetzky, W. S, Press, F, "Elastic Waves in Layered Media," McGraw-Hill, New York, 1957.
19. Desi, C. S, and Christian, J. T, "Numerical Methods in Geotechnical Engineering," McGraw-Hill, New York, 1977.
20. Richart, F. E, Hall, J. R, and Woods, R. D, "Vibrations of Soils and Foundations," Prentice-Hall, Inc, Englewood Cliffs, New Jersey, 1970.

21. Selig, E. T, "Characteristics of Stress Wave Propagation in Soils," Proceedings of the Symposium on Soil Interaction, University of Arizona, Tucson, Arizona, Sept. 1964.
22. Bahar, L. Y, and Ebner, A. M, "Transfer Matrix Approach to Earthquake Amplification Through Layered Soils," Nuclear Engineering and Design, Vol. 35, 1975, pp 59-67.
23. Idriss, I. M, and Seed, H. B, "Response of Earth Banks During Earthquakes," Proceedings of ASCE Journal of the Soil Mechanics and Foundations Division, Vol. 93, No. SM3, May, 1967, pp 61-82.
24. Gazetas, G, and Roesset, J. M, "Vertical Vibration of Machine Foundations," Journal of the Geotechnical Engineering Division, ASCE, Vol. 105, No. GT12, Dec. 1979, pp 1435-1469.
25. Gazetas, G, "Static and Dynamic Displacements of Foundations on Heterogeneous Multilayered Soils," Geotechnique, Vol. 30, No. 2, 1980, pp 159-177.
26. Costantino, C. J, "Finite Element Approach to Stress Wave Problems," Proceedings of ASCE, Journal of the Engineering Mechanics Division, Vol. 93, No. EM2, April 1967, pp 153-175.

27. Alfredo, H. S, and Rainer, J. H, "Model for Wave Motions in Axi-Symmetric Solids," Proceedings of ASCE, Journal of the Engineering Mechanics Division, Vol. 90, No. EM2, April, 1964, pp 195-223.
28. Thakkar, S. K, and Stagg, K. G, "Nonlinear Dynamic Analysis of Stress-Wave-Propagation Problems," Proceedings of the International Conference held at University College Swansea, 2nd-5th September, 1980, pp 237-258.
29. Costantino, C. J, Wachowski, A, and Barnwell, U. L, "Finite Element Solution for Wave Propagation in Layered Media Caused by a Nuclear Detonation," Proceedings, Symposium, University of New Mexico, Aug. 1967.
30. Lysmer, J, and Kuhlemeyer, R. L, "Finite Dynamic Model for Infinite Media," Proceedings of ASCE, Journal of the Engineering Mechanics Division, Vol. 95, No. EM4, Aug. 1969, pp 859-877.
31. Kuhlemeyer, R. L, and Lysmer, J, "Finite Element Method Accuracy for Wave Propagation Problems," Proceedings of ASCE, Journal of Soil Mechanics and Foundation Division, Vol. 99, No. SM5, May 1973, pp 421-427.

32. Shipley, S. A, Leistner, H. G, and Jones, R. E,
"A Comparison Between Finite Elements Predictions
and Exact Solutions," Proceedings of ASCE, Symposium
on Wave Propagation, University of Mexico, Aug. 1967.
33. Kausel, E, Roesset, J. M, and Waas, G, "Dynamic
Analysis of Footings on Layered Media," Proceeding
of the ASCE, Journal of the Engineering Mechanics
Division, Vol. 101, No. EM5, 1975, pp 679-693.
34. Tassoulas, J. L, and Kausel, E, "Elements for the
Numerical Analysis of Wave Motion in Layered Strata,"
International Journal for Numerical Methods in
Engineering, Vol. 19, 1983, pp 1005-1032.
35. Lazan, B. J, "Damping of Materials and Members in
Structural Mechanics," Pergamon Press Inc, 1968,
1st Edn.
36. Graft-Johnson, J. W. S, "The Damping Capacity of
Compacted Kaolinite Under Low Stresses," Proceedings
of ASCA Symposium on Wave Propagation, University of
New Mexico, Aug. 1967.
37. Clough, R. W, and Penzin, J, "Dynamics of Structures,"
McGraw-Hill, Inc, 1975.

38. Ewins, D. J, "Measurement and Application of Mechanical Impedance Data," Journal of the Society of Environmental Engineers, Dec. 1975, March 1976 and June 1976.
39. Wilson, E. L, and Penzien, J. "Evaluation of Orthogonal Damping Matrices," International Journal for Numerical Methods in Engineering, Vol. 4, 1972, pp 5-10.
40. Heukelom, W, and Klomp, J, G, "Road Design and Dynamic Loading," Proceedings of the Association of Asphalt Paving Technologists," Feb. 1964, pp 92-125.
41. Idriss, I. M, and Seed, H. B, "Seismic Response of Horizontal Soil Layers," Proceedings of ASCE, Journal of the Soil Mechanics and Foundation Division, Vol. 94, No. SM4, July 1968, pp 1003-1029.
42. Idriss, I. M, and Seed, H. B, "Seismic Response by Variable Damping Finite Elements," Journal of the Geotechnical Engineering Division, ASCE, Vol. 100, No. GT1, Jan. 1974, pp 1-13.
43. Roesset, J. M, Whitman, R. V, and Dorby, R, "Modal Analysis for Structures with Foundation Interaction," Journal of Structural Division, ASCE, Vol. 99, No. ST3, 1973, pp 399-416.

44. Bathe, K. J, and Wilson, E. L, "Numerical Methods in Finite Element Analysis," Prentice-Hall, Inc, New Jersey, 1976.
45. Riera, J. D, "On the Stress Analysis of Structures Subjected to Aircraft Impact Forces," Nuclear Engineering and Design, Vol. 8, 1968, pp 415-426.
46. Bathe, K. J, Ramm, E, and Wilson, E. L, "Finite Element Formulations for Large Deformation Dynamic Analysis," International Journal for Numerical Methods in Engineering, Vol. 9, 1975, pp 353-386.
47. Barez, F, Goldsmith, W, and Sackman, J. L, "Longitudinal Wave Propagation in Axisymmetric Structures with Material and/or Aereal Discontinuity," Experimental Mechanics, Oct. 1980, pp 325-333.
48. Zienkiewics, O. C, "The Finite Element Method," McGraw-Hill, 1977, 3rd Edn.
49. Hinton, E, and Owen, D. R. J, "An Introduction to Finite Element Computation," Pineridge Press, Swansea, 1979.
50. Boswell, L. F, and Scott, C. R, "A Flexible Circular Plate on a Heterogeneous Elastic Half-Space: Influence Coefficients for Contact Stress and Settlement," Geotechnique, Vol. 25, No. 3, 1976, pp 604-610.

51. Dungar, R, Eldred, P. J. L, and Severn, R. T, "Dynamic Interaction of the Structure-Fluid-Foundation System of Gravity Platforms," BOSS '76, Behaviour of Off-Shore Structures, The Norwegian Institute of Technology.
52. Kausel, E, and Roesset, J. M," Soil-Structure Interaction Problems for Nuclear Containment Structures," ASCE Power Div. Spec. Conf, Denver, Colo. 1974.
53. Tasi, N. C, "Modal Damping for Soil-Structure Interaction," Journal of the Engineering Mechanics Division, Vol. 100, No. EM2, April 1974, pp 323-341.
54. Jennings, A, "Matrix Computation for Engineers and Scientists," John Wiley and Sons Ltd, 1980.
55. Gupta, K. K, "Development of a Unified Numerical Procedure for Free Vibration Analysis of Structures," International Journal for Numerical Methods in Engineering, Vol. 17, 1981, pp 187-198.
56. Sinitsyn, A. P, "The Interaction Between a Surface Wave and a Structure," International Symposium on Wave Propagation, University of Mexico, New Mexico, Aug. 1967.

57. Zienkiewicz, O. C, Valliappan, S, and King, I. P, "Stress Analysis of Rock as a 'No Tension' Material," Geometrique, Vol. 18, No. 1, 1968, pp 56-66.
58. Francavilla, A, and Zienkiewicz, O. C, "A Note on Numerical Computation of Elastic Contact Problems," International Journal for Numerical Methods in Engineering, Vol. 9, 1975, pp 913-924.
59. Sachdeva, T. D, and Ramakrishnan, C. V, "A Finite Element Solution for the Two-Dimensional Elastic Contact Problems with Friction," International Journal for Numerical Methods in Engineering, Vol. 17, 1981, pp 1257-1271.
60. Bathe, K. J, and Wilson, E. L, "Stability and Accuracy Analysis of Direct Integration Methods," Earthquake Engineering and Structural Dynamics, Vol. 1, 1973, pp 283-291.
61. Hinton, E, and Owen, D. R. J, "Finite Element Programming," Academic Press Inc. (London), 1979.
62. Parekh, C. H, "Finite Element Solution System," Ph.D. Thesis, University of Wales, Swansea, 1969.

63. King, I. P, "Finite Element Solution System Fess," International Report, Dept. of Civil Engineering, University of Wales, Swansea, May 1967.
64. Digambar, P. M, and Graham, H. P, Report No. 75-37, Earthquake Engineering Research Centre, College of Engineering, University of California, Berkeley, California, Dec. 1975.
65. Wilson, E. L, Farhoomand, I, and Bathe, K. J, "Nonlinear Dynamic Analysis of Complex Structures," Earthquake Engineering and Structural Dynamics, Vol. 1, 1973, pp 241-252.
66. Yamada, Y, and Nagai, Y, "Analysis of One-Dimensional Stress Wave by the Finite Element Method," Journal of Industrial Science, University of Tokyo, Japan, Vol. 23, No. 5, May 1971, pp 186-189.
67. Duns, C. S, and Butterfield, R, "The Dynamic Analysis of Soil-Structure System Using the Finite Element Method," International Symposium on Wave Propagation, University of New Mexico, Aug. 1967.
68. Frocht, M. M, "Photoelasticity," John Wiley and Sons, Inc. 1962, Vol. I.

69. Durelli, A. J, and Riley, W. F, "Introduction to Photomechanics," Prentice-Hall Inc. 1965.
70. Dally, J. W, "Applications of Photoelasticity to Elastodynamics," Proceedings of Symposium held at Stanford University, California, June 1971.
71. McNicholas, J. B, and Rankilor, P. R, "The Mechanical Properties of Some Polyurethane Rubbers at Room Temperature," Strain, Vol. 5, No. 2, April 1969.
72. Rankilor, P. R, and McNicholas, J. B, "The Preparation and Use of a Stress-Sensitive Material in Multi-Layer Photoelastic Models," International Journal of Rock Mechanics Mining Sciences, Vol. 5, No. 6, Nov. 1968.
73. Kolsky, H, "Some Recent Experimental Investigations in Stress-Wave Propagation and Fracture," Proceedings of Symposium held at Stamford University, California, June 1971.
74. Dalley, J. W, "An Introduction to Dynamic Photoelasticity," Experimental Mechanics, Dec. 1980, pp 409-416.
75. Dalley, J. W, Henzi, A, and Lewis, D, "On the Fidelity of High-Speed Photographic Systems for Dynamic Photoelasticity, Proc. SESA, 26-2, 394, 1969.

76. Durelli, A. J, and Mulzet, A. P, "Large Strain Analysis and Stresses in Linear Materials," Journal of Engineering Mechanics Division, ASCE, No. EM3, June 1965, pp 65-91.
77. Robert, J. S, "Application of the Least-Squares Method to Photoelastic Analysis," Experimental Mechanics, June 1980, pp 192-197.
78. Dally, J. W, "Data Analysis in Dynamic Photoelasticity," Experimental Mechanics, Aug. 1967, pp 332-338.
79. Segerlind, L. J, "Stress-Difference Elasticity and Its Application to Photomechanics, Experimental Mechanics, Oct. 1971, pp 440-445.
80. Meyer, M. L. Mehrotra, C. L, and Pabani, S. A, "A Note On Special Photographic Techniques Applicable to Photoelasticity," Journal of Strain Analysis, Vol. 10, No. 3, 1975, pp 163-166.
81. Mehrotra, C. L, and Meyer, M. L, "Equidensometry Applied to Photoelasticity," Experimental Mechanics, Oct. 1976, pp 383-388.

82. Ahlvin, R. G, "Developments in Pavement Design in the USA - Flexible Pavements," Proceedings of the Symposium Organized by the Institution of Civil Engineers in London, Nov. 1970.
83. Moraldi, I. G, "Developments of Pavement Design Both Rigid and Flexible on the Continent of Europe," Proceedings of the Symposium Organized by the Institution of Civil Engineers, London, Nov. 1970.
84. Jennings, H, and Straw, F. L. H, "Strengthening of Pavements," Proceedings of the Symposium Organized by the Institution of Civil Engineers, London, Nov. 1970.
85. Martin, F. R, Judge, R. F. A, and Chammings, M. B, "Design and Evaluation of Aircraft Pavements," Transportation Engineering Journal, No. TE4, Nov. 1973, pp 785-799.
86. Witczak, M. W, and Shook, J. F, "Full-Depth Asphalt Airfield Pavements," Proceedings of ASCE, Transportation Engineering Journal, Vol. 101, No. TE2, May 1975, pp 297-309.
87. Kingham, R. I, "Failure Criteria Developed from AASHO Road Test Data," Proceedings, Third international Conference on the Structural Design of Asphalt Pavements, London, 1972.

88. Hsuch, T. M, and Penzin, J, "Dynamic Response of Airplanes in Ground Operation," Transportation Engineering Journal, No. TE3, Aug. 1974, pp 743-756.
89. Taylor, J, "Manual on Aircraft Loads," Pergamon Press Ltd, First Edition, 1965.
90. Nijboer, L. W, and Van Der Poel, C, "A Study of Vibration Phenomena in Asphaltic Road Constructions," Asphalt Paving Technologist, Vol. 22, 1953, pp 197-231.
91. Heukelom, W, and Foster, C. R, "Dynamic Testing of Pavements," Proceedings of ASCE, Journal of the Structural Division, No. SM1, Feb. 1960, pp 1-27.
92. Avramesco, A, "Dynamic Phenomena in Pavements Considered as Elastic Layered Structures," Second International Conference on the Structural Design of Asphalt Pavements, University of Michigan, Aug. 1967.
93. Bruhn, "Analysis and Design of Flight Vehicle Structures," Tri-State Offest Company, Jan. 1965.
94. Torenbeek, E, "Synthesis of Subsonic Airplane Design," Sdeft University Press, 1982.

95. Westmann, R. A, "Stress Analysis by Finite Elements," Highway Research Record, 228, University of California, Los Angeles, 1968, pp 46-58.

96. Duncan, J. M, Monismith, C. L, and Wilson, E. L, "Finite Element Analysis of Pavements," Highway Research Record, 228, University of California, Berkeley, 1968, pp 18-33.

97. Barker, W. R, "Nonlinear Finite Element Analysis of Heavily Loaded Airfield Pavement Systems, Proceedings, Symposium of Appl. Finite Element Method, Geotech. Engineering, Mississippi, May 1972.

APPENDIX 1

=====

C
C

```

COMMON/CONTR/TITLE (12) , NP, NE, NB, NDF, NCN, NSFR, NSZF, L
&V, NGAUSR, NPP,
&NSK, NSIZ, NBUF, NI, IT, ILL, ND, NNP, NAVE, NLD, NMAT, NIT, IC
&S, NCORD, NL,
&NRE, DV, KE, KP, IAY, NDLY, NRG, NRT, NRPP, NRC, NRPRS, NSTRS,
&NGAUST, NBAR
COMMON/GEP/NBC (50) , NF IX (50) , U (100) , R1 (300) , ALFA (50)
&, BETA (50) ,
&NOP (70, 8) , THICK, ANG (50) , WGT (50) , AA (60, 4) , BB (60, 4) , B
&AREA (60, 4)
COMMON/ELS/
&IMAT (70) , CORD (200, 3) , D (4, 4) , AX, AY, GX, GY, TD, E1, E2, C1
&, C2, G2, Q (2, 200)
&, ORT (10, 9) , XM (16, 16) , QN (2, 16) , XG (16) , UAST (300) , RT (3
&00) , UD2 (16)
&, UAC (16) , UAC2 (16) , UVE (16) , UDE (16) , RT1 (300) , XR (300) ,
&UV2 (16) , ZZ (6)
COMMON/DK/NDYN, DELT, ROE, ANOT, BNOT, AONE, ATO, ATHRE, AF
&OR, BONE, AF IV,
&ASIX, ASEVN, AET, ANIN, ATEN, SETA, DALPHA, DBETA, IFIAG, GR
&AV, GTH, NCASE
&, LNBC (50) , LNFI (50) , DANG (50) , DUS (50, 2) , XMU (16) , LCAS (
&6) , NLAY (6, 20)
&, KFAC (6, 20) , KLD, LELEM, R3 (300) , INTER, YF (250) , XF (250)
&, NPULS, COFR
COMMON/ADY/SK (24000) , R      , ESTIFM (24, 24) , NN (12)
COMMON
& US (50, 2) ,
& T (200) , PP (200) , IONARY (70)

```

C
C
C
C

DYNAMIC ANALYSIS OF PLANE STRESS/STRAIN AND AXISYMMETRIC CONDITION
FOR LINEAR PARABOLIC OR CUBIC ELEMENTS

```

IFIAG=0
REWIND 8
REWIND 15
REWIND 11
READ , NPROB, NDYN, NCASE, IAY, NDLY, KE, KP, LELEM, INTER
READ , DELT, SETA, GRAV, GTH
write (6, 1) nprob, ndyn, delt, seta
1 format (v)
DO 60 NPR=1, NPROB

```

C
C
C

NPROB=TOTAL NO. OF PROBLEMS

C
C
C
C
C

```

CALL PTIME (TIME1)
WRITE (6, 101) NPR, TIME1
READ (41, 7) TITLE
WRITE (6, 7) TITLE
DATA FOR ANALYSIS OF EX. PULSE
READ CONTROL DATA

```

```

      READ , NP, NE, NB, NLD, NDF, MMAT, NSFR, NGAUSR, NGAUST, NPP
&, NT, NL, NSIZ,
&      NCORD, NBAR, NONLIN, NTRANG, NRECT
      N11=NGAUSR*NRECT+NGAUST*NTRANG
      WRITE (11)NLD, N11, NE, NP
      IF (NCORD .EQ. 0) NCORD=2
      WRITE (6, 112)NP, NE, NB, NLD, NDF, MMAT, NSFR, NGAUSR, NGAU
&ST, NPP, NT, NL,
&NSIZ, NCORD, NBAR
112 FORMAT(1H ,15(I4))
C      IF (NCASE .NE. 7) GO TO 222
C      DO 322 I=1, 250
C 322 YF(I)=0.0
C      REWIND 19
C      READ(19, 22)(YF(I), I=1, 31)
C      PRINT, (YF(I), I=1, 31)
C      REWIND 19
C      GO TO 422
C 222 REWIND 19
C 422 CONTINUE
C 22 FORMAT(V)
C      READ MATERIAL PROPERTIES
C
      WRITE (6, 108)
C FOR SPRING ELEMENT (SL/SS/THETA/5X0) FOR ORT
      READ , (N, (ORT(N, I), I=1, 9), L=1, MMAT)
      WRITE (6, 118) ((N, (ORT(N, I), I=1, 6)), N=1, MMAT)
118 FORMAT(1H ,14, 6F16.3)
C
C      PRESET TAPES
C
      REWIND 3
      REWIND 4
C
      ICS=3
      IF (NPP .EQ. 2) ICS=4
      NCN=4*NSFR
      NSZF=NP*NDF
      LV=NCN*NDF
      WRITE (6, 105) NCN, LV, NSZF
      CALL GDATA
CDO 5432 N=1, NP
C5432 WRITE (6, 6543)N, (CORD(N, M), M=1, NCORD)
      6543 FORMAT(1H ,13, 6X, F8.2, 2X, F8.2)
C
C      NLD=NO OF LOAD CASES
      KLD=1
      DO 40 ILD=1, NLD
      IF(ILD .GT. 1) GO TO 72
      CALL SET
      CALL STIFM
72 CONTINUE
      CALL LDATA
      IF (INTER .LT. 2) GO TO 35

```

```

        IF (ILD .EQ. 1.AND.KLD.EQ.2) CALL STRESS
35 CONTINUE
        IF (INTER .LT. 2) GO TO 37
        IF (ILD .EQ. 1.AND.KLD.EQ.2) GO TO 30
37 CONTINUE
        IF (ILD .GT. 1) GO TO 75
        CALL PTIME(TIME3)
        CALL SOLVE
        WRITE(6,103) TIME3
        GO TO 80
75 CONTINUE
        IF (NDYN .GT. 1) GO TO 55
        CALL RESOLV
        GO TO 80
55 CALL RESOLV
80 CONTINUE
        CALL BSUB
        IF (ILD .GT. 1) CALL STRESS
C      CALL STRESS
        IF (NBAR.EQ.0) GOTO 50
        CALL BSTRESS
50 CONTINUE
C200 CONTINUE
        CALL PTIME(TIME2)
C      WRITE(6,102) TIME2
30 CONTINUE
        IF (INTER .LT. 2) GO TO 32
        KLD=KLD+1
        IF (INTER .GT. 2.AND.KLD.EQ.2) GO TO 72
32 CONTINUE
40 CONTINUE
60 CONTINUE
7 FORMAT(12A4)
101 FORMAT(1H1,13H PROBLEM NO,, I3,3X,21HEXECUTION STA
&RTED AT ,F8.4)
C 102 FORMAT(1H0,3X,23HEXECUTION FINISHED AT ,F8.4)
103 FORMAT(1H0,34H STIFFNESS FORMULATION FINISHED AT
&,F8.4)
C104 FORMAT(1H0, 29H RESULTANT FORCES OBTAINED AT ,A8)
105 FORMAT(1H0,22HNO. OF NODES/ELEMENT =, I3,2X,18HSIZE
& OF K MATRIX = ,
&I3,2X,19HMAX.NO.OF UNKNOWNNS=, I4)
108 FORMAT(1H0,20H MATERIAL PROPERTIES )
        STOP
        END
C===== START SUBROUTINE =====
        SUBROUTINE GDATA
C
        COMMON
        & US(50,2),R(3),
        & T(200),PP(200),IONARY(70)
C
C      GEOMETRICAL DATA, BOUNDARY CONDITIONS AND GAUSS INTEGRATION DATA
C

```

```

      READ , NNP,NNE,NNBB,NIAP,II,IMOD
      WRITE(6,111) NNP,NNE,NNBB,NIAP,II,IMOD
111  FORMAT(1H ,7I6)
      DO 10 II=1,NP
      DO 10 JJ=1,NCORD
      10 CORD(II,JJ) = 0.
C
C
      DO 20 L=1,NNP
      20 READ , N,(CORD(N,M),M=1,NCORD)
C20 WRITE(6,109)N,(CORD(N,M),M=1,NCORD)
      109 FORMAT(1H ,I6,6H * ,F8.1,2H ,F8.1)
C
C      READ ELEMENT DATA
C
      IF(NBAR.NE.0) GOTO 50
C FOR SPRING (END1 END2 6X0 PROPERTY NO.
C
      READ,(N,(NOP(N,M),M=1,8),IMAT(N),L=1,NNE)
      GOTO 41
      50 CONTINUE
C PRESET REINFORCEMENT COORDS TO ZERO
      DO 45 L=1,NNE
      DO 45 M=1,4
      AA(L,M)=0.
      BB(L,M)=.0
      45 CONTINUE
      DO 40 L=1,NNE
      READ,(N,(NOP(N,M),M=1,8),IMAT(N),NBARS)
CWRITE(6,106)(N,(NOP(N,M),M=1,8),IMAT(N),NBARS)
      BAREA(N,1)=0.0
      IF(NBARS.EQ.0) GOTO 40
      READ,((AA(N,M),BB(N,M),BAREA(N,M)),M=1,NBARS)
      WRITE(6,107)((AA(N,M),BB(N,M),BAREA(N,M)),M=1,NBAR
&S)
      106 FORMAT(1H ,11I6)
      107 FORMAT(1H ,3E15.4)
      40 CONTINUE
C BAR DATA READ IN
C
C      READ BOUNDARY DATA
      41 IF (NNBB .LE. 0) GO TO 480
      DO 450 I=1,NNBB
      450 READ,NBC(I),NFIX(I),ANG(I),(US(I,J),J=1,NDF)
      480 CONTINUE
C
C NODEXY IS REMOVED: GAUSS CONTAINS INTEGRATION DATA
      CALL GAUSS
      IF (II .NE. 0) GO TO 500
CWRITE(6,102)
CDO 30 N=1,NP
C30CWRITE(6,112) N,(CORD(N,M),M=1,NCORD)
      112 FORMAT(1H ,I4,6H ++ ,F10.2,2X,F10.2)
      WRITE(6,103)

```



```

CWRITE (6,113) (N, (NOP(N,M),M=1,8), IMAT(N),N=1,NE)
113 FORMAT(1H ,10I4)
    IF (NB .EQ. 0) GO TO 500
    WRITE (6,104)
    DO 490 I=1,NB
490 WRITE (6,114)NBC(I),NFIX(I),ANG(I), (US(I,J),J=1,NDF
&)
114 FORMAT(1H ,2I4,3(F12.3,2X))
500 CONTINUE
    IC=0
    DO 650 I=1,NB
    DO 650 J=1,NDF
    IC=IC+1
650 U(IC)=US(I,J)
C
102 FORMAT(20H1 NODAL POINTS          )
103 FORMAT(20H1  ELEMENTS            )
104 FORMAT(21H0 BOUNDARY CONDITIONS)
C105 FORMAT(32H0 GAUSSIAN INTEGRATION CONSTANTS )
    RETURN
    END
C===== START SUBROUTINE =====
    SUBROUTINE GAUSS
    COMMON
    & US(50,2),R(3),
    & T(200),PP(200),IONARY(70)
C THIS SUB CONTAINS GAUSS QUADRATURE INTEGRATION DATA.RECTANGULAR THEN
C TRIANGULAR ELEMENT ARE PROVIDED FOR. 2*2,3*3$4*4:RECTANGULAR ELMS.  :
C4*4$5*5
C TRIANGULAR.ARRAYS-ALFA/BETA/WGT.
    A1=.577350269189626
    A2=.774596669241483
    A3=.000000000000000
    A4=.8611363115
    A5=.3399810435
    W1=1.000000000000000
    W2=.5555555555555556
    W3=.88888888889
    W4=.3478548451
    W5=.6521451548
C FOR NO RECTANGLES.
    IF (NGAUSR.EQ.0)GOTO 3
    IF (NGAUSR.GT.4)GOTO 1
C 2*2=RECTANGULAR
    ALFA(1)=-A1
    ALFA(2)=A1
    ALFA(3)=-A1
    ALFA(4)=A1
    BETA(1)=-A1
    BETA(2)=-A1
    BETA(3)=A1
    BETA(4)=A1
    DO 10 I=1,4
    WGT(I)=W1

```

```

10 CONTINUE
   GOTO 3
  1 CONTINUE
    IF (NGAUSR.GT.9)GOTO 2
C 3*3 RECTANGULAR
   DO 20 I=1,7,3
     ALFA(I)=-A2
     ALFA(I+1)=A3
     ALFA(I+2)=A2
  20 CONTINUE
     DO 30 I=1,3,1
       BETA(I)=-A2
       BETA(I+3)=A3
       BETA(I+6)=A2
  30 CONTINUE
     DO 40 I=2,8,2
       WGT(I)=W2*W3
  40 CONTINUE
     DO 50 I=1,9,2
       WGT(I)=W2*W2
  50 CONTINUE
     WGT(5)=W3*W3
     GOTO 3
  2 CONTINUE
C 4*4 RECTANGULAR
   DO 60 I=1,13,4
     ALFA(I)=-A4
     ALFA(I+1)=-A5
     ALFA(I+2)=A5
     ALFA(I+3)=A4
  60 CONTINUE
     DO 70 I=1,4,1
       BETA(I)=-A4
       BETA(I+4)=-A5
       BETA(I+8)=A5
       BETA(I+12)=A4
  70 CONTINUE
     DO 80 I=2,15,1
       WGT(I)=W4*W5
       W42=W4**2
  80 CONTINUE
     WGT(1)=W42
     WGT(4)=W42
     WGT(13)=W42
     WGT(16)=W42
     W52=W5**2
     WGT(6)=W52
     WGT(7)=W52
     WGT(10)=W52
     WGT(11)=W52
  3 CONTINUE
    IF (NGAUST.EQ.0)GOTO 4
C 4*4 TRIANGULAR
   DO 90 I=30,33,1

```

```

ALFA(I)=.0694318443
ALFA(I+4)=.3300094783
ALFA(I+8)=.6699905218
ALFA(I+12)=.9305681558
90 CONTINUE
  I=45
  DO 100 M=30,42,4
  DO 100 N=30,42,4
  BETA(I)=ALFA(M)*ALFA(N)
  I=I-1
100 CONTINUE
  WGT(30)=.05630076615
  WGT(31)=.1055505547
  WGT(32)=.1055505547
  WGT(33)=.05630076615
  WGT(34)=.0759942953
  WGT(35)=.1424712409
  WGT(36)=.1424712409
  WGT(37)=.0759942953
  WGT(38)=.0374316306
  WGT(39)=.0701754105
  WGT(40)=.0701754105
  WGT(41)=.0374316306
  WGT(42)=.0042007305
  WGT(43)=.0078537125
  WGT(44)=.0078537125
  WGT(45)=.0042007305
  DO 110 JI=30,45
  WGT(JI)=WGT(JI)/2.
110 CONTINUE
C   WRITE(6,6)((ALFA(I),BETA(I),WGT(I)),I=1,45)
  4 CONTINUE
  RETURN
  END
C===== START SUBROUTINE =====
  SUBROUTINE SET
  COMMON US(50,2),R(3),T(200),PP(200),IONARY(9,200)
C
  DO 156 J=1,9
  DO 156 I=1,NP
156 IONARY(J,I)=0
C
C=====SELECT SPACING=====
C
  DO 205 L=1,NE
  NCN=8
  IF(NOP(L,7).EQ.0)NCN=6
C
  IF(NOP(L,3).EQ.0)NCN=2
  IST=NOP(L,1)
  MAX=IST
  MIN=IST
  DO 165 N=2,NCN
  NTH=NOP(L,N)

```

```

      IF (NTH .EQ. 0) GO TO 166
      ND=N
      IF ( MAX .LT. NTH) MAX=NTH
      IF (MIN .LE. NTH) GO TO 165
      MIN=NTH
      I=N-1
165 CONTINUE
166 IF (NSIZ .LT. (MAX-MIN)*NDF) NSIZ=(MAX-MIN)*NDF
      I=MIN
      DO 200 M=1,9
      IF (IONARY(M,I) .NE. 0) GO TO 200
      IONARY(M,I)=L
      GO TO 205
200 CONTINUE
205 CONTINUE
      L=1
      DO 230 I=1,NP
      DO 225 M=1,9
      IF (IONARY(M,I) .EQ. 0) GO TO 230
      IONARY(L,1)=IONARY(M,I)
225 L=L+1
230 CONTINUE
      IONARY(L,1)=0
      NSK=((NSIZ+NDF)*(NSIZ+NDF+1))/2+1
      IF (NSK .LT. NSZF+1) NSK=NSZF+1
C PRINT, 'YOUR BAND WIDTH IS TOO LARGE DUE TO THE MAX
C&NODE NUMBERING DIFFERENCE BEING',NSIZ,'/2 THEREFOR
C&GREATER THAN 65 '
      IF (NSK .LE. 24000) RETURN
      WRITE (6,111)
111 FORMAT(50H0 PROGRAM HALTED IN SET STIFFNESS SPACE
& EXCEEDED )
      STOP
      END
C===== START SUBROUTINE =====
      SUBROUTINE LDATA
      COMMON
& US (50,2),R(3),
& T(200),PP(200),IONARY(70)
& ,P(12),DEL(2,12),COJ(2,2),COJIN(2,2),DET,DI(2,12)
&,DIJ(2,2)
& ,NOPE(12),XYE(3,12),DISE(2,12)
& ,XYP(3),RP,STRN(4),STRS(4),STRSP(4)
& ,ESTIFM(24,24),B(4,24),DVDB(4,24),DVD(4,4)
&,FORCE(16),SFORCE(16),R2(100),DIS(2,200)
      IF (ILD .GT. 1) GO TO 822
      DO 50 J=1,NSZF
      RT(J)=0.0
      R1(J)=0.
      XR(J)=0.0
50 CONTINUE
      READ(41,7) TITLE
      READ, NSTRS
      WRITE(6,100) TITLE,ILD,NSTRS

```

```

C     READ BOUNDARY CONDITION FOR LOAD CASES
      IF (ILD.EQ. 1.AND.KLD.EQ.1) GO TO 800
      READ, NNBB
      DO 777 I=1, NNBB
777  READ, NBC(I), NFIX(I), ANG(I), (US(I,J), J=1, NDF)
      NB=NNBB
800  CONTINUE
C     READ EXTERNAL LOADS AT NODES
C
CWRITE(6,108)
      65 CONTINUE
      READ, NQ, (R(K), K=1, NDF)
CC   WRITE(6,119) NQ, (R(K), K=1, NDF)
C119 FORMAT(1H , I4, 2(F12.3, 2X))
      DO 70 K=1, NDF
      IC=(NQ-1)*NDF+K
      RT(IC)=R(K)
70   CONTINUE
      IF (NQ.LT. NP) GO TO 65
      7 FORMAT(12A4)
108  FORMAT(1H0,17H LOADS FROM CARDS )
100  FORMAT(1H1,12A4,5X,10HLOAD CASE= , I3, I5)
C   WRITE LOAD VECTOR TO DISC 2
      c     REWIND 2
      c     WRITE(2) (R1(I), I=1, NSZF)
      IF (NDYN.LT. 2) GO TO 300
      IF (ILD.GT. 1) GO TO 822
      IF (ILD.EQ. 1.AND.KLD.EQ.2) GO TO 822
      READ, (LCAS(I), I=1, 6)
      IF (LAY.LT. 2) GO TO 135
      READ, ((NLAY(I,J), J=1, NDLY), I=1, IAY)
      PRINT, ((NLAY(I,J), J=1, NDLY), I=1, IAY)
      READ, (ZZ(L), L=1, IAY)
      READ, ((KFAC(I,J), J=1, LELEM), I=1, IAY)
135  CONTINUE
      DO 202 J=1, NSZF
      RT1(J)=0.0
202  CONTINUE
      REWIND 15
      DO 424 LN=1, NE
      DO 402 I=1, 8
402  NOPE(I)=0
C
      READ(15) LNEW, (NOPE(I), I=1, 8), ((XM(II,J), J=1, LV), I
& I=1, LV), (XG(II)
&, II=1, LV)
C     PRINT, LNEW, (NOPE(I), I=1, 8), ((XM(II,J), J=1, LV), II=1, LV)
      LNEW=IONARY(LN)
      NCN=8
      DO 406 K=1, NCN
406  NOPE(K)=NOP(LNEW, K)
      DO 408 I=1, NCN
      NRR=NOPE(I)
      NR1=NRR*2-1

```

```

NR=NRF* 2
K21=2*I-1
K2=2*I
XR(NR1)=XR(NR1)+XG(K21)
XR(NR)=XR(NR)+XG(K2)
408 CONTINUE
424 CONTINUE
C
C
C
C      DO 206 I=1,NSZF
C      R1(I)=XR(I)+RT(I)
C      RT1(I)=RT(I)
C 206 CONTINUE
822 CONTINUE
      IF (ILD .EQ. 1.AND.KLD.EQ.1) GO TO 833
      CALL LDYN
      IF (INTER .LT. 2) GO TO 833
      IF (ILD .EQ. 1.AND.KLD.EQ.2) GO TO 844
833 CONTINUE
      CALL CASES
      DO 606 I=1,NSZF
      RT1(I)=RT(I)
606 CONTINUE
      GO TO 500
300 DO 330 I=1,NSZF
      R1(I)=RT(I)
330 CONTINUE
      GO TO 477
500 CONTINUE
      IF (INTER .LT. 2) GO TO 477
C      EFFECT OF REFLECTION AND REFRACTION OF STRESS WAVE PROPAGATION
C      PRINT, ((ORT(L, I), I=1, 8), L=1, NMAT)
      ZZ(1)=SQRT(ORT(2, 2))/SQRT(ORT(1, 2))
      ZZ(2)=SQRT(ORT(3, 2))/SQRT(ORT(2, 2))
      ZZ(3)=SQRT(ORT(4, 2))/SQRT(ORT(3, 2))
C      PRINT, (ZZ(I), I=1, IAY)
      IF (ILD .EQ. 1) GO TO 477
      DO 455 I=1, IAY
      DO 466 K=1, NDLY
      KK=NLAY(I, K)
      K21=2*KK+1
      K2=2*KK
      R1(K21)=R1(K21)+ZZ(I)*R3(K21)
      R1(K2)=R1(K2)+ZZ(I)*R3(K2)
466 CONTINUE
455 CONTINUE
477 CONTINUE
      REWIND 2
      WRITE (2) (R1(I), I=1, NSZF)
C      PRINT, (R1(I), I=1, NSZF)
844 CONTINUE
      RETURN
      END

```

```

C===== START SUBROUTINE =====
  SUBROUTINE CASES
  COMMON
  & US (50, 2), R (3),
  & T (200), PP (200), IONARY (70)
  & , P (12), DEL (2, 12), COJ (2, 2), COJIN (2, 2), DET, DI (2, 12)
  & , DIJ (2, 2)
  & , NOPE (12), XYE (3, 12), DISE (2, 12)
  & , XYP (3), RP, STRN (4), STRS (4), STRSP (4)
  & , ESTIFM (24, 24), B (4, 24), DVDB (4, 24), DVD (4, 4)
  & , FORCE (16), SFORCE (16), R2 (100), DIS (2, 200)

```

```

C
  IF (NCASE .EQ. 1) GO TO 111
  IF (NCASE .EQ. 2) GO TO 222
  IF (NCASE .EQ. 3) GO TO 333
  IF (NCASE .EQ. 4) GO TO 444
  IF (NCASE .EQ. 5) GO TO 555
  IF (NCASE .EQ. 6) GO TO 666
  IF (NCASE .EQ. 7) GO TO 777
111 IF (ILD .GT. 1) GO TO 112
    DO 206 II=1, NSZF
206 R1 (II)=XR (II)+RT (II)
    GO TO 500
112 DO 603 II=1, NSZF
    R1 (II)=XR (II)+RT1 (II)+SETA* (RT (II)-RT1 (II))
603 CONTINUE
    GO TO 500

```

```

C
C
C
C
C
C
  CASE OF RECTANGULAR PULSE
222 IF (ILD .GT. 1) GO TO 223
    DO 224 I=1, NSZF
224 R1 (I)=XR (I)+RT (I)
    GO TO 500
223 IF (ILD .GT. ICAS (1)) GO TO 226
    DO 225 I=1, NSZF
225 R1 (I)=XR (I)+RT (I)+SETA* (RT (I)-RT1 (I))
    GO TO 500
226 DO 227 I=1, NSZF
227 R1 (I)=XR (I)
    GO TO 500

```

```

C
  CASE OF TRINGULAR PULSE
333 IF (ILD .GT. 1) GO TO 342
    DO 353 I=1, NSZF
353 R1 (I)=XR (I)+0.5*RT (I)*SETA
    GO TO 500
342 IF (ILD .GT. ICAS (1)) GO TO 363
    DO 373 I=1, NSZF
373 R1 (I)=XR (I)+0.5*RT (I)+(ILD-2)*RT (I)+SETA*RT (I)
    GO TO 500
363 IF (ILD .GT. ICAS (2)) GO TO 383
    DO 393 I=1, NSZF

```

```

393 R1(I)=XR(I)+LCAS(1)*RT(I)-(ILD-LCAS(1)+1)-SETA*RT(
&I)+0.5*RT(I)
GO TO 500
383 DO 394 I=1, NSZF
394 R1(I)=XR(I)
GO TO 500
C CASE OF TRAPEZOIDAL PULSE
444 IF (ILD .GT. 1) GO TO 414
DO 424 I=1, NSZF
424 R1(I)=XR(I)+0.5*RT(I)*SETA
GO TO 500
414 IF (ILD .GT. LCAS(1)) GO TO 454
DO 404 I=1, NSZF
404 R1(I)=XR(I)+0.5*RT(I)+(ILD-2)*RT(I)+SETA*RT(I)
GO TO 500
454 IF (ILD .GT. LCAS(2)) GO TO 464
DO 474 I=1, NSZF
474 R1(I)=XR(I)+LCAS(1)*RT(I)
GO TO 500
464 IF (ILD .GT. LCAS(2)) GO TO 484
DO 494 I=1, NSZF
494 R1(I)=XR(I)+LCAS(1)*RT(I)-(ILD-LCAS(2)+1)*RT(I)-(S
&ETA-0.5)*RT(I)
GO TO 500
484 DO 488 I=1, NSZF
488 R1(I)=XR(I)
GO TO 500
C CASE OF SURFACE BURSTS OF NUCLEAR WEAPONS
555 IF (ILD .GT. 1) GO TO 515
DO 525 I=1, NSZF
525 R1(I)=XR(I)+((0.5*RT(I)*SETA)/LCAS(1))
GO TO 500
515 IF (ILD .GT. LCAS(1)) GO TO 535
DO 545 I=1, NSZF
CAS=0.0
CAS=RT(I)/LCAS(1)
R1(I)=XR(I)+0.5*CAS+(ILD-2)*CAS+SETA*CAS
545 CONTINUE
GO TO 500
535 IF (ILD .GT. LCAS(2)) GO TO 533
DO 565 I=1, NSZF
565 R1(I)=XR(I)+RT(I)
GO TO 500
533 IF (ILD .GT. LCAS(3)) GO TO 575
DO 585 I=1, NSZF
CAS=0.0
CAS=(0.66*RT(I))/(LCAS(3)-LCAS(2))
R1(I)=XR(I)+RT(I)-(ILD-LCAS(2)+1)*CAS-SETA*CAS+0.5
&*CAS
585 CONTINUE
GO TO 500
575 IF (ILD .GT. LCAS(4)) GO TO 516
DO 517 I=1, NSZF
CAS=0.0

```



```

      CAS=0.20*RT(I)/(LCAS(4)-LCAS(3))
      R1(I)=XR(I)+RT(I)-(ILD-LCAS(3)+1)*CAS-SETA*CAS+0.5
&*CAS
517 CONTINUE
      GO TO 500
516 IF (ILD .GT. LCAS(5)) GO TO 518
      DO 519 I=1,NSZF
      CAS=0.0
      CAS=0.14*RT(I)/(LCAS(5)-LCAS(4))
      R1(I)=XR(I)+0.14*RT(I)-(ILD-LCAS(4)+1)*CAS-SETA*CA
&S+0.5*CAS
519 CONTINUE
      GO TO 500
518 DO 520 I=1,NSZF
520 R1(I)=XR(I)
      GO TO 500
C
C      CASE OF SIN AND HALF SIN WAVE PULSE
666 TIM=0.0
      TIM=DELT*ILD
      PI=3.1415927
      IF (ILD .GT. LCAS(1)) GO TO 626
      DO 616 I=1,NSZF
      R1(I)=XR(I)+RT(I)*SIN((PI*TIM)/(LCAS(1)*DELT))
616 CONTINUE
      GO TO 500
626 IF (LCAS(2) .EQ. 1) GO TO 636
      DO 646 I=1,NSZF
646 R1(I)=XR(I)+RT(I)*SIN((PI*TIM)/(LCAS(1)*DELT))
      GO TO 500
636 DO 656 I=1,NSZF
656 R1(I)=XR(I)
      GO TO 500
C      CASE OF ACTUAL IMPACT FORCE FROM EXPERIMENTS
777 IF (ILD .GT. 1) GO TO 705
      DO 710 II=1,NSZF
710 R1(II)=XR(II)+0.5*SETA*YF(ILD+1)*RT(II)
      GO TO 500
705 KPULS=NPULS-2
      IF(ILD .GT. KPULS) GO TO 730
      DO 720 II=1,NSZF
      R1(II)=XR(II)+RT(II)*YF(ILD)+SETA*(YF(ILD+1)-YF(IL
&D))*RT(II)*.5
720 CONTINUE
      GO TO 500
730 DO 740 II=1,NSZF
      R1(II)=XR(II)
740 CONTINUE
500 CONTINUE
      RETURN
      END
C===== START SUBROUTINE =====
      SUBROUTINE LDYN
      COMMON

```

```

& US (50, 2), R(3),
& T(200), PP(200), IONARY(70)
& ,P(12), DEL(2, 12), COJ(2, 2), COJIN(2, 2), DET, DI(2, 12)
& ,DIJ(2, 2)
& ,NOPE(12), XYE(3, 12), DISE(2, 12)
& ,XYP(3), RP, STRN(4), STRS(4), STRSP(4)
& ,ESTIFM(24, 24), B(4, 24), DVDB(4, 24), DVD(4, 4)
& ,FORCE(16), SFORCE(16), R2(100), DIS(2, 200)
C   PRINT, (UAST(I), I=1, NSZF)
   IF (ILD .GT. 1) GO TO 235
   DO 291 I=1, 50
   LNBC(I)=0
   LNF I(I)=0
   DANG(I)=0.0
   DO 292 J=1, 2
292 DUS(I, J)=0.0
291 CONTINUE
   NNBB=NB
   DO 220 I=1, NNBB
   LNBC(I)=NBC(I)
   LNF I(I)=NF IX(I)
   DANG(I)=ANG(I)
   DO 230 J=1, NDF
230 DUS(I, J)=US(I, J)
220 CONTINUE
   IC=0
   DO 232 I=1, NB
   DO 232 J=1, NDF
   IC=1+IC
232 U(IC)=US(I, J)
   GO TO 250
235 CONTINUE
   DO 262 I=1, NDF
   DO 262 J=1, NP
262 Q(I, J)=0.0
   DO 260 J=1, NSZF
   XR(J)=0.0
260 R1(J)=0.0
   DO 240 I=1, NNBB
   NBC(I)=LNBC(I)
   NF IX(I)=LNF I(I)
   ANG(I)=DANG(I)
   DO 244 J=1, NDF
244 US(I, J)=DUS(I, J)
240 CONTINUE
   IC=0
   DO 246 I=1, NB
   DO 246 J=1, NDF
   IC=IC+1
246 U(IC)=US(I, J)
250 CONTINUE
C   CALL FDUMP
   CALL SET
   LV=16

```

```

    IF (IFIAG .EQ. 1) GO TO 555
    L1=16
    L2=17
    IFIAG=1
    GO TO 590
555 L1=17
    L2=16
    IFIAG=0
590 CONTINUE
    REWIND 15
    REWIND 16
    REWIND 17
    DO 600 N=1,NE
C
    READ(9) LNEW, (NOPE(I), I=1, 8), ((XM(II,J), J=1, LV), II=1, LV)
C
    DO 204 I=1, LV
    UAC2(I)=0.0
    UAC(I)=0.0
    UV2(I)=0.0
    UVE(I)=0.0
    UD2(I)=0.0
    UDE(I)=0.0
204 CONTINUE
    IF (INTER .LT. 2) GO TO 707
    IF (INTER .GT. 2) GO TO 704
707 IF (ILD .GT. 2) GO TO 404
704 IF (ILD .GT. 1) GO TO 404
    WRITE(16) LNEW, (NOPE(I), I=1, 8), (UAC(J), J=1, LV), (UV
    &E(J), J=1, LV)
    &, (UDE(J), J=1, LV)
404 CONTINUE
    DO 208 I=1, 8
    NOPE(I)=0.0
208 CONTINUE
C
    READ(15) LNEW, (NOPE(I), I=1, 8), ((XM(II,J), J=1, LV), I
    &I=1, LV), (XG(II)
    &, II=1, LV)
    LC=IMAT(LNEW)
    IF (LC .GT. NMAT) LC=LC-100
    DALPHA=ORT(LC, 7)
    DBETA=ORT(LC, 8)
    CALL CONDY
C
    PRINT, LNEW, (NOPE(I), I=1, 8), ((XM(II,J), J=1, LV), II=1, LV)
    IF (ILD .EQ. 2) GO TO 505
    READ(L1) LNEW, (NOPE(I), I=1, 8), (UAC(J), J=1, LV), (UVE
    &(J), J=1, LV)
    &, (UDE(J), J=1, LV)
C
    PRINT, LNEW, (NOPE(I), I=1, 8), (UAC(J), J=1, LV)
505 CONTINUE
    NCN=8
    LNEW=IONARY(N)
    DO 288 I=1, 12
    NOPE(I)=0

```

```

288 CONTINUE
   NCN=8
   DO 289 K=1,NCN
   NOPE (K)=NOP (LNEW,K)
289 CONTINUE
   DO 304 JJ=1,NCN
   NNCN=NOPE (JJ)
   LR2=NNCN*2-1
   LR=NNCN*2
   N21=2*JJ-1
   N2=2*JJ
C      PRINT,N21,N2,LR2,LR
C      PRINT,LR2,LR
   UAC2 (N21)= ((AFOR*UAST (LR2))+(AFIV*UDE (N21)))+(ASIX*
&UVE (N21))+
&(ASEVN*UAC (N21)))
   UAC2 (N2)= ((AFOR*UAST (LR))+(AFIV*UDE (N2)))+(ASIX*UVE
&(N2))+
&(ASEVN*UAC (N2)))
   UV2 (N21)= (UVE (N21)+(AET*(UAC2 (N21)+UAC (N21))))
   UV2 (N2)= (UVE (N2)+(AET*(UAC2 (N2)+UAC (N2))))
   UD2 (N21)= (UDE (N21)+(DELT*UVE (N21)))+(ANIN*UAC (N21))
&+(ATEN*UAC2 (N21)))
   UD2 (N2)= (UDE (N2)+(DELT*UVE (N2)))+(ANIN*UAC (N2))+(AT
&EN*UAC2 (N2)))
304 CONTINUE
   DO 305 L=1,LV
   UAC (L)=UAC2 (L)
   UVE (L)=UV2 (L)
   UDE (L)=UD2 (L)
305 CONTINUE
C
   DO 306 I=1,LV
   XMU (I)=0.0
   DO 308 J=1,LV
   XMU (I)=XMU (I)+XM (I,J)*(AONE*UDE (J)+ATO*UVE (J)+ATH
&RE*UAC (J))
308 CONTINUE
306 CONTINUE
   DO 309 I=1,NCN
   NRR=NOPE (I)
   NR1=NRR*2-1
   NR=NRR*2
   K21=2*I-1
   K2=2*I
C      PRINT,NR1,NR,K21,K2
   XR (NR1)=XR (NR1)+XMU (K21)
   XR (NR)=XR (NR)+XMU (K2)
309 CONTINUE
   DO 370 I=1,NCN
   KD1=2*I-1
   KD2=2*I
   KD3=NOPE (I)
   Q (1,KD3)=UDE (KD1)

```

```

      Q(2,KD3)=UDE(KD2)
370 CONTINUE
      IF(N.EQ.KE) WRITE(6,307)UDE(KP)
      IF(N.EQ.KE) WRITE(19)ILD,UAC(KP),UVE(KP),UDE(K
&P)
307 FORMAT(V)
      WRITE(L2) LNEW,(NOPE(I),I=1,8),(UAC(J),J=1,LV),(U
&VE(J),J=1,LV)
&,(UDE(J),J=1,LV)
600 CONTINUE
C      READ(9) LNEW,(NOPE(I),I=1,8),((XM(II,J),J=1,LV),II=1,LV)
      IF(INTER.LT.2) GO TO 601
      IF(KLD.NE.2) GO TO 601
      DO 602 K=1,NE
      DO 603 I=1,LV
      UAC2(I)=0.0
      UAC(I)=0.0
      UV2(I)=0.0
      UVE(I)=0.0
      UD2(I)=0.0
      UDE(I)=0.0
603 CONTINUE
      WRITE(L2) LNEW,(NOPE(I),I=1,8),(UAC(J),J=1,LV),(U
&VE(J),J=1,LV)
&,(UDE(J),J=1,LV)
602 CONTINUE
601 CONTINUE
      RETURN
      END

```

```

C===== START SUBROUTINE =====
      SUBROUTINE CONDY
      COMMON
& US(50,2),R(3),
& T(200),PP(200),IONARY(70)
& ,P(12),DEL(2,12),COJ(2,2),COJIN(2,2),DET,DI(2,12
&),DIJ(2,2)
& ,NOPE(12),XYE(3,12),DISE(2,12)
& ,XYP(3),RP,STRN(4),STRS(4),STRSP(4)
& ,ESTIFM(24,24),B(4,24),DVDB(4,24),DVD(4,4)
& ,FORCE(16),SFORCE(16),R2(100),DIS(2,200)
      TAW=SETA*DELT
      ANOT=(6.+3.*DALPHA*TAW)/(TAW**2+3.*DBETA*TAW)
      BNOT=DALPHA-DBETA*ANOT
      AONE=(6/(TAW**2))+3.*BNOT/TAW
      ATO=(6/TAW)+2.*BNOT
      ATHRE=2.+TAW*BNOT/2.0
      AFOR=6./(SETA*(3.*DBETA*TAW+TAW**2))
      BONE=DBETA*AFOR
      AFIV=(3.*BONE/TAW)-6./((TAW**2)*SETA)
      ASIX=2.*BONE-6./(TAW*SETA)
      ASEVN=BONE*TAW/2.0+1.0-3.0/SETA
      AET=DELT/2.0
      ANIN=DELT**2/3.0
      ATEN=ANIN/2.0

```

```

GTH=GTH/57.295779514
c  write(6,1)taw,anot,bnot,aone,ato,athre,afor
c  write(6,1)bone,afiv,asix,asevn,aet,anin,aten
1 FORMAT (V)
RETURN
C===== START SUBROUTINE =====
END
SUBROUTINE STIFM
COMMON
& US (50,2),R(3),
& T(200),PP(200),IONARY(70)
& ,P(12),DEL(2,12),COJ(2,2),COJIN(2,2),DET,DI(2,12
&),DIJ(2,2)
& ,NOPE(12),XYE(3,12),DISE(2,12)
& ,XYP(3),RP,STRN(4),STRS(4),STRSP(4)
& ,ESTIFM(24,24),B(4,24),DVDB(4,24),DVD(4,4)
& ,FORCE(16),SFORCE(16),R2(100),DIS(2,200)
DO 400 M=1,NE
NCN=8
DO 11 J=1,8
NOPE(J)=0
11 CONTINUE
C INITIAL ESTIFM AND B
DO 2 I=1,16
DO 2 J=1,16
ESTIFM(I,J)=.0
XM(I,J)=0.0
IF(I.LE.4)B(I,J)=.0
2 CONTINUE
LNEW=IONARY(M)
CWRITE(6,987)LNEW
987 FORMAT(1H ,6HLNEW= ,I3)
IF(NOP(LNEW,3) .GT. 0.01E-8) GO TO 12
C SPRING ELEMENT
CALL SPRING(LNEW)
DO 13 K=1,NCN
NOPE(K)=NOP(LNEW,K)
13 CONTINUE
GOTO 350
12 CONTINUE
NCN=8
DO 955 I=1,16
XG(I)=0.0
955 CONTINUE
LV=16
KK=1
NGAUS=NGAUSR
IF(NOP(LNEW,7) .NE.0) GOTO 30
C
NCN=6
LV=12
KK=30
NGAUS=45
30 CONTINUE

```

```

C CORRECTION FOR TRIANGLES
C FORMATION OF STIFFNESSES AND CALCULATION OF BODY FORCES
C
      L=IMAT(LNEW)
C
C NOTE MATERIAL NO OF ELEMENT ALONG SLOPING BOUNDARY IS GT.BY.100
C
      IF(L.GT.NMAT)L=L-100
      DO 200 K=1,NCN
      MASH=NOP(LNEW,K)
      DO 300 I=1,NCORD
      XYE(I,K)=CORD(MASH,I)
300 CONTINUE
      NOPE(K)=MASH
200 CONTINUE
      E1=ORT(L,1)
      E2=ORT(L,2)
      G2=ORT(L,3)
      C1=ORT(L,4)
      C2=ORT(L,5)
      ROE=ORT(L,6)
      DALPHA=ORT(L,7)
      DBETA=ORT(L,8)
      THICK=ORT(L,9)
      CALL CONDY
      CALL MODU
C
C FORMULATION OF STIFFNESS
C
      DO 100 IGAUS=KK,NGAUS
      G=ALFA(IGAUS)
      H=BETA(IGAUS)
C WRITE(6,10)G,H
C10 FORMAT(1H ,^G =^,F13.8,^H =^,F13.8)
      CALL SFR(G,H)
      CALL AUX(LNEW)
      IJAUS=IGAUS
      CALL FEM(IJAUS)
C WRITE(6,5000)((DI(I,J),J=1,8),I=1,2)
C5000 FORMAT(1H ,^DI I,J^,8E15.4)
      DO 21 I=1,NDF
      DO 22 J=1,IV
      QN(I,J)=0.0
22 CONTINUE
21 CONTINUE
      NASH=0
      DO 10 I=1,NCN
      MASH=NASH+1
      NASH=MASH+1
      QN(1,MASH)=P(I)
      QN(2,MASH)=P(I)
10 continue
      GXC=ROE*GRAV*SIN(GTH)
      GYC=-ROE*GRAV*COS(GTH)

```

```

do 900 i=1,ncn
lr=(i-1)*ndf+1
lrr=(i-1)*ndf+2
XG(LR)=XG(LR)+GXC*DV*P(I)
XG(LRR)=XG(LRR)+GYC*DV*P(I)
900 continue
DO 910 I=1, LV
DO 910 J=1, LV
DO 915 K=1, NDF
XM(I,J)=XM(I,J)+QN(K,I)*QN(K,J)*ROE*DV
915 CONTINUE
910 CONTINUE
C
DO 20 I=1, LV
DO 20 J=I, LV
GASH=ESTIFM(I,J)
DO 18 K=1, ICS
GASH=GASH+B(K,I)*DVDB(K,J)
18 CONTINUE
ESTIFM(I,J)=GASH
ESTIFM(J,I)=GASH
20 CONTINUE
100 CONTINUE
IF (IMAT(LNEW) .GT. NMAT) CALL ROSB(LNEW)
C FOR BAR REINFORCEMENT IN QUAD ELEMENTS.
C IF NBAR GT 0 THEN REINFORCED.
IF (NBAR.EQ.0.OR.NCN.EQ.6) GOTO 350
IF (BAREA(LNEW,1) .LT. 0.01E-8) GO TO 350
CALL BAR(LNEW)
350 CONTINUE
C DO 915 I=1,16
C DO 915 J=1,16
C XM(I,J)=0.0
C XM(I,I)=1.0
C 915 CONTINUE
C DO 920 I=1,16
C DO 920 J=1,16
C 920 XM(I,J)=ROE*1.0*2.0/8.0*(XM(I,J))
IF (NDYN .LT. 2) GO TO 935
DO 930 I=1,16
DO 930 J=1,16
930 ESTIFM(I,J)=ESTIFM(I,J)+ANOT*(XM(I,J))
935 CONTINUE
WRITE (3) LNEW, (NOPE(I), I=1, 8), ((ESTIFM(I,J), J=1, 1
&6), I=1, 16)
WRITE (15) LNEW, (NOPE(I), I=1, 8), ((XM(II,J), J=1, LV)
&, II=1, LV), (XG(II)
&, II=1, LV)
IF (ILD .GT. 1) GO TO 400
WRITE (6,3) LNEW, (NOPE(I), I=1, 8)
C WRITE (6,4) ((ESTIFM(I,J), J=1, 16), I=1, 16)
3 FORMAT(' ', 'ELEMENT NO.', I3, 'NODES', 8I4)
4 FORMAT(8 (2X, E9.3), /8 (2X, E9.3))
400 CONTINUE

```



```

A=0.
N=0
WRITE (3) N, (N, I=1, 8), ((A, J=1, 16), I=1, 16)
C PUT TERMINATER IN FOR BAR DATA
A1=.0
B1=.0
C FOR CASE OF REINFOCIMENT DELE 5342, 5344 KAREAM
ASTEEL=0.0
ESTEEL=0.0
WRITE (8) (ASTEEL, ESTEEL, LNEW, A1, B1, (NOPE (I), I=1, 8)
&, ((B(I, J
& ( ), J=1, 16), I=1, 4))
REWIND 3
RETURN
END
C===== START SUBROUTINE =====
SUBROUTINE ROSB(LNEW)
COMMON
& US (50, 2), R (3),
& T (200), PP (200), IONARY (70)
& , P (12), DEL (2, 12), COJ (2, 2), COJIN (2, 2), DET, DI (2, 12)
& , DIJ (2, 2)
& , NOPE (12), XYE (3, 12), DISE (2, 12)
& , XYP (3), RP, STRN (4), STRS (4), STRSP (4)
& , ESTIFM (24, 24), B (4, 24), DVDB (4, 24), DVD (4, 4)
& , FORCE (16), SFORCE (16), R2 (100), DIS (2, 200)
C
C WRITE (6, 30) ((ESTIFM(I, J), I=1, LV), J=1, LV)
DO 250 I=1, NCN
DO 150 M=1, NB
IF (NOP(LNEW, I) .EQ. NBC(M)) GO TO 140
150 CONTINUE
GO TO 250
140 IF (ANG(M) .LT. 0.01E-8) GO TO 250
GASH=ANG(M)*0.017453292
CS=COS(GASH)
TN=TAN(GASH)
MASH=2*I-1
NASH=MASH+1
DO 20 K=1, LV
STFUC=ESTIFM(MASH, K)*CS
STFVC=ESTIFM(NASH, K)*CS
ESTIFM(MASH, K)=STFUC+STFVC*TN
ESTIFM(NASH, K)=STFVC-STFUC*TN
20 CONTINUE
DO 40 K=MASH, NASH
STFUC=ESTIFM(K, MASH)*CS
STFVC=ESTIFM(K, NASH)*CS
ESTIFM(K, MASH)=STFUC+STFVC*TN
ESTIFM(K, NASH)=STFVC-STFUC*TN
40 CONTINUE
DO 60 J=MASH, NASH
DO 60 K=1, LV
ESTIFM(K, J)=ESTIFM(J, K)

```

```

60 CONTINUE
250 CONTINUE
C   WRITE (6, 30) ((ESTIFM(I, J), I=1, LV), J=1, LV)
C
      RETURN
C===== START SUBROUTINE =====
      END
      SUBROUTINE FEM(IGAUS)
      COMMON
      & US (50, 2), R(3),
      & T(200), PP(200), IONARY(70)
      & , P(12), DEL(2, 12), COJ(2, 2), COJIN(2, 2), DET, DI(2, 12
      &), DIJ(2, 2)
      & , NOPE(12), XYE(3, 12), DISE(2, 12)
      & , XYP(3), RP, STRN(4), STRS(4), STRSP(4)
      & , ESTIFM(24, 24), B(4, 24), DVDB(4, 24), DVD(4, 4)
      & , FORCE(16), SFORCE(16), R2(100), DIS(2, 200)
C
C   CALCULATE B MATRIX FROM DI MATRIX
C
      NASH=0
      DO 10 I=1, NCN
      MASH=NASH+1
      NASH=MASH+1
      B(1, MASH)=DI(1, I)
      B(2, NASH)=DI(2, I)
      B(3, MASH)=DI(2, I)
      B(3, NASH)=DI(1, I)
      IF (NPP .EQ. 2) B(4, MASH)=P(I)/RP
10 CONTINUE
      DV=ABS(DET)*WGT(IGAUS)
      IF (NPP .EQ. 2) DV=DV*RP*6.2831853072
      IF (NCORD .EQ. 3) DV=DV*XYP(3)
      IF (NCORD .EQ. 2) DV=DV*THICK
C   CALCULATE DVD MATRIX
C
      DO 12 I=1, ICS
      DO 12 J=1, ICS
      DVD(I, J)=DV*D(I, J)
12 CONTINUE
      DO 16 I=1, ICS
      DO 16 J=1, LV
      GASH=0.
      DO 14 K=1, ICS
      GASH=GASH+DVD(I, K)*B(K, J)
14 CONTINUE
      DVDB(I, J)=GASH
16 CONTINUE
      RETURN
      END
C===== START SUBROUTINE =====
      SUBROUTINE AUX(LNEW)
      COMMON
      & US (50, 2), R(3),

```

```

& T(200),PP(200),IONARY(70)
& ,P(12),DEL(2,12),COJ(2,2),COJIN(2,2),DET,DI(2,12
& ),DIJ(2,2)
& ,NOPE(12),XYE(3,12),DISE(2,12)
& ,XYP(3),RP,STRN(4),STRS(4),STRSP(4)
& ,ESTIFM(24,24),B(4,24),DVDB(4,24),DVD(4,4)
& ,FORCE(16),SFORCE(16),R2(100),DIS(2,200)

C
C   CREATE COORDINATE JACOBIAN 0 INTERPOLATE X,YOCOJ(I,J),XY(1),XY(2)
C   ARE COORDINATE JACOBIAN MATRIX, X COORDINATE AND Y COORDINATE
C
C   WRITE(6,19)NCN
C19 FORMAT(1H ,^NCN=^,I4)
C   WRITE(6,20)((XYE(I,J),I=1,2),J=1,NCN)
C   WRITE(6,20)((DEL(I,J),I=1,2),J=1,NCN)
C   WRITE(6,20)(P(I),I=1,NCN)
C20 FORMAT(1H ,2E15.7)
    DO 8 I=1,2
    DO 8 J=1,2
    GASH=0.
    DO 4 K=1,NCN
    GASH=GASH+XYE(I,K)*DEL(J,K)
4 CONTINUE
    COJ(I,J)=GASH
8 CONTINUE
C   WRITE(6,20)((COJ(I,J),I=1,2),J=1,NCN)
    DO 16 I=1,NCORD
    GASH=0.
    DO 6 K=1,NCN
    GASH=GASH+XYE(I,K)*P(K)
6 CONTINUE
    XYP(I)=GASH
16 CONTINUE
    RP=XYP(1)

C
C   CALCULATE DETERMINATE AND INVERSE OF COORDINATE JACOBIAN
C   DET AND COJIN(I,J) ARE DETERMINANT AND INVERSE COORD. JACOBIAN
C
    DET=COJ(1,1)*COJ(2,2)-COJ(1,2)*COJ(2,1)
    DET=ABS(DET)
C   WRITE(6,20)DET
C   IF (DET) 100,200,300
C   IF (DET) 300,200,300
C100 CONTINUE
C   WRITE(6,101) LNEW
C 101 FORMAT(1H0,38H NEGATIVE DET STOPPED AT ELEMENT NO = ,I3)
C   STOP
200 DET=0.0000000001
300 CONTINUE
    COJIN(1,1)=COJ(2,2)/DET
    COJIN(2,2)=COJ(1,1)/DET
    COJIN(1,2)=-COJ(1,2)/DET
    COJIN(2,1)=-COJ(2,1)/DET
C

```

```

C      CALCULATE CARTESIAN DERIVATIVES OF SHAPE FUNCTIONS,DI (I,K),I=X,Y,
C
      DO 14 I=1,2
      DO 12 K=1,NCN
      GASH=0.
      DO 10 J=1,2
      GASH=GASH+DEL(J,K)*COJIN(J,I)
10 CONTINUE
      DI (I,K)=GASH
12 CONTINUE
14 CONTINUE
      RETURN
      END
C===== START SUBROUTINE =====
      SUBROUTINE MODU
      CN=E1/E2
      CQ=CN*C2*C2
      D(3,3)=G2
      D(1,3)=0.
      D(3,1)=0.
      D(2,3)=0.
      D(3,2)=0.
      IF(NPP .NE. 0) GO TO 20
C
C      D MATRIX FOR PLANE STRESS CASE
C
      CD=E2/(1.-CQ)
      D(1,1)=CD*CN
      D(2,2)=CD
      D(1,2)=CD*CN*C2
      D(2,1)=CD*CN*C2
      GO TO 24
20 CONTINUE
C
C      D MATRIX FOR PLANE STRAIN CASE
C
      CD=E2/((1.+C1)*(1.-C1-2.*CQ))
      D(1,1)=CD*CN*(1.-CQ)
      D(2,2)=CD*(1.-C1*C1)
      D(1,2)=CD*CN*(1.+C1)*C2
      D(2,1)=D(1,2)
      IF (NPP .NE. 2) GO TO 24
C
C      D MATRIX FOR AXISYMMETRIC CASE
C
      D(4,4)=D(1,1)
      D(4,1)=CD*(C1+CQ)
      D(1,4)=D(4,1)
      D(4,2)=D(1,2)
      D(2,4)=D(1,2)
      D(3,4)=0.
      D(4,3)=0.
24 CONTINUE
      RETURN

```

```

      END
C===== START SUBROUTINE =====
      SUBROUTINE STRP (LNEW)
      COMMON
      & US (50, 2), R (3),
      & T (200), PP (200), IONARY (70)
      & , P (12), DEL (2, 12), COJ (2, 2), COJIN (2, 2), DET, DI (2, 12
      &), DIJ (2, 2)
      & , NOPE (12), XYE (3, 12), DISE (2, 12)
      & , XYP (3), RP, STRN (4), STRS (4), STRSP (4)
      & , ESTIFM (24, 24), B (4, 24), DVDB (4, 24), DVD (4, 4)
      & , FORCE (16), SFORCE (16), R2 (100), DIS (2, 200)
C
      DO 18 I=1, 2
      DO 18 J=1, 2
      GASH=0.
      DO 16 K=1, NCN
      GASH= GASH + DISE (I, K)*DI (J, K)
16 CONTINUE
      DIJ (I, J)=GASH
18 CONTINUE
      DO 9 I=1, 3
      DO 9 J=1, LV
      B (I, J)=0.
      9 CONTINUE
C LOOP 10 IS FOR NON-LINEARISATION OF MATERIAL RESPONSE.
      NASH=0
      DO 10 I=1, NCN
      MASH=NASH+1
      NASH=MASH+1
      B (1, MASH)=DI (1, I)
      B (2, MASH)=DI (2, I)
      B (3, MASH)=DI (2, I)
      B (3, MASH)=DI (1, I)
10 CONTINUE
      IF (NPP .NE. 2) GO TO 30
      GISH=0.
      DO 20 K=1, NCN
      GISH=GISH+DISE (1, K)*P (K)
20 CONTINUE
      IF (RP .EQ. 0.0) RP=0.000001
      STRN (4)=GISH/RP
30 CONTINUE
C
C      CALCULATE STRAIN AT A POINT
C
      STRN (1)=DIJ (1, 1)
      STRN (2)=DIJ (2, 2)
      STRN (3)=DIJ (1, 2)+DIJ (2, 1)
C
C      CALCULATE STRESSES AT A POINT
C
      DO 24 I=1, ICS
      GASH=0.

```

```

DO 22 J=1, ICS
  GASH=GASH+D(I,J)*STRN(J)
22 CONTINUE
  STRS(I)=GASH
24 CONTINUE
  IF (NPP-1) 26, 28, 32
26 STRN(4)=0.
  STRS(4)=C1*STRS(1)+C2*STRS(2)*E1/E2
  GO TO 32
28 STRS(4)=0.
  STRN(4)=- (C1*STRS(1)/E1)-(C2*STRS(2)/E2)
32 CONTINUE
  GASH=(STRS(1)+STRS(2))*0.5
  GISH=STRS(1)-GASH
  GESH=STRS(3)
  GOSH=SQRT(GISH*GISH+GESH*GESH)
  STRSP(1)=GASH+GOSH
  STRSP(2)=GASH-GOSH
  STRSP(3)=45.0
  IF (GISH.NE.0.0) STRSP(3)=ATAN(GESH/GISH)*28.6478
&89757
  STRSP(4)=STRS(4)
  RP=GOSH
C
CICN=1
C   WRITE(19,50) ICN,XYP(1),XYP(2),(STRSP(I),I=1,3)
C   WRITE(6,51)(STRS(I),I=1,4)
C   WRITE(6,51)((B(I,J),J=1,LV),I=1,3)
C51 FORMAT(1H,8E15.3)
C LOOP 11 IS FOR NON-LINEAR WORK.
  DO 11 J=1, LV
    SUM=0.
    DO 12 I=1, 3
      SUM=SUM+STRS(I)*B(I,J)
    12 CONTINUE
    FORCE(J)=SUM
  11 CONTINUE
C FORCE VECTOR FOR ELEMENT POINT.
  RETURN
  END
C===== START SUBROUTINE =====
  SUBROUTINE STRESS
  COMMON
  & US(50,2),R(3),
  & T(200),PP(200),IONARY(70)
  & ,P(12),DEL(2,12),COJ(2,2),COJIN(2,2),DET,DI(2,12)
  & ,DIJ(2,2)
  & ,NOPE(12),XYE(3,12),DISE(2,12)
  & ,XYP(3),RP,STRN(4),STRS(4),STRSP(4)
  & ,ESTIFM(24,24),B(4,24),DVDB(4,24),DVD(4,4)
  & ,FORCE(16),SFORCE(16),R2(100),DIS(2,200)
C INITIALISE R2 VECTOR
  DO 900 I=1, NSZF
  900 R3(I)=0.0

```

```

REWIND 2
READ(2) (R2(I), I=1, NSZF)
C APPLIED LOAD READ FROM DISC 2.
DO 402 I=1, NSZF
R2(I)=R1(I)+R2(I)
402 CONTINUE
C R1 IS THE REACTIVE LOAD VECTOR.
C WRITE(6, 403) (R1(I), I=1, NSZF)
C WRITE(6, 403) (R2(I), I=1, NSZF)
403 FORMAT(1H , 8E13.4)
DO 902 I=1, 2
DO 902 J=1, 200
902 DIS(I, J)=0.0
DO 400 N=1, NE
C IF(N .GT. 1) GO TO 4444
IF(NOP(N, 3).EQ.0)GOTO 405
NCN=8
C
C
LV=16
KK=1
NGAUS=NGAUSR
C
IF(NOP(N, 7) .NE. 0)GOTO 30
NCN=6
LV=12
KK=30
NGAUS=45
30 CONTINUE
L=IMAT(N)
IF (L .GT. NMAT) L=L-100
E1=ORT(L, 1)
E2=ORT(L, 2)
G2=ORT(L, 3)
C1=ORT(L, 4)
C2=ORT(L, 5)
CALL MODU
DO 500 K=1, NCN
MASH=NOP(N, K)
DO 600 I=1, 2
IF(NDYN.EQ. 1) DISE(I, K)=DIS(I, MASH)
IF(NDYN.GT. 1) DISE(I, K)=Q(I, MASH)
XYE(I, K)=CORD(MASH, I)
600 CONTINUE
NOPE(K)=MASH
500 CONTINUE
C WRITE(6, 7) N
7 FORMAT(1H0, 13H ELEMENT NO = , I3)
IF (NSTRS .EQ. 1) GO TO 300
C AL ULATE STRAINS AND STRESSES AT GAUSSIAN POINTS
C WRITE(6, 8)
C WRITE(6, 9)
C
8 FORMAT(' ', ' STRAINS AND STRESSES AT GAUSSIAN PO

```

```

&INTS.
& PRINCIPAL VALUES')
9 FORMAT(' ', 'COORDS (X, Y),      XX      ZZ      XZ
&   YY
&   (1)      (2)      THETA      MAX SHEAR' )
C LOOP 101 IS FOR NON-L WORK.
DO 101 I=1, LV
SFORCE(I)=0.
101 CONTINUE
DO 100 IGAUS=KK, NGAUS
ICN=IGAUS
G=ALFA(IGAUS)
H=BETA(IGAUS)
CALL SFR(G, H)
NNNN=N
CALL AUX(NNNN)
CALL STRP(NNNN)
C WRITE(6, 2) ICN, XYP(1), XYP(2), (STRS(J), J=1, 4), (STRSP(J), J=1, 3), RP
2 FORMAT(I4, 2F9.3, 4(E13.5, 2X), 2X, 2(E12.4, 2X),
&F8.3, E12.4)
C WRITE(6, 5) (STRN(J), J=1, 4)
5 FORMAT(14X, 8HSTRAINS , 4(E13.5, 2X))
C WRITE(11) XYP(1), XYP(2), (STRS(J), J=1, 4), (STRSP(J), J=1, 4),
C & (STRN(I), I=1, 4)
C LOOP 102 IS FOR NON-L WORK.
DO 102 I=1, LV
SFORCE(I)=SFORCE(I)+FORCE(I)*WGT(IGAUS)*DET
102 CONTINUE
100 CONTINUE
C WRITE(6, 104) (SFORCE(I), I=1, LV)
300 CONTINUE
IF (NSTRS .EQ. 2) GO TO 401
C
C CALCULATE STRAINS AND STRESSES AT NODAL POINTS
C
C PRINT, ' STRAINS AND STRESSES AT NODE POINTS
C& PRINCIPAL VALUES '
IF (NCN.EQ.6)GOTO 140
XI1=-1.
ETA1=-1.
ETA2=-1.
XI2=1.
ANSFR=NSFR
DO 200 NLV=1, NCN, NSFR
DO 80 I=1, NSFR
KNEW=NLV+I-1
GISH=I-1
GOSH=ANSFR-GISH
G=(GOSH*XI1+GISH*XI2)/ANSFR
H=(GOSH*ETA1+GISH*ETA2)/ANSFR
CALL SFR(G, H)
CALL AUX(NNNN)
CALL STRP(NNNN)
MNEW=NOPE (KNEW)

```



```

      IF (N .EQ. 3) GO TO 222
      IF (N .EQ. 9) GO TO 222
      GO TO 224
222 CONTINUE
      WRITE (6, 2) MNEW, XYP (1), XYP (2), (STRS (J), J=1, 4), (ST
&RSP (J), J=1, 3), RP
C      WRITE (11) ILD, MNEW, XYP (1), XYP (2), (STRS (J), J=1, 4), (STRSP (J), J=1, 3), RP
C      IF (MNEW .EQ. 14) WRITE (19) MNEW, ILD, STRS (2)
C      WRITE (6, 5) (STRN (J), J=1, 4)
224 CONTINUE
80 CONTINUE
      GISH=-X11
      GOSH=-ETA1
      X11=XI2
      ETA1=ETA2
      XI2=GISH
      ETA2=GOSH
200 CONTINUE
      GOTO 400
140 CONTINUE
      DO 150 IKI=1, 6
      FIKI=IKI
      IF (IKI. GT. 3) GOTO 160
      G=(3.-F IKI)/2.
      H=0.0
      GOTO 180
160 IF (IKI. GT. 5) GOTO 170
      G=0.0
      H=(FIKI-3.)/2.
      GOTO 180
170 CONTINUE
      G=.5
      H=.5
180 CONTINUE
      CALL SFR (G, H)
      CALL AUX (NNNN)
      CALL STRP (NNNN)
      MNEW=NOPE (IKI)
C      PRINT, G, H, MNEW, XYP (1), XYP (2), (STRS (J), J=1, 4), (STRSP (J), J=1, 3)
C      PRINT, (STRN (J), J=1, 4)
150 CONTINUE
401 CONTINUE
      IF (NSTRS.NE.2) GOTO 400
C LOOP 103 IS FOR NON-L WORK
      DO 103 I=1, NCN
      NNCN=NOPE (I)
      N21=NNCN*2-1
      N2=NNCN*2
      R2 (N21)=-SFORCE (2*I-1)+R2 (N21)
      R2 (N2)=-SFORCE (I*2)+R2 (N2)
103 CONTINUE
C      INCREMENTAL LOAD FOR INTERFACE EFFECT
      DO 701 I=1, IAY
      DO 701 J=1, LELEM

```

```

      KJJ=KFAC(I,J)
      IF (KJJ .EQ. N) GO TO 702
701 CONTINUE
      GO TO 703
702 DO 704 K=1,NCN
      K2=K*2-1
      K1=K*2
      KNCN=NOPE(K)
      KN2=KNCN*2-1
      KN=KNCN*2
      IF (K .GT. 3) SFORCE(K2)=0.0
      IF (K .GT. 3) SFORCE(K1)=0.0
      R3(KN2)=-SFORCE(K2)+R3(KN2)
      R3(KN)=-SFORCE(K1)+R3(KN)
704 CONTINUE
703 CONTINUE
C
C
C
      GOTO 400
405 CONTINUE
      N1=NOP(N,1)
      N2=NOP(N,2)
      DD1=DIS(1,N1)-DIS(1,N2)
      DD2=DIS(2,N1)-DIS(2,N2)
      F1=ORT(IMAT(N),4)
      F2=ORT(IMAT(N),5)
      F3=ORT(IMAT(N),6)
      F1=F1*DD1+F2*DD2
      F3=F2*DD1+F3*DD2
      WRITE(6,37)N,N1,N2
      WRITE(6,38)F1,F3
37 FORMAT(1H ,"FORCES ON SPRING ELEMENT ",I5,"NODES"
&,2I5)
38 FORMAT(1H ,"X COMP. = ",E16.3," Y COMP. = ",E16.3
&)
400 CONTINUE
4444 CONTINUE
C   WRITE(6,104)(R3(I),I=1,NSZF)
104 FORMAT(1H ,8E12.3)
CWRITE(6,105)((J,(DIS(I,J),I=1,2)),J=1,NSZF)
105 FORMAT(1H ,I3,3X,2E16.3)
      RETURN
      END
C===== START SUBROUTINE =====
      SUBROUTINE BSTRESS
      COMMON
& US(50,2),R(3),
& T(200),PP(200),IONARY(70)
& ,P(12),DEL(2,12),COJ(2,2),COJIN(2,2),DET,DI(2,12
&),DIJ(2,2)
& ,NOPE(12),XYE(3,12),DISE(24)
& ,XYP(3),RP,STRN(4),STRS(4),STRSP(4)
& ,ESTIFM(24,24),B(4,24),DVDB(4,24),DVD(4,4)

```

```

&,FORCE(16),SFORCE(16),R2(100),DIS(2,200)
REWIND 8
NCN=8
WRITE(6,20)
10 CONTINUE
READ(8)(ASTEEL,ESTEEL,LNEW,A1,B1,(NOPE(I),I=1,8)
&,(B(I,J),J=1,16),I=1,4)
CWRITE(6,600)ASTEEL,ESTEEL,LNEW,A1,B1,(NOPE(I),I=1,8)
600 FORMAT(1H ,20H A E LNEW A B NELS ,2E10.3,I4,2E10
&.3,8I10)
CWRITE(6,601)((B(I,J),J=1,16),I=1,4)
601 FORMAT(1H ,8E10.3)
C MUST SELECT DIRECTION OF DISPLACEMENT IE X OR Y BUT FIRST
C TEST FOR LAST BAR DATA
IF(A1 .LT. 0.01E-8.AND.B1 .LT. 0.01E-8) GO TO 500
K=1
IF(B1 .LT. 0.01E-8)K=2
C K=1 FOR BAR ALONG X AXIS.
KF=14+K
DO 100 I=1,NCN
100 DISE(I)=DIS(K,NOPE(I))
C WRITE(6,602)(DISE(I),I=1,NCN)
602 FORMAT(1H ,8E10.3)
C STRAIN STRESS AND FORCE AT EACH G POINT
DO 300 I=1,4
STRN(I)=.0
300 CONTINUE
DO 400 I=1,4
JJJ=0
DO 200 J=K,KF,2
JJJ=JJJ+1
STRN(I)=STRN(I)+B(I,J)*DISE(JJJ)
200 CONTINUE
STRS(I)=ESTEEL*STRN(I)
STRSP(I)=ASTEEL*STRS(I)
400 CONTINUE
WRITE(6,21)LNEW,A1,B1
WRITE(6,22)((STRN(I),STRS(I),STRSP(I)),I=1,4)
GOTO 10
500 CONTINUE
20 FORMAT(1H ,"ELEMENT X Y STRAIN STRESS FOR
&CE")
21 FORMAT(1H ,I4,10X,F9.3,10X,F9.3)
22 FORMAT(1H ,E15.4,10X,E15.4,10X,E15.4)
RETURN
END
C===== START SUBROUTINE =====
SUBROUTINE SFR(G,H)
COMMON
& US(50,2),R(3),
& T(200),PP(200),IONARY(70)
& ,P(12),DEL(2,12),COJ(2,2),COJIN(2,2),DET,DI(2,12)
& ,DIJ(2,2)
& ,NOPE(12),XYE(3,12),DISE(2,12)

```

```

& ,XYP(3),RP,STRN(4),STRS(4),STRSP(4)
& ,ESTIFM(24,24),B(4,24),DVDB(4,24),DVD(4,4)
& ,FORCE(16),SFORCE(16),R2(100),DIS(2,200)

```

C

```
IF(NCN.EQ.6)GOTO 10
```

C

```
G AND H DENOTE THE XI AND ETA VALUES AT THE POINT COSIDERED
```

C

```
GH = G*H
GG = G*G
HH = H*H
GGH = GG*H
GHH =G*HH
```

C

C

C

C

C

C

```
PARABOLIC SHAPE FUNCTIONS AND THEIR FIRST DERIVATIVES FOR
CURVED 8-NODAL ARBITRARY QUADRILATERAL
```

```

G2 = G*2.
H2 = H*2.
GH2 = GH*2.
P( 1)= (-1.+GH+GG+HH-GGH-GHH)/4.
P( 2) = ( 1.-H-GG+GGH)/2.
P( 3) = (-1.-GH+GG+HH-GGH+GHH)/4.
P( 4) = ( 1.+G-HH-GHH)/2.
P( 5) = (-1.+GH+GG+HH+GGH+GHH)/4.
P( 6) = ( 1.+H-GG-GGH)/2.
P( 7) = (-1.-GH+GG+HH+GGH-GHH)/4.
P( 8) = ( 1.-G-HH+GHH)/2.
DEL(1,1)=(H+G2-GH2-HH)/4.
DEL(1,2)=-G+GH
DEL(1,3)=(-H+G2-GH2+HH)/4.
DEL(1,4)=(1.-HH)/2.
DEL(1,5)=(H+G2+GH2+HH)/4.
DEL(1,6)=-G-GH
DEL(1,7)=(-H+G2+GH2-HH)/4.
DEL(1,8)=(-1.+HH)/2.
DEL(2,1)=(G+H2-GG-GH2)/4.
DEL(2,2)=(-1.+GG)/2.
DEL(2,3)=(-G+H2-GG+GH2)/4.
DEL(2,4)=-H-GH
DEL(2,5)=(G+H2+GG+GH2)/4.
DEL(2,6)=(1.-GG)/2.
DEL(2,7)=(-G+H2+GG-GH2)/4.
DEL(2,8)=-H+GH

```

C

```
GOTO 20
```

```
10 CONTINUE
```

```
C SHAPE FUNCTIONS FOR TRIANGLE ELEMENT
```

```
C 6 NODE TRIANGLE
```

```

X2G2=2.*G*G
X2H2=2.*H*H
X2GH=2.*G*H
P(1)=X2G2-G

```

```

P(2)=4.*G-2.*(X2G2+X2GH)
P(3)=1.-3.*(G+H)+X2G2+X2H2+2.*X2GH
P(4)=4.*H-2.*(X2GH+X2H2)
P(5)=X2H2-H
P(6)=2.*X2GH
DEL(1,1)=4.*G-1.
DEL(1,2)=4.-8.*G-4.*H
DEL(1,3)=-3.+4.*(G+H)
DEL(1,4)=-4.*H
DEL(1,5)=0.
DEL(1,6)=4.*H
DEL(2,1)=0.
DEL(2,2)=-4.*G
DEL(2,3)=-3.+4.*(G+H)
DEL(2,4)=4.-4.*G-8.*H
DEL(2,5)=4.*H-1.
DEL(2,6)=4.*G
20 CONTINUE
RETURN
END
C===== START SUBROUTINE =====
SUBROUTINE SOLVE
COMMON/ADY/SK(24000),R,ESTIFM(24,24),NN(12)
C
C WRITE(6,50)
C50 FORMAT(1H,^REACTIONS^)
C WRITE(6,51)(R1(I),I=1,NSZF)
C51 FORMAT(1H,60E15.4)
NCN=8
C CORRECT FOR 8. OR 6.
NBF=24000
NSIZ=0
NNP=0
NBUF=NSK-1
NZ=1
ND=1
NLKI=0
C
L=0
IF (NT) 230,235,230
230 WRITE(6,101)
READ, NRON, NROF, NCON, NCOF, XST
WRITE(6,1) NRON, NROF, NCON, NCOF, XST
1 FORMAT(1H,4I3,2X,E9.3)
101 FORMAT(13H0 STIFFNESSES)
235 CONTINUE
DO 236 N=1,NBF
236 SK(N)=0.
NC=1
READ(3)
& N, (NN(I), I=1,8), ((ESTIFM(I,J), J=1,16), I=1,16)
CWRITE(6,265)(N, (NN(I), I=1,8))
265 FORMAT(1H,"ELEMENT NO.",I4,"STIFF ...NODES",8I4)
C WRITE(6,266)((ESTIFM(I,J), J=1,16), I=1,16)

```

```

C266 FORMAT(1H ,8E12.4)
      NCN=8
      IF (NN(7).EQ.0)NCN=6
      IF (NN(3).EQ.0)NCN=2
C CORRECT FOR 8. OR 6.
  242 L=L+1
      DO 300 M=1,9
      IF (N.EQ.0) GO TO 303
      DO 245 I=1,NCN
      IF (NN(I).EQ. L) GO TO 250
  245 CONTINUE
      GO TO 303
  250 NC=NC+1
      DO 280 I=1,NCN
      IF (NN(I).EQ.0) GO TO 280
      II=(NN(I)-L)*NDF
      DO 270 J=1,NCN
      IF (NN(J).EQ. 0) GO TO 270
      JJ=(NN(J)-L)*NDF
      DO 260 IL=1,NDF
      IA=II+IL
      IC=(I-1)*NDF+IL
      DO 260 JM=1,NDF
      JB=JJ+JM
      IF (IA.GT.JB) GO TO 260
      JD=(J-1)*NDF+JM
      IAB=((JB-1)*JB)/2+IA
CC WRITE(6,3000)IC,JD,ESTIFM(IC,JD),IAB
C3000 FORMAT(1H ,^E(^,2I3,^)=^,E12.3,^ ON SK(^,I3,^)^)
      SK(IAB)=SK(IAB)+ESTIFM(IC,JD)
  260 CONTINUE
  270 CONTINUE
      NX=(NN(I)-L)*NDF
      IF (NSIZ.LT.NX) NSIZ=NX
  280 CONTINUE
      READ(3)
      & N, (NN(I), I=1, 8), ((ESTIFM(I,J), J=1, 16), I=1, 16)
CWRITE(6,265) (N, (NN(I), I=1, 8))
CC WRITE(6,266) ((ESTIFM(I,J), J=1, 16), I=1, 16)
      NCN=8
      IF (NN(7).EQ.0)NCN=6
      IF (NN(3).EQ.0)NCN=2
  300 CONTINUE
C
C=====SET UP LOAD=====
C
  303 CONTINUE
      IF (NT) 318,318,304
  304 IF (L-NRON) 318,305,318
  305 JB = NDF*(NCON-NRON) + NCOF
      IA = (JB*(JB-1))/2 + NROF
      SK(IA) = SK(IA) + XST
      READ , NRON,NROF,NCON,NCOF,XST
CWRITE(6,1) NRON,NROF,NCON,NCOF,XST

```

```

      GO TO 304
318 CONTINUE
      NSZ=NSIZ+NDF
      JZ = 0
      IF (NZ.EQ.NB+1) GO TO 320
      IF (L.NE.NBC(NZ)) GO TO 320
      JZ =NFI X(NZ)
      IZ=10** (NDF-1)
      NZ=NZ+1
320 DO 500 I=1,NDF
      NSZ=NSZ-1
      IC= I+NDF* (L-1)
      R=R1(IC)
      NBD=0
      IF (JZ.EQ.0) GO TO 400
      IF (JZ.LT.IZ) GO TO 340
      LZ =(NZ-2)*NDF+I
      U(ND)=U(LZ)
      RS=-R
      R=U(ND)
      ND=ND+1
      NBD=1
      JZ=JZ-IZ
340 IZ=IZ/10
400 CONTINUE
      IF (SK(1) .GE. 0.) GO TO 700
CWRITE(6,701) L,I,SK(1)
701 FORMAT(1H0,8HNODE NO. ,I5,I10,6H D.F. ,7HSK(1) =
      & ,E15.6)
700 CONTINUE
      NBLK=NSZ+4
      IF ((NBUF+NBLK).LE.NBF) GO TO 408
      NLKI=NLKI+1
      WRITE(4) NLKI, NBUF, (SK(J),J=NSK,NBUF)
      PRINT,'WRITING',NLKI,' RECORD TO DISC 4 SK(NBUF
      &),' ,SK(NBUF)
      NBUF=NSK-1
      NNP=0
408 NNP=NNP+1
      NBUF=NBUF+1
      SK(NBUF)=NSZ
      NBUF=NBUF+1
      SK(NBUF)=NBD
      NBUF=NBUF+1
      IA=NBUF+1

```

```

C
=====INVERT DIAGONAL TERM=====
C

```

```

      IF (NBD.EQ.1) GO TO 411
      IF (SK(1) .NE. 0.) GO TO 99
      PRINT,'PROGRAM HALTED IN ELIM '
      PRINT,'NEGATIVE OR ZERO DIAGONAL STIFFNESS NODE N
      &O',L,'
      &      ',I,' DEGREE OF FREEDOM'

```

```

STOP
99 CONTINUE
   XK=1./SK(1)
   SK(NBUF)=XK
C
C=====MODIFY LOADS AND OFF DIAGONAL TERMS=====
C
410 R1(IC)=XK*R
   GO TO 412
411 SK(NBUF)=-SK(1)
   R1(IC)=SK(1)*R+RS
   XK=1.
   R=-R
412 CONTINUE
   IF (L+I-NP-NDF) 415,600,415
415 NBUF=NBUF+1
   KJ=1
   DO 420 J=1,NSZ
   KJ=KJ+J
   SK(NBUF)=XK*SK(KJ)
   IF(NBD.EQ.1) SK(NBUF)=-SK(NBUF)
420 NBUF=NBUF+1
   SK(NBUF)=NSZ
   NBUF=NBUF+1
   SK(NBUF)=NNP
   DO 440 J=1,NSZ
   IF(SK(IA).EQ.0.) GO TO 440
   IF(NBD.EQ.1) GO TO 435
   JB=(J*(J+1))/2+1
   KJ=1
   DO 430 K=1,J
   KJ=KJ+K
   IJ =JB+K
430 SK(IJ)=SK(IJ)-SK(KJ)*SK(IA)
435 JB=IC+J
   R1(JB)=R1(JB)-SK(IA)*R
440 IA=IA+1
   DO 460 J=1,NSZ
   IK=(J*(J-1))/2
   IJ=IK+J+1
   DO 460 K=1,J
   IA =IK+K
   JB=IJ+K
460 SK(IA)=SK(JB)
   IJ=(NSZ*(NSZ+1))/2+1
   IK=IJ+NSZ
   DO 480 K=IJ,IK
480 SK(K)=0.
500 CONTINUE
   NSIZ=NSIZ-NDF
   GO TO 242
600 CONTINUE
   NLKI=NLKI+1
   WRITE(4) NLKI,NBUF,(SK(J),J=NSK,NBUF )

```



```

PRINT, 'WRITING', NLKI, ' RECORD TO DISC*4* SK(NBUF
&)' ,SK(NBUF)
IF(NSIZ.EQ.0) NSIZ=NDF
PRINT, 'THERE ARE ', NLKI, ' RECORDS ON DISC FILE 4'
RETURN
END

```

C===== START SUBROUTINE =====

```

SUBROUTINE RESOLV
COMMON/ADY/SK(24000),R
REWIND 4
READ(4) NLKI, NTP, (SK(I), I=NSK, NTP)
NBUF=NSK-1
ND=1
NNP=1
DO 500 L=1, NP
DO 490 I=1, NDF
IC=I+NDF*(L-1)
R=R1(IC)
NBUF=NBUF+1
NSZ=SK(NBUF)
NBUF=NBUF+1
NBD=SK(NBUF)
NBUF=NBUF+1
IF(NBD.EQ.0) GO TO 420
RS=-R
R=-U(ND)
ND=ND+1
R1(IC)=SK(NBUF)*R+RS
GO TO 425
420 CONTINUE
R1(IC)=SK(NBUF)*R
425 CONTINUE
IF(L+I-NP-NDF) 450, 600, 450
450 NBUF=NBUF+1
DO 470 J=1, NSZ
IK=IC+J
R1(IK)=R1(IK)-SK(NBUF)*R
470 NBUF=NBUF+1
NBUF=NBUF+1
IF(NBUF.LT.NTP) GO TO 490
READ(4) NLKI, NTP, (SK(II), II=NSK, NTP)
NBUF=NSK-1
NNP=0
490 NNP=NNP+1
500 CONTINUE
600 RETURN
END

```

C===== START SUBROUTINE =====

```

SUBROUTINE BSUB
DIMENSION DIS(2, 200)
COMMON/ADY/SK(24000),R
EQUIVALENCE (SK(1), DIS(1, 1))
C
C WRITE(6, 49)

```

```

C49 FORMAT(1H , ^REACTIONS^ )
C   WRITE(6,50) (R1(I), I=1, NSZF)
C50 FORMAT(1H , 60E15.4)
    REWIND 3
C   BACKSPACE 4
C   PRINT, 'BACKSPACE 4 AT 15820'
      ND=ND-1
      KJ=NDF* NP
      DIS (NDF, NP)=R1 (KJ)
      R1 (KJ)=0.
      I=NDF
      L=NP
      NBUF=NBUF-1
      NBD=SK (NBUF)
      NBUF=NBUF-2
C   IF (NNP.EQ.1) BACKSPACE 4
C   IF (NNP.EQ.1) PRINT, 'BACKSPACE 4 AT 15920'
      GO TO 641
C
C=====START SYSTEMATIC BACK SUBSTITN=====
C
620 L=L-1
625 I=I-1
      NNP=SK (NBUF)
C   IF (NNP.EQ.1.AND.KLMI.NE.1) BACKSPACE 4
C   IF (NNP.EQ.1.AND.KLMI.NE.1) PRINT, 'BACKSPACE 4 AT 16000'
      NBUF=NBUF-1
      NSZ=SK (NBUF)
      IA=NBUF-NSZ
      NBUF=IA-2
      NBD=SK (NBUF)
      NBUF=NBUF-2
      KJ=NDF* (L-1)+I
      DIS (I, L)=R1 (KJ)
      R1 (KJ)=0.
      DO 640 J=1, NSZ
      LJ=L+(J+I-1)/NDF
      K=I+J-(LJ-L)*NDF
      DIS (I, L)=DIS (I, L)-SK (IA)*DIS (K, LJ)
640 IA=IA+1
641 IF (NBD.EQ. 0) GO TO 642
      R1 (KJ)=DIS (I, L)
      DIS (I, L)=U (ND)
      ND=ND-1
642 CONTINUE
      IF (I+L-2) 645, 655, 645
645 IF (NNP.NE.1) GO TO 650
      READ(4) KLMI, NBUF, (SK (II), II=NSK, NBUF)
C   PRINT, 'READING', KLMI, ' RECORD ON 4   SK (NBUF)=' , SK (NBUF)
C   BACKSPACE 4
C   PRINT, 'BACKSPACE 4 AT 16230'
650 IF (I.NE.1) GO TO 625
652 I=NDF+1
      GO TO 620

```

```

655 CONTINUE
C
C   BOUNDARY DISPLACEMENTS AND REACTION TRANSFORMATION
C
C   WRITE (6, 113)
C   PRINT, NB
C   WRITE (6, 704) (NBC(M), M=1, NB)
C   DO 250 M=1, NB
C     N=NBC(M)
C     MASH=2*N-1
C     NASH=MASH+1
C   WRITE (6, 111) N, (DIS(I, N), I=1, NDF), (R1(J), J=MASH, NASH)
C   IF (ANG(M) .EQ. 0.0) GO TO 250
C   GASH=ANG(M)*0.017453292
C   CS=COS(GASH)
C   TN=TAN(GASH)
C   DXC=DIS(1, N)*CS
C   DYC=DIS(2, N)*CS
C   DIS(1, N)=DXC-DYC*TN
C   DIS(2, N)=DYC+DXC*TN
C   RXC=R1(MASH)*CS
C   RYC=R1(NASH)*CS
C   RX=RXC-RYC*TN
C   RY=RYC+RXC*TN
C   WRITE (6, 111) N, (DIS(I, N), I=1, NDF), RX, RY
250 CONTINUE
C
C WRITE (6, 10)
C 10 FORMAT(' ', 'NODAL DISPLACEMENTS', ' FORCES ')
C WRITE (6, 11) ( N, DIS(1, N), DIS(2, N), R1(N*2-1), R1(N*2), N=1, NP)
C   PRINT, (DIS(1, N), DIS(2, N), R1(N*2-1), R1(N*2), N=1, NP)
C 11 FORMAT(' ', 'NODE NO.', I3, ' U=', E9.3, ' V=', E9.3, ' RX=', E9.3,
C&' RY=', E9.3)
C   IF (NDYN .LT. 2) GO TO 700
C   DO 701 I=1, NSZF
C     UAST(I)=0.0
701 CONTINUE
C   DO 702 J=1, NP
C     DO 703 I=1, NDF
C       N=I+2*(J-1)
C       UAST(N)=DIS(I, J)
703 CONTINUE
702 CONTINUE
C   WRITE (6, 704) (UAST(N), N=1, NSZF)
704 FORMAT(V)
700 CONTINUE
C   WRITE (6, 110)
C WRITE TO TAPE SPECIAL ELEMENT DATA.
C   DO 600 N=1, NE
C     IF (NOP(N, 7) .GT. 0.01E-8) GO TO 600
C   WRITE (19, 500) (N, (NOP(N, I), I=1, 6))
C   CALL SFWRITE (NOP(N, 1), 6, IRELPHY)
C   DO 610 NN=1, 6
C     K=NOP(N, NN)

```

```

C      WRITE (19, 501) ((CORD(K, I), I=1, 2), (DIS(I, K), I=1, 2))
      610 CONTINUE
C500 FORMAT(7I5)
C501 FORMAT(4E12.6)
      600 CONTINUE
C      CALL SFWCLOSE (IREPLY)
C
C      110 FORMAT(1H0, 14H DISPLACEMENTS )
      111 FORMAT(1I10, 6(F12.3, 2X))
      113 FORMAT(1H0, 14H DISPLACEMENTS , 40X, 10H REACTIONS
&)
C
C      WRITE (6, 49)
C      WRITE (6, 50) (R1(I), I=1, NSZF)
      RETURN
      END

```

Input data for pavement analysis

```
1 3 1 3 13 1 14 6 5
0 .0001 1.4 0.0 0.0
  AXY
133 36 37 600 2 4 2 4 16 1 0 0 0 2 0 0 0 36
  1 1500000.0 1500000.0 506756.7 0.48 0.48 0.0002 .5 .0003
  2 1080000.0 1080000.0 385714.3 0.4 0.4 0.00015 .5 .0003
  3 225000.0 225000.0 80357.142 0.4 0.4 0.000149 0.5 .0003
  4 44000.0 44000.0 15714.285 0.4 0.4 0.000127 0.5 0.0003
133 36 37 0 0 0
  1 0.0 81.0
  2 4.7623 81.0
  3 9.5246 81.0
  4 14.7623 81.0
  5 20.0 81.0
  6 26.0 81.0
  7 32.0 81.0
  8 38.0 81.0
  9 44.0 81.0
 10 50.0 81.0
 11 56.0 81.0
 12 62.0 81.0
 13 68.0 81.0
 14 0.0 79.5
 15 9.5246 79.5
 16 20.0 79.5
 17 32.0 79.5
 18 44.0 79.5
 19 56.0 79.5
 20 68.0 79.5
 21 0.0 78.5
 22 4.7623 78.0
 23 9.5246 78.0
 24 14.7624 78.0
 25 20.0 78.0
 26 26.0 78.0
 27 32.0 78.0
 28 38.0 78.0
 29 44.0 78.0
 30 50.0 78.0
 31 56.0 78.0
 32 62.0 78.0
 33 68.0 78.0
 34 0.0 75.0
 35 9.5246 75.0
 36 20.0 75.0
 37 32.0 75.0
 38 44.0 75.0
 39 56.0 75.0
 40 68.0 75.0
 41 0.0 72.0
 42 4.7623 72.0
 43 9.5246 72.0
 44 14.7623 72.0
 45 20.0 72.0
```

46 26.0 72.0
47 32.0 72.0
48 38.0 72.0
49 44.0 72.0
50 50.0 72.0
51 56.0 72.0
52 62.0 72.0
53 68.0 72.0
54 0.0 66.0
55 9.5246 66.0
56 20.0 66.0
57 32.0 66.0
58 44.0 66.0
59 56.0 66.0
60 68.0 66.0
61 0.0 60.0
62 4.7623 60.0
63 9.5246 60.0
64 14.7623 60.0
65 20.0 60.0
66 26.0 60.0
67 32.0 60.0
68 38.0 60.0
69 44.0 60.0
70 50.0 60.0
71 56.0 60.0
72 62.0 60.0
73 68.0 60.0
74 0.0 54.0
75 9.5246 54.0
76 20.0 54.0
77 32.0 54.0
78 44.0 54.0
79 56.0 54.0
80 68.0 54.0
81 0.0 48.0
82 4.7623 48.0
83 9.5246 48.0
84 14.7623 48.0
85 20.0 48.0
86 26.0 48.0
87 32.0 48.0
88 38.0 48.0
89 44.0 48.0
90 50.0 48.0
91 56.0 48.0
92 62.0 48.0
93 68.0 48.0
94 0.0 36.0
95 9.5246 36.0
96 20.0 36.0
97 32.0 36.0
98 44.0 36.0
99 56.0 36.0

100 68.0 36.0
 101 0.0 24.0
 102 4.7623 24.0
 103 9.5246 24.0
 104 14.7623 24.0
 105 20.0 24.0
 106 26.0 24.0
 107 32.0 24.0
 108 38.0 24.0
 109 44.0 24.0
 110 50.0 24.0
 111 56.0 24.0
 112 62.0 24.0
 113 68.0 24.0
 114 0.0 12.0
 115 9.5246 12.0
 116 20.0 12.0
 117 32.0 12.0
 118 44.0 12.0
 119 56.0 12.0
 120 68.0 12.0
 121 0.0 0.0
 122 4.7623 0.0
 123 9.5246 0.0
 124 14.7623 0.0
 125 20.0 0.0
 126 26.0 0.0
 127 32.0 0.0
 128 38.0 0.0
 129 44.0 0.0
 130 50.0 0.0
 131 56.0 0.0
 132 62.0 0.0
 133 68.0 0.0

1 21 22 23 15 3 2 1 14 1
 2 23 24 25 16 5 4 3 15 1
 3 25 26 27 17 7 6 5 16 1
 4 27 28 29 18 9 8 7 17 1
 5 29 30 31 19 11 10 9 18 1
 6 31 32 33 20 13 12 11 19 1
 7 41 42 43 35 23 22 21 34 2
 8 43 44 45 36 25 24 23 35 2
 9 45 46 47 37 27 26 25 36 2
 10 47 48 49 38 29 28 27 37 2
 11 49 50 51 39 31 30 29 38 2
 12 51 52 53 40 33 32 31 39 2
 13 61 62 63 55 43 42 41 54 3
 14 63 64 65 56 45 44 43 55 3
 15 65 66 67 57 47 46 45 56 3
 16 67 68 69 58 49 48 47 57 3
 17 69 70 71 59 51 50 49 58 3
 18 71 72 73 60 53 52 51 59 3
 19 81 82 83 75 63 62 61 74 3
 20 83 84 85 76 65 64 63 75 3

21 85 86 87 77 67 66 65 76 3
22 87 88 89 78 69 68 67 77 3
23 89 90 91 79 71 70 69 78 3
24 91 92 93 80 73 72 71 79 3
25 101 102 103 95 83 82 81 94 4
26 103 104 105 96 85 84 83 95 4
27 105 106 107 97 87 86 85 96 4
28 107 108 109 98 89 88 87 97 4
29 109 110 111 99 91 90 89 98 4
30 111 112 113 100 93 92 91 99 4
31 121 122 123 115 103 102 101 114 4
32 123 124 125 116 105 104 103 115 4
33 125 126 127 117 107 106 105 116 4
34 127 128 129 118 109 108 107 117 4
35 129 130 131 119 111 110 109 118 4
36 131 132 133 120 113 112 111 119 4
1 10 0.0 0.0 0.0
13 10 0.0 0.0 0.0
14 10 0.0 0.0 0.0
20 10 0.0 0.0 0.0
21 10 0.0 0.0 0.0
33 10 0.0 0.0 0.0
34 10 0.0 0.0 0.0
40 10 0.0 0.0 0.0
41 10 0.0 0.0 0.0
53 10 0.0 0.0 0.0
54 10 0.0 0.0 0.0
60 10 0.0 0.0 0.0
61 10 0.0 0.0 0.0
73 10 0.0 0.0 0.0
74 10 0.0 0.0 0.0
80 10 0.0 0.0 0.0
81 10 0.0 0.0 0.0
93 10 0.0 0.0 0.0
94 10 0.0 0.0 0.0
100 10 0.0 0.0 0.0
101 10 0.0 0.0 0.0
113 10 0.0 0.0 0.0
114 10 0.0 0.0 0.0
120 10 0.0 0.0 0.0
121 11 0.0 0.0 0.0
122 11 0.0 0.0 0.0
123 11 0.0 0.0 0.0
124 11 0.0 0.0 0.0
125 11 0.0 0.0 0.0
126 11 0.0 0.0 0.0
127 11 0.0 0.0 0.0
128 11 0.0 0.0 0.0
129 11 0.0 0.0 0.0
130 11 0.0 0.0 0.0
131 11 0.0 0.0 0.0
132 11 0.0 0.0 0.0
133 11 0.0 0.0 0.0

LOAD

2

```
1 0.0 -250.66
2 0.0 -501.32
3 0.0 -250.66
133 0.0 0.0
5 795 800 0 0 0
21 22 23 24 25 26 27 28 29 30 31 32 33
41 42 43 44 45 46 47 48 49 50 51 52 53
81 82 83 84 85 86 87 88 89 90 91 92 93
0 .0 0.0 0.0
1 2 3 4 5 6
7 8 9 10 11 12
19 20 21 22 23 24
LOAD
```

2

37

```
1 10 0.0 0.0 0.0
13 10 0.0 0.0 0.0
14 10 0.0 0.0 0.0
20 10 0.0 0.0 0.0
21 10 0.0 0.0 0.0
33 10 0.0 0.0 0.0
34 10 0.0 0.0 0.0
40 10 0.0 0.0 0.0
41 10 0.0 0.0 0.0
53 10 0.0 0.0 0.0
54 10 0.0 0.0 0.0
60 10 0.0 0.0 0.0
61 10 0.0 0.0 0.0
73 10 0.0 0.0 0.0
74 10 0.0 0.0 0.0
80 10 0.0 0.0 0.0
81 10 0.0 0.0 0.0
93 10 0.0 0.0 0.0
94 10 0.0 0.0 0.0
100 10 0.0 0.0 0.0
101 10 0.0 0.0 0.0
113 10 0.0 0.0 0.0
114 10 0.0 0.0 0.0
120 10 0.0 0.0 0.0
121 11 0.0 0.0 0.0
122 11 0.0 0.0 0.0
123 11 0.0 0.0 0.0
124 11 0.0 0.0 0.0
125 11 0.0 0.0 0.0
126 11 0.0 0.0 0.0
127 11 0.0 0.0 0.0
128 11 0.0 0.0 0.0
129 11 0.0 0.0 0.0
130 11 0.0 0.0 0.0
131 11 0.0 0.0 0.0
132 11 0.0 0.0 0.0
133 11 0.0 0.0 0.0
```

APPENDIX I I

THE WILSON θ -METHOD

Let the acceleration, velocity and displacement at time t , i.e, \ddot{U}_t , \dot{U}_t and U_t , where the subscript denotes time t , be known quantities. For solution of $\ddot{U}_{t+\Delta t}$, $\dot{U}_{t+\Delta t}$ and $U_{t+\Delta t}$, assuming that the acceleration varies linearly during the time interval $\theta \Delta t$, where $\theta > 1$.

The parameter θ is chosen to obtain accuracy and stability in the integration. The linear acceleration method is defined by $\theta = 1$ and is known to be only conditionally stable. In Wilson's averaging method θ equals 2 and the integration is unconditionally stable. Without losing unconditional stability, θ can be selected to obtain a scheme which has less integration error.

If τ denotes the increase in time, where $\theta \Delta t \leq \tau \leq \theta \Delta t$, then for the time interval t to $t + \theta \Delta t$

$$\ddot{U}_{t+\tau} = \ddot{U}_t + (\ddot{U}_{t+\Delta t} - \ddot{U}_t) \frac{\tau}{\Delta t} \quad \dots \quad \dots \quad \dots \quad (1)$$

$$\dot{U}_{t+\tau} = \dot{U}_t + \ddot{U}_t \tau + \frac{\tau^2}{2\theta \Delta t} (\ddot{U}_{t+\theta \Delta t} - \ddot{U}_t) \quad \dots \quad (2)$$

$$U_{t+\tau} = U_t + \dot{U}_t \tau + \frac{1}{2} \ddot{U}_t \tau^2 + (\ddot{U}_{t+\Delta t} - \ddot{U}_t) \frac{\tau^3}{6\Delta t} \quad \dots \quad (3)$$

At time $t + \Delta t$

$$\dot{U}_{t+\Delta t} = \dot{U}_t + (\ddot{U}_{t+\Delta t} + \ddot{U}_t) \frac{\Delta t}{2} \dots \dots \dots \dots \quad (4)$$

$$U_{t+\Delta t} = U_t + \dot{U}_t \Delta t + (2\ddot{U}_t + \ddot{U}_{t+\Delta t}) \frac{\Delta t^2}{6} \dots \dots \dots \dots \quad (5)$$

Writing the equation governing the motion of a single degree of freedom system with free vibration period T , damping ratio ζ and applied load R

$$\ddot{U} + 2\zeta \omega \dot{U} + \omega^2 U = R \dots \dots \dots \dots \dots \quad (6)$$

Equation (6) should be satisfied at time $t + \theta \Delta t$, which gives

$$\ddot{U}_{t+\theta \Delta t} + 2\zeta \omega \dot{U}_{t+\theta \Delta t} + \omega^2 U_{t+\theta \Delta t} = R_{t+\theta \Delta t} \dots \dots \dots \dots \quad (7)$$

Using Equations(1) and (3) at time $\tau = \theta \Delta t$ and substitute into Equation (7), an equation is obtained with $\ddot{U}_{t+\Delta t}$ as the only unknown. Solving for $\ddot{U}_{t+\Delta t}$ and substituting into Equations(4) and (5) the following relationship is established

$$\begin{bmatrix} \ddot{U}_{t+\Delta t} \\ \dot{U}_{t+\Delta t} \\ U_{t+\Delta t} \end{bmatrix} = A \begin{bmatrix} \ddot{U}_t \\ \dot{U}_t \\ U_t \end{bmatrix} + L R_{t+\theta \Delta t} \dots \dots \dots \dots \quad (8)$$

where A is the approximation operator and L is the load operator; both are given in Table 1. This recurrence relation is used to study the stability and accuracy of the integration scheme, when the solution at time $t + n \Delta t$ with an integer is given by

$$\begin{bmatrix} \ddot{U}_{t+n \Delta t} \\ \dot{U}_{t+n \Delta t} \\ U_{t+n \Delta t} \end{bmatrix} = A^n \begin{bmatrix} \ddot{U}_t \\ \dot{U}_t \\ U_t \end{bmatrix} + A^{n-1} L R_{t+\Delta t+(\theta-1)\Delta t} + \dots + L R_{t+n \Delta t+(\theta-1)\Delta t} \dots \dots \dots (9)$$

The complete algorithm used in the integration is given in Table (2).

Table (1), Load Operator at the Wilson- Θ -Method.

$$A = \begin{pmatrix} (1 - \frac{\beta\theta^2}{3} - \frac{1}{\theta} - K\theta)\frac{1}{\Delta t}(-\beta\theta - 2K)\frac{1}{\Delta t^2}(-\beta) \\ \Delta t(1 - \frac{1}{2\theta} - \frac{\beta\theta^2}{6} - \frac{K\theta}{2})(1 - \frac{\beta\theta}{2} - K)\frac{1}{\Delta t}(\frac{-\beta}{2}) \\ \Delta t^2(\frac{1}{2} - \frac{1}{6\theta} - \frac{\beta\theta^2}{18} - \frac{K\theta}{6})\Delta t(1 - \frac{\beta\theta}{6} - \frac{K}{3})(1 - \frac{\beta}{6}) \end{pmatrix}$$

and

$$L = \begin{pmatrix} \frac{\beta}{\omega^2 \Delta t^2} \\ \frac{\beta}{2\omega^2 \Delta t} \\ \frac{\beta}{6\omega^2} \end{pmatrix}$$

where $\beta = (\frac{\theta}{\omega^2 \Delta t^2} + \frac{\zeta\theta^2}{\omega\Delta t} + \frac{\theta^3}{6})^{-1}$

; $K = \frac{\zeta\beta}{\omega\Delta t}$

Table (2) Step-by-Step Solution

Using Wilson- θ Integration Method (44)

A INITIAL CALCULATION

1. Formation of stiffness matrix $[K]$, mass matrix $[M]$ and damping matrix $[C]$.

2. Initialize U_0 , \dot{U}_u and \ddot{U}_0

3. Select time step Δt and calculate integration constants

$$\theta = 1.4$$

$$a_0 = \frac{6}{(\theta \Delta t)^2} ; a_1 = \frac{3}{\theta \Delta t} ; a_2 = 2a_1 ; a_3 = \frac{\theta \Delta t}{2} ;$$

$$a_4 = \frac{a_0}{\theta} ; a_5 = \frac{-a_2}{\theta} ; a_6 = 1 - \frac{3}{\theta} ; a_7 = \frac{\Delta t}{2} ;$$

$$a_8 = \frac{\Delta t^2}{6}$$

4. Formation of effective stiffness matrix K^*

$$K^* = K + a_0 M + a_1 C$$

5. Triangularize K^* : $K^* = LDL^T$

B For Each time step

1. Calculation of effective load vector at time $t + \Delta t$:

$$R_{t+\theta\Delta t} = R_t + \theta(R_{t+\Delta t} - R_t) + M(a_0 b + a_2 \dot{U}_t + 2\ddot{U}_t)$$

2. Solve for displacements at time $t + \theta \Delta t$:

$$LDL^T U_{t+\theta \Delta t} = R_{t+\theta \Delta t}^*$$

3. Calculate displacements, velocities and accelerations at time $t + \Delta t$:

$$\ddot{U}_{t+\Delta t} = a_4(U_{t+\theta} \Delta t) + a_5 \dot{U}_t + a_6 \ddot{U}_t$$

$$\dot{U}_{t+\Delta t} = \dot{U}_t + a_7(\ddot{U}_{t+\Delta t} + \ddot{U}_t)$$

$$U_{t+\Delta t} = U_t + \Delta t \dot{U}_t + a_8(\ddot{U}_{t+\Delta t} + 2\ddot{U}_t)$$

APPENDIX III

THE EIGENPROBLEM

VECTOR ITERATION METHODS

The basic relation considered is

$$K \phi = \lambda M \phi \quad \dots \quad \dots \quad \dots \quad \dots \quad \dots \quad \dots \quad \dots \quad (1)$$

The aim is to satisfy the above equation by directly operating upon it. Two techniques of inverse iteration are used, inverse iteration and forward iteration.

(a) INVERSE ITERATION

Assuming that $[K]$ is positive definite, $[M]$ is the diagonal mass matrix or alternatively it may be a handed matrix. The basic equations used are presented in the following.

Assuming a starting iteration vector X_1 evaluate in each iteration step $K = 1, 2 \dots$ as follows

$$K \bar{X}_{k+1} = M X_k \quad \dots \quad \dots \quad \dots \quad \dots \quad \dots \quad \dots \quad \dots \quad (2)$$

and

$$K_{k+1} = \frac{\bar{X}_{k+1}}{(\bar{X}_{k+1}^T M \bar{X}_{k+1})^{1/2}} \quad \dots \quad \dots \quad \dots \quad \dots \quad (3)$$

where provided that x_1 is not M-orthogonal to ϕ_1 meaning that $X_1^T M \phi_1 \neq 0$

then $X_{k+1} \xrightarrow{\phi_1} \phi_1$ as $K \rightarrow \infty$

the basic step in the iteration is the solution of Equation (2). In the actual computer program it is assumed that

$$Y_1 = MX_1$$

$$K \quad \bar{X}_{k+1} = Y_k \quad \dots \quad \dots \quad \dots \quad \dots \quad \dots \quad \dots \quad \dots \quad (4)$$

$$\bar{Y}_{k+1} = M \bar{X}_{k+1} \quad \dots \quad \dots \quad \dots \quad \dots \quad \dots \quad \dots \quad \dots \quad (5)$$

$$P(\bar{X}_{k+1}) = \frac{\bar{X}_{k+1}^T Y}{\bar{X}_{k+1}^T \bar{Y}_{k+1}} \quad \dots \quad \dots \quad \dots \quad \dots \quad \dots \quad (6)$$

$$Y_{k+1} = \frac{\bar{Y}_{k+1}}{(\bar{X}_{k+1}^T \bar{Y}_{k+1})^{1/2}} \quad \dots \quad \dots \quad \dots \quad \dots \quad (7)$$

where provided that $Y_1^T \phi_1 \neq 0$

$$Y_{k+1} \quad M \phi_1 \quad \text{and} \quad P(\bar{X}_{k+1}) \rightarrow \lambda_1$$

as $K \rightarrow \infty$

Using the second iteration procedure, an approximation to the eigenvalue λ_1 is given by the Rayleigh quotient $P(\bar{X}_{k+1})$. The solution has convergence when

$$\frac{[\lambda_1^{(k+1)} - \lambda_1^{(k)}]}{\lambda_1^{(k+1)}} \leq \text{Tol} \quad \dots \quad \dots \quad \dots \quad \dots \quad \dots \quad (8)$$

where Tol should be 10^{-25} or smaller when the eigenvalue λ_1 is required to 25 digit accuracy. The eigenvector will then be accurate to about 8 or more digits. If ℓ is the last iteration then

$$\lambda_1 = P(\bar{x}_{(\ell+1)}) \quad \dots \quad \dots \quad \dots \quad \dots \quad \dots \quad \dots \quad (9)$$

and

$$\phi_1 = \frac{\bar{x}_{(\ell+1)}}{(\bar{x}_{\ell+1}^T \bar{Y}_{\ell+1})^{1/2}} \quad \dots \quad \dots \quad \dots \quad \dots \quad \dots \quad (10)$$

(b) FORWARD ITERATION

The method of forward iteration is complementary to the inverse iteration technique. The method yields the eigenvector corresponding to the largest eigenvalue. M is assumed positive definite. Adopting the same procedure as in the previous section and assuming that $Y_1 = K x_1$ for $K = 1, 2 \dots$

$$M \bar{x}_{k+1} = Y_k \dots \dots \dots \dots \dots \dots \dots \dots \dots \dots \quad (11)$$

$$\bar{y}_{k+1} = K \bar{x}_{k+1} \dots \dots \dots \dots \dots \dots \dots \dots \dots \dots \quad (12)$$

$$P(\bar{x}_{k+1}) = \frac{\bar{x}_{k+1}^T \bar{y}_{k+1}}{\bar{x}_{k+1}^T Y_k} \dots \dots \dots \dots \dots \dots \dots \quad (13)$$

$$Y_{k+1} = \frac{\bar{y}_{k+1}}{(\bar{x}_{k+1}^T Y_k)^{1/2}} \dots \dots \dots \dots \dots \dots \dots \quad (14)$$

Provided that $\phi_n^T Y_1 \neq 0$

$$Y_{k+1} \longrightarrow K \phi_n$$

and $P(\bar{x}_{k+1}) \longrightarrow \lambda_n$ as $K \longrightarrow \infty$

Convergence in the iteration could again be measured as given in Equ.(8) and if ℓ is the last iteration, then

$$\lambda_n = P(\bar{x}_{\ell+1}) \dots \dots \dots \dots \dots \dots \dots \quad (15)$$

and

$$\phi_n = \frac{\bar{x}_{\ell+1}}{(\bar{x}_{\ell+1}^T Y_\ell)^{1/2}} \dots \dots \dots \dots \dots \dots \dots \quad (16)$$

Appendix IV

Programme for analysis of experimental results

```
COMMON/CD/NC1 (2400) ,NC2 (2400) ,X (2400) ,Y (2400) ,CHROM
& (1200) ,
&XX (1200) ,YY (1200) ,XF (1200) ,YF (1200) ,TXY (1200) ,XCL (1
&200)
& ,NOEF (1200) ,AZ (1500) ,XC (1200) ,YC (1200) ,CL (1200) ,W (3
&000)
& ,CLINIC (1200) ,YCL (1200) ,PQS (40, 40)
C
COMMON/ELS/N, II, NI, NV1, NV2, XV, XY, SCALEX, SCALEY, XNOT
& , YNOT,
&NCC, NX, NY, KK2, KK2X, FRTXS (40, 40) ,XL, XH, YL, YH
COMMON/STRE/SHXY (1200) ,FMQ (1200) ,DSH (1200) ,STYC (120
&0)
& ,STXY (1200) ,XST (40, 40) ,YST (40, 40) ,STXC (100) ,DXST (10
&0)
NV1=0.0
NV2=0.0
XV=0.0
YV=0.0
C
C CALCULATION OF UNIT FRINGE VALUE
UNIF=1.0
10 FORMAT (V)
READ (41, 10) NTF
C NTF ARE NO. OF TOTAL FRAMES IN THE FILM
READ (41, 10) (NOEF (I) , I=1, NTF)
C NOEF IS THE NO. OF EACH FRAME
II=0
DO 555 N=1, NTF
II=II+1
NI=II+9
CALL CONTP
CALL ISOCH
IF (NCC .EQ. 1) GO TO 20
C IF (N .GT. 2) GO TO 600
CALL ISOCL
600 CONTINUE
CALL EXST
20 CONTINUE
555 CONTINUE
STOP
END
C
```

```

SUBROUTINE CONTP
COMMON/CD/NC1(2400),NC2(2400),X(2400),Y(2400),CHROM
&(1200),
&XX(1200),YY(1200),XF(1200),YF(1200),TXY(1200),XCL(1
&200)
&,NOEF(1200),AZ(1500),XC(1200),YC(1200),CL(1200),W(3
&000)
&,CLINIC(1200),YCL(1200),PQS(40,40)
COMMON/ELS/N,II,NI,NV1,NV2,XV,XY,SCALEX,SCALEY,XNOT
&,YNOT,
&NCC,NX,NY,KK2,KK2X,FRTXS(40,40),XL,XH,YL,YH
READ(41,10)(NC1(I),NC2(I),X(I),Y(I),RX,RY,I=II,NI)
10 FORMAT(V)
DO 11 I=II,NI
X(I)=100.0+X(I)
Y(I)=100.0+Y(I)
11 CONTINUE
C CALCULATION OF SCALE AND COORDINATES OF ORIGEN
SCALEX=10.0/(X(II+6)-X(II+4))
SCALEY=5.0/(Y(II+6)-Y(II+9))
DO 12 I=II,NI
X(I)=X(I)*SCALEX
Y(I)=Y(I)*SCALEY
12 CONTINUE
KK=II+4
XBAR=0.0
YBAR=0.0
DO 15 I=KK,NI
XBAR=XBAR+X(I)
YBAR=YBAR+Y(I)
15 CONTINUE
XBAR=XBAR/((NI-KK)+1)
YBAR=YBAR/((NI-KK)+1)
XNOT=XBAR-3*((X(II+9)-X(II+7))/4)
YNOT=YBAR-(Y(II+4)-Y(II+7))- (Y(II+6)-Y(II+9))
C PRINT," VALUES OF XBAR AND YBAR"
C PRINT, XBAR ,YBAR
C PRINT," VALUES OF XNOT AND YNOT "
C PRINT, XNOT ,YNOT
C CALCULATION OF SCALE FACTOR
C PRINT," VALUES OF SCALEX AND SCALEY "
C PRINT, SCALEX ,SCALEY
RETURN
END

```

```

C
C
SUBROUTINE ISOCH
COMMON/CD/NC1(2400),NC2(2400),X(2400),Y(2400),CHRO
&M(1200),
&XX(1200),YY(1200),XF(1200),YF(1200),TXY(1200),XCL(
&1200)
&,NOEF(1200),AZ(1500),XC(1200),YC(1200),CL(1200),W(
&3000)
&,CLINIC(1200),YCL(1200),PQS(40,40)
COMMON/ELS/N,II,NI,NV1,NV2,XV,XY,SCALEX,SCALEY,XNO
&T,YNOT,
&NCC,NX,NY,KK2,KK2X,FRTXS(40,40),XL,XH,YL,YH
C DATA FOR ISOCHROMATIC FRINGES

```

```

II=NI
20 CONTINUE
NC1 (II)=NV1
NC2 (II)=NV2
X (II)=XV
Y (II)=YV
II=II+1
READ (41, 10) NV1, NV2, XV, YV, RX, RY
10 FORMAT (V)
IF (NV1 .LT. 9999) GO TO 20
C   TRANSFER OF COORDINATES
NCC=(II-NI)
IF (NCC .EQ. 1) GO TO 222
II=II-1
NI=NI+1
C
DO 22 I=NI, II
X (I)=100.0+X (I)
Y (I)=100.0+Y (I)
22 CONTINUE
C
DO 25 J=NI, II
X (J)=X (J)*SCALEX
Y (J)=Y (J)*SCALEY
X (J)=X (J)-XNOT
Y (J)=Y (J)-YNOT
25 CONTINUE
C   WRITE (6, 30) (X (I), Y (I), I=NI, II)
30 FORMAT (2 (8X, F8.4))
C   CALCULATION OF MAXIMUM AND MINIMUM VALUES
XL=100000.0
XH=0.00000
YL=100000.0
YH=0.000000
DO 35 I=NI, II
X2=X (I)
IF (I .EQ. II) GO TO 31
X3=X (I+1)
31 CONTINUE
Y2=Y (I)
IF (I .EQ. II) GO TO 32
Y3=Y (I+1)
32 CONTINUE
IF (I .GT. NI) GO TO 70
XL=AMIN1 (X2, X3)
70 CONTINUE
XL=AMIN1 (XL, X2, X3)
XH=AMAX1 (XH, X2, X3)
IF (I .GT. NI) GO TO 80
YL=AMIN1 (Y2, Y3)
80 CONTINUE
YL=AMIN1 (YL, Y2, Y3)
YH=AMAX1 (YH, Y2, Y3)
35 CONTINUE
PRINT, "   VALUES OF MINX  MAXX           MINY  MAXY
&"
WRITE (6, 37) XL, XH, YL, YH
37 FORMAT (4 (5X, F8.4))

```

```

UNIF=1.0
DO 40 I=NI,II
K=(I-NI)+1
XX(K)=X(I)
YY(K)=Y(I)
CHROM(K)=(NCL(I)-NOEF(N))/100.0
CHROM(K)=CHROM(K)*UNIF
40 CONTINUE
DO 86 I=1,K
IF(CHROM(K).GT.9.)PRINT,"CHECK DATA OF LAST FR
&AM "
86 CONTINUE
PRINT," NUMBER OF FRAME AS FOLLOW ,"
PRINT,NOEF(N)
C PRINT," VALUES OF XX YY CHROM"
NP=II-NI
NP=II-NI
PRINT," VALUES OF NX NY NP "
NXL=(XL+1.0)
XL=NXL
NXH=XH
XH=NXH
NYL=(YL+1.0)
YL=NYL
NYH=YH
YH=NYH
NX=(XH-XL)*2+1
NY=(YH-YL)*2+1
PRINT, NX ,NY ,NP
WRITE(6,37)XL,XH,YL,YH
DO 82 I=1,3000
82 W(I)=0.0
DO 84 I=1,1500
84 AZ(I)=0.0
CALL RANGRD(NP,XX,YY,CHROM,NX,XL,XH,NY,YL,YH,AZ,30
&00,W)
DO 45 I=1,1200
XX(I)=0.0
YY(I)=0.00
xf(i)=0.00
yf(i)=0.0
CHROM(I)=0.0
45 CONTINUE
H=(XH-XL)/(NX-1)
HK=(YH-YL)/(NY-1)
DO 50 I=1,NX
XX(I)=XL+(I-1)*H
50 CONTINUE
DO 52 I=1,NY
YY(I)=YL+(I-1)*HK
52 CONTINUE
DO 55 J=1,NY
DO 55 I=1,NX
K=I+(J-1)*NX
XF(K)=XX(I)
YF(K)=YY(J)
55 CONTINUE
C SIGM1-SIGMA2 AT GRID POINTS

```

```

30 FORMAT(' VALUES OF SHEAR STRESS AT GRID POIN
&TS')
WRITE(6,8) (SHXY(I),I=1,KN2)
IF (NCC .GT. 1) GO TO 44
C   NORMAL STRESSES ACROSS CENTER LINE OF THE MODEL
C   FIRST STEP SUMMATION OF SHEAR STRESS DIFRENCE ON LINES
C   SYMMETRICALLY LOCATED WITH AXES OF SYMMETRY
C
DO 12 I=1,NY
L=(NX*I)-1
DSH(I)=(SHXY(L)*2+DSH(I))
12 CONTINUE
STYC(1)=2*TXY(14)
C
C   ASSUMING AT END OF CL SEGMA X EQ ZERO
DO 14 I=1,NY
STYC(I)=STYC(1)-DSH(I)
STXC(I)=(2*TXY(NX*(I-1)+14))+STYC(I)
14 CONTINUE
C
PRINT," VALUES OF NORMAL STRESS ON CENTER LINE
& OF MODDEL"
WRITE(6,16) (STYC(I),STXC(I),I=1,NY)
16 FORMAT(2(8X,F8.4))
C
C   NORMALL STRESS AT ALL GRID POINTS
DO 18 I=2,NY
DO 20 J=1,NX
K=(NX*I)-(J-1)
KH=K+NX
KL=K-NX
C   IF (KH .GT. K) TXY(KH)=0.0
C   IF (KL .LT. 1) TXY(KL)=0.0
DXST(J)=(DXST(J)+(SHXY(KH)-SHXY(KL)))
XST(I,J)=STXC(I)-DXST(J)
PQS(I,J)=(TXY(K)**2)**2
FRTXS(I,J)=4*(SHXY(K)**2)
YST(I,J)=XST(I,J)-SQRT(PQS(I,J)-FRTXS(I,J))
20 CONTINUE
18 CONTINUE
C
PRINT," VALUES OF NORMALL STRESSES AT GRID
&POINTS"
C   WRITE(6,22) ((XST(I,J),YST(I,J),J=1,NX),I=2,NY)
22 FORMAT(4(8X,F8.4))
44 CONTINUE
RETURN
END
C
SUBROUTINE ISOCL
COMMON/CD/NC1(2400),NC2(2400),X(2400),Y(2400),CHRO
&M(1200),
&XX(1200),YY(1200),XF(1200),YF(1200),TXY(1200),XCL(
&1200)
&,NOEF(1200),AZ(1500),XC(1200),YC(1200),CL(1200),W(
&3000)
&,CLINIC(1200),YCL(1200),PQS(40,40)

```



```

C      DO 60 I=1,NY
C      DO 60 J=1,NX
C      K=J+(I-1)*NY
C      TXY(K)=AZ(I,J)
C      TXY(K)=2*TXY(K)
C 60   CONTINUE
      WRITE(6,90)
90   FORMAT('      VALUES      OF      SIGMA2-SIGM1      AT
&GRID POINTS')
      NT=NX*NY
      DO 60 I=1,NT
60   TXY(I)=2*AZ(I)
      WRITE(6,65)(TXY(I),I=1,NT)
65   FORMAT(3(6X,F8.4))
      GO TO 220
222  WRITE(6,95)
95   FORMAT(' THE FORMER IS THE CASE OF FIRST FRAME OF
& ZERO FRINGES ')
220  CONTINUE
      RETURN
      END

C      SUBROUTINE EXST
      COMMON/CD/NC1(2400),NC2(2400),X(2400),Y(2400),CHRO
&M(1200),
&XX(1200),YY(1200),XF(1200),YF(1200),TXY(1200),XCL(
&1200)
&,NOEF(1200),AZ(1500),XC(1200),YC(1200),CL(1200),W(
&3000)
&,CLINIC(1200),YCL(1200),PQS(40,40)

C      COMMON/ELS/N,II,NI,NV1,NV2,XV,XY,SCALEX,SCALEY,XNO
&T,YNOT,
&NCC,NX,NY,KK2,KK2X,FRTXS(40,40),XL,XH,YL,YH
      COMMON/STRE/SHXY(1200),PMQ(1200),DSH(1200),STYC(12
&00)
&,STXY(1200),XST(40,40),YST(40,40),STXC(100),DXST(1
&00)

C      SHEAR STRESS AT GRID POINTS
      DO 2 I=1,KK2
      CL(I)=CL(I)*3.1415/180.0
2     CONTINUE
      C      KK2X=KK2+NX
      C      DO 4 I=NX,KK2X
      C      K=(I-NX)+1
      C      CL(I)=CLINIC(K)
      C      4 CONTINUE
      C      DO 6 I=1,NX
      C      CL(I)=0.0
      C      6 CONTINUE
      C      PRINT," VALUES OF ISOCLINIC AT GRID POI
&NTS "

C      WRITE(6,8)(CL(I),I=1,KK2X)
8     FORMAT(6(3X,F8.4))
      DO 10 I=1,KK2
      SHXY(I)=TXY(I)*SIN(2*CL(I))
10    CONTINUE
      WRITE(6,30)

```

```

C      COMMON/ELS/N, II, NI, NV1, NV2, XV, XY, SCALEX, SCALEY, XNO
      &T, YNOT,
      &NCC, NX, NY, KK2, KK2X, FRTXS (40, 40), XL, XH, YL, YH
C      DATA AND CALCULATION OF ISOCLINIC VALUES AT GRID POINTS
      IF (N .GT. 2) GO TO 600
      READ (5, 10) NCL
      READ (5, 10) (XCL(I), YCL(I), CLINIC(I), I=1, NCL)
600 CONTINUE
      KCL=NCL
      10 FORMAT (V)
C      THE FOLOWING DO LOOP TO FORMULATE VALUES OF ISOCLINIC IN THE
C      HALF PART OF MODEL BY SYMETRY
      DO 24 I=1, 1200
      XC(I)=0.0
      YC(I)=0.0
      CL(I)=0.0
      24 CONTINUE
      DO 602 I=1, KCL
      N2=(2*I)-1
      N21=2*I
      XC(N2)=XCL(I)
      XC(N21)=(7.5-XCL(I))+7.5
      YC(N2)=YCL(I)
      YC(N21)=YCL(I)
      CL(N2)=CLINIC(I)
      CL(N21)=90.0-CLINIC(I)
602 CONTINUE
C      DO 12 I=1, NCL
C      XC(I)=XCL(I)
C      YC(I)=YCL(I)
C      CL(I)=CLINIC(I)
C 12 CONTINUE
      DO 14 I=1, 1500
      AZ(I)=0.0
      14 CONTINUE
      DO 16 I=1, 3000
      16 W(I)=0.0
C      CALCULATION OF MAXIMUM AND MINUMUM VALUES FOR ISOCLINIC
      IF (N .GT. 2) GO TO 22
      NCL=2*NCL
      22 CONTINUE
      CALL RANGRD (NCL, XC, YC, CL, NX, XL, XH, NY, YL, YH, AZ, 3000
      &, W)
      DO 604 I=1, 1200
      XC(I)=0.0
      YC(I)=0.0
      Yf(I)=0.0
      Xf(I)=0.0
      CL(I)=0.0
604 CONTINUE
      H=(XH-XL)/(NX-1)
      HK=(YH-YL)/(NY-1)
      DO 606 I=1, NX
      XC(I)=XL+(I-1)*H
606 CONTINUE
      DO 607 I=1, NY
      YC(I)=YL+(I-1)*HK

```

```

607 CONTINUE
  DO 608 J=1,NY
  DO 608 I=1,NX
  K=I+(J-1)*NX
  Xf(K)=XC(I)
  Yf(K)=YC(J)
608 CONTINUE
  DO 610 I=1,NY
  DO 610 J=1,NX
  K=J+(I-1)*NX
  KK2=K
  CL(K)=AZ(K)
610 CONTINUE
C   PRINT," VALUES OF ISOCLINIC VALUES AT GRID POINTS"
  NIT=NX*NY
  2 FORMAT(3(8X,F8.4))
  RETURN
  END
F:/SUBR/
IB

```

EXPERIMENTAL RESULTS OF MODEL 3 (SAMPLE RESULT)
 THE FORMER IS THE CASE OF FIRST FRAME OF ZERO FRINGES

VALUES	OF	SIGMA2-SIGM1	AT	GRID	POINTS
====X-COR	Y-COR	SIG1-SIG2====			
2.7510	8.6206	9.8343	14.2803		
3.0000	8.0000	10.0000	14.0000		
3.0000	10.0000	2.0000	3.5000	10.0000	2.0000
4.0000	10.0000	2.0000	4.5000	10.0000	2.0000
5.0000	10.0000	2.0000	5.5000	10.0000	2.0000
6.0000	10.0000	1.9871	6.5000	10.0000	1.8610
7.0000	10.0000	1.6269	7.5000	10.0000	1.3516
8.0000	10.0000	1.0377	3.0000	10.5000	2.0000
3.5000	10.5000	2.0002	4.0000	10.5000	2.0000
4.5000	10.5000	2.0000	5.0000	10.5000	2.0002
5.5000	10.5000	1.9100	6.0000	10.5000	1.6358
6.5000	10.5000	2.0000	7.0000	10.5000	2.0000
7.5000	10.5000	0.4271	8.0000	10.5000	-0.5124
3.0000	11.0000	2.0000	3.5000	11.0000	2.0000
4.0000	11.0000	2.0000	4.5000	11.0000	2.0000
5.0000	11.0000	2.0000	5.5000	11.0000	2.0000
6.0000	11.0000	2.0000	6.5000	11.0000	2.0000
7.0000	11.0000	2.0000	7.5000	11.0000	2.0000
8.0000	11.0000	1.9998	3.0000	11.5000	2.0000
3.5000	11.5000	2.0000	4.0000	11.5000	2.0000
4.5000	11.5000	2.0000	5.0000	11.5000	2.0000
5.5000	11.5000	2.0000	6.0000	11.5000	2.0000
6.5000	11.5000	1.9516	7.0000	11.5000	1.7568
7.5000	11.5000	1.2673	8.0000	11.5000	0.3493
3.0000	12.0000	2.0000	3.5000	12.0000	2.0000
4.0000	12.0000	2.0000	4.5000	12.0000	2.0000
5.0000	12.0000	2.0000	5.5000	12.0000	1.9993
6.0000	12.0000	1.9777	6.5000	12.0000	1.7737
7.0000	12.0000	1.4717	7.5000	12.0000	0.8505
8.0000	12.0000	-0.2030	3.0000	12.5000	2.0000
3.5000	12.5000	2.0109	4.0000	12.5000	2.0000
4.5000	12.5000	2.0000	5.0000	12.5000	1.9990
5.5000	12.5000	1.9824	6.0000	12.5000	1.9813
6.5000	12.5000	1.8176	7.0000	12.5000	1.6608
7.5000	12.5000	1.4226	8.0000	12.5000	0.9464
3.0000	13.0000	2.0000	3.5000	13.0000	1.9718
4.0000	13.0000	2.0000	4.5000	13.0000	2.0000
5.0000	13.0000	1.8828	5.5000	13.0000	1.6843
6.0000	13.0000	1.8257	6.5000	13.0000	1.9812
7.0000	13.0000	2.0724	7.5000	13.0000	2.6296
8.0000	13.0000	2.4775	3.0000	13.5000	2.0000
3.5000	13.5000	1.6402	4.0000	13.5000	2.0000
4.5000	13.5000	1.9997	5.0000	13.5000	1.2522
5.5000	13.5000	1.1743	6.0000	13.5000	1.5875
6.5000	13.5000	2.1259	7.0000	13.5000	3.3328
7.5000	13.5000	4.0674	8.0000	13.5000	3.8623
3.0000	14.0000	1.9877	3.5000	14.0000	0.7426
4.0000	14.0000	2.0000	4.5000	14.0000	1.8664
5.0000	14.0000	0.5147	5.5000	14.0000	0.6504
6.0000	14.0000	1.1625	6.5000	14.0000	2.0572
7.0000	14.0000	3.5416	7.5000	14.0000	4.4179
8.0000	14.0000	3.8224			

====VALUES OF SHEAR STRESS AT GRID POINTS					
====X-COR	Y-COR	SH. ST====			
3.0000	10.0000	1.8907	3.5000	10.0000	1.8692
4.0000	10.0000	1.7469	4.5000	10.0000	1.8035
5.0000	10.0000	1.8794	5.5000	10.0000	1.9448
6.0000	10.0000	1.9850	6.5000	10.0000	1.8533
7.0000	10.0000	1.6237	7.5000	10.0000	1.3516
8.0000	10.0000	0.0657	3.0000	10.5000	1.8024
3.5000	10.5000	1.7798	4.0000	10.5000	1.7375
4.5000	10.5000	1.7666	5.0000	10.5000	1.8927
5.5000	10.5000	1.8700	6.0000	10.5000	1.6357
6.5000	10.5000	1.9969	7.0000	10.5000	1.9827
7.5000	10.5000	0.3020	8.0000	10.5000	-0.0672
3.0000	11.0000	1.7047	3.5000	11.0000	1.6807
4.0000	11.0000	1.6732	4.5000	11.0000	1.7320
5.0000	11.0000	1.8794	5.5000	11.0000	1.9350
6.0000	11.0000	1.9967	6.5000	11.0000	1.9978
7.0000	11.0000	1.9696	7.5000	11.0000	2.0000
8.0000	11.0000	0.3473	3.0000	11.5000	1.5831
3.5000	11.5000	1.5637	4.0000	11.5000	1.5917
4.5000	11.5000	1.6824	5.0000	11.5000	1.7916
5.5000	11.5000	1.8419	6.0000	11.5000	1.9183
6.5000	11.5000	1.9224	7.0000	11.5000	1.7285
7.5000	11.5000	0.8961	8.0000	11.5000	0.0625
3.0000	12.0000	1.4799	3.5000	12.0000	1.4799
4.0000	12.0000	1.5139	4.5000	12.0000	1.5793
5.0000	12.0000	1.6471	5.5000	12.0000	1.7183
6.0000	12.0000	1.8238	6.5000	12.0000	1.6805
7.0000	12.0000	1.4493	7.5000	12.0000	0.8505
8.0000	12.0000	-0.0353	3.0000	12.5000	1.3671
3.5000	12.5000	1.4028	4.0000	12.5000	1.3990
4.5000	12.5000	1.4464	5.0000	12.5000	1.5115
5.5000	12.5000	1.6152	6.0000	12.5000	1.7658
6.5000	12.5000	1.7090	7.0000	12.5000	1.5593
7.5000	12.5000	1.0059	8.0000	12.5000	0.3257
3.0000	13.0000	1.0161	3.5000	13.0000	1.2030
4.0000	13.0000	1.2017	4.5000	13.0000	1.2465
5.0000	13.0000	1.2457	5.5000	13.0000	1.2443
6.0000	13.0000	1.4998	6.5000	13.0000	1.7158
7.0000	13.0000	1.9187	7.5000	13.0000	2.6296
8.0000	13.0000	0.9361	3.0000	13.5000	0.5829
3.5000	13.5000	0.7232	4.0000	13.5000	0.7459
4.5000	13.5000	0.8708	5.0000	13.5000	0.6158
5.5000	13.5000	0.7173	6.0000	13.5000	1.1997
6.5000	13.5000	1.8169	7.0000	13.5000	2.9955
7.5000	13.5000	2.8760	8.0000	13.5000	1.6930
3.0000	14.0000	0.5379	3.5000	14.0000	0.2765
4.0000	14.0000	0.2466	4.5000	14.0000	0.4157
5.0000	14.0000	0.1663	5.5000	14.0000	0.2781
6.0000	14.0000	0.6937	6.5000	14.0000	1.4650
7.0000	14.0000	3.0671	7.5000	14.0000	4.4179
8.0000	14.0000	1.9112			

====VALUES ====X-COR	OF Y-COR	SIGMA2-SIGM1 SIG1-SIG2====	AT GRID	POINTS	
6.0000	11.0000	2.0000	6.5000	11.0000	2.0000
7.0000	11.0000	2.0000	7.5000	11.0000	2.0000
8.0000	11.0000	2.0000	8.5000	11.0000	2.0000
9.0000	11.0000	2.0000	6.0000	11.5000	2.0000
6.5000	11.5000	2.0000	7.0000	11.5000	2.0000
7.5000	11.5000	2.0000	8.0000	11.5000	2.0000
8.5000	11.5000	2.0000	9.0000	11.5000	2.0000
6.0000	12.0000	2.0000	6.5000	12.0000	2.4731
7.0000	12.0000	2.6800	7.5000	12.0000	3.6009
8.0000	12.0000	3.0981	8.5000	12.0000	2.9396
9.0000	12.0000	2.0000	6.0000	12.5000	2.0000
6.5000	12.5000	2.7921	7.0000	12.5000	4.0000
7.5000	12.5000	4.0004	8.0000	12.5000	4.0003
8.5000	12.5000	1.9091	9.0000	12.5000	3.2736
6.0000	13.0000	2.4794	6.5000	13.0000	3.1687
7.0000	13.0000	0.5061	7.5000	13.0000	1.8283
8.0000	13.0000	1.3457	8.5000	13.0000	3.2045
9.0000	13.0000	3.6250	6.0000	13.5000	2.6426
6.5000	13.5000	2.6389	7.0000	13.5000	4.0011
7.5000	13.5000	4.9230	8.0000	13.5000	4.2810
8.5000	13.5000	2.9997	9.0000	13.5000	2.7639
6.0000	14.0000	1.9234	6.5000	14.0000	2.6604
7.0000	14.0000	5.1295	7.5000	14.0000	7.8684
8.0000	14.0000	5.8770	8.5000	14.0000	3.1339
9.0000	14.0000	2.0533			

====VALUES ====X-COR	OF SHEAR Y-COR	STRESS AT SH. ST====	AT GRID	POINTS	
6.0000	11.0000	1.9967	6.5000	11.0000	1.9978
7.0000	11.0000	1.9696	7.5000	11.0000	2.0000
8.0000	11.0000	0.3473	8.5000	11.0000	-0.0939
9.0000	11.0000	0.1148	6.0000	11.5000	1.9183
6.5000	11.5000	1.9701	7.0000	11.5000	1.9677
7.5000	11.5000	1.4142	8.0000	11.5000	0.3580
8.5000	11.5000	0.3446	9.0000	11.5000	0.5656
6.0000	12.0000	1.8444	6.5000	12.0000	2.3430
7.0000	12.0000	2.6392	7.5000	12.0000	3.6009
8.0000	12.0000	0.5380	8.5000	12.0000	0.9405
9.0000	12.0000	0.7734	6.0000	12.5000	1.7825
6.5000	12.5000	2.6252	7.0000	12.5000	3.7555
7.5000	12.5000	2.8287	8.0000	12.5000	1.3769
8.5000	12.5000	0.6501	9.0000	12.5000	1.4845
6.0000	13.0000	2.0367	6.5000	13.0000	2.7441
7.0000	13.0000	0.4685	7.5000	13.0000	1.8283
8.0000	13.0000	0.5085	8.5000	13.0000	1.6022
9.0000	13.0000	2.0670	6.0000	13.5000	1.9971
6.5000	13.5000	2.2553	7.0000	13.5000	3.5962
7.5000	13.5000	3.4810	8.0000	13.5000	1.8765
8.5000	13.5000	1.5574	9.0000	13.5000	1.8099
6.0000	14.0000	1.1477	6.5000	14.0000	1.8944
7.0000	14.0000	4.4422	7.5000	14.0000	7.8684
8.0000	14.0000	2.9384	8.5000	14.0000	2.2002
9.0000	14.0000	1.6476			

====VALUES ====X-COR	OF Y-COR	SIGMA2-SIGM1 SIG1-SIG2====	AT GRID	POINTS	
2.0000	11.0000	2.0000	2.5000	11.0000	2.0000
3.0000	11.0000	2.0000	3.5000	11.0000	2.0000
4.0000	11.0000	2.0000	4.5000	11.0000	2.0000
5.0000	11.0000	2.0000	5.5000	11.0000	2.0000
6.0000	11.0000	2.0000	6.5000	11.0000	2.0000
7.0000	11.0000	2.7198	7.5000	11.0000	2.7129
8.0000	11.0000	2.5011	8.5000	11.0000	2.0000
9.0000	11.0000	2.0000	9.5000	11.0000	2.0000
10.0000	11.0000	2.0000	10.5000	11.0000	2.0000
11.0000	11.0000	2.0000	11.5000	11.0000	2.0000
12.0000	11.0000	2.0000	2.0000	11.5000	2.0000
2.5000	11.5000	2.0000	3.0000	11.5000	2.0000
3.5000	11.5000	2.0000	4.0000	11.5000	2.0000
4.5000	11.5000	2.0000	5.0000	11.5000	2.0000
5.5000	11.5000	2.0000	6.0000	11.5000	2.7880
6.5000	11.5000	3.0758	7.0000	11.5000	3.3691
7.5000	11.5000	3.4225	8.0000	11.5000	3.3100
8.5000	11.5000	3.2173	9.0000	11.5000	2.4071
9.5000	11.5000	2.0000	10.0000	11.5000	2.0000
10.5000	11.5000	2.0000	11.0000	11.5000	2.0000
11.5000	11.5000	2.0000	12.0000	11.5000	2.0000
2.0000	12.0000	2.0000	2.5000	12.0000	2.0000
3.0000	12.0000	2.0000	3.5000	12.0000	2.0000
4.0000	12.0000	2.0000	4.5000	12.0000	2.0000
5.0000	12.0000	2.0000	5.5000	12.0000	2.3662
6.0000	12.0000	3.1750	6.5000	12.0000	2.7734
7.0000	12.0000	1.2711	7.5000	12.0000	1.3372
8.0000	12.0000	0.7771	8.5000	12.0000	2.8261
9.0000	12.0000	2.9868	9.5000	12.0000	2.0575
10.0000	12.0000	2.0000	10.5000	12.0000	2.0000
11.0000	12.0000	2.0000	11.5000	12.0000	2.0000
12.0000	12.0000	2.0000	2.0000	12.5000	2.0000
2.5000	12.5000	2.0000	3.0000	12.5000	2.0000
3.5000	12.5000	2.0000	4.0000	12.5000	2.0000
4.5000	12.5000	2.0000	5.0000	12.5000	2.0000
5.5000	12.5000	3.2074	6.0000	12.5000	3.0313
6.5000	12.5000	2.1147	7.0000	12.5000	3.4353
7.5000	12.5000	3.9613	8.0000	12.5000	3.4651
8.5000	12.5000	2.1472	9.0000	12.5000	3.3165
9.5000	12.5000	3.0156	10.0000	12.5000	2.0000
10.5000	12.5000	2.0000	11.0000	12.5000	2.0000
11.5000	12.5000	2.0000	12.0000	12.5000	2.0000
2.0000	13.0000	2.0000	2.5000	13.0000	2.0000
3.0000	13.0000	2.0000	3.5000	13.0000	2.0000
4.0000	13.0000	2.0000	4.5000	13.0000	2.0000
5.0000	13.0000	2.0213	5.5000	13.0000	3.1050
6.0000	13.0000	3.1391	6.5000	13.0000	3.6321
7.0000	13.0000	4.6226	7.5000	13.0000	4.8140

Appendix V

```

    IMPLICIT REAL*8 (A-H,O-Z)
    DIMENSION N(800),G(800),GTOP(800),GP(800),GPO(800),X(800)
    &,Y(800),AM(800,4),C(4,4),B(800),Z(4),aa(20,20),wks1(4),wks2(4)
    &,xam(4,800),NCF(800),NT1(800),NT2(800),XNF(800)
c    program for least squar method for unit fringe value
    READ(3,20)M,R,T,PIE
20  FORMAT(V)
    READ(3,20)(N(I),NCF(I),NT1(I),X(I),Y(I),NT2(I),I=1,M)
c    the folowing statement for scale of foto
    ORX=(X(3)+X(8))/2
    ORY=(Y(3)+Y(8))/2
    SCX=(X(5)-X(1))/5.08
    SCY=(Y(6)-Y(10))/5.08
    do 22 i=1,m
    X(I)=(X(I)-ORX)*SCX
    Y(I)=(Y(I)-ORY)*SCY
    XNF(I)=(N(I)-N(1))*0.124*32.2*12.0
22  continue
    DO 40 I=1,M
    F=0.0
    GTOP(I)=R**2-(X(I)**2+Y(I)**2)
    GP(I)=(X(I)**2+Y(I)**2+R**2)**2
    GPO(I)=GP(I)-4*(Y(I)**2*r**2)
    F=XNF(I)
    G(I)=(4*F*R*GTOP(I))/(PIE*T*GPO(I))
40  CONTINUE
    DO 50 I=1,M
    xaM(1,i)=G(I)
    xaM(2,i)=X(I)
    xaM(3,i)=Y(I)
    xaM(4,i)=1.0d0
50  CONTINUE
    do 45 i=1,4
    do 45 j=1,M
45  am(j,i)=xam(i,j)
    DO 35 I=1,4
    DO 35 J=1,4
    C(I,J)=0.0d0
    DO 35 K=1,M
    C(I,J)=C(I,J)+AM(K,J)*AM(K,I)
35  CONTINUE
    DO 55 I=1,4
    DO 55 J=1,M
    B(I)=B(I)+(AM(J,I)*N(J))
55  CONTINUE
    IA=4
    IAA=4
    L=4
    IFAIL=0
    CALL F04ATF(C,IA,B,L,Z,AA,IAA,WKS1,WKS2,IFAIL)
    DO 60 I=1,L
    WRITE(6,70)Z(I)
60  CONTINUE
70  FORMAT(V)
    STOP
    END

```